Hydrodynamic Stability of Non-Newtonian Rotating Boundary-Layer Flows

by

Paul Travis Griffiths

A thesis submitted to the
University of Birmingham
for the degree of
Doctor of Philosophy

School of Mathematics
University of Birmingham
July 2015

This thesis is dedicated to my grandfather

Norman William Knight.

Abstract

The stability of the boundary-layer on a rotating disk is considered for fluids that adhere to a non-Newtonian governing viscosity relationship. For fluids with shear-rate dependent viscosity the base flow is no longer an exact solution of the Navier-Stokes equations, however, in the limit of large Reynolds number the flow inside the three-dimensional boundary-layer can be determined via a similarity solution.

The convective instabilities associated with flows of this nature are described both asymptotically and numerically via separate linear stability analyses. Akin to previous Newtonian studies it is found that there exists two primary modes of instability; the upper-branch type I modes, and the lower-branch type II modes. Results show that both these modes can be stabilised or destabilised depending on the choice of non-Newtonian viscosity model. A number of comments are made regarding the suitability of some of the more well-known non-Newtonian constitutive relationships within the context of the rotating disk model.

Key words: non-Newtonian, boundary-layer, rotating disk flow, convective instability

Acknowledgements

First and foremost I would like to thank Professor Stephen Garrett for his advice, guidance and the numerous opportunities he has afforded me. I am indebted to him for his willingness to take me on as a Ph.D. student. I must also thank Dr. Sharon Stephen for the excellent supervision I received during the initial stages of my studies. Additionally I would like to acknowledge, firstly, Dr. Zahir Hussain, for the many useful discussions relating to this work, secondly, Professor Jim Denier, without his suggestions large parts of this thesis may never have materialised and thirdly, Dr. Jamal Uddin, for guiding me towards a career in academia. Financial support from the Engineering and Physical Sciences Research Council is also gratefully acknowledged.

I am extremely grateful for the continued support of my parents, without which I wouldn't be in the position I find myself now. Dad, I appreciate the important life lessons you have taught me, not forgetting to mention 'the only equation I will ever need'...

$$\text{Buy Bananas (50p)} + \text{Sell Bananas (£1)} = \text{Profit},$$

I have no doubt that remembering this will prove useful, especially in the unlikely event that I one day open a greengrocers.

Lastly, I would like to thank my partner Natalie Ainge, without her my years as a Ph.D. student would not have been so enjoyable.

Contents

Chapter 1

Introduction

The stability and transition of the boundary-layer on a rotating disk is a classical fluid mechanics problem that has attracted a great deal of attention from numerous authors over many decades. The first theoretical investigation of this three-dimensional problem was performed by von Kármán (1921). He showed that the steady incompressible flow induced by the rotation of an infinite plane with uniform angular velocity is an exact solution of the Navier-Stokes equations. The governing partial differential equations (PDEs) can be reduced to a set of ordinary differential equations (ODEs) via the introduction of a suitable similarity solution.

The boundary-layer flow is characterised by the lack of a radial pressure gradient near to the disk to balance the centrifugal forces so the fluid spirals outwards. The disk acts as a centrifugal fan, the fluid emanating from the disk being replaced by an axial flow directed back towards the surface.

Batchelor (1951) showed that this type of flow is in fact just a limiting case of a whole number of flows with similarity solutions in which both the infinite plane and the fluid at infinity rotate with differing angular velocities. The corresponding limiting case, when the infinite plane is stationary and the fluid at infinity rotates at a constant angular velocity, was first described by Bödewadt (1940).

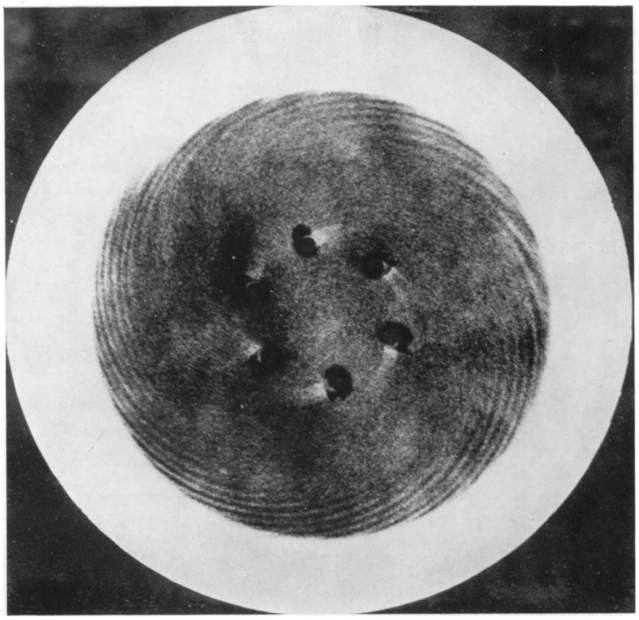

Figure 1.1: Experimental image reproduced from Gregory *et al.* (1955) showing the china-clay record of the instability and transition on a rotating disk.

A vast wealth of material exists concerning the solutions of the Newtonian rotating disk equations; the interested reader is referred to Zandbergen & Dijkstra (1987). The authors provide a thorough review of the major contributions made postdating von Kármán's seminal work.

The stability of the von Kármán boundary-layer was first investigated by Gregory, Stuart & Walker (1955). The motivation for this study stemmed from the desire to better understand the boundary-layer flow on a swept wing. Both flows are susceptible to cross-flow instabilities as both exhibit inflectional velocity profiles. However, the rotating disk problem is somewhat simpler to analyse as it offers an exact solution of the Navier-Stokes equations and is easier to model experimentally. The authors observed spiral modes of instability in the form of co-rotating vortices. Gregory & Walker conducted an experimental analysis using china-clay techniques to observe the transition from laminar to turbulent flow, measuring the angle between the normal to the radius vector and the tangent to the vortices to be approximately 13°. Stuart conducted the theoretical study,

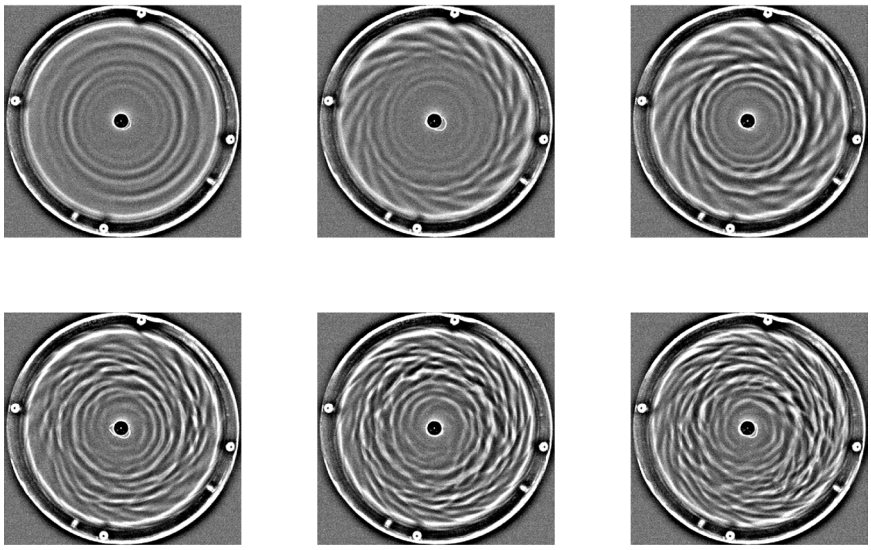

Figure 1.2: Experimental image reproduced from Cros, Floriani, Le Gal & Lima (2005) showing the transition from laminar to turbulent flow within the Bödewadt boundary-layer. The radius of the disk is $R = 140$ mm and Ω, the angular velocity of the fluid, increases from 9 rpm - top left to 20 rpm - bottom right.

a high Reynolds number linear stability analysis that modelled the cross-flow instabilities. His predictions for the wave angle of the disturbances were in excellent agreement with the experimental results of Gregory & Walker. Figure 1.1, taken from the experimental study, shows with increasing disk radii: laminar flow, spiral vortices and fully developed turbulent flow. Clearly these visualisation experiments are only able to indicate the existence of stationary waves, those disturbances that are fixed relative to the motion of the disk. However, the rotating disk boundary-layer is also susceptible to travelling wave disturbances, and experimental studies have since been conducted to investigate instabilities of this nature, see for example, Lingwood (1996).

Figure 1.2 shows the laminar to turbulent transition within the Bödewadt boundary-layer. Akin to the von Kármán boundary-layer study of Gregory *et al.* (1955) we observe, at relatively low values of the Reynolds number ($Re = \Omega R^2/\nu$), purely laminar flow in the form of circular wave patterns. As the Reynolds number is increased spiral vortices begin to appear and coexist with the circular wave formations. Increasing the Reynolds

number further still we see that these circular waves all but disappear and the spiral vortices become the dominate feature of the flow. Above the critical Reynolds number the flow transitions and here a weak state of turbulence is observed where the coherent spiral structures are no longer recognisable.

Malik (1986) presents the first comprehensive numerical study of the stationary mode disturbances with the rotating disk boundary-layer, computing the curves of neutral stability using a sixth-order system of linear disturbance equations. By utilising a parallel-flow approximation, and therefore restricting attention to the local stability characteristics of the flow, Malik includes the effects of streamline curvature and Coriolis force and demonstrates that there exists two distinct neutral branches. An upper-branch, due to the cross-flow instability, termed type I and a lower-branch, attributed to external streamline curvature, termed type II. These numerical results were verified by the linear asymptotic analysis of Hall (1986). He recovered the type I solution presented by Gregory *et al.* (1955) (later corrected by Gajjar 2007) and showed that an additional short-wavelength mode exists, its structure being fixed by a balance between viscous and Coriolis forces. This mode corresponds directly to the type II branch.

If localised disturbances are unbounded for large time and propagate both upstream and downstream, the flow is said to be absolutely unstable. Conversely, if disturbances are swept away from the source the flow is said to be convectively unstable. Figure 1.3 outlines examples of (i) stable, (ii) convectively unstable and (iii) absolutely unstable disturbances. For case (ii) the disturbance grows as it convects downstream, whilst for case (iii) the disturbance grows at the initial location and spreads into regions on both sides of the source. The studies of Gregory *et al.* (1955), Malik (1986) and Hall (1986) are examples of convective instability investigations. The subject matter of this thesis will also concern convectively unstable flows[1]. However, there are numerous studies concerning

[1]That is not to say that these flows do not also exhibit absolute instabilities, they do, we simply do not consider them here.

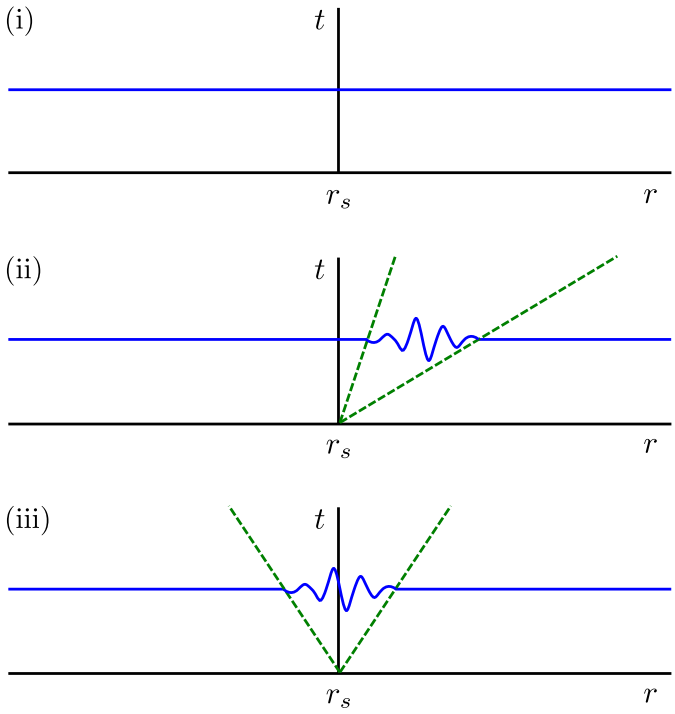

Figure 1.3: Space-time diagrams of (i) stable, (ii) convectively unstable and (iii) absolutely unstable disturbances. The disturbances are introduced at the dimensionless position $r = r_s$ and grow exponentially within the dashed lines.

the absolute instability characteristics of the rotating disk boundary-layer.

Lingwood (1995*a*) investigated the role of absolute instability showing that the boundary-layer on a rotating disk of infinite extent is locally absolutely unstable at Reynolds numbers in excess of a critical value. The value of the critical Reynolds number agrees exceptionally well with experimental data, leading to Lingwood's hypothesis that absolute instability plays a part in turbulent transition on the rotating disk. Subsequently, Davies & Carpenter (2003) investigated the global behaviour of the absolute instability of the rotating disk boundary-layer. By direct numerical simulations of the linearised governing equations they were able to show that the local absolute instability does not produce a linear global instability, instead suggesting that convective behaviour eventually dominates at all the Reynolds numbers. Their conclusion was that absolute instability was not involved in the transition process through linear effects. More recently, Pier (2003)

demonstrated explicitly that a nonlinear approach is required to explain the self-sustained behaviour of the rotating disk flow. Using the result of Huerre & Monkewitz (1990) that the presence of local absolute instability does not necessarily give rise to linear global instability, Pier suggested that the flow has a primary nonlinear global mode (fixed by the onset of the local absolute instability) which has a secondary absolute instability that triggers the transition to turbulence.

Using the complex Ginzburg-Landau equation Healey (2010) investigated both the linear and non-linear global modes associated with the rotating disk boundary-layer. In this study the author suggests that so called 'edge effects' are of paramount importance and that linear global instability can be induced by local absolute instability at the edge of the disk. Healey (2010) supports this claim by comparing his global mode theory with previous experimentally observed transition Reynolds numbers plotted against the Reynolds number at the edge of the disk, finding a suitable agreement between the two. These theoretical predictions for the edge effects were then studied experimentally by Imayama, Alfredsson & Lingwood (2013). Using different edge configurations and edge Reynolds numbers the experimental results show that there appears to be little correlation between the proximity of the edge of the disk and the transition Reynolds number, as suggested by Healey (2010). Instead, the authors hypothesise that the agreement obtained by Healey (2010) is largely due to the inconsistency, with respect to previous experimental procedures, of the definition of 'transition'. The exact mechanisms governing the laminar to turbulent transition with the rotating disk boundary-layer remains an area of active research and is not yet fully understood. The interested reader is referred to the very recent review article by Lingwood & Alfredsson (2015) for a thorough discussion on the history of these studies and the potential directions for future research.

Extending the rotating disk theory Lingwood (1997) and Lingwood & Garrett (2011) considered the BEK system of rotating boundary-layer flows, named as such as it en-

compasses a family of rotating flows including the Bödewadt, Ekman and von Kármán boundary layers. They show that as the Rossby number (the dimensionless parameter that quantifies changes in differential rotation rate) increases, the flows become increasingly unstable in both the convective and absolute senses, noting that the onset of convective and absolute instability occurs almost simultaneously at very low Reynolds number in the Bödewadt boundary-layer.

In an attempt to develop drag reduction techniques Cooper, Harris, Garrett, Özkan & Thomas (2015) investigate the use of roughness to delay laminar to turbulent transition. For practical and theoretical reasons the authors choose the rotating disk model in order to investigate the effect of roughness on boundary-layer flows that exhibit cross-flow instabilities. Both anisotropic and isotropic surface roughnesses are modelled via partial slip conditions at the wall. The convective stability analysis reveals that the introduction of surface roughness results in a stabilisation of the type I mode. However, for anisotropic roughness in the form of concentric grooves the type II mode is significantly destabilised, so much so that in fact this mode becomes the primary and most dangerous mode in terms of critical Reynolds number. Generally the results suggest that a delay in laminar to turbulent transition is possible, although it appears imperative that the 'correct' type of surface roughness is used. Certainly there is a great deal of scope for future investigations regarding this problem and it is believed that the authors are currently undertaking an experimental study in the hope of validating these theoretical results.

More recent research interests have concerned the stability and transition of the boundary-layer flow over rotating cones and spheres. Being intrinsically linked with spinning projectile applications this work has been motivated by the need to better understand, and hopefully delay, laminar-turbulent transition within such systems. Garrett & Peake (2002) show that, with respect to the rotating sphere boundary-layer, for latitudes below $\theta = 66^\circ$ the cross-flow instability mode dominates, whilst above this latitude the

streamline curvature mode is the most dangerous. Garrett, Hussain & Stephen (2009) investigate the stability of the boundary-layer on a rotating cone and note that for broad cones the instability mechanism manifests as co-rotating vortices, whereas for slender cones counter-rotating vortices are observed. This cross-flow study shows favourable agreement with experimental results for cones with a half-angle greater than forty degrees. For cones with a half angle below this value an alternative formulation that focuses on centrifugal effects is required, see Hussain, Garrett & Stephen (2014). In this case favourable agreement with experimental results is again observed, this time for cones with a reduced half-angle.

1.1 Motivation for this work

The motivation for this study has stemmed from a problem originally posed by Schlumberger PLC concerning rotating disk experiments that are commonplace in the petrochemical industry. Schlumberger are interested in the erosion of calcite disks when rotated and submersed in acidic solutions. The problem was presented to a study group at the King Abdullah University of Science and Technology (KAUST) in association with the Oxford Centre for Collaborative Applied Mathematics (OCCAM) in early 2011 and a report was published thereafter. A copy of the report entitled 'Modelling mass transfer in a rotating disk reaction vessel' is readily available online[2].

The report served to model the reaction between the calcite rotating disks and the acidic fluids, hence both a mathematical and chemical analysis of the problem needed to be considered. During the construction of the mathematical model the fluids were assumed to be Newtonian. However, in practice, gelling agents were often added to the acidic fluids in order to slow the reaction rate of the fluids with the calcite disks. The introduction of these gelling agents changes the viscous structure of the fluids entirely.

[2] http://www.maths-in-industry.org/miis/349/1/SLB-disk.pdf

Figure 1.4: Calcite disks used during experimental testing. Reproduced from Nasr-El-Din *et al.* (2008). The angular velocity at which each disk has been spun (and hence the Reynolds number of each of the respective flows) increases from 100 rpm - top left to 1000 rpm - bottom right

It transpires that the gelled acids used in these experiments behaved as non-Newtonian shear-thinning fluids.

In addition to the experimental data, representatives at Schlumberger also provided the study group with supplementary material that detailed experimental set-up and procedure. These studies provided the group with accompanying experimental results, see for example, Nasr-El-Din, Al-Mohammad, Al-Aamri & Al-Fuwaires (2008).

The gelled acidic fluids were modelled by Nasr-El-Din *et al.* (2008) using the power-law constitutive relationship. As can be seen in figure 1.4 swirling flow patterns have been etched into the calcite disks, becoming more pronounced as the Reynolds number of the flow increases. The resemblance between these experimental images and those taken by Gregory *et al.* (1955) is clear to see. This observation naturally raises the question of whether the instability and transition of the boundary-layer flow on a rotating disk can be modelled for non-Newtonian fluids. If so, are the properties of the non-Newtonian fluid stabilising or destabilising? These questions provide the motivation for the current study

and form a basis for the content of this thesis.

1.2 Non-Newtonian boundary-layer flows

Considerably less attention has been given to the non-Newtonian rotating disk problem[3]. Mitschka (1964) modified the von Kármán similarity solution to incorporate a power-law governing viscosity relationship. In this case the base flow is not an exact solution of the generalised Navier-Stokes equations and a boundary-layer approximation is required. Both Mitschka & Ulbrecht (1965) and Andersson, de Korte & Meland (2001) present basic flow solutions for shear-thickening and shear-thinning power-law fluids. However, those authors overlooked the importance of matching these boundary-layer solutions to an external flow. Denier & Hewitt (2004) addressed this problem and presented corrected solutions for both cases, noting that the structure of the solutions is intrinsically different for shear-thickening and shear-thinning fluids.

Due to the relative simplicity of the power-law model it has been utilised by a number of other studies in order to investigate non-Newtonian effects. Hansford & Litt (1968) considered the mass transport from a rotating disk into power-law fluids, noting that the rate of mass transfer would be increased for shear-thinning fluids. Ming, Zheng & Zhang (2011) extend the work of Andersson *et al.* (2001) and investigate the addition of heat transfer in the context of the power-law rotating disk model. Assuming thermal conductivity can also be described by a power-law relationship, the authors show that at a fixed Prandtl number (the ratio of momentum diffusivity to thermal diffusivity) the temperature distribution within the boundary-layer will decay to zero further from and closer to the disk for shear-thinning and shear-thickening fluids, respectively.

The study of viscoplastic fluids has been the subject of some more recent research

[3]Within this section, without any prior introduction, we have the need to reference some of the more commonly used non-Newtonian viscosity models. Specific details regarding these models, and others, are outlined in chapter 2.

interests, specifically fluids that adhere to the Bingham governing viscosity relationship. Rashaida, Bergstrom & Sumner (2006) once again considered the mass transfer whilst using a boundary-layer approximation in order to obtain solutions for the basic flow, whereas Ahmadpour & Sadeghy (2013) make no such boundary-layer approximation and present base flow solutions whilst retaining all the additional viscous terms associated with the Bingham viscosity model. An in depth review of this study appears in chapter 3.

The two-dimensional flat-plate boundary-layer problem has received considerably more attention in the literature, perhaps for obvious reasons. As it is not of primary interest we provide just a brief overview of two of the more notable studies. Acrivos, Shah & Petersen (1960), in their Falkner-Skan type investigation, were the first to show that the classical boundary-layer similarity solution can be extended to incorporate a power-law constitutive relationship. Interestingly, the authors give the prediction that there exists a 'finite-width' boundary-layer for shear-thickening fluids. Denier & Dabrowski (2004) reconsidered this problem and demonstrated that this finite-width crisis is due to a singularity in the solutions. The authors addressed this problem by introducing an additional viscous layer in order to smooth out these singularities.

Having performed a relatively exhaustive search of the literature there appears to be very little material concerning the stability characteristics of non-Newtonian boundary-layer flows. Indeed before the commencement of this work there had been no previous investigations regarding stability and transition in the context of three-dimensional non-Newtonian boundary-layers.

1.3 Aims of this study

The intention of this work is to improve upon the current understanding of non-Newtonian rotating boundary-layer flows. Within this thesis we will consider three different gener-

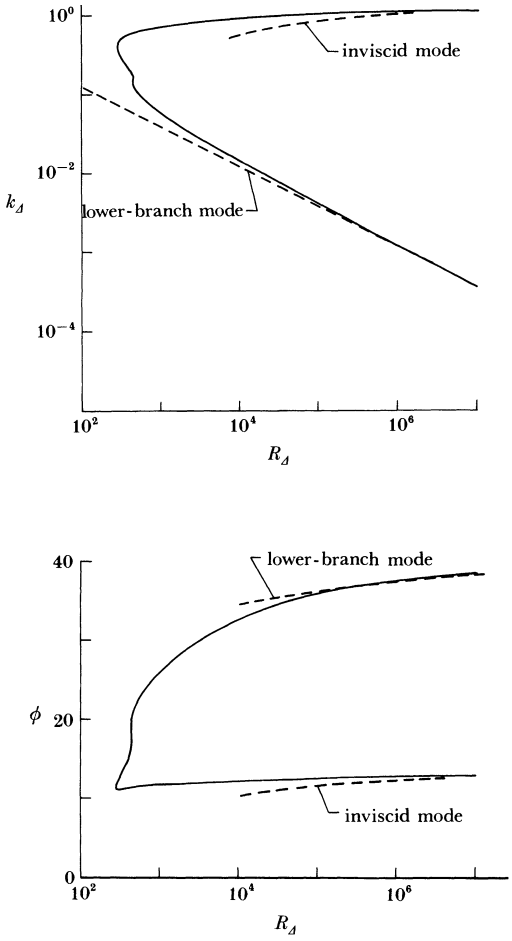

Figure 1.5: Plots of the Newtonian stability results reproduced from Hall (1986). Malik's neutral curves are given by the solid lines whilst Hall's asymptotic predictions are given by the dashed lines. The modified Reynolds number is R_Δ, the effective wavenumber is k_Δ and ϕ is the wave angle.

alised Newtonian fluid models[4]. Firstly, we will look to provide a detailed account of the base flow solutions. We will follow the study of Denier & Hewitt (2004) to ensure the consistency of all our solutions. Having done so, we will then consider the convective stability characteristics of these flows, utilising both asymptotic and numerical techniques. It has been shown, in the Newtonian limit, that there is an excellent agreement between these two sets of solutions, see figure 1.5. We hope to reproduce results such as this for flows with

[4]The exact definition of a generalised Newtonian fluid is given in chapter 2. For the time being it is enough to note that these fluids are non-Newtonian in nature and moreover satisfy certain regularising conditions.

non-constant viscosity. We will follow the Newtonian studies of Hall (1986) and Lingwood (1995*b*) when considering our asymptotic and numerical investigations, respectively.

This thesis is organised as follows: in chapter 2 we give a brief introduction to the class of non-Newtonian fluids known as generalised Newtonian fluids. We then go on to determine the governing boundary-layer equations for this problem. We solve these equations and present the corresponding base flow profiles in chapter 3. In chapter 4 we formulate the three-dimensional linear stability problem for each of our generalised Newtonian fluid models. An asymptotic analysis is presented in the limit of large Reynolds number and results for the upper-branch neutral modes are detailed here. The numerical investigation is the subject matter of chapter 5, where we find that the form of the viscosity profile within the boundary-layer plays a pivotal role in determining the curves of neutral stability. These numerically computed solutions are then compared with the upper-branch asymptotic results. In chapter 6 we present an initial investigation into the asymptotic structure of the lower-branch neutral modes. Finally, in chapter 7, we conclude and summarise our findings and comment on possible extensions of this work.

A considerable amount of the work detailed herein has already been published and appears in the literature as:

- **Griffiths, P. T.**, Stephen, S. O., Bassom, A. P. & Garrett, S. J. 2014*a* Stability of the boundary layer on a rotating disk for power-law fluids. *J. Non-Newtonian Fluid Mech.* **207**, 1-6

- **Griffiths, P. T.**, Garrett, S. J. & Stephen, S. O. 2014*b* The neutral curve for stationary disturbances in rotating disk flow for power-law fluids *J. Non-Newtonian Fluid Mech.* **213**, 73-81

- **Griffiths, P. T.** 2015 Flow of a generalised Newtonian fluid due to a rotating disk *J. Non-Newtonian Fluid Mech.* **221**, 9-17

A fourth publication is currently being prepared for submission to the Journal of Fluid Mechanics (JFM).

Chapter 2

Problem Formulation

In this chapter we derive the governing equations that describe the boundary-layer flow of a non-Newtonian fluid due to a rotating disk. Specifically, we will focus our attention on fluids that satisfy a generalised Newtonian relationship, where the fluid viscosity is said to be dependent on the shear rate of the flow.

However, before doing so, we will first discuss some of the features that certain generalised Newtonian fluids exhibit, outlining a number of the more common empirical relationships that are used to describe these fluids. Perhaps the most well-known of these relationships being the Ostwald-de Waele or 'power-law' model.

2.1 Generalised Newtonian fluids

Newtonian fluids are defined as having a constant viscosity at all shear rates. Owing from this definition we arrive at the following governing relationship

$$\boldsymbol{\tau} = \mu_n \dot{\boldsymbol{\gamma}}, \tag{2.1.1}$$

where $\boldsymbol{\tau}$ is the shear stress tensor, μ_n is the constant viscosity and $\dot{\boldsymbol{\gamma}} = \boldsymbol{\nabla u} + (\boldsymbol{\nabla u})^{\mathrm{T}}$ is the rate-of-strain tensor for any arbitrary flow field $\boldsymbol{u} = \boldsymbol{u}(x_1, x_2, x_3, t)$, in an arbitrary coordinate system. Thus for Newtonian fluids shear stress is a linear function of the shear

rate.

The viscosity of a generalised Newtonian fluid is no longer constant, instead it is a function of the shear rate, so that

$$\mu(\dot{\boldsymbol{\gamma}}) = \frac{\dot{\boldsymbol{\gamma}}}{\boldsymbol{\tau}}, \tag{2.1.2}$$

where here μ is a scalar and therefore must be a function of the invariants of the tensor $\dot{\boldsymbol{\gamma}}$. The invariants of a tensor are defined such that their values are independent of the choice of coordinate system. For example, a single, independent scalar invariant can be constructed from a vector. Taking an arbitrary vector $\boldsymbol{v} = (v_1, v_2, v_3)$, in three dimensions, we have that the magnitude of the vector is $|\boldsymbol{v}| = v = \sqrt{v_1^2 + v_2^2 + v_3^2} = \sqrt{\sum_i v_i^2}$. This is known as the scalar invariant of $\boldsymbol{v}$ and is independent of the choice of coordinate system. We find that three independent scalars can be formed from a tensor of rank two, such as the rate-of-strain tensor.

The invariants of $\dot{\boldsymbol{\gamma}}$ are given in Bird, Armstrong & Hassager (1977) as

$$\begin{aligned}
I &= \operatorname{tr} \dot{\boldsymbol{\gamma}} = \sum_i \dot{\gamma}_{ii}, \\
II &= \operatorname{tr} \dot{\boldsymbol{\gamma}}^2 = \sum_i \sum_j \dot{\gamma}_{ij}\dot{\gamma}_{ji} = \sum_i \sum_j \dot{\gamma}_{ij}^2, \\
III &= \operatorname{tr} \dot{\boldsymbol{\gamma}}^3 = \sum_i \sum_j \sum_k \dot{\gamma}_{ij}\dot{\gamma}_{jk}\dot{\gamma}_{ki}.
\end{aligned}$$

For the second invariant II we have utilised the fact that the rate-of-strain tensor is symmetric. Given that $\dot{\boldsymbol{\gamma}} = \boldsymbol{\nabla u} + (\boldsymbol{\nabla u})^{\mathrm{T}}$, it is relatively simple to show that the first invariant $I = 2(\boldsymbol{\nabla} \cdot \boldsymbol{u})$, and thus I is zero for incompressible fluids[1]. The magnitude of the rate-of-strain tensor is given by $|\dot{\boldsymbol{\gamma}}| = \dot{\gamma} = \sqrt{(\dot{\boldsymbol{\gamma}} : \dot{\boldsymbol{\gamma}})/2}$ where the double dot operation

[1]This computation is outlined in the appendix A.

is defined as follows

$$
\begin{aligned}
(\dot{\boldsymbol{\gamma}} : \dot{\boldsymbol{\gamma}}) &= \left[\left(\sum_i \sum_j \boldsymbol{\delta}_i \boldsymbol{\delta}_j \dot{\gamma}_{ij} \right) : \left(\sum_k \sum_l \boldsymbol{\delta}_k \boldsymbol{\delta}_l \dot{\gamma}_{kl} \right) \right] \\
&= \sum_i \sum_j \sum_k \sum_l (\boldsymbol{\delta}_i \boldsymbol{\delta}_j : \boldsymbol{\delta}_k \boldsymbol{\delta}_l) \dot{\gamma}_{ij} \dot{\gamma}_{kl} \\
&= \sum_i \sum_j \sum_k \sum_l (\boldsymbol{\delta}_j \cdot \boldsymbol{\delta}_k)(\boldsymbol{\delta}_i \cdot \boldsymbol{\delta}_l) \dot{\gamma}_{ij} \dot{\gamma}_{kl} = \sum_i \sum_j \sum_k \sum_l \delta_{il} \delta_{jk} \dot{\gamma}_{ij} \dot{\gamma}_{kl} \\
&= \sum_i \sum_j \dot{\gamma}_{ij} \dot{\gamma}_{ji} = \sum_i \sum_j \dot{\gamma}_{ij}^2 = II.
\end{aligned}
$$

Hence we are able to write $\dot{\gamma}$ solely in terms of the II. Bird *et al.* (1977) note that the third invariant III is identically zero for shearing flows such as; axial annular flow, tube flow and the flow between rotating disks. Thus, for the types of flows considered within this thesis, μ depends only on the second invariant of the rate-of-strain tensor. It is commonplace in literature regarding flows of this nature to write the generalised Newtonian viscosity as a function of the shear rate, so that, $\mu = \mu(\dot{\gamma})$. Hence (2.1.2) is perhaps better written as $\boldsymbol{\tau} = \mu(\dot{\gamma})\dot{\boldsymbol{\gamma}}$.

One of the simplest generalised Newtonian models is given by

$$
\mu(\dot{\gamma}) = m(\dot{\gamma})^{n-1}. \tag{2.1.3}
$$

This is known as the Ostwald-de Waele or power-law model, where $m(\mathrm{Pa\,s}^n)$ is the consistency coefficient and n the dimensionless power-law index. Fluids that adhere to this relationship are known as power-law fluids. The relationship was first formulated by Armand de Waele (see de Waele 1923), a British chemist and, again, slightly later by the German chemist and biologist Carl Wilhelm Wolfgang Ostwald (see Ostwald 1925). Other

commonly used models include:

$$\text{Carreau-Yasuda model} \qquad \mu = \mu_\infty + (\mu_0 - \mu_\infty)[1 + (\lambda\dot{\gamma})^a]^{(n-1)/a}, \tag{2.1.4a}$$

$$\text{Powell-Eyring model} \qquad \mu = \mu_\infty + (\mu_0 - \mu_\infty)(\lambda\dot{\gamma})^{-1}\text{arcsinh}(\lambda\dot{\gamma}), \tag{2.1.4b}$$

$$\text{Bingham model} \qquad \mu = \begin{cases} \infty & \text{for} \quad \tau < \tau_y, \\ \mu_p + \tau_y(\dot{\gamma})^{-1} & \text{for} \quad \tau \geq \tau_y. \end{cases} \tag{2.1.4c}$$

Here μ_∞ is the infinite-shear-rate viscosity, μ_0 is the zero-shear-rate viscosity, λ is the characteristic time constant, often referred to as the 'relaxation time' and a is the power-law scale factor. For $n > 1$ the fluid is said to be shear-thickening, whilst for $n < 1$ the fluid is said to be shear-thinning. The Newtonian viscosity relationship is recovered when $\mu_0 = \mu_\infty$ and $\tau_y = 0$. The plastic-shear-rate viscosity is μ_p, the magnitude of the shear stress tensor is $\tau = \sqrt{(\boldsymbol{\tau} : \boldsymbol{\tau})/2}$ and τ_y is the yield stress. We note here that when $a = 2$ the Carreau-Yasuda model reduces to the better known Carreau model.

Encapsulating the correct non-Newtonian behaviour of a fluid is achieved by the correct choice of material constants of the model. For shear-thickening (dilatant) flows with $n > 1$, the fluid's viscosity increases with increasing shear rate. Whilst for shear-thinning (pseudoplastic) flows, the fluid's viscosity decreases with increasing shear rate. Substituting $n = 1$ into the power-law model returns the Newtonian viscosity relationship where $m = \mu_n$. However, this model is not without its limitations. For shear-thinning fluids the model predicts an infinite viscosity at rest and a vanishing viscosity as the shear rate approaches infinity, and vice-versa for shear-thickening fluids. Clearly this behaviour is unphysical:

$$\text{for} \quad n < 1 \quad : \quad \lim_{\dot{\gamma}\to 0} \mu(\dot{\gamma}) \to \infty, \quad \lim_{\dot{\gamma}\to \infty} \mu(\dot{\gamma}) \to 0,$$

$$\text{for} \quad n > 1 \quad : \quad \lim_{\dot{\gamma}\to 0} \mu(\dot{\gamma}) \to 0, \quad \lim_{\dot{\gamma}\to \infty} \mu(\dot{\gamma}) \to \infty.$$

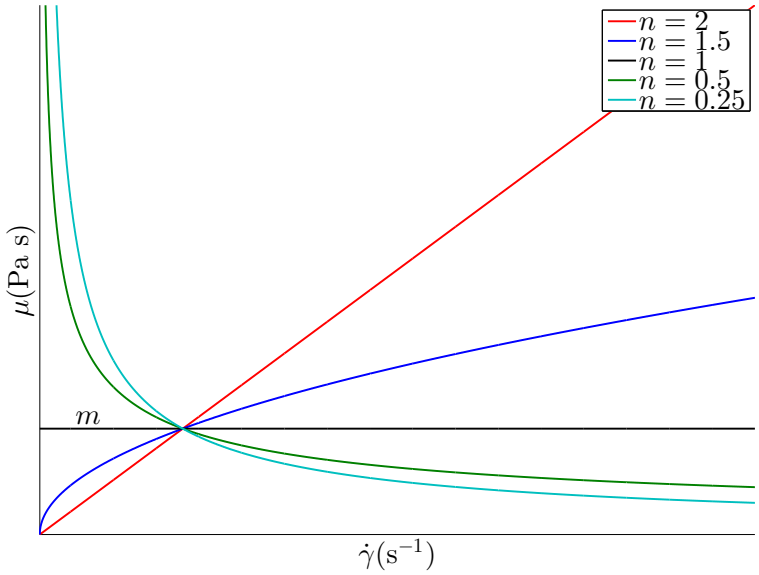

Figure 2.1: Viscosity as a function of shear rate for shear-thickening and shear-thinning power-law fluids and Newtonian fluids. The plots intersect at the point $(1, m)$.

Hence the power-law relationship is only applicable over a finite range of shear rates.

The Carreau-Yasuda and Powell-Eyring models are not subject to such flaws and are able to describe both shear-thickening and shear-thinning flows for $\dot{\gamma} \gg 1$ and $\dot{\gamma} \ll 1$. However, due to the complex nature of these respective constitutive relationships the power-law model is often the favoured model when considering a mathematical analysis of generalised Newtonian fluid flow.

Setting $a = 2$ in (2.1.4a) returns the Carreau model, first developed by Pierre Carreau[2] (see Carreau 1972). We see that this model is able to provide a physical description of fluid behaviour in regions of both very high and very low shear:

$$\text{for} \quad n < 1 \quad : \quad \lim_{\dot{\gamma}\to 0} \mu(\dot{\gamma}) \to \mu_0, \quad \lim_{\dot{\gamma}\to \infty} \mu(\dot{\gamma}) \to \mu_\infty,$$

$$\text{for} \quad n > 1 \quad : \quad \lim_{\dot{\gamma}\to 0} \mu(\dot{\gamma}) \to \mu_0, \quad \lim_{\dot{\gamma}\to \infty} \mu(\dot{\gamma}) \to \infty.$$

[2]Currently serving as Professor Emeritus at Ècole Polytechnique de Montrèal.

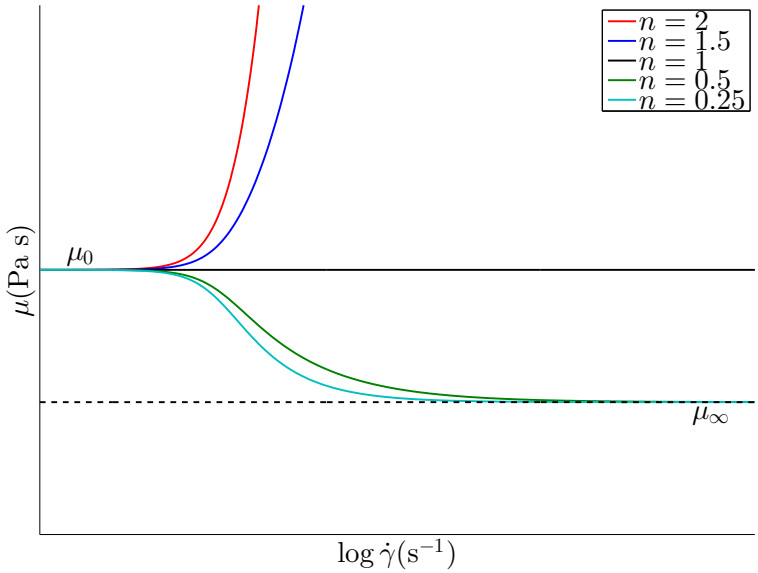

Figure 2.2: Viscosity as a function of shear rate for shear-thickening and shear-thinning Carreau fluids and Newtonian fluids.

Clearly, when compared to the power-law model, this is preferable. The major disadvantage being the requirement of stipulating four material constants, μ_0, μ_∞, λ and n as opposed to just two, m and n in the power-law regime.

The Bingham model was first introduced by American rheologist Eugene Bingham (see Bingham 1916). He observed that many real fluids would appear not to flow until the magnitude of the applied shear stress increased above a fixed value, known as the yield stress. Having observed this physical relationship between applied shear stress and viscosity, Bingham formulated the constitutive mathematical relationship that describes fluid viscosity of this nature. Certainly the Bingham relationship does appear to model the behaviour of some real fluids very well. However, at zero shear rate the viscosity function changes instantaneously from an infinite value to a constant finite value. Papanastasiou (1987) proposed an alternate version of the model that regularises this shift from infinite to finite viscosity. Known as the Bingham-Papanastasiou model, this is simply an extension

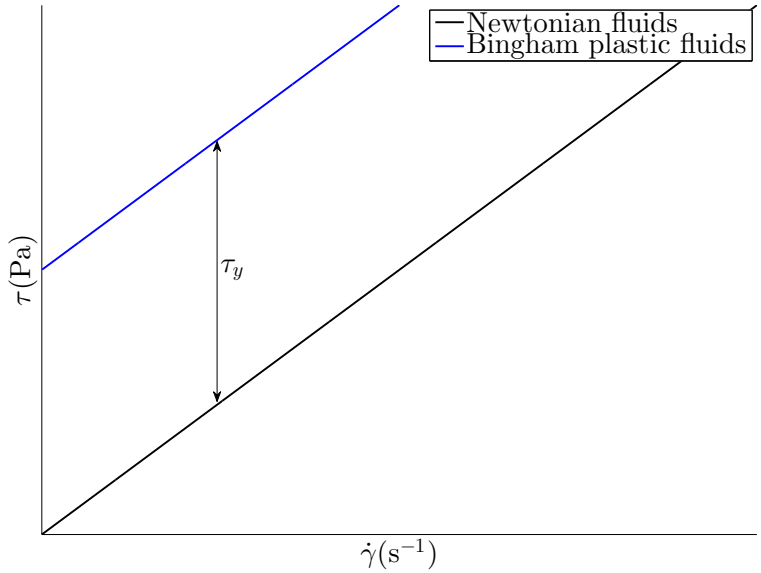

Figure 2.3: Shear stress as a function of shear rate for Bingham plastic and Newtonian fluids.

of the Bingham model that allows for fluids that exhibit gradual yield. By introducing the parameter k(s), which controls the exponential growth of the shear stress as a function of shear rate, Papanastasiou was able to formulate a constitutive relationship that is valid in both the yielded and unyielded regions. The viscosity function is given by

$$\mu = \mu_p + \tau_y[1 - \exp(-k\dot{\gamma})](\dot{\gamma})^{-1}.$$

This is very useful in practice as it avoids the need to know explicitly the location of the yield of any particular fluid. We see that as $k \to 0$ the Newtonian model is recovered, whilst as $k \to \infty$ the Bingham model is recovered. The Papanastasiou modification has also been introduced to a number of other, more complex models that describe flows of this nature, namely, the Herschel-Bulkley model and the Casson model.

Some examples of shear-thinning fluids include: blood, ketchup, paint and a number of cosmetic products. Fluids that adhere to the Bingham model are often referred to

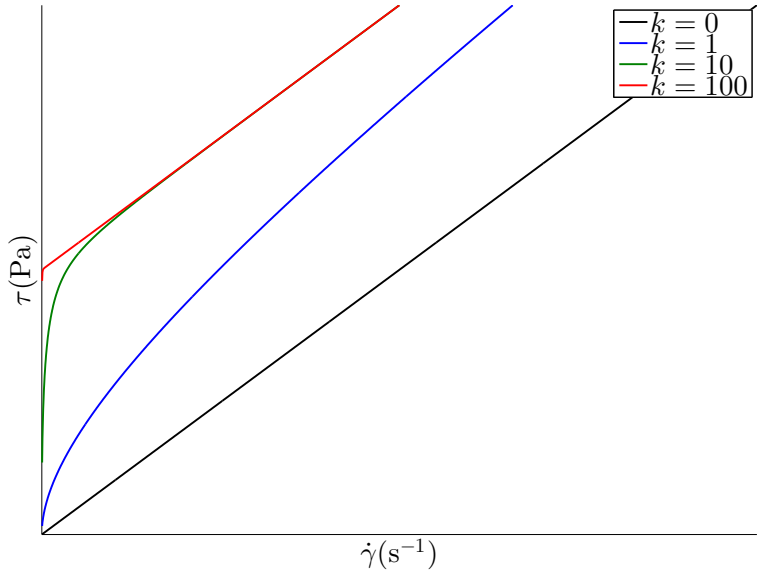

Figure 2.4: Shear stress as a function of shear rate for Bingham–Papanastasiou fluids with $k = 0$, 1, 10, 100.

as Bingham plastic fluids and examples of such include: paints, mud, toothpaste and a variety of foodstuffs from mayonnaise to chocolate. In reality shear-thickening fluids are much less common than both shear-thinning and Bingham plastic fluids, nonetheless, examples include: mixtures of corn starch and water (often referred to as oobleck) and solutions of certain surfactants. However, there does exist a growing interest in the use of shear-thickening fluids in the development of liquid body armour. See for instance: Lee, Wetzel & Wagner (2003) and Decker, Halbach, Nam, Wager & Wetzel (2007).

2.2 The governing boundary-layer equations

Let us now consider the flow of an incompressible generalised Newtonian fluid due to an infinite rotating disk located at $z^* = 0$. The disk rotates about the z^*-axis with angular velocity Ω^*. The motion of the fluid is in the positive z^* direction, the fluid is infinite in extent and the only boundary is at $z^* = 0$. Working in a reference frame that rotates

with the disk, the continuity and Navier-Stokes equations are expressed as

$$\boldsymbol{\nabla}\cdot\boldsymbol{u}^{*}=0, \tag{2.2.1}$$

$$\frac{\partial\boldsymbol{u}^{*}}{\partial t^{*}}+\boldsymbol{u}^{*}\cdot\boldsymbol{\nabla}\boldsymbol{u}^{*}+\boldsymbol{\Omega}^{*}\times(\boldsymbol{\Omega}^{*}\times\boldsymbol{r}^{*})+2\boldsymbol{\Omega}^{*}\times\boldsymbol{u}^{*}=-\frac{1}{\rho^{*}}\nabla p^{*}+\frac{1}{\rho^{*}}\boldsymbol{\nabla}\cdot\boldsymbol{\tau}^{*}. \tag{2.2.2}$$

Here $\boldsymbol{u}^{*}=(u^{*},v^{*},w^{*})$ are the velocity components in cylindrical coordinates (r^{*},θ,z^{*}), t^{*} is time, the angular velocity and position vectors are $\boldsymbol{\Omega}^{*}=(0,0,\Omega^{*})$ and $\boldsymbol{r}^{*}=(r^{*},0,z^{*})$, respectively. The fluid density is ρ^{*} and p^{*} is the fluid pressure. For generalised Newtonian fluids the stress tensor is given by

$$\boldsymbol{\tau}^{*}=\mu^{*}\dot{\boldsymbol{\gamma}}^{*}\quad\text{with}\quad\mu^{*}=\mu^{*}(\dot{\gamma}^{*}), \tag{2.2.3}$$

where $\dot{\boldsymbol{\gamma}}^{*}=\boldsymbol{\nabla}\boldsymbol{u}^{*}+(\boldsymbol{\nabla}\boldsymbol{u}^{*})^{\mathrm{T}}$ is the rate-of-strain tensor and $\mu^{*}(\dot{\gamma}^{*})$ is the non-Newtonian viscosity. The magnitude of the symmetric rate-of-strain tensor is

$$\dot{\gamma}^{*}=\sqrt{\frac{\dot{\boldsymbol{\gamma}}^{*}:\dot{\boldsymbol{\gamma}}^{*}}{2}}. \tag{2.2.4}$$

In the succeeding analysis it is advantageous to forgo the use of vector notation, so that now (2.2.1) and (2.2.2) are expressed as

$$\frac{1}{r^{*}}\frac{\partial(r^{*}u^{*})}{\partial r^{*}}+\frac{1}{r^{*}}\frac{\partial v^{*}}{\partial\theta}+\frac{\partial w^{*}}{\partial z^{*}}=0, \tag{2.2.5}$$

$$\mathcal{L}^{*}u^{*}-\frac{(v^{*}+r^{*}\Omega^{*})^{2}}{r^{*}}=-\frac{1}{\rho^{*}}\frac{\partial p^{*}}{\partial r^{*}}+\frac{1}{\rho^{*}}\left[\frac{1}{r^{*}}\frac{\partial(r^{*}\tau^{*}_{r^{*}r^{*}})}{\partial r^{*}}+\frac{1}{r^{*}}\frac{\partial\tau^{*}_{r^{*}\theta}}{\partial\theta}+\frac{\partial\tau^{*}_{r^{*}z^{*}}}{\partial z^{*}}-\frac{\tau^{*}_{\theta\theta}}{r^{*}}\right], \tag{2.2.6a}$$

$$\mathcal{L}^{*}v^{*}+\frac{u^{*}v^{*}}{r^{*}}+2u^{*}\Omega^{*}=-\frac{1}{r^{*}\rho^{*}}\frac{\partial p^{*}}{\partial\theta}+\frac{1}{\rho^{*}}\left[\frac{1}{r^{*2}}\frac{\partial(r^{*2}\tau^{*}_{\theta r^{*}})}{\partial r^{*}}+\frac{1}{r^{*}}\frac{\partial\tau^{*}_{\theta\theta}}{\partial\theta}+\frac{\partial\tau^{*}_{\theta z^{*}}}{\partial z^{*}}\right], \tag{2.2.6b}$$

$$\mathcal{L}^{*}w^{*}=-\frac{1}{\rho^{*}}\frac{\partial p^{*}}{\partial z^{*}}+\frac{1}{\rho^{*}}\left[\frac{1}{r^{*}}\frac{\partial(r^{*}\tau^{*}_{z^{*}r^{*}})}{\partial r^{*}}+\frac{1}{r^{*}}\frac{\partial\tau^{*}_{z^{*}\theta}}{\partial\theta}+\frac{\partial\tau^{*}_{z^{*}z^{*}}}{\partial z^{*}}\right], \tag{2.2.6c}$$

where

$$\mathcal{L}^* = \frac{\partial}{\partial t^*} + u^* \frac{\partial}{\partial r^*} + \frac{v^*}{r^*}\frac{\partial}{\partial \theta} + w^* \frac{\partial}{\partial z^*}.$$

We find that $\dot{\gamma}^*$ takes the form

$$\dot{\gamma}^* = \left\{ 2\left[\left(\frac{\partial u^*}{\partial r^*} \right)^2 + \left(\frac{1}{r^*}\frac{\partial v^*}{\partial \theta} + \frac{u^*}{r^*} \right)^2 + \left(\frac{\partial w^*}{\partial z^*} \right)^2 \right] + \left[r^* \frac{\partial}{\partial r^*}\left(\frac{v^*}{r^*} \right) + \frac{1}{r^*}\frac{\partial u^*}{\partial \theta} \right]^2 + \left(\frac{\partial u^*}{\partial z^*} + \frac{\partial w^*}{\partial r^*} \right)^2 + \left(\frac{\partial v^*}{\partial z^*} + \frac{1}{r^*}\frac{\partial w^*}{\partial \theta} \right)^2 \right\}^{1/2}, \quad (2.2.7)$$

the details of this calculation are provided in the appendix A. The components of the stress tensor specified in (2.2.6a)-(2.2.6c) are found to be

$$\tau^*_{r^*r^*} = 2\mu^* \left(\frac{\partial u^*}{\partial r^*} \right), \quad (2.2.8a)$$

$$\tau^*_{\theta\theta} = 2\mu^* \left(\frac{1}{r^*}\frac{\partial v^*}{\partial \theta} + \frac{u^*}{r^*} \right), \quad (2.2.8b)$$

$$\tau^*_{z^*z^*} = 2\mu^* \left(\frac{\partial w^*}{\partial z^*} \right), \quad (2.2.8c)$$

$$\tau^*_{r^*\theta} = \mu^* \left[r^* \frac{\partial}{\partial r^*}\left(\frac{v^*}{r^*} \right) + \frac{1}{r^*}\frac{\partial u^*}{\partial \theta} \right] = \tau^*_{\theta r^*}, \quad (2.2.8d)$$

$$\tau^*_{r^*z^*} = \mu^* \left(\frac{\partial u^*}{\partial z^*} + \frac{\partial w^*}{\partial r^*} \right) = \tau^*_{z^*r^*}, \quad (2.2.8e)$$

$$\tau^*_{\theta z^*} = \mu^* \left(\frac{\partial v^*}{\partial z^*} + \frac{1}{r^*}\frac{\partial w^*}{\partial \theta} \right) = \tau^*_{z^*\theta}. \quad (2.2.8f)$$

In a rotating frame of reference this system of equations are closed subject to the boundary conditions

$$u^* = v^* = w^* = 0 \quad \text{at} \quad z^* = 0, \quad (2.2.9a)$$

$$u^* \to 0, \quad v^* \to -r^*\Omega^* \quad \text{as} \quad z^* \to \infty. \quad (2.2.9b)$$

The first of these equations represents the no-slip condition at the surface of the disk, the second represents the Coriolis force balance condition at the outer-edge of the disk boundary-layer.

Independent of the choice of non-Newtonian viscosity model, the system is reduced to non-dimensional form via the introduction of the following dimensionless variables

$$r = \frac{r^*}{l^*}, \quad Z = \frac{z^*}{\delta l^*}, \quad U(r,\theta,Z) = \frac{u^*(r^*,\theta,z^*)}{l^*\Omega^*}, \quad V(r,\theta,Z) = \frac{v^*(r^*,\theta,z^*)}{l^*\Omega^*}, \tag{2.2.10a}$$

$$W(r,\theta,Z) = \frac{w^*(r^*,\theta,z^*)}{\delta l^*\Omega^*}, \quad t = \Omega^* t^*, \quad P(r,\theta,Z) = \frac{p^*(r^*,\theta,z^*)}{\rho^*(l^*\Omega^*)^2}, \tag{2.2.10b}$$

here $l^*\Omega^*$ and l^* are natural velocity and length scales respectively. We regard δ as a general non-dimensional boundary-layer thickness that will be determined later. Substituting (2.2.10) into (2.2.5)-(2.2.6c) gives the dimensionless continuity equation

$$\frac{1}{r}\frac{\partial(rU)}{\partial r} + \frac{1}{r}\frac{\partial V}{\partial \theta} + \frac{\partial W}{\partial Z} = 0, \tag{2.2.11}$$

and the non-dimensionalised Navier-Stokes equations

$$\mathcal{L}U - \frac{(V+r)^2}{r} = -\frac{\partial P}{\partial r} + \frac{1}{\rho^*(l^*\Omega^*)^2}\left[\frac{1}{r}\frac{\partial(r\tau_{rr})}{\partial r} + \frac{1}{r}\frac{\partial \tau_{r\theta}}{\partial \theta} + \frac{\partial \tau_{rZ}}{\partial Z} - \frac{\tau_{\theta\theta}}{r}\right], \tag{2.2.12a}$$

$$\mathcal{L}V + \frac{UV}{r} + 2U = -\frac{1}{r}\frac{\partial P}{\partial \theta} + \frac{1}{\rho^*(l^*\Omega^*)^2}\left[\frac{1}{r^2}\frac{\partial(r^2\tau_{\theta r})}{\partial r} + \frac{1}{r}\frac{\partial \tau_{\theta\theta}}{\partial \theta} + \frac{\partial \tau_{\theta Z}}{\partial Z}\right], \tag{2.2.12b}$$

$$\delta\mathcal{L}W = -\frac{1}{\delta}\frac{\partial P}{\partial Z} + \frac{1}{\rho^*(l^*\Omega^*)^2}\left[\frac{1}{r}\frac{\partial(r\tau_{Zr})}{\partial r} + \frac{1}{r}\frac{\partial \tau_{Z\theta}}{\partial \theta} + \frac{\partial \tau_{ZZ}}{\partial Z}\right], \tag{2.2.12c}$$

where

$$\mathcal{L} = \frac{\partial}{\partial t} + U\frac{\partial}{\partial r} + \frac{V}{r}\frac{\partial}{\partial \theta} + W\frac{\partial}{\partial Z}.$$

The dimensionless forms of the τ_{ij} terms appearing in (2.2.12) are dependent on the choice of non-Newtonian viscosity model, as such these will defined subsequently. Independent of the model in question we write $\dot{\gamma} = \dot{\gamma}^*(\delta/\Omega^*)$, thus it is trivial to show that

$$\begin{aligned}\dot{\gamma}^2 = &\left(\frac{\partial U}{\partial Z}\right)^2 + \left(\frac{\partial V}{\partial Z}\right)^2 + \delta^4\left[\frac{1}{r^2}\left(\frac{\partial W}{\partial \theta}\right)^2 + \left(\frac{\partial W}{\partial r}\right)^2\right] \\ &+\delta^2\Bigg\{2\left(\frac{\partial U}{\partial r}\right)^2 + 2\left(\frac{1}{r}\frac{\partial V}{\partial \theta} + \frac{U}{r}\right)^2 + 2\left(\frac{\partial W}{\partial Z}\right)^2 + \left[r\frac{\partial}{\partial r}\left(\frac{V}{r}\right) + \frac{1}{r}\frac{\partial U}{\partial \theta}\right]^2 \\ &+\frac{2}{r}\frac{\partial V}{\partial Z}\frac{\partial W}{\partial \theta} + 2\frac{\partial U}{\partial Z}\frac{\partial W}{\partial r}\Bigg\}. \end{aligned} \tag{2.2.13}$$

It proves useful to split the remainder of the analysis in to three parts, considering in turn, power-law, Bingham and Carreau fluid models. This style of presentation will persist throughout the remainder of this thesis. It should be noted that definitions of the Reynolds number, for example, may change within each section. However, in order to be consistent, the same notation will be used across all sections.

2.2.1 Case I: Power-law

For power-law fluids we have that

$$\mu^* = m^*\left(\frac{\Omega^*\dot{\gamma}}{\delta}\right)^{n-1}.$$

Thus, having made the previous considerations, we are now able to determine the dimensionless form of the viscous terms appearing in (2.2.12). For fluids that adhere to the power-law relationship we find that

$$\frac{1}{r}\frac{\partial(r\tau_{rr})}{\partial r} = m^*\Omega^*\left(\frac{\Omega^*}{\delta}\right)^{n-1}\frac{2}{r}\frac{\partial}{\partial r}\left(\tilde{\mu}r\frac{\partial U}{\partial r}\right), \tag{2.2.14a}$$

$$\frac{1}{r}\frac{\partial \tau_{r\theta}}{\partial \theta} = m^*\Omega^*\left(\frac{\Omega^*}{\delta}\right)^{n-1}\frac{1}{r}\frac{\partial}{\partial \theta}\left\{\tilde{\mu}\left[r\frac{\partial}{\partial r}\left(\frac{V}{r}\right) + \frac{1}{r}\frac{\partial U}{\partial \theta}\right]\right\}, \tag{2.2.14b}$$

$$\frac{\tau_{\theta\theta}}{r} = m^*\Omega^*\left(\frac{\Omega^*}{\delta}\right)^{n-1}\frac{2\tilde{\mu}}{r^2}\left(\frac{\partial V}{\partial\theta}+U\right), \tag{2.2.14c}$$

$$\frac{\partial\tau_{rZ}}{\partial Z} = m^*\Omega^*\left(\frac{\Omega^*}{\delta}\right)^{n-1}\frac{1}{\delta^2}\frac{\partial}{\partial Z}\left[\tilde{\mu}\left(\frac{\partial U}{\partial Z}+\delta^2\frac{\partial W}{\partial r}\right)\right], \tag{2.2.14d}$$

$$\frac{1}{r^2}\frac{\partial\left(r^2\tau_{\theta r}\right)}{\partial r} = m^*\Omega^*\left(\frac{\Omega^*}{\delta}\right)^{n-1}\frac{1}{r^2}\frac{\partial}{\partial r}\left\{\tilde{\mu}\left[r^3\frac{\partial}{\partial r}\left(\frac{V}{r}\right)+r\frac{\partial U}{\partial\theta}\right]\right\}, \tag{2.2.14e}$$

$$\frac{1}{r}\frac{\partial\tau_{\theta\theta}}{\partial r} = m^*\Omega^*\left(\frac{\Omega^*}{\delta}\right)^{n-1}\frac{2}{r}\frac{\partial}{\partial\theta}\left[\tilde{\mu}\left(\frac{1}{r}\frac{\partial V}{\partial\theta}+\frac{U}{r}\right)\right], \tag{2.2.14f}$$

$$\frac{\partial\tau_{\theta Z}}{\partial Z} = m^*\Omega^*\left(\frac{\Omega^*}{\delta}\right)^{n-1}\frac{1}{\delta^2}\frac{\partial}{\partial Z}\left[\tilde{\mu}\left(\frac{\partial V}{\partial Z}+\frac{\delta^2}{r}\frac{\partial W}{\partial\theta}\right)\right], \tag{2.2.14g}$$

$$\frac{1}{r}\frac{\partial\left(r\tau_{Zr}\right)}{\partial r} = m^*\Omega^*\left(\frac{\Omega^*}{\delta}\right)^{n-1}\frac{1}{\delta}\left\{\frac{1}{r}\frac{\partial}{\partial r}\left[\tilde{\mu}r\left(\frac{\partial U}{\partial Z}+\delta^2\frac{\partial W}{\partial r}\right)\right]\right\}, \tag{2.2.14h}$$

$$\frac{1}{r}\frac{\partial\tau_{Z\theta}}{\partial\theta} = m^*\Omega^*\left(\frac{\Omega^*}{\delta}\right)^{n-1}\frac{1}{\delta}\left\{\frac{1}{r}\frac{\partial}{\partial\theta}\left[\tilde{\mu}\left(\frac{\partial V}{\partial Z}+\frac{\delta^2}{r}\frac{\partial W}{\partial\theta}\right)\right]\right\}, \tag{2.2.14i}$$

$$\frac{\partial\tau_{ZZ}}{\partial Z} = m^*\Omega^*\left(\frac{\Omega^*}{\delta}\right)^{n-1}\frac{1}{\delta}\left[2\frac{\partial}{\partial Z}\left(\tilde{\mu}\frac{\partial W}{\partial Z}\right)\right], \tag{2.2.14j}$$

where $\tilde{\mu} = (\dot{\gamma})^{n-1}$. Thus (2.2.12) becomes

$$\mathcal{L}U - \frac{(V+r)^2}{r} = -\frac{\partial P}{\partial r}+\frac{m^*{\Omega^*}^{n-2}}{\rho^* l^{*2}\delta^{n+1}}\left[\frac{\partial}{\partial Z}\left(\tilde{\mu}\frac{\partial U}{\partial Z}\right)+\mathcal{O}(\delta^2)\right], \tag{2.2.15a}$$

$$\mathcal{L}V + \frac{UV}{r}+2U = -\frac{1}{r}\frac{\partial P}{\partial\theta}+\frac{m^*{\Omega^*}^{n-2}}{\rho^* l^{*2}\delta^{n+1}}\left[\frac{\partial}{\partial Z}\left(\tilde{\mu}\frac{\partial V}{\partial Z}\right)+\mathcal{O}(\delta^2)\right], \tag{2.2.15b}$$

$$\begin{aligned}\mathcal{L}W = &-\frac{1}{\delta^2}\frac{\partial P}{\partial Z}+\frac{m^*{\Omega^*}^{n-2}}{\rho^* l^{*2}\delta^{n+1}}\left[\frac{1}{r}\frac{\partial}{\partial r}\left(\tilde{\mu}r\frac{\partial U}{\partial Z}\right)\right.\\ &\left.+\frac{1}{r}\frac{\partial}{\partial\theta}\left(\tilde{\mu}\frac{\partial V}{\partial Z}\right)+2\frac{\partial}{\partial Z}\left(\tilde{\mu}\frac{\partial W}{\partial Z}\right)+\mathcal{O}(\delta^2)\right].\end{aligned} \tag{2.2.15c}$$

Where the $\mathcal{O}(\delta^2)$ terms are easily obtained from (2.2.14). Clearly to ensure the consistency of these equations we require that

$$\frac{m^*{\Omega^*}^{n-2}}{\rho^* l^{*2}\delta^{n+1}} = \mathcal{O}(1).$$

Let us now introduce the dimensionless parameter

$$Re = \frac{\rho^* {\Omega^*}^{2-n} {l^*}^2}{m^*}, \tag{2.2.16}$$

often referred to as the 'power-law' Reynolds number. It is noteworthy to mention here that by setting $n = 1$ and $m^* = \mu_n^*$ this reduces to the familiar form of the Reynolds number for the flow of a Newtonian fluid. Making use of this parameter we require that

$$\left(\frac{1}{Re}\right)\left(\frac{1}{\delta^{n+1}}\right) = \mathcal{O}(1).$$

So we have that the boundary-layer thickness for the flow of a power-law fluid driven by a rotating disk is given by

$$\delta = \mathcal{O}(Re^{-\frac{1}{n+1}}). \tag{2.2.17}$$

Again, we see here that by setting $n = 1$ we return to the familiar Newtonian result.

Thus we have that the scaled governing equations for this problem, when considering the flow of a power-law fluid, are given by

$$\mathcal{L}U - \frac{(V+r)^2}{r} = -\frac{\partial P}{\partial r} + \frac{\partial}{\partial Z}\left(\tilde{\mu}\frac{\partial U}{\partial Z}\right) + \mathcal{O}(Re^{-\frac{2}{n+1}}), \tag{2.2.18a}$$

$$\mathcal{L}V + \frac{UV}{r} + 2U = -\frac{1}{r}\frac{\partial P}{\partial \theta} + \frac{\partial}{\partial Z}\left(\tilde{\mu}\frac{\partial V}{\partial Z}\right) + \mathcal{O}(Re^{-\frac{2}{n+1}}), \tag{2.2.18b}$$

$$\begin{aligned}\mathcal{L}W = &-Re^{2/(n+1)}\frac{\partial P}{\partial Z} + \frac{1}{r}\frac{\partial}{\partial r}\left(\tilde{\mu} r \frac{\partial U}{\partial Z}\right) \\ &+\frac{1}{r}\frac{\partial}{\partial \theta}\left(\tilde{\mu}\frac{\partial V}{\partial Z}\right) + 2\frac{\partial}{\partial Z}\left(\tilde{\mu}\frac{\partial W}{\partial Z}\right) + \mathcal{O}(Re^{-\frac{2}{n+1}}),\end{aligned} \tag{2.2.18c}$$

where

$$\tilde{\mu} = \left[\left(\frac{\partial U}{\partial Z} \right)^2 + \left(\frac{\partial V}{\partial Z} \right)^2 + \mathcal{O}(Re^{-\frac{2}{n+1}}) + \mathcal{O}(Re^{-\frac{4}{n+1}}) \right]^{(n-1)/2}, \tag{2.2.18d}$$

is the dimensionless viscosity function defined by

$$\tilde{\mu} = \frac{[Re^{1/(n+1)}\Omega^*]^{1-n}\mu^*}{m^*}.$$

The continuity equation (2.2.11) remains unchanged.

We now proceed by making a boundary-layer approximation, eliminating terms involving inverse powers of the Reynolds number by assuming that $Re \gg 1$. Inside the boundary-layer we assume a solution to (2.2.11) and (2.2.18) given that the velocity components, pressure and viscosity have the following asymptotic expansions

$$\begin{aligned}
U(r,\theta,z) &= U_0(r,\theta,Z) + Re^{-2/(n+1)}U_1(r,\theta,Z) + \cdots, \\
V(r,\theta,z) &= V_0(r,\theta,Z) + Re^{-2/(n+1)}V_1(r,\theta,Z) + \cdots, \\
W(r,\theta,z) &= W_0(r,\theta,Z) + Re^{-2/(n+1)}W_1(r,\theta,Z) + \cdots, \\
P(r,\theta,z) &= P_0(r,\theta,Z) + Re^{-2/(n+1)}P_1(r,\theta,Z) + \cdots, \\
\tilde{\mu}(r,\theta,z) &= \tilde{\mu}_0(r,\theta,Z) + Re^{-2/(n+1)}\tilde{\mu}_1(r,\theta,Z) + \cdots,
\end{aligned}$$

where $z = z^*/l^* = Re^{-1/(n+1)}Z$ is the coordinate corresponding to the region outside of the boundary-layer, the outer region coordinate. To leading order we see that $P_0 = P_0(r,\theta)$, however, since it is assumed that inside the boundary-layer the pressure is a function of Z only, we have that $P_0 \equiv 0$. Thus the boundary-layer equations at lowest order are

$$\frac{1}{r}\frac{\partial(rU_0)}{\partial r} + \frac{1}{r}\frac{\partial V_0}{\partial \theta} + \frac{\partial W_0}{\partial Z} = 0, \tag{2.2.19a}$$

$$\frac{\partial U_0}{\partial t}+U_0\frac{\partial U_0}{\partial r}+\frac{V_0}{r}\frac{\partial U_0}{\partial \theta}+W_0\frac{\partial U_0}{\partial Z}-\frac{(V_0+r)^2}{r}=\frac{\partial}{\partial Z}\left(\tilde{\mu}_0\frac{\partial U_0}{\partial Z}\right), \tag{2.2.19b}$$

$$\frac{\partial V_0}{\partial t}+U_0\frac{\partial V_0}{\partial r}+\frac{V_0}{r}\frac{\partial V_0}{\partial \theta}+W_0\frac{\partial V_0}{\partial Z}+\frac{U_0V_0}{r}+2U_0=\frac{\partial}{\partial Z}\left(\tilde{\mu}_0\frac{\partial V_0}{\partial Z}\right), \tag{2.2.19c}$$

$$\begin{aligned}\frac{\partial W_0}{\partial t}+U_0\frac{\partial W_0}{\partial r}+\frac{V_0}{r}\frac{\partial W_0}{\partial \theta}+W_0\frac{\partial W_0}{\partial Z}=&-\frac{\partial P_1}{\partial Z}+\frac{1}{r}\frac{\partial}{\partial r}\left(\tilde{\mu}_0 r\frac{\partial U_0}{\partial Z}\right)\\&+\frac{1}{r}\frac{\partial}{\partial \theta}\left(\tilde{\mu}_0\frac{\partial V_0}{\partial Z}\right)\\&+2\frac{\partial}{\partial Z}\left(\tilde{\mu}_0\frac{\partial W_0}{\partial Z}\right),\end{aligned} \tag{2.2.19d}$$

where

$$\tilde{\mu}_0=\left[\left(\frac{\partial U_0}{\partial Z}\right)^2+\left(\frac{\partial V_0}{\partial Z}\right)^2\right]^{(n-1)/2}. \tag{2.2.19e}$$

2.2.2 Case II: Bingham

Having derived system (2.2.19) which governs the boundary-layer flow of a power-law fluid it remains for us to reformulate the derivation to arrive at the corresponding equations for a Bingham plastic fluid. For brevity we exclude rewriting each component of the stress tensor, instead we note that the multiplicative quantity, $m^*\Omega^*(\Omega^*/\delta)^{n-1}$, that appears in each of the dimensionless viscous terms of system (2.2.14) reduces to simply $\mu_p^*\Omega^*$ when considering the flow of a Bingham plastic fluid. Thus by fixing $m^*=\mu_p^*$ and $n=1$ in (2.2.14) we determine an analogous set of viscous terms where now $\tilde{\mu}=1+2rB_n\dot{\gamma}^{-1}$ with $B_n=\tau_y^*l^*\delta/(2r^*\mu_p^*\Omega^*)$. As before, δ is yet to be determined. Thus (2.2.12) becomes

$$\mathcal{L}U-\frac{(V+r)^2}{r}=-\frac{\partial P}{\partial r}+\frac{\mu_p^*}{\rho^*\Omega^*(l^*\delta)^2}\left[\frac{\partial}{\partial Z}\left(\tilde{\mu}\frac{\partial U}{\partial Z}\right)+\mathcal{O}(\delta^2)\right], \tag{2.2.20a}$$

$$\mathcal{L}V+\frac{UV}{r}+2U=-\frac{1}{r}\frac{\partial P}{\partial \theta}+\frac{\mu_p^*}{\rho^*\Omega^*(l^*\delta)^2}\left[\frac{\partial}{\partial Z}\left(\tilde{\mu}\frac{\partial V}{\partial Z}\right)+\mathcal{O}(\delta^2)\right], \tag{2.2.20b}$$

$$\mathcal{L}W = -\frac{1}{\delta^2}\frac{\partial P}{\partial Z} + \frac{\mu_p^*}{\rho^*\Omega^*(l^*\delta)^2}\left[\frac{1}{r}\frac{\partial}{\partial r}\left(\tilde{\mu}r\frac{\partial U}{\partial Z}\right)\right.$$
$$\left.+\frac{1}{r}\frac{\partial}{\partial\theta}\left(\tilde{\mu}\frac{\partial V}{\partial Z}\right) + 2\frac{\partial}{\partial Z}\left(\tilde{\mu}\frac{\partial W}{\partial Z}\right) + \mathcal{O}(\delta^2)\right]. \tag{2.2.20c}$$

Again, to ensure the consistency of these equations we require that

$$\frac{\mu_p^*}{\rho^*\Omega^*(l^*\delta)^2} = \mathcal{O}(1).$$

By introducing the Reynolds number scaled by the plastic-shear-rate viscosity

$$Re = \frac{\rho^*\Omega^*{l^*}^2}{\mu_p^*}, \tag{2.2.21}$$

we require that

$$\left(\frac{1}{Re}\right)\left(\frac{1}{\delta^2}\right) = \mathcal{O}(1).$$

So that the boundary-layer thickness for the flow of a Bingham plastic fluid driven by a rotating disk is given by

$$\delta = \mathcal{O}(Re^{-\frac{1}{2}}). \tag{2.2.22}$$

Thus the scaled governing equations for this problem, when considering the flow of a Bingham plastic fluid, are given by

$$\mathcal{L}U - \frac{(V+r)^2}{r} = -\frac{\partial P}{\partial r} + \frac{\partial}{\partial Z}\left(\tilde{\mu}\frac{\partial U}{\partial Z}\right) + \mathcal{O}(Re^{-1}), \tag{2.2.23a}$$
$$\mathcal{L}V + \frac{UV}{r} + 2U = -\frac{1}{r}\frac{\partial P}{\partial\theta} + \frac{\partial}{\partial Z}\left(\tilde{\mu}\frac{\partial V}{\partial Z}\right) + \mathcal{O}(Re^{-1}), \tag{2.2.23b}$$

$$\mathcal{L}W = -Re\frac{\partial P}{\partial Z} + \frac{1}{r}\frac{\partial}{\partial r}\left(\tilde{\mu} r \frac{\partial U}{\partial Z}\right) + \frac{1}{r}\frac{\partial}{\partial \theta}\left(\tilde{\mu}\frac{\partial V}{\partial Z}\right) + 2\frac{\partial}{\partial Z}\left(\tilde{\mu}\frac{\partial W}{\partial Z}\right) + \mathcal{O}(Re^{-1}), \tag{2.2.23c}$$

where

$$\tilde{\mu} = 1 + 2rB_n\left[\left(\frac{\partial U}{\partial Z}\right)^2 + \left(\frac{\partial V}{\partial Z}\right)^2 + \mathcal{O}(Re^{-1}) + \mathcal{O}(Re^{-2})\right]^{-1/2}, \tag{2.2.23d}$$

is the dimensionless viscosity function. The continuity equation (2.2.11) remains unchanged.

As with Matsumoto, Takashima, Kamiya, Kayano & Ohta (1982), we define the Bingham number, B_n by

$$B_n = \frac{\tau_y^* l^* \delta}{2r^*\mu_p^*\Omega^*} = \frac{\tau_y^*}{2r^*\Omega^*\sqrt{\mu_p^*\rho^*\Omega^*}} = \frac{\tau_y^*}{2\mu_p^*\Omega^* R}. \tag{2.2.24}$$

We note here that the Bingham number is a function of the radius of the disk, this therefore restricts our attention to a local analysis whereby B_n is evaluated at a specific radial location along the disk. In order to simplify the expression for B_n we have utilised the form of the modified Reynolds number, $R = rRe^{1/2}$, based on the boundary-layer thickness and the local azimuthal velocity of the disk.

We again proceed by making a boundary-layer approximation, eliminating terms involving inverse powers of the Reynolds number by assuming that $Re \gg 1$. Inside the boundary-layer we assume a solution to (2.2.11) and (2.2.23) given that the velocity components, pressure and viscosity have the following asymptotic expansions

$$U(r,\theta,z) = U_0(r,\theta,Z) + Re^{-1}U_1(r,\theta,Z) + \cdots,$$
$$V(r,\theta,z) = V_0(r,\theta,Z) + Re^{-1}V_1(r,\theta,Z) + \cdots,$$

$$W(r,\theta,z) = W_0(r,\theta,Z) + Re^{-1}W_1(r,\theta,Z) + \cdots,$$
$$P(r,\theta,z) = P_0(r,\theta,Z) + Re^{-1}P_1(r,\theta,Z) + \cdots,$$
$$\tilde{\mu}(r,\theta,z) = \tilde{\mu}_0(r,\theta,Z) + Re^{-1}\tilde{\mu}_1(r,\theta,Z) + \cdots,$$

where here $z = z^*/l^* = Re^{-1/2}Z$ is the coordinate corresponding to the region outside of the boundary-layer. Again, to leading order we see that $P_0 = P_0(r,\theta)$, so by the preceding argument $P_0 \equiv 0$. Thus the boundary-layer equations at lowest order are identical to (2.2.19a)-(2.2.19d) where now

$$\tilde{\mu}_0 = 1 + 2rB_n\left[\left(\frac{\partial U_0}{\partial Z}\right)^2 + \left(\frac{\partial V_0}{\partial Z}\right)^2\right]^{-1/2}, \tag{2.2.25}$$

is the zero-order viscosity function.

2.2.3 Case III: Carreau

The procedure here can be viewed as a simple extension of the previous case. Where before we non-dimensionalised with respect to μ_p^* we instead choose to non-dimensionalise with respect to μ_∞^*. Thus we determine an analogous set of viscous terms where now $\tilde{\mu} = 1 + c_0[1 + (r^{-1}k\dot{\gamma})^2]^{(n-1)/2}$, here $c_0 = (\mu_0^* - \mu_\infty^*)/\mu_\infty^*$ is the viscosity ratio and $k = r^*\lambda^*\Omega^*/(l^*\delta)$ is the dimensionless equivalent of the constant λ^*. Again, δ remains, as of yet, undetermined. Thus (2.2.12) becomes

$$\mathcal{L}U - \frac{(V+r)^2}{r} = -\frac{\partial P}{\partial r} + \frac{\mu_\infty^*}{\rho^*\Omega^*(l^*\delta)^2}\left[\frac{\partial}{\partial Z}\left(\tilde{\mu}\frac{\partial U}{\partial Z}\right) + \mathcal{O}(\delta^2)\right], \tag{2.2.26a}$$
$$\mathcal{L}V + \frac{UV}{r} + 2U = -\frac{1}{r}\frac{\partial P}{\partial \theta} + \frac{\mu_\infty^*}{\rho^*\Omega^*(l^*\delta)^2}\left[\frac{\partial}{\partial Z}\left(\tilde{\mu}\frac{\partial V}{\partial Z}\right) + \mathcal{O}(\delta^2)\right], \tag{2.2.26b}$$
$$\begin{aligned}\mathcal{L}W = &-\frac{1}{\delta^2}\frac{\partial P}{\partial Z} + \frac{\mu_\infty^*}{\rho^*\Omega^*(l^*\delta)^2}\left[\frac{1}{r}\frac{\partial}{\partial r}\left(\tilde{\mu}r\frac{\partial U}{\partial Z}\right)\right.\\ &\left.+\frac{1}{r}\frac{\partial}{\partial \theta}\left(\tilde{\mu}\frac{\partial V}{\partial Z}\right) + 2\frac{\partial}{\partial Z}\left(\tilde{\mu}\frac{\partial W}{\partial Z}\right) + \mathcal{O}(\delta^2)\right].\end{aligned} \tag{2.2.26c}$$

As before, to ensure the consistency of these equations we require that

$$\frac{\mu_\infty^*}{\rho^*\Omega^*(l^*\delta)^2} = \mathcal{O}(1).$$

By introducing the Reynolds number scaled by the infinite-shear-rate viscosity

$$Re = \frac{\rho^*\Omega^* l^{*^2}}{\mu_\infty^*}. \tag{2.2.27}$$

We determine that the boundary-layer thickness for the flow of a Carreau fluid driven by a rotating disk is also given by

$$\delta = \mathcal{O}(Re^{-\frac{1}{2}}). \tag{2.2.28}$$

Thus the scaled governing equations for this problem, when considering the flow of a Carreau fluid, are given by

$$\mathcal{L}U - \frac{(V+r)^2}{r} = -\frac{\partial P}{\partial r} + \frac{\partial}{\partial Z}\left(\tilde{\mu}\frac{\partial U}{\partial Z}\right) + \mathcal{O}(Re^{-1}), \tag{2.2.29a}$$

$$\mathcal{L}V + \frac{UV}{r} + 2U = -\frac{1}{r}\frac{\partial P}{\partial \theta} + \frac{\partial}{\partial Z}\left(\tilde{\mu}\frac{\partial V}{\partial Z}\right) + \mathcal{O}(Re^{-1}), \tag{2.2.29b}$$

$$\begin{aligned}\mathcal{L}W = &-Re\frac{\partial P}{\partial Z} + \frac{1}{r}\frac{\partial}{\partial r}\left(\tilde{\mu}r\frac{\partial U}{\partial Z}\right)\\ &+\frac{1}{r}\frac{\partial}{\partial \theta}\left(\tilde{\mu}\frac{\partial V}{\partial Z}\right) + 2\frac{\partial}{\partial Z}\left(\tilde{\mu}\frac{\partial W}{\partial Z}\right) + \mathcal{O}(Re^{-1}),\end{aligned} \tag{2.2.29c}$$

where

$$\tilde{\mu} = 1 + c_0\left\{1 + \left(\frac{k}{r}\right)^2\left[\left(\frac{\partial U}{\partial Z}\right)^2 + \left(\frac{\partial V}{\partial Z}\right)^2 + \mathcal{O}(Re^{-1}) + \mathcal{O}(Re^{-2})\right]\right\}^{(n-1)/2}, \tag{2.2.29d}$$

is the dimensionless viscosity function. The continuity equation (2.2.11) remains unchanged.

As in the previous section we make use of the modified Reynolds number to simplify our dimensionless expression

$$k = \frac{r^*\lambda^*\Omega^*}{l^*\delta} = r^*\lambda^*\Omega^*\sqrt{\frac{\rho^*\Omega^*}{\mu^*_\infty}} = \lambda^*\Omega^* R, \tag{2.2.30}$$

here we see that k is also a function of the radius of the disk and again we note that this restricts our attention to a strictly local analysis.

Using the asymptotic expansions outlined in §2.2.2, where now the Reynolds number is scaled by the infinite-shear-rate viscosity, we determine that the boundary-layer equations at lowest order are identical to (2.2.19a)-(2.2.19d) where

$$\tilde{\mu}_0 = 1 + c_0\left\{1 + \left(\frac{k}{r}\right)^2\left[\left(\frac{\partial U_0}{\partial Z}\right)^2 + \left(\frac{\partial V_0}{\partial Z}\right)^2\right]\right\}^{(n-1)/2}, \tag{2.2.31}$$

is the zero-order viscosity function.

Chapter 3

Basic Flow Solutions

In this chapter we solve our boundary-layer equations and determine the resulting steady mean flow profiles. Mitschka (1964) was the first to consider this problem in the power-law regime. Other notable contributions have been made by Mitschka & Ulbrecht (1965) and more recently by Andersson *et al.* (2001), among others. Mitschka & Ulbrecht (1965) present numerical results for both shear-thickening and shear-thinning power-law fluids. Andersson *et al.* (2001) revisited this problem and considered the accuracy of these results. However, in both the aforementioned cases the authors fail to interpret their respective numerical solutions in the context of the global flow. Since we have used a boundary-layer approximation in the formulation of the governing equations, one must ask questions about how this boundary-layer flow will match the flow in the outer region. In the Newtonian limit no such questions need to be taken into consideration as the similarity solution first proposed by von Kármán (1921) is in fact an exact solution of the Navier-Stokes equations and hence no matching constraints are necessary.

More recently Ahmadpour & Sadeghy (2013) formally addressed the problem of the flow due to a rotating disk when considering fluids that adhere to the Bingham model. Claiming to have found an exact solution to the problem, the authors are only able to present numerical solutions for specific values of the Reynolds number (Re) and dimen-

sionless radius of the disk (r). Having not appealed to a boundary-layer formulation the authors find that terms dependent on Re and r appear in the governing base flow ODEs, and thus have the need to specify these values during their numerical solution process. Two other studies of note are those of Matsumoto *et al.* (1982) and Rashaida *et al.* (2006). Matsumoto *et al.* (1982) consider the film thickness of a Bingham plastic fluid on a rotating disk, presenting both theoretical and experimental results. This work is an extension of the Newtonian problem the authors addressed previously (see Matsumoto, Salto & Takashima 1973). Rashaida *et al.* (2006) investigated the mass transfer from a rotating disk to a Bingham plastic fluid. Comparing their results to those of Levich (1962), who considered the Newtonian problem; the authors find that the rate of mass transfer is generally increased for Bingham plastic fluids.

In the context of the rotating disk problem, no previous studies have utilised the form of the Carreau rheological model. This is perhaps due to its relative complexity when to compared to say, the simpler power-law model. This is not to say that the literature is completely void of generalised Newtonian boundary-layer flows of this type. The corresponding Falkner-Skan boundary-layer problem has been considered by Dabrowski (2004), he presents an analysis for both power-law and Carreau fluids and is therefore able to comment on the respective failings and merits of each model.

Within this chapter we determine steady mean flow solutions for power-law, Bingham and Carreau fluid models. This appears in the literature as Griffiths (2015). The power-law results are essentially a review of the work of Denier & Hewitt (2004) although significantly more detail is provided regarding the asymptotic form of the solutions. Having introduced the modified Bingham number used by Matsumoto *et al.* (1982) in their film thickness investigation, we are able to determine a governing set of ODEs dependent solely on this parameter. These results are then compared to those of Ahmadpour & Sadeghy (2013). Additionally, we present solutions for shear-thickening and shear-thinning Carreau

fluids where now the flow is controlled by not one, but three dimensionless parameters. We begin by introducing the classical Newtonian results.

3.1 The von Kármán solution

In the Newtonian case we find that the steady, axisymmetric, continuity and Navier-Stokes equations in a frame of reference rotating with the disk, at an angular velocity Ω^*, are given by

$$\begin{aligned}
\frac{1}{r}\frac{\partial(ru)}{\partial r} + \frac{\partial w}{\partial z} &= 0, \\
u\frac{\partial u}{\partial r} + w\frac{\partial u}{\partial z} - \frac{(v+r)^2}{r} &= -\frac{\partial p}{\partial r} + \frac{1}{Re}\left[\frac{1}{r}\frac{\partial}{\partial r}\left(r\frac{\partial u}{\partial r}\right) - \frac{u}{r^2} + \frac{\partial^2 u}{\partial z^2}\right], \\
u\frac{\partial v}{\partial r} + w\frac{\partial v}{\partial z} + \frac{uv}{r} + 2u &= \frac{1}{Re}\left[\frac{1}{r}\frac{\partial}{\partial r}\left(r\frac{\partial v}{\partial r}\right) - \frac{v}{r^2} + \frac{\partial^2 v}{\partial z^2}\right], \\
u\frac{\partial w}{\partial r} + w\frac{\partial w}{\partial z} &= -\frac{\partial p}{\partial z} + \frac{1}{Re}\left[\frac{1}{r}\frac{\partial}{\partial r}\left(r\frac{\partial w}{\partial r}\right) + \frac{\partial^2 w}{\partial z^2}\right],
\end{aligned}$$

where r and z have been made dimensionless with respect to some reference length l^*, the radial, azimuthal and axial velocity components, u, v and w have been made dimensionless with respect to $l^*\Omega^*$ and the pressure p has been made dimensionless with respect to $\rho^*(l^*\Omega^*)^2$. The Reynolds number for this flow is

$$Re = \frac{\rho^*\Omega^* {l^*}^2}{\mu_n^*},$$

and the boundary-layer thickness is given by $\delta = Re^{-1/2}$. In his pioneering 1921 study von Kármán suggested that the flow above a rotating plane is self-similar and is scaled by the boundary-layer thickness. Hence he proposed a similarity solution of the form

$$\begin{aligned}
[u(z), v(z), w(z)] &= [r\bar{u}(z/\delta), r\bar{v}(z/\delta), \delta\bar{w}(z/\delta)], \\
p(z) &= \delta^2\bar{p}(z/\delta).
\end{aligned}$$

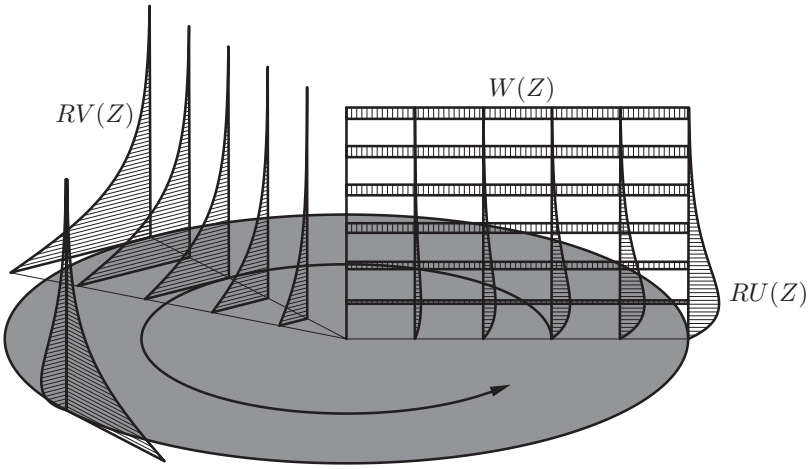

Figure 3.1: The flow due to a rotating disk. Here U, V and W are the velocity components in the radial, azimuthal and axial directions respectively, R is the dimensionless radial coordinate and Z is the dimensionless boundary-layer coordinate. Reproduced from Siddiqui, Mukund, Scott & Pier (2013).

Thus the radial ($\bar{u}$), azimuthal ($\bar{v}$) and axial ($\bar{w}$) velocity components are obtained from

$$-2\bar{u} = \bar{w}', \tag{3.1.1a}$$

$$\bar{u}^2 - (\bar{v}+1)^2 + \bar{w}\bar{u}' = \bar{u}'', \tag{3.1.1b}$$

$$2\bar{u}\,(\bar{v}+1) + \bar{w}\bar{v}' = \bar{v}'', \tag{3.1.1c}$$

where the primes denote differentiation with respect to z. The pressure is determined by

$$\bar{p}' = -\bar{w}\bar{w}' + \bar{w}'' \implies \bar{p} - \bar{p}_0 = -\bar{w}^2/2 - 2\bar{u}, \tag{3.1.2}$$

where $\bar{p}_0 \equiv 0$ as we stipulate that $\bar{p} = 0$ at $z = 0$. Owing to (2.2.9) the non-dimensional boundary conditions are

$$\bar{u} = \bar{v} = \bar{w} = 0 \quad \text{at} \quad z = 0, \tag{3.1.3a}$$

$$\bar{u} \to 0, \quad \bar{v} \to -1 \quad \text{as} \quad z \to \infty. \tag{3.1.3b}$$

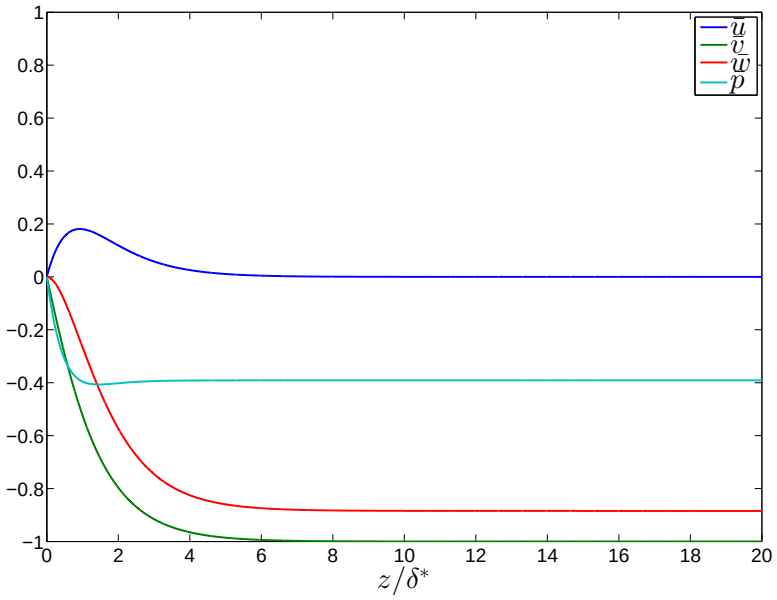

Figure 3.2: The Newtonian base flow profiles: $\bar{u}$, $\bar{v}$, $\bar{w}$ and $\bar{p}$ versus the similarity coordinate z/δ.

In order to determine $\bar{u}$, $\bar{v}$ and $\bar{w}$ (and hence $\bar{p}$) we solve (3.1.1) subject to the boundary conditions (3.1.3), this requires a full numerical solution of the non-linear ordinary differential equations. We employ a shooting method that utilises a fourth-order Runge-Kutta quadrature routine to perform the numerical integration of the differential equations twinned with a Newton iteration scheme to determine the values of the unknowns $\bar{u}'(0) = \bar{u}_0$ and $\bar{v}'(0) = \bar{v}_0$.

3.2 Case I: Power-law

Having isolated the dominant viscous terms via a boundary-layer approximation we arrived at the scaled governing equations (2.2.11) and (2.2.19), let us now return to an unscaled frame of reference. Assuming that the flow is steady and axisymmetric we rewrite the velocity functions (U_0, V_0, W_0), pressure P_1 and modified viscosity function $\tilde{\mu}_0$ in terms of the outer region coordinate z, whilst also removing the boundary-layer scaling

on the axial velocity component so that

$$[u_0(r,z), v_0(r,z), w_0(r,z)] = [U_0(r,\theta,Z), V_0(r,\theta,Z), Re^{-1/(n+1)}W_0(r,\theta,Z)], \tag{3.2.1a}$$

$$p_1(r,z) = P_1(r,\theta,Z), \quad \mu_0(r,z) = \tilde{\mu}_0(r,\theta,Z). \tag{3.2.1b}$$

Then we arrive at the unscaled leading order equations that must be solved in order to determine the steady mean flow

$$\frac{1}{r}\frac{\partial(ru_0)}{\partial r} + \frac{\partial w_0}{\partial z} = 0, \tag{3.2.2a}$$

$$u_0\frac{\partial u_0}{\partial r} + w_0\frac{\partial u_0}{\partial z} - \frac{(v_0+r)^2}{r} = \frac{1}{Re}\frac{\partial}{\partial z}\left(\mu_0\frac{\partial u_0}{\partial z}\right), \tag{3.2.2b}$$

$$u_0\frac{\partial v_0}{\partial r} + w_0\frac{\partial v_0}{\partial z} + \frac{u_0 v_0}{r} + 2u_0 = \frac{1}{Re}\frac{\partial}{\partial z}\left(\mu_0\frac{\partial v_0}{\partial z}\right), \tag{3.2.2c}$$

$$\begin{aligned} u_0\frac{\partial w_0}{\partial r} + w_0\frac{\partial w_0}{\partial z} = -\frac{\partial p_1}{\partial z} + \frac{1}{Re}\Bigg[\frac{1}{r}\frac{\partial}{\partial r}\left(\mu_0 r\frac{\partial u_0}{\partial z}\right) \\ + 2\frac{\partial}{\partial z}\left(\mu_0\frac{\partial w_0}{\partial z}\right)\Bigg], \end{aligned} \tag{3.1.2d}$$

with

$$\mu_0 = \left[\left(\frac{\partial u_0}{\partial z}\right)^2 + \left(\frac{\partial v_0}{\partial z}\right)^2\right]^{(n-1)/2}. \tag{3.2.2e}$$

It should be noted here that substituting $n = 1$ into (3.2.2) does not admit the governing equations in the Newtonian limit. This is because a number of viscous terms have been removed via the application of our boundary-layer approximation. Essentially, only the second order derivatives with respect to z are retained in this case.

In order to solve (3.2.2) we introduce a modified von Kármán similarity solution of the form

$$\boldsymbol{u} = [r\bar{u}(\eta), r\bar{v}(\eta), r^{(n-1)/(n+1)}Re^{-1/(n+1)}\bar{w}(\eta)],$$

$$p_1(r,z) = r^{2(n-1)/(n+1)} Re^{-2/(n+1)} \bar{p}(\eta),$$

where $\boldsymbol{u} = [u_0(r,z), v_0(r,z), w_0(r,z)]$ and the similarity variable η is given by

$$\eta = r^{(1-n)/(n+1)} Re^{1/(n+1)} z.$$

Substituting this form for the similarity solution into (3.2.2) produces the following non-linear ODEs that $\bar{u}$, $\bar{v}$ and $\bar{w}$ must satisfy

$$-2\bar{u} - \frac{1-n}{n+1}\eta\bar{u}' = \bar{w}', \tag{3.2.3a}$$

$$\bar{u}^2 - (\bar{v}+1)^2 + \left(\bar{w} + \frac{1-n}{n+1}\eta\bar{u}\right)\bar{u}' = (\bar{\mu}\bar{u}')', \tag{3.2.3b}$$

$$2\bar{u}(\bar{v}+1) + \left(\bar{w} + \frac{1-n}{n+1}\eta\bar{u}\right)\bar{v}' = (\bar{\mu}\bar{v}')', \tag{3.2.3c}$$

where $\bar{\mu} = [\bar{u}'^2 + \bar{v}'^2]^{(n-1)/2}$ and the primes denote differentiation with respect to η. The pressure is determined by

$$\bar{p}' = \frac{1-n}{n+1}\left[\bar{u}(\bar{w} - \eta\bar{w}') - 2\bar{\mu}\bar{u}'\right] - 2\bar{\mu}'\bar{u} - \bar{w}\bar{w}' + (\bar{\mu}\bar{w}')'. \tag{3.2.4}$$

Here we note the difference between (3.2.4) and equation (A1) as reported by Denier & Hewitt (2004). Using the authors' notation, the term $(n-1)/(n+1)(\hat{\mu}F')'$ should read $\eta(1-n)/(n+1)(\hat{\mu}F')'$, thus allowing for the simplification of the pressure correction term p_1. We see that the Newtonian similarity ODEs, (3.1.1) and (3.1.2), are returned with the application of $n = 1$, as is to be expected.

Rearranging (3.2.3b) and (3.2.3c) gives

$$\bar{u}'' = \frac{(\bar{u}'^2 + n\bar{v}'^2)[\bar{u}^2 - (\bar{v}+1)^2 + (\bar{w} + \hat{\eta}\bar{u})\bar{u}'] - \bar{u}'\bar{v}'(n-1)[2\bar{u}(\bar{v}+1) + (\bar{w} + \hat{\eta}\bar{u})\bar{v}']}{n\bar{\mu}(\bar{u}'^2 + \bar{v}'^2)},$$

$$\bar{v}'' = \frac{(n\bar{u}'^2 + \bar{v}'^2)[2\bar{u}(\bar{v}+1) + (\bar{w} + \hat{\eta}\bar{u})\bar{v}'] - \bar{u}'\bar{v}'(n-1)[\bar{u}^2 - (\bar{v}+1)^2 + (\bar{w}+\hat{\eta}\bar{u})\bar{u}']}{n\bar{\mu}(\bar{u}'^2 + \bar{v}'^2)},$$

with $\hat{\eta} = (1-n)/(n+1)\eta$. Having $\bar{u}''$ and $\bar{v}''$ in this form allows us to formulate a system of five first order ordinary differential equations in five unknowns, $\bar{u}$, $\bar{u}'$, $\bar{v}$, $\bar{v}'$ and $\bar{w}$. The non-dimensional boundary conditions are

$$\bar{u} = \bar{v} = \bar{w} = 0 \quad \text{at} \quad \eta = 0, \tag{3.2.5a}$$

$$\bar{u} \to 0, \quad \bar{v} \to -1 \quad \text{as} \quad \eta \to \infty. \tag{3.2.5b}$$

Before going on to obtain numerical solutions of (3.2.3) subject to (3.2.5) we must first consider the asymptotic form of the functions $\bar{u}$, $\bar{v}$ and $\bar{w}$ as $\eta \to \infty$. By doing so we are able to ensure the correct decay of these functions to the far-field. Here we will follow closely the approach of Denier & Hewitt (2004) for shear-thinning power-law fluids. For shear-thickening fluids the analysis is somewhat more involved. Denier & Hewitt (2004) showed that the solutions for $n > 1$ become non-differentiable at a critical location $\eta = \eta_c$. However, it is noted that in this case the singularity can be completely regularised and thus the solutions can be matched to an external flow. We will not consider shear-thickening power-law fluids here. The interested reader is referred to Denier & Hewitt (2004) for the full details regarding flows with $n > 1$ and for a lengthy discussion on shear-thinning flows for the three distinct cases when $0 < n < 0.5$, $n = 0.5$ and $0.5 < n < 1$.

We begin by integrating (3.2.3a) to arrive at the following

$$\bar{w} = \frac{n-1}{n+1}\eta\bar{u} - \frac{(3n+1)}{(n+1)}\int_0^\eta \bar{u}\,\mathrm{d}\eta. \tag{3.2.6}$$

Now $\bar{w}$ is bounded as $\eta \to \infty$ given that $\bar{u}$ is $o(\eta^{-1})$ as $\eta \to \infty$. Let us assume that

$$\bar{w} \to -\frac{(3n+1)}{(n+1)}\int_0^\infty \bar{u}\,\mathrm{d}\eta = \bar{w}_\infty.$$

Since $\bar{u} \to 0$ and $\bar{v} \to -1$ as $\eta \to \infty$ we find that the dominant balance of terms in (3.2.3b) and (3.2.3c) is given by

$$\bar{w}_\infty \bar{u}' \sim (\bar{\mu}\bar{u}')', \tag{3.2.7a}$$

$$\bar{w}_\infty \bar{v}' \sim (\bar{\mu}\bar{v}')', \tag{3.2.7b}$$

as $\eta \to \infty$. These equations are most easily solved by setting $(\bar{u}', \bar{v}') = R(\cos\theta, \sin\theta)$, where the amplitude R and phase angle θ satisfy

$$\bar{w}_\infty R^{2-n} = nR',$$

$$\theta' = 0.$$

Solving for the amplitude we have that

$$R - R_0 = \left[\frac{(n-1)\bar{w}_\infty \eta}{n}\right]^{1/(n-1)}.$$

Hence we have that $R \sim \eta^{1/(n-1)}$ as $\eta \to \infty$ and thus we see that

$$(\bar{u}, \bar{v}) \sim \eta^{n/(n-1)} \quad \text{as} \quad \eta \to \infty. \tag{3.2.8}$$

For the case when $n = 1$ this relationship becomes singular, due to the fact that in the Newtonian limit the decay of the functions $\bar{u}$ and $\bar{v}$ is exponential. Cochran (1934) showed that in this case

$$(\bar{u}, \bar{v}) \sim e^{\bar{w}_\infty \eta} \quad \text{as} \quad \eta \to \infty,$$

where here we note that $\eta|_{n=1} = Re^{1/2}z$ and that in the Newtonian case the limiting value

of $\bar{w}$ is simplified such that

$$\bar{w}_\infty = -2\int_0^\infty \bar{u}\,\mathrm{d}\eta.$$

In order for $\bar{w}$ to be bounded as $\eta \to \infty$ we require that $n/(n-1) < -1$, thus (3.2.8) is valid only for values of the power-law index in the range $0.5 < n < 1$ and hence $\bar{w} \to \infty$ as $\eta \to \infty$ in the case when $0 < n \leq 0.5$. This analysis shows that bounded solutions will only exist in the shear-thinning case when $0.5 < n < 1$. In order to obtain physical solutions for highly shear-thinning fluids, $0 < n \leq 0.5$, one must seek an alternate solution methodology.

Differentiating (3.2.8) we obtain two asymptotic boundary conditions that can be applied at some suitably large η to ensure the correct asymptotic behaviour as $\eta \to \eta_\infty$

$$(\bar{u}', \bar{v}') \sim \frac{n}{\eta(n-1)}(\bar{u}, \bar{v}) \quad \text{as} \quad \eta \to \infty. \tag{3.2.9}$$

The same can be performed in the Newtonian case, finding that

$$(\bar{u}', \bar{v}') \sim \bar{w}_\infty(\bar{u}, \bar{v}) \quad \text{as} \quad \eta \to \infty. \tag{3.2.10}$$

Numerical solutions of (3.2.3) subject to (3.2.5) are presented in figures 3.3 & 3.4, the value of η_∞ employed for each calculation along with the calculated values of $\bar{u}_0$, $\bar{v}_0$, $\bar{w}(\eta_\infty)$ and $\bar{p}(\eta_\infty)$ for power-law indices in the range $0.6 \leq n \leq 0.9$ are presented in table 3.1. These solutions were obtained using the numerical scheme as described previously and in the shear-thinning case the scheme iterated until the asymptotic boundary conditions (3.2.9) were satisfied to within the desired tolerance of (10^{-10}) at some $\eta = \eta_\infty$.

Here we have reproduced the results presented by Denier & Hewitt (2004) for power-law indices in the range, $0.6 \leq n \leq 0.9$, whilst also including the Newtonian results

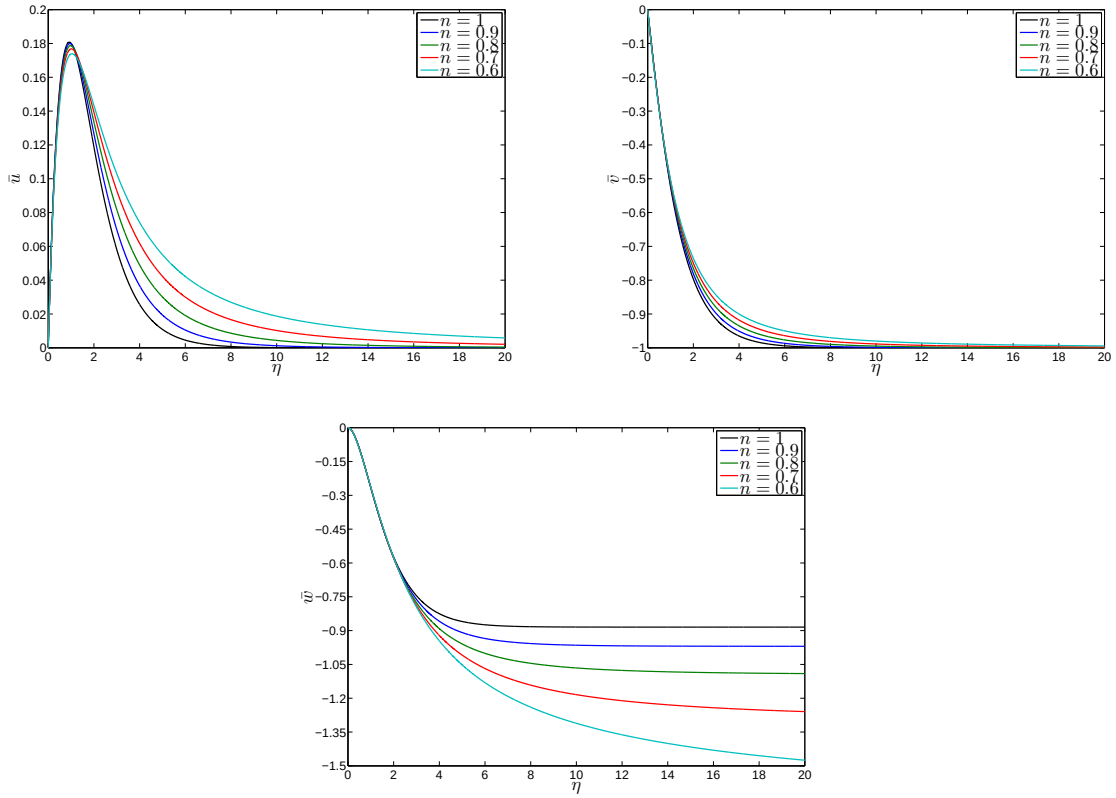

Figure 3.3: The radial ($\bar{u}$), azimuthal ($\bar{v}$) and axial ($\bar{w}$) velocity functions versus η for power-law fluids with $n = 1$, 0.9, 0.8, 0.7, 0.6.

obtained in §3.1. As is to be expected our results are in complete agreement with Denier & Hewitt (2004), however, here we also present values for $\bar{u}_0$, $\bar{v}_0$ and $\bar{p}(\eta_\infty)$ for each value of n. The results in the Newtonian case are in agreement with those presented by Healey (2006).

We observe from figure 3.3 that the shear-thinning velocity profiles are comparable to the Newtonian solution with the radial, azimuthal and axial velocity components decaying to their respective far-field values further from the disk surface with decreasing n. This slow decay to the far-field is most notable in the case of the axial velocity component; we look to the asymptotic form of the solution to give us an insight in to why this is the case.

From (3.2.8) we have that $\bar{u} = A\eta^{n/(n-1)} + \cdots$ and $\bar{v} = B\eta^{n/(n-1)} + \cdots$, as $\eta \to \infty$,

n	$\bar{u}_0$	$-\bar{v}_0$	η_∞	$-\bar{w}(\eta_\infty)$	$-\bar{p}(\eta_\infty)$
1	0.5102	0.6159	20	0.8845	0.3911
0.9	0.5069	0.6243	55	0.9698	0.5565
0.8	0.5039	0.6362	100	1.0957	0.8317
0.7	0.5017	0.6532	175	1.3051	1.3694
0.6	0.5005	0.6778	645	1.7329	2.7935

Table 3.1: Numerical values of the basic flow parameters for power-law fluids with $n = 1$, 0.9, 0.8, 0.7, 0.6. For $n = 1$ the value of η_∞ represents the dimensionless distance away from the disk at which the solutions have sufficiently converged to their respective limiting values, as in this case the asymptotic boundary condition (3.2.10) has no specific dependence on η.

where A and B are constants. Hence using (3.2.6) we arrive at the following

$$\bar{w} = \bar{w}_\infty + \frac{n-1}{n+1} A\eta^{(2n-1)/(n-1)} - \frac{(3n+1)}{(n+1)} \int_0^\eta A\chi^{n/(n-1)}\, \mathrm{d}\chi + \cdots \quad \text{as} \quad \eta \to \infty,$$

so that

$$\bar{w} = \bar{w}_\infty + \frac{(n+2)(1-n)}{(n+1)(2n-1)} A\eta^{(2n-1)/(n-1)} + \cdots \quad \text{as} \quad \eta \to \infty.$$

Thus we see that the slow decay of the axial velocity function to $\bar{w}_\infty$ is due to the strong dependence of $\bar{w}$ on the power-law index n.

As noted by Denier & Hewitt (2004) the decay is $\mathcal{O}(\eta^{-8})$ for $n = 0.9$ whilst for $n = 0.6$ the decay is $\mathcal{O}(\eta^{-1/2})$. We see that for $n = 0.5$ the function will not converge to any limiting value, as predicted. As a point of interest we note that in the Newtonian case the decay of $\bar{w}$ to $\bar{w}_\infty$ is $\mathcal{O}(e^{-\eta})$. Both $\bar{u}$ and $\bar{v}$ decay to their respective far-field values, 0 and -1 like $\mathcal{O}(\eta^{-9})$ for $n = 0.9$, like $\mathcal{O}(\eta^{-3/2})$ for $n = 0.6$ and again like $\mathcal{O}(e^{-\eta})$ in the Newtonian limit.

Having this asymptotic form for the solutions for large η also allows us to comment on the structure of the viscosity function, $\bar{\mu}$, as $\eta \to \infty$. Again, assuming the form for $\bar{u}$ and $\bar{v}$

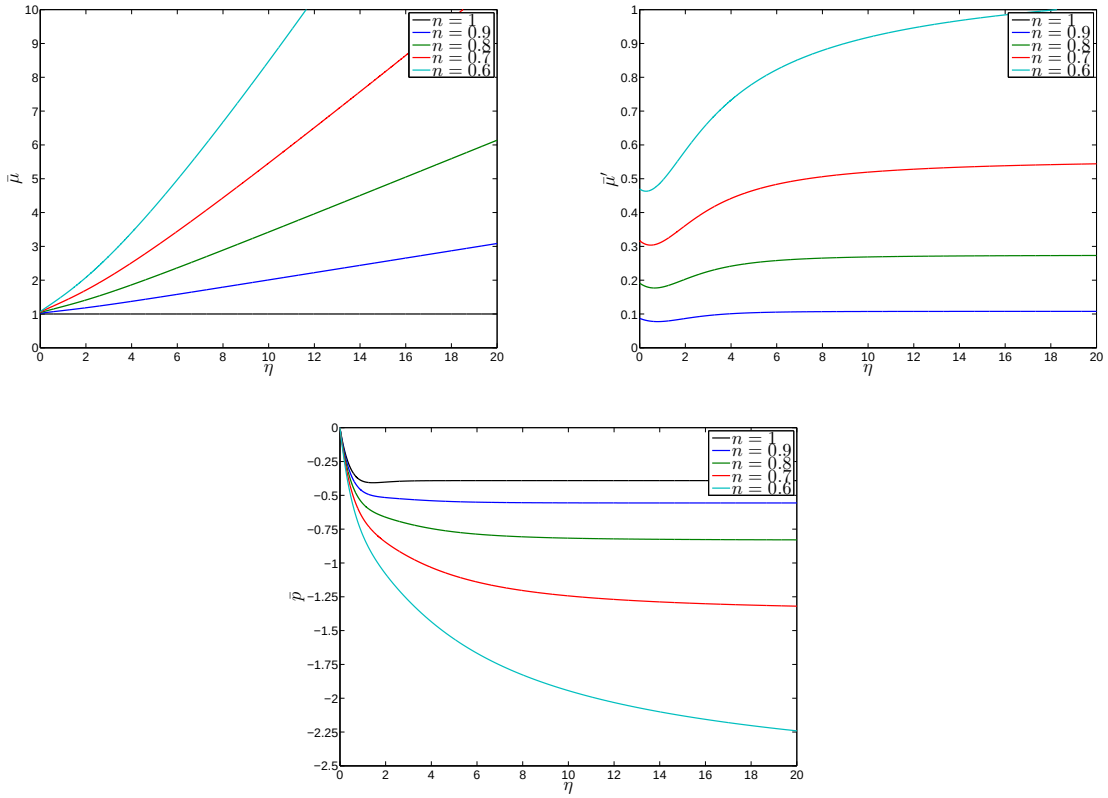

Figure 3.4: The viscosity function ($\bar{\mu}$), its first derivative ($\bar{\mu}'$) and the pressure function ($\bar{p}$) versus η for power-law fluids with $n = 1$, 0.9, 0.8, 0.7, 0.6.

as $\eta \to \infty$, we find that $\bar{\mu} = C\eta + \cdots$ as $\eta \to \infty$, where $C = [n^2(A^2+B^2)/(n-1)^2]^{(n-1)/2}$. Thus, the viscosity function does not decay to a well-defined limit and instead remains unbounded in the far-field. Clearly this behaviour is unphysical, predicting that fluid is entrained into the boundary-layer with unbounded viscosity as the axial distance is increased. This being a result of the failure of the power-law model to accurately model shear-thinning flows in the limit as $\dot{\gamma}^* \to 0$. Analogously, one would find that $\bar{\mu} \to 0$ as $\eta \to \eta_c$ for shear-thickening power-law fluids for the same reason.

Since $\bar{\mu} = C\eta + \cdots$ as $\eta \to \infty$ we expect that $\bar{\mu}' \to \bar{\mu}'_\infty$ as $\eta \to \infty$, where $\bar{\mu}'_\infty$ is constant. To see this we again utilise the far-field form of the equations given by (3.2.7),

so that

$$(\bar{u}'', \bar{v}'') \sim \frac{(\bar{w}_\infty - \bar{\mu}'_\infty)}{\bar{\mu}}(\bar{u}', \bar{v}') \quad \text{as} \quad \eta \to \infty. \tag{3.2.11}$$

Now $\bar{\mu}'$ can be written in terms of $\bar{\mu}$

$$\bar{\mu}' = \frac{(n-1)\bar{\mu}(\bar{u}'\bar{u}'' + \bar{v}'\bar{v}'')}{\bar{u}'^2 + \bar{v}'^2}.$$

Thus using (3.2.11) we find that

$$\bar{\mu}' \to \bar{\mu}'_\infty = \frac{(n-1)\bar{w}_\infty}{n} = \frac{(1-n)(3n+1)}{n(n+1)} \int_0^\infty \bar{u}\,\mathrm{d}\eta \quad \text{as} \quad \eta \to \infty. \tag{3.2.12}$$

The existence of this limit is observed in figure 3.4.

As noted in §3.1 the pressure correction term, $\bar{p}$, is realisable once the velocity functions have been calculated. The pressure profiles have been determined using a standard trapezoidal numerical integration scheme where the unit step-size has been reduced until sufficiently converged results were obtained. In the Newtonian limit this scheme was validated against the analytic solution given by (3.1.2). The slow decay to the far-field can again be quantified asymptotically, by integrating (3.2.4) we arrive at

$$\bar{p} = \bar{\mu}\bar{w}' - 2\bar{u}\bar{\mu} - \frac{\bar{w}^2}{2} + \frac{1}{n+1}\int_0^\eta 4n\bar{u}'\bar{\mu} + (1-n)\bar{u}(\bar{w} - \eta\bar{w}')\,\mathrm{d}\eta, \tag{3.2.13}$$

thus

$$\bar{p} \to -\frac{\bar{w}_\infty^2}{2} + \frac{1}{n+1}\int_0^\infty 4n\bar{u}'\bar{\mu} + (1-n)\bar{u}(\bar{w} - \eta\bar{w}')\,\mathrm{d}\eta = \bar{p}_\infty.$$

Utilising the large η asymptotic forms for $\bar{u}$, $\bar{v}$, $\bar{w}$ and $\bar{\mu}$ gives

$$\begin{aligned}\bar{p} = \bar{p}_\infty &- \frac{(n+2)}{(n+1)} AC\eta^{(2n-1)/(n-1)} - 2AC\eta^{(2n-1)/(n-1)} \\ &- \frac{(n+2)(1-n)}{(n+1)(2n-1)} A\bar{w}_\infty \eta^{(2n-1)/(n-1)} + \mathcal{O}(\eta^{\frac{4n-2}{n-1}}) \\ &+ \frac{A[4n^2C - (n-1)^2\bar{w}_\infty]}{(n+1)(n-1)} \int_0^\eta \chi^{n/(n-1)} + \mathcal{O}(\chi^{\frac{3n-1}{n-1}})\,\mathrm{d}\chi \quad \text{as} \quad \eta \to \infty.\end{aligned}$$

Hence we find that

$$\bar{p} = \bar{p}_\infty + \frac{[4 - n(2n+5)]C + 3(n-1)\bar{w}_\infty}{(n+1)(2n-1)} A\eta^{(2n-1)/(n-1)} + \cdots \quad \text{as} \quad \eta \to \infty. \tag{3.2.14}$$

3.3 Case II: Bingham

As in the previous section we wish to return to an unscaled frame of reference and we assume that the flow is both steady and axisymmetric. By rewriting the velocity functions (U_0, V_0, W_0), pressure P_1 and modified viscosity function $\tilde{\mu}_0$ in terms of the outer region coordinate z, whilst also removing the boundary-layer scaling on the axial velocity component we have that

$$[u_0(r,z), v_0(r,z), w_0(r,z)] = [U_0(r,\theta,Z), V_0(r,\theta,Z), Re^{-1/2}W_0(r,\theta,Z)], \tag{3.3.1a}$$

$$p_1(r,z) = P_1(r,\theta,Z), \quad \mu_0(r,z) = \tilde{\mu}_0(r,\theta,Z). \tag{3.3.1b}$$

Thus our leading order equations, (3.2.2a)-(3.1.2d), are as before with the exception of μ_0 which is now given by

$$\mu_0 = 1 + 2rRe^{1/2}B_n \left[\left(\frac{\partial u_0}{\partial z} \right)^2 + \left(\frac{\partial v_0}{\partial z} \right)^2 \right]^{-1/2}, \tag{3.3.2}$$

we recall that in this case the definition of the Reynolds number is slightly different as Re has been scaled by the plastic-shear-rate viscosity, μ_p^*.

As outlined in §3.2, the leading order equations are solved via the introduction of a similarity solution. Here the solution takes the form

$$\boldsymbol{u} = [r\bar{u}(\zeta), r\bar{v}(\zeta), Re^{-1/2}\bar{w}(\zeta)],$$
$$p_1(z) = Re^{-1}\bar{p}(\zeta),$$

where $\boldsymbol{u_B} = [u_0(z), v_0(z), w_0(z)]$ and the similarity variable ζ is given by

$$\zeta = Re^{1/2}z.$$

We note here that ζ takes the same form as the Newtonian similarity variable and unlike η, the power-law variable, is independent of the radius of the disk r. Substituting this form for the similarity solution into (3.2.2a)-(3.1.2d) with (3.3.2) produces the following equations that $\bar{u}$, $\bar{v}$ and $\bar{w}$ must satisfy

$$-2\bar{u} = \bar{w}', \tag{3.3.3a}$$
$$\bar{u}^2 - (\bar{v}+1)^2 + \bar{w}\bar{u}' = (\bar{\mu}\bar{u}')', \tag{3.3.3b}$$
$$2\bar{u}(\bar{v}+1) + \bar{w}\bar{v}' = (\bar{\mu}\bar{v}')', \tag{3.3.3c}$$

where the primes denote differentiation with respect to ζ and the pressure is determined by

$$\bar{p}' = (1-\bar{\mu})\bar{u}' - 2\bar{\mu}'\bar{u} - \bar{w}\bar{w}' + (\bar{\mu}\bar{w}')'. \tag{3.3.4}$$

B_n	$\bar{u}_0$	$-\bar{v}_0$	$-\bar{w}_\infty$
0	0.5102	0.6159	0.8845
0.1	0.4247	0.5900	0.7815
0.2	0.3586	0.5685	0.7158
0.3	0.3077	0.5489	0.6668
0.4	0.2681	0.5308	0.6282
0.5	0.2368	0.5141	0.5968

Table 3.2: Numerical values of the basic flow parameters for Bingham plastic fluids with $B_n = 0,\ 0.1,\ 0.2,\ 0.3,\ 0.4,\ 0.5$. We find that suitably converged results are obtained when $\zeta_\infty = 20$.

Here $\bar{\mu} = 1 + 2B_n[\bar{u}'^2 + \bar{v}'^2]^{-1/2}$. Rearranging (3.3.3b) and (3.3.3c) gives

$$\bar{u}'' = \frac{[\bar{u}^2 - (\bar{v}+1)^2 + \bar{w}\bar{u}'](\bar{\mu}\bar{u}'^2 + \bar{v}'^2) - \bar{u}'\bar{v}'(1-\bar{\mu})[2\bar{u}(\bar{v}+1) + \bar{w}\bar{v}']}{\bar{\mu}(\bar{u}'^2 + \bar{v}'^2)},$$
$$\bar{v}'' = \frac{[2\bar{u}(\bar{v}+1) + \bar{w}\bar{v}'](\bar{u}'^2 + \bar{\mu}\bar{v}'^2) - \bar{u}'\bar{v}'(1-\bar{\mu})[\bar{u}^2 - (\bar{v}+1)^2 + \bar{w}\bar{u}']}{\bar{\mu}(\bar{u}'^2 + \bar{v}'^2)}.$$

The appropriate boundary conditions for this problem are identical to those stated in (3.2.5) with η being replaced by ζ.

Following the methodology of §3.2 it is possible to show that the velocity functions $\bar{u}$, $\bar{v}$ and $\bar{w}$ decay at an exponential rate, as in the Newtonian case. We find that

$$\bar{u} = Ae^{\bar{w}_\infty \zeta} + \cdots,$$
$$\bar{v} = Be^{\bar{w}_\infty \zeta} + \cdots,$$
$$\bar{w} = \bar{w}_\infty - \frac{2A}{\bar{w}_\infty} e^{\bar{w}_\infty \zeta} + \cdots,$$

as $\zeta \to \infty$. Here A and B are constants to be determined. Thus the velocity solutions will be bounded as $\zeta \to \infty$ for all values of B_n, provided that $\bar{w}_\infty \leq 0$. In fact, the large ζ asymptotic form of the solutions has no specific dependence on the Bingham number whatsoever. Hence no additional asymptotic conditions are required during the numerical

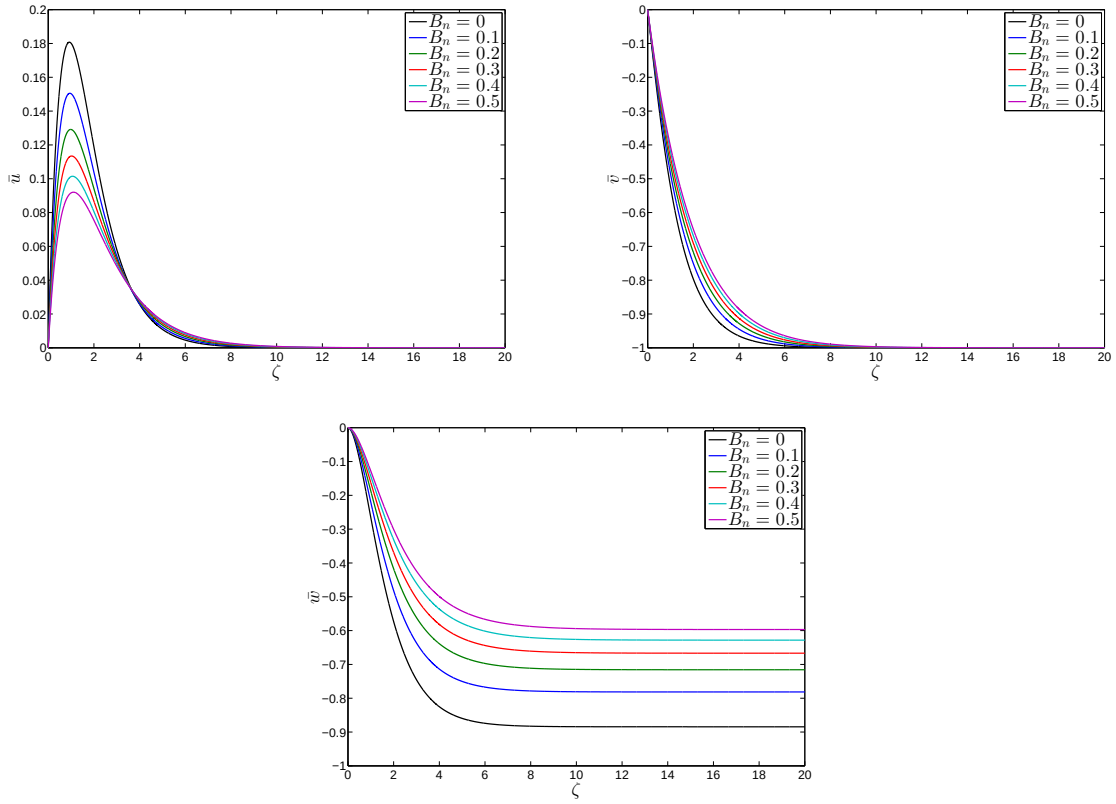

Figure 3.5: The radial ($\bar{u}$), azimuthal ($\bar{v}$) and axial ($\bar{w}$) velocity functions versus ζ for Bingham plastic fluids with $B_n = 0$, 0.1, 0.2, 0.3, 0.4, 0.5.

solution process.

In figure 3.5 we observe a significant reduction in the peak of the cross-flow velocity component, $\bar{u}$, as B_n increases from zero, whilst the component of the azimuthal velocity, $\bar{v}$, increases in absolute value with the Bingham number. We find that the von Kármán pumping rate, $-\bar{w}_\infty$, is decreased for increasing values of the yield stress, this being a direct consequence of the reduction in the peak of the radial velocity profile. Since, in this case, the velocity functions decay to the far-field exponentially one finds that

$$\bar{\mu} = 1 + \frac{2B_n e^{-\bar{w}_\infty \zeta}}{\bar{w}_\infty \sqrt{A^2 + B^2}} + \cdots \quad \text{as} \quad \zeta \to \infty.$$

Therefore for $B_n > 0$ the viscosity function grows exponentially in the far-field, as is

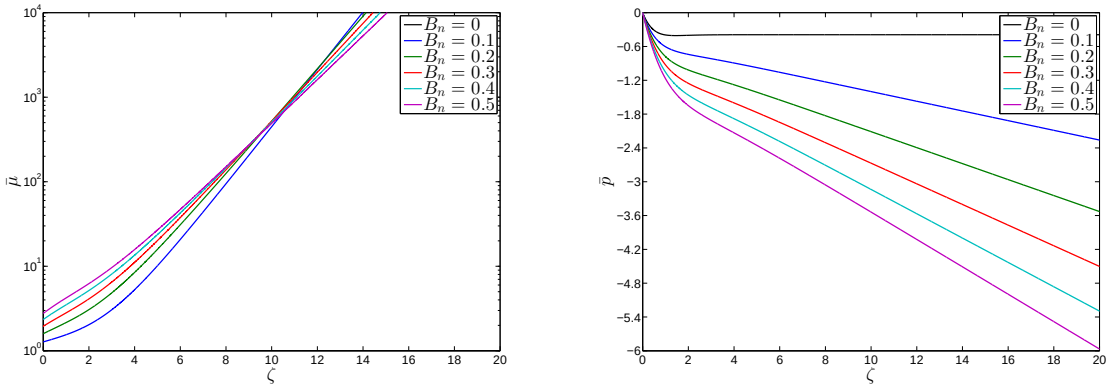

Figure 3.6: The viscosity ($\bar{\mu}$) and pressure ($\bar{p}$) functions versus ζ for Bingham plastic fluids with $B_n = 0,\ 0.1,\ 0.2,\ 0.3,\ 0.4,\ 0.5$.

observed in figure 3.6. This unphysical result owes from the inability of the Bingham model to describe apparent viscosity at vanishing shear-rates, as noted by Zhu, Kim & De Kee (2005).

It appears as though the value of $\bar{p}$ decreases linearly for increasing ζ, hence why no values for $\bar{p}_\infty$ are given in table 3.2. This prediction of unbounded pressure at the outer-edge of the boundary-layer is due to the unphysical nature of the viscosity function $\bar{\mu}$. By integrating (3.3.4) we obtain

$$\bar{p} = 2\bar{u}(1 - 2\bar{\mu}) - \frac{\bar{w}^2}{2} + \int_0^\zeta (\bar{\mu} - 1)\bar{u}' \,\mathrm{d}\zeta, \tag{3.3.5}$$

so that as $\zeta \to \infty$

$$\bar{p} \to -\frac{\bar{w}_\infty^2}{2} - \frac{8AB_n}{\bar{w}_\infty\sqrt{A^2 + B^2}} + \int_0^\infty \frac{2AB_n}{\sqrt{A^2 + B^2}} \,\mathrm{d}\zeta. \tag{3.3.6}$$

Hence $\bar{p} = \bar{p}_\infty + \mathcal{O}(\zeta) + \cdots$ as $\zeta \to \infty$.

3.3.1 Comparative results

A number of the previous comments have been outlined by Ahmadpour & Sadeghy (2013) who considered the full system of non-linear governing equations by numerically integrating a three parameter system. Because of our boundary-layer formulation of this problem the governing equations introduced here are reduced to a one parameter system, dependent only on B_n. In order to validate our results we present comparative solutions between this work and that of Ahmadpour & Sadeghy (2013) (subsequently referred to herein as AS). Having retained all of the viscous terms, AS obtain a three parameter system dependent on[1]

$$B_y = \frac{\tau_y^*}{\mu_p^* \Omega^*}, \quad Re = \frac{\rho^* \Omega^* {l^*}^2}{\mu_p^*} \quad \text{and} \quad r,$$

thus AS must specify values for all of the parameters before a numerical solution can be obtained.

However, recalling (2.2.24) we see that B_n can be expressed simply as a function of r, Re and B_y. Hence we are able to construct comparative solutions given the data used by AS, that being $r = 1$ and $Re = 2950$. So that when performing numerical computations our lone parameter B_n is now given by $B_n(r) = B_y/(10\sqrt{118})$. AS have obtained solutions with $B_y = 0$, 10, 20, 30, 50 (for $r = 1$ and $Re = 2950$) in a stationary frame of reference. In order to produce comparative results we transform our system from a rotating reference frame to a stationary one and solve the resulting equations.

Here we have reproduced the numerical solutions of AS using their three parameter numerical scheme. The results of these calculations are presented in figure 3.7. Although AS do not provide solutions for the viscosity profiles we are able to infer these results

[1] Although the notation used here is not consistent with that of AS the results are directly comparable. AS have made no attempt to solve for the resulting pressure profiles, as such no comparison is achievable in this case.

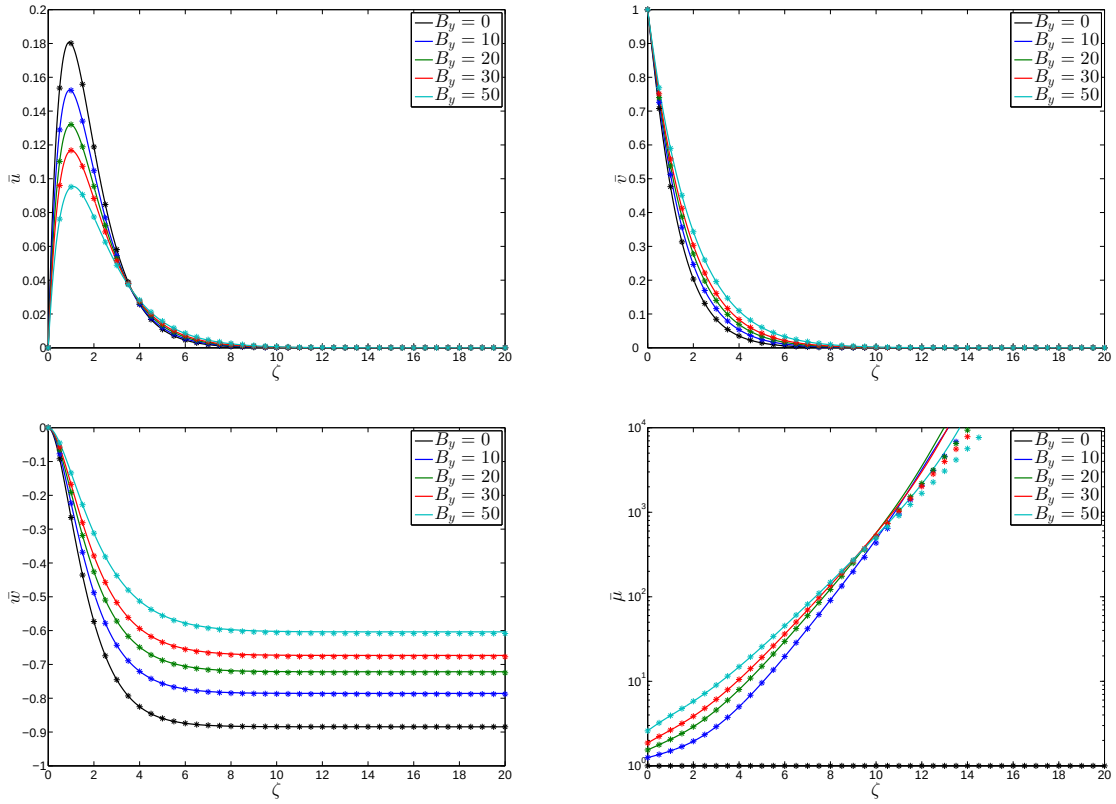

Figure 3.7: Comparative plots of $\bar{u}$, $\bar{v}$, $\bar{w}$ and $\bar{\mu}$ versus ζ with $B_y = 0$, 10, 20, 30, 50. The solid line curves are reproductions of Ahmadpour and Sadeghy's solutions, the $*$ markers are the corresponding boundary-layer results.

given the authors' stated form for the apparent viscosity (labelled equation (13)). The solid line curves are the solutions obtained from the work of AS whilst the $*$ markers represent the solutions owing from the boundary-layer formulation of the problem. We note here that both sets of velocity profiles decay to the far-field exponentially, as was outlined previously for the one parameter system.

It is clear from figure 3.7 that our results are in excellent agreement with those of AS. We find that there is in fact negligible discrepancy between the two sets of solutions. This serves to confirm the boundary-layer approximation made previously. We see that the elimination of the higher order viscous terms from the problem has little to no effect on the steady mean flow solutions.

Here we choose to appeal to the boundary-layer approximation as having the solutions in this form easily allows for the construction of an asymptotic stability analysis. That is not to say that an equivalent study could not be performed using the formulation provided by AS. However, we have shown here that the analysis of AS is unnecessarily extensive. Analogous results are obtained from a considerably simplified system of equations. This suggests that the resulting stability analysis will also be considerably simplified in this case.

3.4 Case III: Carreau

Using the methodology outlined in the previous section we arrive at our leading order equations, (3.2.2a)-(3.1.2d), with the exception that now μ_0 takes the form

$$\mu_0 = 1 + c_0\left\{1 + \left(\frac{k}{rRe^{1/2}}\right)^2\left[\left(\frac{\partial u_0}{\partial z}\right)^2 + \left(\frac{\partial v_0}{\partial z}\right)^2\right]\right\}^{(n-1)/2}. \tag{3.4.1}$$

We recall that in this case the definition of the Reynolds number is slightly different as here Re has been scaled by the infinite-shear-rate viscosity, μ^*_∞.

The leading order equations are again solved via the introduction of a similarity solution

$$\boldsymbol{u} = [r\bar{u}(\xi), r\bar{v}(\xi), Re^{-1/2}\bar{w}(\xi)],$$
$$p_1(z) = Re^{-1}\bar{p}(\xi),$$

where $\boldsymbol{u_B} = [u_0(z), v_0(z), w_0(z)]$ and the similarity coordinate $\xi = Re^{1/2}z$. Thus we determine that

$$-2\bar{u} = \bar{w}', \tag{3.4.2a}$$
$$\bar{u}^2 - (\bar{v}+1)^2 + \bar{w}\bar{u}' = (\bar{\mu}\bar{u}')', \tag{3.4.2b}$$

$$2\bar{u}\,(\bar{v}+1)+\bar{w}\bar{v}'=(\bar{\mu}\bar{v}')', \tag{3.4.2c}$$

$$\bar{w}\bar{w}'+\bar{p}'=2\bar{\mu}'(\bar{\nu}\bar{u}'-\bar{u})+(\bar{\mu}\bar{w}')', \tag{3.4.2d}$$

where the primes denote differentiation with respect to ξ. The viscosity function is given by $\bar{\mu}=1+c_0[1+k^2(\bar{u}'^2+\bar{v}'^2)]^{(n-1)/2}$ and $\bar{\nu}^{-1}=[\ln(\bar{u}'^2+\bar{v}'^2)]'$.

Rearranging (3.4.2b) and (3.4.2c) gives

$$\bar{u}''=\frac{[\bar{u}^2-(\bar{v}+1)^2+\bar{w}\bar{u}'](\bar{\varsigma}_1+\bar{\varsigma}_2\bar{v}'^2)-\bar{u}'\bar{v}'\bar{\varsigma}_2[2\bar{u}(\bar{v}+1)+\bar{w}\bar{v}']}{\bar{\mu}[\bar{\varsigma}_1+\bar{\varsigma}_2(\bar{u}'^2+\bar{v}'^2)]},$$
$$\bar{v}''=\frac{[2\bar{u}(\bar{v}+1)+\bar{w}\bar{v}'](\bar{\varsigma}_1+\bar{\varsigma}_2\bar{v}'^2)-\bar{u}'\bar{v}'\bar{\varsigma}_2[\bar{u}^2-(\bar{v}+1)^2+\bar{w}\bar{u}']}{\bar{\mu}[\bar{\varsigma}_1+\bar{\varsigma}_2(\bar{u}'^2+\bar{v}'^2)]},$$

where

$$\bar{\varsigma}_1=\bar{\mu}[1+k^2(\bar{u}'^2+\bar{v}'^2)]\quad\text{and}\quad\bar{\varsigma}_2=k^2(\bar{\mu}-1)(n-1).$$

The appropriate boundary conditions for this problem are identical to those stated in (3.2.5) with η being replaced by ξ.

In the limit of large ξ we solve (3.4.2b) and (3.4.2c) by setting $(\bar{u}',\bar{v}')=S(\cos\psi,\sin\psi)$, where the amplitude S and phase angle ψ are given by

$$\bar{w}_\infty S[1+c_0(1+k^2S^2)^{(n-3)/2}(1+nk^2S^2)]^{-1}=S',$$
$$\psi'=0,$$

with $\bar{w}_\infty=2\int_0^\infty\bar{u}\,\mathrm{d}\xi$. By assuming that $nk^2S^2\ll1$, which holds in the limit as $\xi\to\infty$, we find that

$$S\sim e^{\bar{w}_\infty\xi/(1+c_0)}\quad\text{as}\quad\xi\to\infty.$$

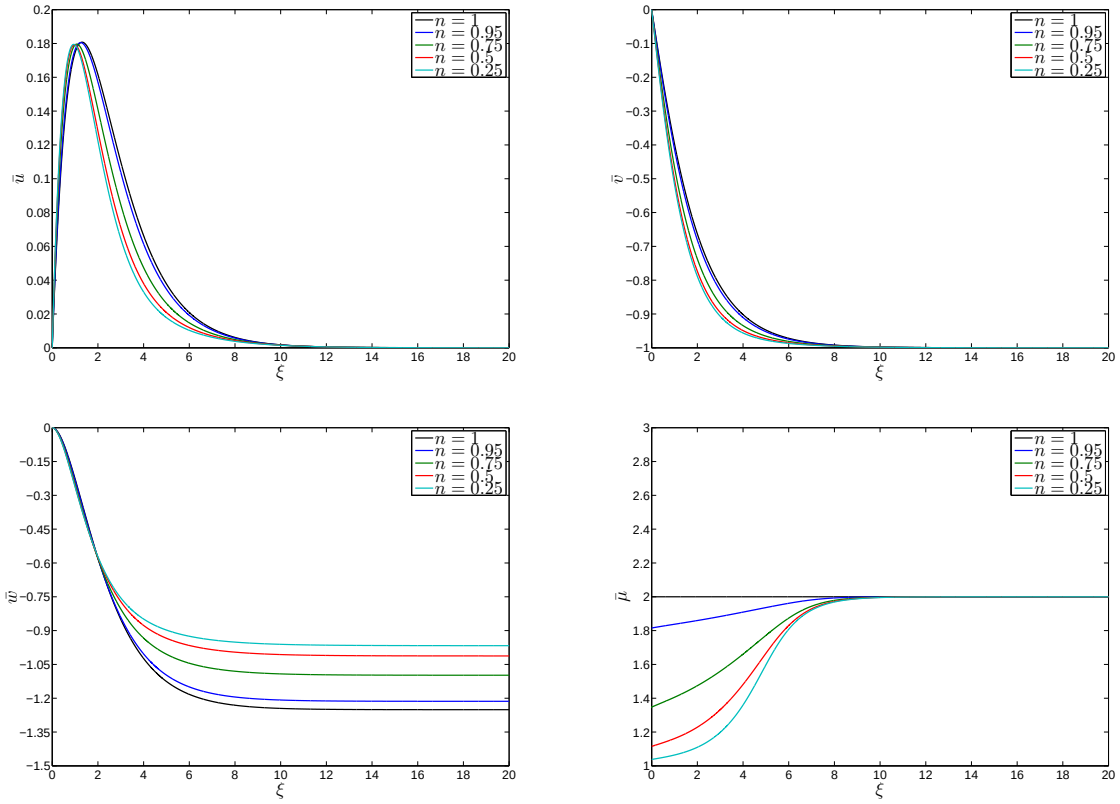

Figure 3.8: Plots of $\bar{u}$, $\bar{v}$, $\bar{w}$ and $\bar{\mu}$ versus ξ for shear-thinning Carreau fluids with $n = 1$, 0.95, 0.75, 0.5, 0.25 and $k = 100$.

Thus

$$\bar{u} = Ae^{\bar{w}_\infty \xi/(1+c_0)} + \cdots ,$$

$$\bar{v} = Be^{\bar{w}_\infty \xi/(1+c_0)} + \cdots ,$$

$$\bar{w} = \bar{w}_\infty - \frac{2A(1+c_0)}{\bar{w}_\infty} e^{\bar{w}_\infty \xi/(1+c_0)} + \cdots ,$$

as $\xi \to \infty$, with A and B being undetermined constants. Since the dimensionless viscosity ratio $c_0 > 0$ and $\bar{w}_\infty < 0$ we expect that the velocity solutions will decay exponentially. Throughout the forthcoming analysis we fix the value of c_0 at unity, as in the Falkner-Skan boundary-layer analysis presented by Dabrowski (2004).

In figures 3.8 & 3.9 basic flow solutions are plotted for shear-thinning and shear-

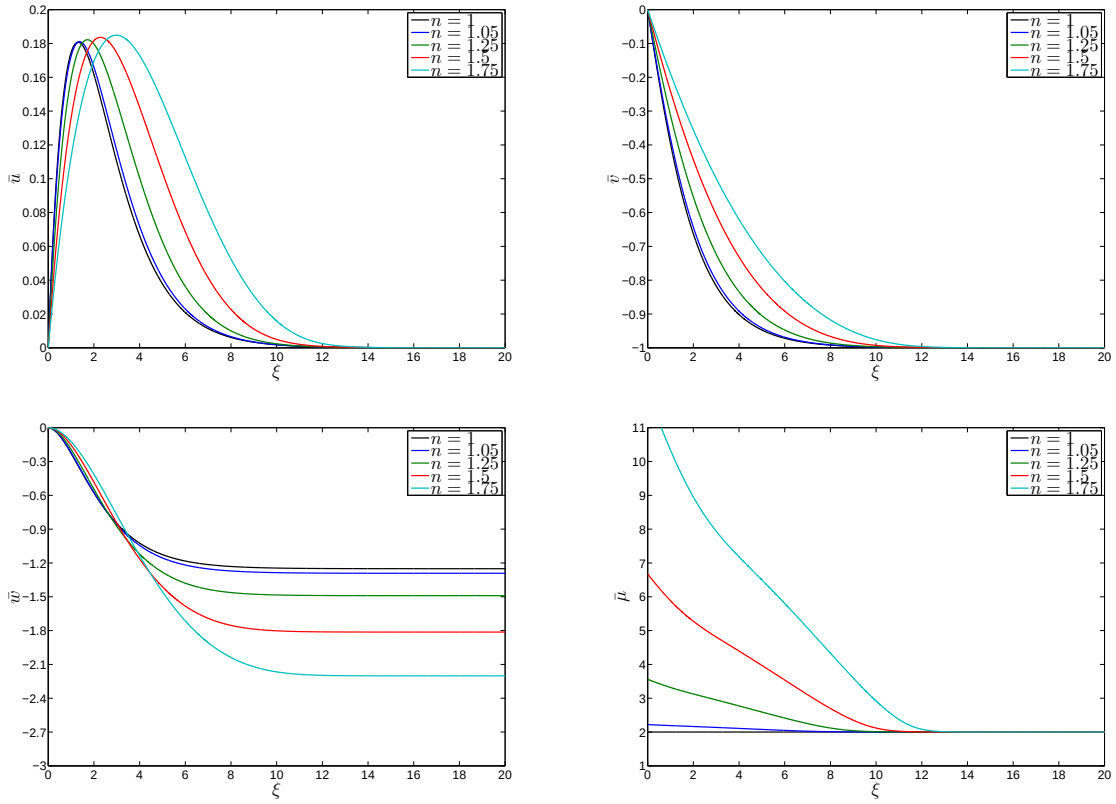

Figure 3.9: Plots of $\bar{u}$, $\bar{v}$, $\bar{w}$ and $\bar{\mu}$ versus ξ for shear-thickening Carreau fluids with $n = 1$, 1.05, 1.25, 1.5, 1.75 and $k = 100$.

thickening Carreau fluids, respectively. For both cases we find that the solutions have fully converged within the confines of the boundary-layer region $0 \leq \xi \leq 20$, which is in stark contrast to the results for shear-thinning power-law fluids presented in figure 3.3. As the power-law index increases from $n = 0.25$ we observe that the peak in the radial cross-flow profile is shifted along the ξ-axis, indicating that the boundary-layer thickness increases with n. As such, the von Kármán pumping rate also increases with increasing n and does so in a non-linear fashion, see figure 3.10. We note the quantitative difference between the power-law and Carreau shear-thinning solutions.

As $\xi \to \infty$ we have that

$$\bar{\mu} \to 1 + c_0[1 + \mathcal{O}(e^{\frac{2\bar{w}_\infty \xi}{1+c_0}}) + \cdots]^{(n-1)/2} = 2.$$

n	$\bar{u}_0$	$-\bar{v}_0$	$-\bar{w}_\infty$	$-\bar{p}_\infty$
0.25	0.5007	0.6026	0.9669	0.5196
0.5	0.4842	0.5789	1.0124	0.5829
0.75	0.4415	0.5250	1.0980	0.6788
0.95	0.3793	0.4554	1.2137	0.7643
1	0.3608	0.4355	1.2508	0.7823
1.05	0.3418	0.4153	1.2916	0.7971
1.25	0.2678	0.3368	1.4902	0.8045
1.5	0.1950	0.2562	1.8131	0.6038
1.75	0.1457	0.1986	2.2015	−0.0120

Table 3.3: Numerical values of the basic flow parameters for shear-thinning and shear-thickening Carreau fluids with $k = 100$. Solutions for $n = 1$ are also included, these differ from the Newtonian results as in this case the viscosity function is effectively set to $\bar{\mu} = 1 + c_0$, rather than unity.

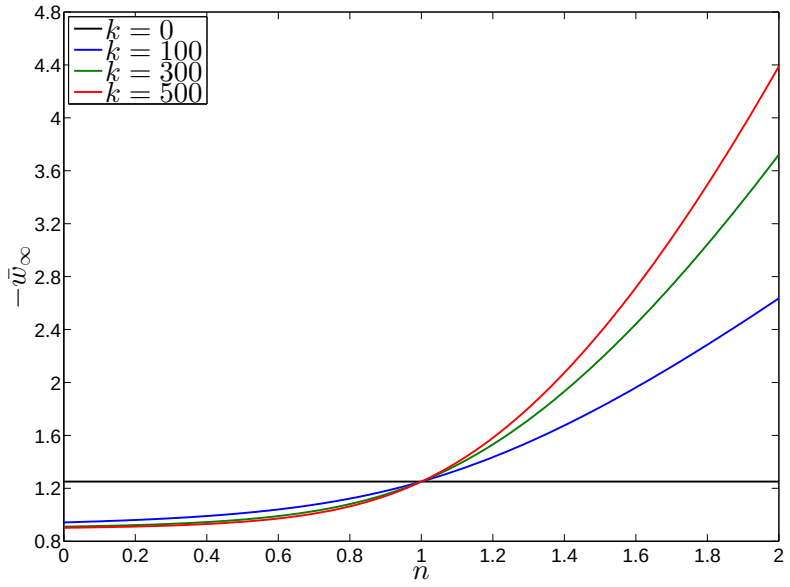

Figure 3.10: Variation of $-\bar{w}_\infty$ versus n for Carreau fluids with $k = 0$, 100, 300, 500.

For shear-thinning and shear-thickening fluids the limit $1 + c_0$ is approached from below and above, respectively. The shear-thinning Carreau model predicts a finite value of viscosity that can never be zero, unlike the power-law model, see figures 2.1 & 3.4. Thus, in the shear-thinning regime at least, this model is able to capture the actual variation

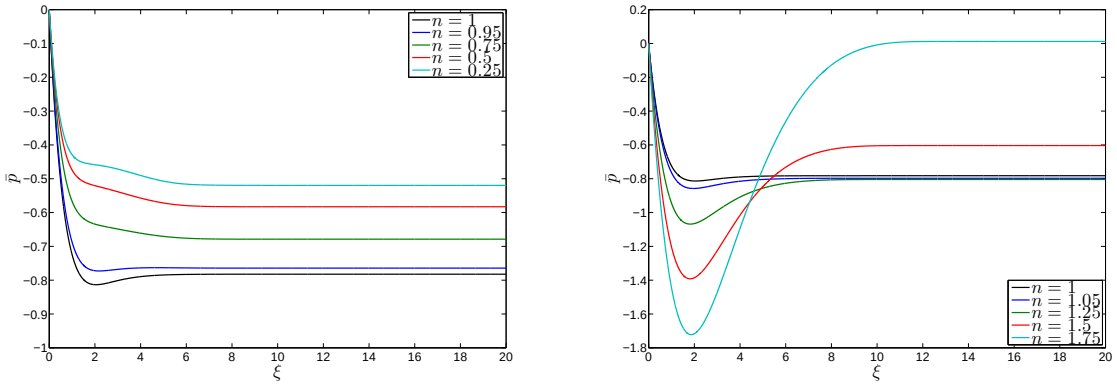

Figure 3.11: Plots of $\bar{p}$ versus ξ for shear-thinning and shear-thickening Carreau fluids with $k = 100$.

of viscosity within the boundary-layer, unlike the simpler power-law model which is only applicable over a finite range of shear rates. In the shear-thickening case a constant viscosity is at least recovered in the limit as $\dot{\gamma}^* \to 0$, although for increasing n ever increasing values of $\bar{\mu}(0) = \bar{\mu}_0$ will be predicted at the disk surface.

Integrating (3.4.2d) we obtain

$$\bar{p} = \bar{\mu}\bar{w}' - \frac{\bar{w}^2}{2} - 2\bar{\mu}\bar{u} + \int_0^\xi \frac{k^2(\bar{\mu}-1)(n-1)(\bar{u}'^2+\bar{v}'^2)}{1+k^2(\bar{u}'^2+\bar{v}'^2)}\bar{u}'\,\mathrm{d}\xi + \int_0^\xi 2\bar{\mu}\bar{u}'\,\mathrm{d}\xi. \tag{3.4.3}$$

Thus

$$\bar{p} \to -\frac{\bar{w}_\infty^2}{2} + \int_0^\infty \hat{a}_1 A e^{\hat{a}_1\xi}\frac{\hat{a}_2 e^{\hat{a}_1\xi}}{1+\hat{a}_3 e^{\hat{a}_1\xi}}\,\mathrm{d}\xi = \bar{p}_\infty, \tag{3.4.4}$$

where for ease of notation we write

$$\begin{aligned}
\hat{a}_1 &= \frac{\bar{w}_\infty}{1+c_0},\\
\hat{a}_2 &= \frac{k^2 c_0(n-1)\bar{w}_\infty^2(A^2+B^2)}{(1+c_0)^2},\\
\hat{a}_3 &= \frac{\hat{a}_2}{(n-1)c_0}.
\end{aligned}$$

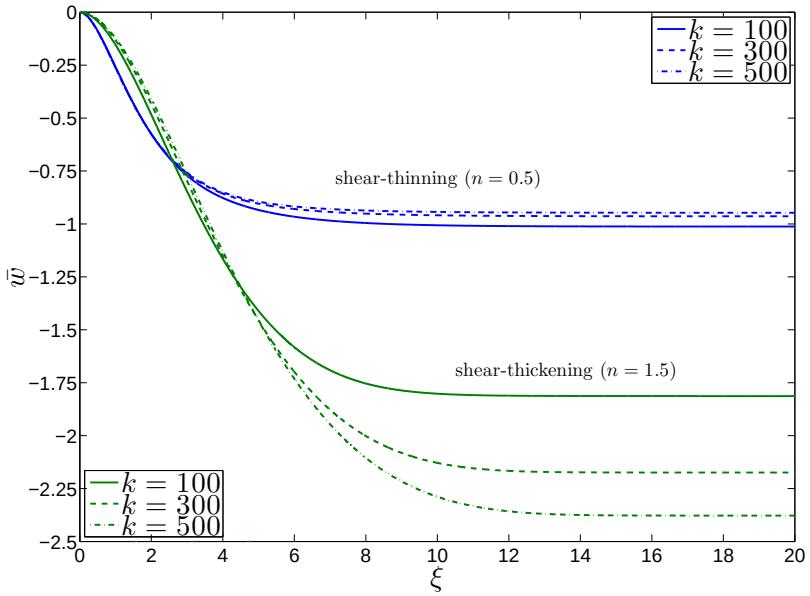

Figure 3.12: The axial velocity function $\bar{w}$ versus ξ for shear-thinning and shear-thickening Carreau fluids with $k = 100$, 300, 500.

Computing the integral above gives

$$\bar{p} = -\frac{\bar{w}_\infty^2}{2} + (n-1)c_0 A\left[\frac{\ln(1+\hat{a}_3)}{\hat{a}_3} - 1\right] + \cdots \quad \text{as} \quad \xi \to \infty. \tag{3.4.5}$$

We see that as n reduces from unity the value of $\bar{p}_\infty$ increases. This is largely due to the increasing nature of $\bar{w}_\infty$ in this case. For shear-thickening fluids we observe that the logarithmic term starts to dominate the decay, although $\bar{w}_\infty$ decreases with n it is not sufficient to overcome the positive correction term and hence, for highly shear-thickening fluids, we see that $\bar{p}_\infty$ again increases. Figure 3.11 suggests that there is a critical value of $n > 1$ at which $\bar{p}_\infty$ attains a minimal value.

In order to investigate the effect the dimensionless relaxation time has on the boundary-layer flow, we fix the value of n whilst varying the value of k, examining both the shear-thinning and shear-thickening cases when $n = 0.5$ and $n = 1.5$, respectively.

Figure 3.12 plots axial velocity profiles against ξ for $0 \leq \xi \leq 20$. We observe that

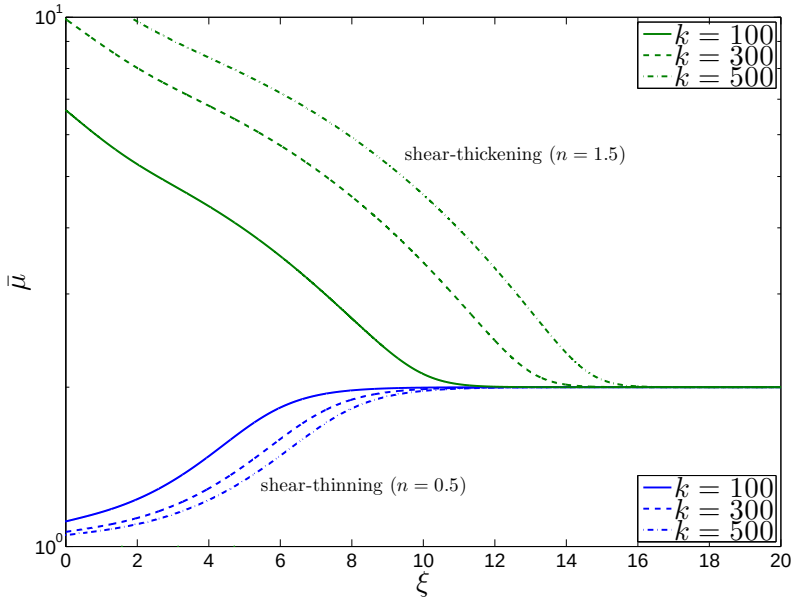

Figure 3.13: The viscosity function $\bar{\mu}$ versus ξ for shear-thinning and shear-thickening Carreau fluids with $k = 100$, 300, 500.

increasing the value of the relaxation parameter has little effect on the velocity profile for shear-thinning fluids, whereas for shear-thickening fluids the effect is much more noticeable. In accordance with Dabrowski (2004) we note that the boundary-layer thickness is increased as k increases for shear-thickening fluids, and whilst marginal, the boundary-layer thickness decreases as k increases for shear-thinning fluids. A similar trend is observed in figure 3.13. Clearly the value k takes has quite a significant effect on the viscosity profile for shear-thickening fluids, much less so for shear-thinning fluids. In order to maintain consistency throughout the remainder of this thesis we choose to fix the value of k at $k = 100$, unless otherwise stated.

Chapter 4

Asymptotic Analysis - The Type I Inviscid Modes

Having obtained solutions for the base flow velocity profiles we are now in a position to proceed with an asymptotic linear stability analysis in the limit of large Reynolds number. In this chapter we will investigate the stability of the inviscid stationary spiral vortices that have been observed in both Newtonian and non-Newtonian rotating disk flows. We will follow the structure presented by Hall (1986). This type of asymptotic study gives predictions for the wavenumber and wave angle of the spiral vortices for both the inviscid and viscous modes of instability. In this chapter we consider the inviscid (type I) modes, corresponding to the upper-branch of the neutral curve. This form of asymptotic analysis has been utilised and extended in a number of previous studies, notably in the problem of the flow due to a rotating cone (see Garrett *et al.* 2009) and also the Bödewadt problem (see MacKerrell 2005). The power-law analysis presented in this chapter appears in the literature as Griffiths *et al.* (2014*a*).

Here, as in the Newtonian analysis, we observe the existence of three distinct layers. An inviscid layer, or zone, a wall layer and a critical layer. The inviscid zone encompasses the entirety of the boundary-layer; the wall layer is needed to ensure the no-slip condition

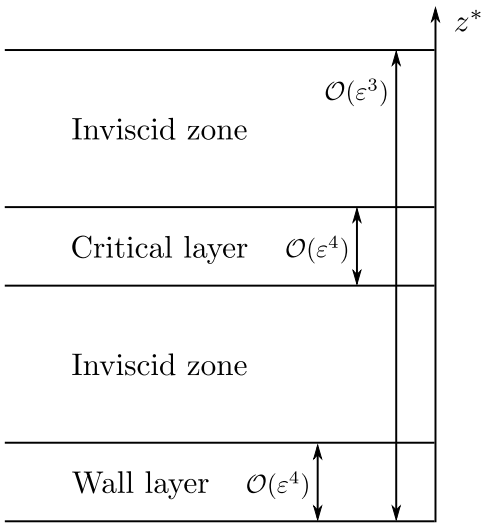

Figure 4.1: Schematic diagram showing the inviscid mode structure inside the rotating disk boundary-layer. The small parameter ε, scaled on the boundary-layer thickness δ, will be defined subsequently.

at the wall is satisfied; and the critical layer exists so that the singularities that arise within the inviscid zone are smoothed out. This structure is outlined schematically in figure 4.1.

A detailed analysis is presented firstly for case I. The analysis for Bingham and Carreau fluid models follows, although for brevity suitably less detail is provided in these cases. Throughout this chapter we will use the notation (u_i, v_i, w_i) and p_i for $i = 0, 1, 2, \cdots$ to define the inviscid zone expansions of the velocity and pressure perturbations. Likewise we use (U_i, V_i, W_i) and P_i for $i = 0, 1, 2, \cdots$ to define the wall layer expansions of the velocity and pressure perturbations. This is consistent with previous investigations, and should not be confused with the notation used in boundary-layer expansions presented in chapters 2 & 3.

4.1 Case I: Power-law

We begin by formulating our disturbance equations. By perturbing the base flow velocity and pressure profiles we determine a new set of equations that govern the structure of

the disturbances. In order to model the initial growth of the disturbances we eliminate non-linear terms and present a linear stability analysis. The corresponding Newtonian non-linear problem has been considered by Gajjar (2007). This non-linear analysis proves to be very involved. It can therefore be foreseen that the inclusion of additional, non-Newtonian, viscous terms would only serve to significantly complicate what is already an extensive mathematical challenge.

4.1.1 Linear disturbance equations

In order to derive the linear disturbance equations we must first recall the full scaled governing equations (2.2.11) and (2.2.18). Again we wish to return to an unscaled frame of reference. So, as before, we rewrite the velocity functions (U, V, W), pressure P and modified viscosity function $\tilde{\mu}$ in terms of the outer region coordinate z, whilst also removing the boundary-layer scaling on the axial velocity component so that

$$[u(r,\theta,z), v(r,\theta,z), w(r,\theta,z)] = [U(r,\theta,Z), V(r,\theta,Z), Re^{-1/(n+1)}W(r,\theta,Z)], \tag{4.1.1a}$$

$$p(r,\theta,z) = P(r,\theta,Z), \quad \mu(r,\theta,z) = \tilde{\mu}(r,\theta,Z). \tag{4.1.1b}$$

Therefore the dimensionless continuity and Navier-Stokes equations in three dimensions are given by

$$\frac{1}{r}\frac{\partial(ru)}{\partial r} + \frac{1}{r}\frac{\partial v}{\partial \theta} + \frac{\partial w}{\partial z} = 0, \tag{4.1.2a}$$

$$\frac{\partial u}{\partial t} + u\frac{\partial u}{\partial r} + \frac{v}{r}\frac{\partial u}{\partial \theta} + w\frac{\partial u}{\partial z} - \frac{(v+r)^2}{r} = -\frac{\partial p}{\partial r} + \frac{1}{Re}\left[\frac{\partial}{\partial z}\left(\mu\frac{\partial u}{\partial z}\right) + \mathcal{T}_r\right], \tag{4.1.2b}$$

$$\frac{\partial v}{\partial t} + u\frac{\partial v}{\partial r} + \frac{v}{r}\frac{\partial v}{\partial \theta} + w\frac{\partial v}{\partial z} + \frac{uv}{r} + 2u = -\frac{1}{r}\frac{\partial p}{\partial \theta} + \frac{1}{Re}\left[\frac{\partial}{\partial z}\left(\mu\frac{\partial v}{\partial z}\right) + \mathcal{T}_\theta\right], \tag{4.1.2c}$$

$$\begin{aligned}\frac{\partial w}{\partial t} + u\frac{\partial w}{\partial r} + \frac{v}{r}\frac{\partial w}{\partial \theta} + w\frac{\partial w}{\partial z} = -\frac{\partial p}{\partial z} + \frac{1}{Re}\Bigg[&\frac{1}{r}\frac{\partial}{\partial r}\left(\mu r\frac{\partial u}{\partial z}\right) \\ &+ \frac{1}{r}\frac{\partial}{\partial \theta}\left(\mu\frac{\partial v}{\partial z}\right) + 2\frac{\partial}{\partial z}\left(\mu\frac{\partial w}{\partial z}\right) + \mathcal{T}_z\Bigg],\end{aligned} \tag{4.1.2d}$$

where

$$\mu = \left[\left(\frac{\partial u}{\partial z}\right)^2 + \left(\frac{\partial v}{\partial z}\right)^2 + \mathcal{T}_\mu\right]^{(n-1)/2}. \tag{4.1.2e}$$

Here the additional viscous terms $\mathcal{T}_r$, $\mathcal{T}_\theta$, $\mathcal{T}_z$ and $\mathcal{T}_\mu$ will not appear in any of the succeeding analyses and have therefore been omitted. The form of these additional terms is given in the appendix B, these are equivalent to the $\mathcal{O}(Re^{-\frac{2}{n+1}})$ and $\mathcal{O}(Re^{-\frac{4}{n+1}})$ terms given in (2.2.18).

We now perturb the base flow by writing

$$(u, v, w) = \boldsymbol{u} + [U_d(r,\theta,z), V_d(r,\theta,z), W_d(r,\theta,z)], \tag{4.1.3}$$

where U_d, V_d and W_d are the disturbance velocities. Substituting (4.1.3) into (4.1.2), assuming steady flow and linearising gives the following disturbance equations

$$\frac{1}{r}\frac{\partial(rU_d)}{\partial r} + \frac{1}{r}\frac{\partial V_d}{\partial \theta} + \frac{\partial W_d}{\partial z} = 0, \tag{4.1.4a}$$

$$\begin{aligned} r\bar{u}\frac{\partial U_d}{\partial r} + \bar{v}\frac{\partial U_d}{\partial \theta} + \bar{\bar{w}}\frac{\partial U_d}{\partial z} + rU_d\frac{\partial \bar{u}}{\partial r} + \bar{u}U_d - 2(\bar{v}+1)V_d + rW_d\frac{\partial \bar{u}}{\partial z} &= -\frac{\partial P_d}{\partial r} \\ &+ \frac{1}{Re}\frac{\partial}{\partial z}\left(\hat{\mu}\frac{\partial U_d}{\partial z} + r\hat{\hat{\mu}}\frac{\partial \bar{u}}{\partial z}\right), \end{aligned} \tag{4.1.4b}$$

$$\begin{aligned} r\bar{u}\frac{\partial V_d}{\partial r} + \bar{v}\frac{\partial V_d}{\partial \theta} + \bar{\bar{w}}\frac{\partial V_d}{\partial z} + rU_d\frac{\partial \bar{v}}{\partial r} + \bar{u}V_d + 2(\bar{v}+1)U_d + rW_d\frac{\partial \bar{v}}{\partial z} &= -\frac{1}{r}\frac{\partial P_d}{\partial \theta} \\ &+ \frac{1}{Re}\frac{\partial}{\partial z}\left(\hat{\mu}\frac{\partial V_d}{\partial z} + r\hat{\hat{\mu}}\frac{\partial \bar{v}}{\partial z}\right), \end{aligned} \tag{4.1.4c}$$

$$\begin{aligned} r\bar{u}\frac{\partial W_d}{\partial r} + \bar{v}\frac{\partial W_d}{\partial \theta} + \bar{\bar{w}}\frac{\partial W_d}{\partial z} + U_d\left[\frac{\bar{\bar{w}}(n-1)}{r(n+1)} + \frac{\partial \bar{\bar{w}}}{\partial r}\right] + W_d\frac{\partial \bar{\bar{w}}}{\partial z} &= -\frac{\partial P_d}{\partial z} \\ &+ \frac{1}{Re}\left\{\frac{1}{r}\frac{\partial}{\partial r}\left[r\left(\hat{\mu}\frac{\partial U_d}{\partial z} + r\hat{\hat{\mu}}\frac{\partial \bar{u}}{\partial z}\right)\right]\right. \\ &+ \frac{1}{r}\frac{\partial}{\partial \theta}\left(\hat{\mu}\frac{\partial V_d}{\partial z} + r\hat{\hat{\mu}}\frac{\partial \bar{v}}{\partial z}\right) \\ &\left.+ 2\frac{\partial}{\partial z}\left(\hat{\mu}\frac{\partial W_d}{\partial z} + \hat{\hat{\mu}}\frac{\partial \bar{\bar{w}}}{\partial z}\right)\right\}, \end{aligned} \tag{4.1.4d}$$

where P_d is the non-dimensional pressure perturbation and $\bar{\bar{w}} = r^{(n-1)/(n+1)} Re^{-1/(n+1)} \bar{w}$. The 'unperturbed' viscosity function $\hat{\mu}$ is given by

$$\hat{\mu} = \left[\left(r \frac{\partial \bar{u}}{\partial z} \right)^2 + \left(r \frac{\partial \bar{v}}{\partial z} \right)^2 \right]^{(n-1)/2}. \tag{4.1.4e}$$

The 'perturbed' viscosity function $\hat{\hat{\mu}}$ appears here due to the first-order cross-product terms associated with the generalised binomial expansion of (4.1.2e). It takes the form

$$\hat{\hat{\mu}} = r(n-1) \left(\frac{\partial \bar{u}}{\partial z} \frac{\partial U_d}{\partial z} + \frac{\partial \bar{v}}{\partial z} \frac{\partial V_d}{\partial z} \right) \left[\left(r \frac{\partial \bar{u}}{\partial z} \right)^2 + \left(r \frac{\partial \bar{v}}{\partial z} \right)^2 \right]^{(n-3)/2}. \tag{4.1.4f}$$

We note that this term is linear with respect to the disturbance quantities.

4.1.2 Zero-order inviscid zone analysis

Since we have assumed a high Reynolds number flow our small parameter ε is defined as $\varepsilon = \delta^{1/3} = Re^{-1/[3(n+1)]}$. Following Hall (1986) we stipulate that the disturbance velocities and pressure take the form

$$U_d = \tilde{u}(r,z)E, \quad V_d = \tilde{v}(r,z)E, \quad W_d = \tilde{w}(r,z)E, \quad P_d = \tilde{p}(r,z)E,$$

where the exponential E is given by

$$E = \exp\left[\frac{\mathrm{i}}{\varepsilon^3} \left(\int^r \alpha(r,\varepsilon)\, \mathrm{d}r + \theta\beta(\varepsilon) \right) \right]. \tag{4.1.5}$$

Here α is the radial wavenumber and β the azimuthal wavenumber. We define the angle of the spiral vortices (or wave angle), denoted throughout by ϕ, as the angle between the normal $\boldsymbol{n}$, to the radius vector $\boldsymbol{r}$ and the tangent to the spiral t. This is depicted in figure

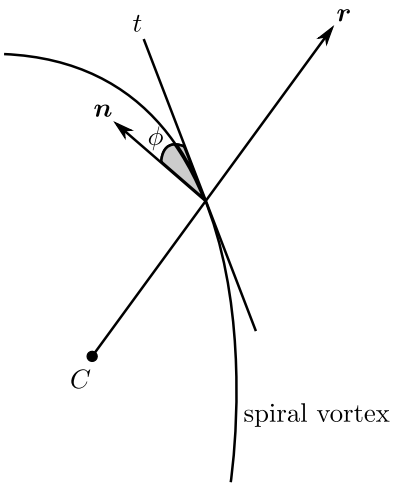

Figure 4.2: Schematic diagram showing the orientation of the wave angle. Here $\boldsymbol{r}$ is the radius vector, t is the tangent to the spiral, $\boldsymbol{n}$ is the normal vector and C is the centre of the disk. The radial wavenumber α propagates along $\boldsymbol{r}$ whilst the azimuthal wavenumber, at a specific radius along the disk, β/r, propagates along $\boldsymbol{n}$.

4.2. From this definition we have that the wave angle ϕ is given by

$$\tan\left(\frac{\pi}{2}-\phi\right)=\frac{\alpha r}{\beta} \implies \phi=\frac{\pi}{2}-\arctan\left(\frac{\alpha r}{\beta}\right). \tag{4.1.6}$$

We see the inclusion of the ε^3 term in (4.1.5) as we expect from Gregory *et al.* (1955) that these modes will have wavelengths scaled on the boundary-layer thickness. Hence we are considering modes with a lengthscale of order $Re^{-1/(n+1)}$ in the radial and azimuthal directions.

We expand the radial and azimuthal wavenumbers α and β as such

$$\alpha=\alpha_0+\varepsilon\alpha_1+\cdots, \tag{4.1.7a}$$

$$\beta=\beta_0+\varepsilon\beta_1+\cdots, \tag{4.1.7b}$$

and seek neutrally stable disturbances, thus $\alpha,\beta\in\mathbb{R}$. The inviscid zone encompasses the entirety of the boundary-layer and therefore has thickness $\mathcal{O}(\varepsilon^3)$. Inside the inviscid zone the velocity and pressure perturbations are expanded in the form

$$\tilde{u} = u_0(\eta) + \varepsilon u_1(\eta) + \cdots , \tag{4.1.8a}$$

$$\tilde{v} = v_0(\eta) + \varepsilon v_1(\eta) + \cdots , \tag{4.1.8b}$$

$$\tilde{w} = w_0(\eta) + \varepsilon w_1(\eta) + \cdots , \tag{4.1.8c}$$

$$\tilde{p} = p_0(\eta) + \varepsilon p_1(\eta) + \cdots , \tag{4.1.8d}$$

where $\eta = r^{(1-n)/(n+1)}\varepsilon^{-3}z$. The preceding expansions are then substituted into the linearised disturbance equations along with the following forms for the differential operators when applied to the disturbance quantities

$$\frac{\partial}{\partial r} = \frac{\eta(1-n)}{r(n+1)}\frac{\partial}{\partial \eta} + \left(\frac{\mathrm{i}}{\varepsilon^3}\right)(\alpha_0 + \varepsilon\alpha_1 + \cdots), \quad \frac{\partial}{\partial \theta} = \left(\frac{\mathrm{i}}{\varepsilon^3}\right)(\beta_0 + \varepsilon\beta_1 + \cdots).$$

Thus (4.1.4) yields

$$\begin{aligned}
&\left[\frac{\eta(1-n)}{r(n+1)}\frac{\partial}{\partial \eta} + \mathrm{i}\varepsilon^{-3}(\alpha_0 + \varepsilon\alpha_1 + \cdots) + \frac{1}{r}\right](u_0 + \varepsilon u_1 + \cdots) \\
&+ \frac{\mathrm{i}\varepsilon^{-3}(\beta_0 + \varepsilon\beta_1 + \cdots)(v_0 + \varepsilon v_1 + \cdots)}{r} + \varepsilon^{-3}r^{(1-n)/(n+1)}\frac{\partial(w_0 + \varepsilon w_1 + \cdots)}{\partial \eta} \\
&= 0,
\end{aligned} \tag{4.1.9a}$$

$$\begin{aligned}
&\left[\frac{\eta\bar{u}(1-n)}{(n+1)}\frac{\partial}{\partial \eta} + \mathrm{i}\varepsilon^{-3}r\bar{u}(\alpha_0 + \varepsilon\alpha_1 + \cdots) + \mathrm{i}\varepsilon^{-3}\bar{v}(\beta_0 + \varepsilon\beta_1 + \cdots) + \bar{w}\frac{\partial}{\partial \eta}\right] \\
&\times (u_0 + \varepsilon u_1 + \cdots) + \frac{\eta\bar{u}'(1-n)}{(n+1)}(u_0 + \varepsilon u_1 + \cdots) + \bar{u}(u_0 + \varepsilon u_1 + \cdots) \\
&- 2(\bar{v}+1)(v_0 + \varepsilon v_1 + \cdots) + \varepsilon^{-3}r^{2/(n+1)}\bar{u}'(w_0 + \varepsilon w_1 + \cdots) \\
&= -\left[\frac{\eta(1-n)}{r(n+1)}\frac{\partial}{\partial \eta} + \mathrm{i}\varepsilon^{-3}(\alpha_0 + \varepsilon\alpha_1 + \cdots)\right](p_0 + \varepsilon p_1 + \cdots) \\
&+ \frac{\partial}{\partial \eta}\left\{\bar{\mu}\frac{\partial(u_0 + \varepsilon u_1 + \cdots)}{\partial \eta} + \frac{\bar{u}'\bar{\mu}(n-1)}{\bar{u}'^2 + \bar{v}'^2}\left[\bar{u}'\frac{\partial(u_0 + \varepsilon u_1 + \cdots)}{\partial \eta}\right.\right. \\
&\left.\left. + \bar{v}'\frac{\partial(v_0 + \varepsilon v_1 + \cdots)}{\partial \eta}\right]\right\},
\end{aligned} \tag{4.1.9b}$$

$$\left[\frac{\eta\bar{u}(1-n)}{(n+1)}\frac{\partial}{\partial\eta}+\mathrm{i}\varepsilon^{-3}r\bar{u}(\alpha_0+\varepsilon\alpha_1+\cdots)+\mathrm{i}\varepsilon^{-3}\bar{v}(\beta_0+\varepsilon\beta_1+\cdots)+\bar{w}\frac{\partial}{\partial\eta}\right]$$
$$\times(v_0+\varepsilon v_1+\cdots)+\frac{\eta\bar{v}'(1-n)}{(n+1)}(u_0+\varepsilon u_1+\cdots)+\bar{u}(v_0+\varepsilon v_1+\cdots)$$
$$+2(\bar{v}+1)(u_0+\varepsilon u_1+\cdots)+\varepsilon^{-3}r^{2/(n+1)}\bar{v}'(w_0+\varepsilon w_1+\cdots)$$
$$=-\frac{\mathrm{i}\varepsilon^{-3}(\beta_0+\varepsilon\beta_1+\cdots)(p_0+\varepsilon p_1+\cdots)}{r}$$
$$+\frac{\partial}{\partial\eta}\left\{\bar{\mu}\frac{\partial(v_0+\varepsilon v_1+\cdots)}{\partial\eta}+\frac{\bar{v}'\bar{\mu}(n-1)}{\bar{u}'^2+\bar{v}'^2}\left[\bar{u}'\frac{\partial(u_0+\varepsilon u_1+\cdots)}{\partial\eta}\right.\right.$$
$$\left.\left.+\bar{v}'\frac{\partial(v_0+\varepsilon v_1+\cdots)}{\partial\eta}\right]\right\}, \tag{4.1.9c}$$

$$\left[\frac{\eta\bar{u}(1-n)}{(n+1)}\frac{\partial}{\partial\eta}+\mathrm{i}r\bar{u}\varepsilon^{-3}(\alpha_0+\varepsilon\alpha_1+\cdots)+\mathrm{i}\bar{v}\varepsilon^{-3}(\beta_0+\varepsilon\beta_1+\cdots)+\bar{w}\frac{\partial}{\partial\eta}\right]$$
$$\times(w_0+\varepsilon w_1+\cdots)+\varepsilon^3r^{-2/(n+1)}\frac{(n-1)}{(n+1)}(\bar{w}-\eta\bar{w}')(u_0+\varepsilon u_1+\cdots)$$
$$+\bar{w}'(w_0+\varepsilon w_1+\cdots)=-\varepsilon^{-3}r^{(1-n)/(n+1)}\frac{\partial(p_0+\varepsilon p_1+\cdots)}{\partial\eta}$$
$$+2\frac{\partial}{\partial\eta}\left\{\bar{\mu}\frac{\partial(w_0+\varepsilon w_1+\cdots)}{\partial\eta}+\varepsilon^3r^{-2/(n+1)}\frac{\bar{w}'\bar{\mu}(n-1)}{\bar{u}'^2+\bar{v}'^2}\left[\bar{u}'\frac{\partial(u_0+\varepsilon u_1+\cdots)}{\partial\eta}\right.\right.$$
$$\left.\left.+\bar{v}'\frac{\partial(v_0+\varepsilon v_1+\cdots)}{\partial\eta}\right]\right\}+\mathcal{O}(\varepsilon^3). \tag{4.1.9d}$$

Due to the relative complexity of the remaining viscous terms associated with the axial linear disturbance equation we do not state them all here, for the succeeding analysis it is enough to note that the remaining terms are of order ε^3.

Equating terms of $\mathcal{O}(\varepsilon^{-3})$ we have that

$$\mathrm{i}\alpha_0u_0+\frac{\mathrm{i}\beta_0v_0}{r}+r^{(1-n)/(n+1)}w_0'=0, \tag{4.1.10a}$$
$$\mathrm{i}\bar{\bar{u}}u_0+r^{2/(n+1)}w_0\bar{u}'+\mathrm{i}\alpha_0p_0=0, \tag{4.1.10b}$$
$$\mathrm{i}\bar{\bar{u}}v_0+r^{2/(n+1)}w_0\bar{v}'+\frac{\mathrm{i}\beta_0p_0}{r}=0, \tag{4.1.10c}$$
$$\mathrm{i}\bar{\bar{u}}w_0+r^{(1-n)/(n+1)}p_0'=0, \tag{4.1.10d}$$

where $\bar{\bar{u}} = \alpha_0 \bar{u} r + \beta_0 \bar{v}$ and the primes denote differentiation with respect to η. Rearranging (4.1.10b) and (4.1.10c) we have that

$$u_0 = \frac{\mathrm{i} r^{2/(n+1)} w_0 \bar{u}' - \alpha_0 p_0}{\bar{\bar{u}}},$$
$$v_0 = \frac{\mathrm{i} r^{(n+3)/(n+1)} w_0 \bar{v}' - \beta_0 p_0}{r \bar{\bar{u}}}.$$

Hence (4.1.10a) becomes

$$r^{(1-n)/(n+1)} w_0' \bar{\bar{u}} = r^{(1-n)/(n+1)} w_0 \bar{\bar{u}}' + \mathrm{i} \gamma_0^2 p_0,$$

where $\gamma_0^2 = \alpha_0^2 + \beta_0^2 / r^2$. Differentiating the above gives

$$r^{(1-n)/(n+1)} w_0'' \bar{\bar{u}} = r^{(1-n)/(n+1)} w_0 \bar{\bar{u}}'' + \mathrm{i} \gamma_0^2 p_0'.$$

Using (4.1.10d) we have that

$$\mathrm{i} \gamma_0^2 p_0' = \gamma_0^2 \bar{\bar{u}} w_0 r^{(n-1)/(n+1)}.$$

Hence w_0 satisfies Rayleigh's equation

$$\bar{\bar{u}} (w_0'' - \kappa_0^2 w_0) - \bar{\bar{u}}'' w_0 = 0, \tag{4.1.11}$$

where $\kappa_0^2 = r^{2(n-1)/(n+1)} (\alpha_0^2 + \beta_0^2 / r^2)$. Here $\bar{\bar{u}}$ is the effective two-dimensional velocity profile, interpreted as the basic flow resolved in the direction of the wavevector of the disturbance. The effective wavenumber of the disturbance is $\kappa_0 = r^{(n-1)/(n+1)} \sqrt{\alpha_0^2 + \beta_0^2 / r^2}$. When considering the Newtonian problem the wavenumber is given as $\gamma_0 = \sqrt{\alpha_0^2 + \beta_0^2 / r^2}$. Thus we see here that the radial and azimuthal wavenumbers are now scaled by $r^{(1-n)/(n+1)}$.

n	λ_0	$\bar{\eta}$	κ_0	ϕ_0
1	4.256	1.458	1.162	13.22°
0.9	4.086	1.455	1.149	13.75°
0.8	3.926	1.445	1.143	14.29°
0.7	3.782	1.423	1.144	14.81°
0.6	3.663	1.388	1.157	15.27°

Table 4.1: Calculated values for λ_0, $\bar{\eta}$, κ_0 and ϕ_0 for power-law fluids with $n = 1,\ 0.9,\ 0.8,\ 0.7,\ 0.6$.

We solve Rayleigh's equation for w_0 subject to the boundary conditions

$$w_0 = 0 \quad \text{at} \quad \eta = 0, \tag{4.1.12a}$$

$$w_0 \to 0 \quad \text{as} \quad \eta \to \infty. \tag{4.1.12b}$$

We choose $\lambda_0 = \alpha_0 r/\beta_0$ such that $\bar{u}$ and $\bar{u}''$ vanish at the same value of $\eta = \bar{\eta}$, ensuring that (4.1.11) is not singular at this point, see figure 4.3. As $\eta \to \bar{\eta}$ we find that

$$u_0 = \frac{\mathrm{i}r^{2/(n+1)} w_0[\bar{u}'_{\bar{\eta}} + (\eta - \bar{\eta})\bar{u}''_{\bar{\eta}} + \cdots] - \alpha_0 p_0}{[\bar{u}_{\bar{\eta}} + (\eta - \bar{\eta})\bar{u}'_{\bar{\eta}} + \cdots]} \sim \frac{\mathrm{i}r^{2/(n+1)} w_0 \bar{u}'_{\bar{\eta}} - \alpha_0 p_0}{(\eta - \bar{\eta})\bar{u}'_{\bar{\eta}}},$$
$$v_0 = \frac{\mathrm{i}r^{(n+3)/(n+1)} w_0[\bar{v}'_{\bar{\eta}} + (\eta - \bar{\eta})\bar{v}''_{\bar{\eta}} + \cdots] - \beta_0 p_0}{r[\bar{u}_{\bar{\eta}} + (\eta - \bar{\eta})\bar{u}'_{\bar{\eta}} + \cdots]} \sim \frac{\mathrm{i}r^{(n+3)/(n+1)} w_0 \bar{v}'_{\bar{\eta}} - \beta_0 p_0}{r(\eta - \bar{\eta})\bar{u}'_{\bar{\eta}}},$$

where the subscript $\bar{\eta}$ denotes evaluation at the point $\eta = \bar{\eta} > 0$. So we see that u_0 and v_0 are singular here and behave like $1/(\eta - \bar{\eta})$. However, the singularity in the combined profile, $\alpha_0 u_0 + \beta_0 v_0/r$, is removable[1]. We see from (4.1.10a) that w_0 depends only on the combination $\alpha_0 u_0 + \beta_0 v_0/r$, thus we do not need to investigate the structure of the functions u_0 and v_0 as $\eta \to \bar{\eta}$.

The eigenvalue problem was solved using a central finite difference method twinned with a Newton iteration scheme to determine the values of the leading order effective wavenumber κ_0. The results are contained within table 4.1. The eigenfunctions have

[1]Gajjar (2007) showed that the combined profile is in fact equal to zero at $\eta = \bar{\eta}$.

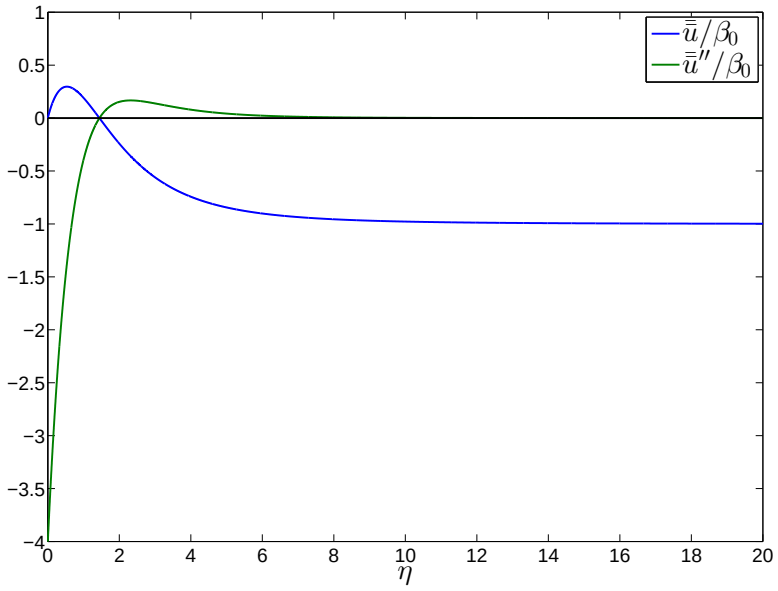

Figure 4.3: Plots of the scaled effective velocity profile $\bar{\bar{u}}/\beta_0$ and its second derivative $\bar{\bar{u}}''/\beta_0$ versus η for the case when $n = 0.8$.

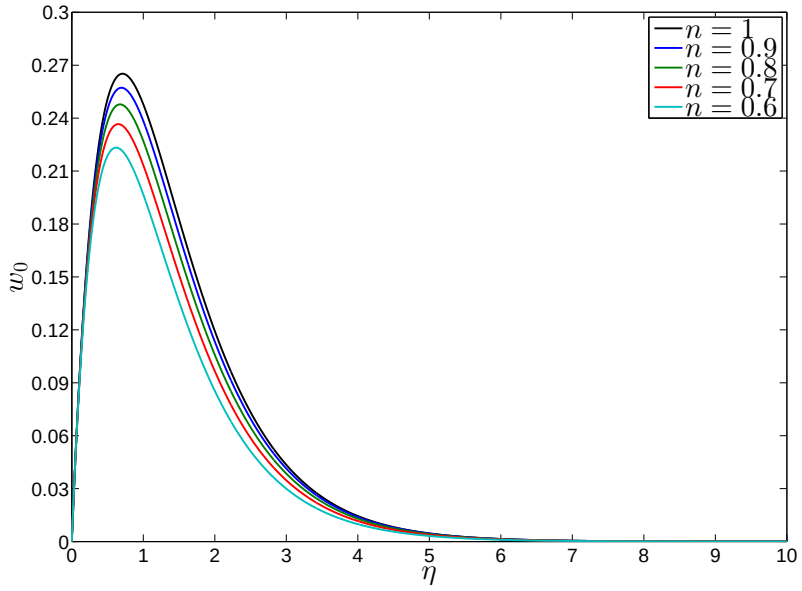

Figure 4.4: The inviscid eigenfunction w_0 versus η for power-law fluids with $n = 1,\ 0.9,\ 0.8,\ 0.7,\ 0.6$.

been normalised with $w_0'(0) = 1$ and are plotted in figure 4.4. Having calculated the ratio of $\alpha_0 r/\beta_0$ we are also able to produce values for the leading order approximation to the wave angle, $\phi_0 = \pi/2 - \arctan \lambda_0$.

4.1.3 First-order inviscid zone analysis

At the next order in the inviscid zone we find that

$$\mathrm{i}(\alpha_0 u_1 + \alpha_1 u_0) + \frac{\mathrm{i}(\beta_0 v_1 + \beta_1 v_0)}{r} + r^{(1-n)/(n+1)} w_1' = 0, \tag{4.1.13a}$$

$$\mathrm{i}\bar{\bar{u}} u_1 + \mathrm{i}\bar{\bar{v}} u_0 + r^{2/(n+1)} w_1 \bar{u}' + \mathrm{i}(\alpha_0 p_1 + \alpha_1 p_0) = 0, \tag{4.1.13b}$$

$$\mathrm{i}\bar{\bar{u}} v_1 + \mathrm{i}\bar{\bar{v}} v_0 + r^{2/(n+1)} w_1 \bar{v}' + \frac{\mathrm{i}(\beta_0 p_1 + \beta_1 p_0)}{r} = 0, \tag{4.1.13c}$$

$$\mathrm{i}\bar{\bar{u}} w_1 + \mathrm{i}\bar{\bar{v}} w_0 + r^{(1-n)/(n+1)} p_1' = 0, \tag{4.1.13d}$$

where $\bar{\bar{v}} = \alpha_1 \bar{u} r + \beta_1 \bar{v}$. Rearranging (4.1.13b) and (4.1.13c) gives respectively

$$u_1 = \frac{\mathrm{i} r^{2/(n+1)} w_1 \bar{u}' - \bar{\bar{v}} u_0 - \alpha_0 p_1 - \alpha_1 p_0}{\bar{\bar{u}}},$$
$$v_1 = \frac{\mathrm{i} r^{(n+3)/(n+1)} w_1 \bar{v}' - r \bar{\bar{v}} v_0 - \beta_0 p_1 - \beta_1 p_0}{r \bar{\bar{u}}}.$$

Hence (4.1.13a) becomes

$$r^{(1-n)/(n+1)}(w_1' \bar{\bar{u}} + w_0' \bar{\bar{v}}) = r^{(1-n)/(n+1)}(w_1 \bar{\bar{u}}' + w_0 \bar{\bar{v}}') + \mathrm{i}\gamma_0^2 p_1 + 2\mathrm{i}\left(\alpha_0\alpha_1 + \frac{\beta_0\beta_1}{r^2}\right) p_0.$$

Differentiating the above gives

$$r^{(1-n)/(n+1)}(w_1'' \bar{\bar{u}} + w_0'' \bar{\bar{v}}) = r^{(1-n)/(n+1)}(w_1 \bar{\bar{u}}'' + w_0 \bar{\bar{v}}'') + \mathrm{i}\gamma_0^2 p_1' + 2\mathrm{i}\left(\alpha_0\alpha_1 + \frac{\beta_0\beta_1}{r^2}\right) p_0'.$$

Using (4.1.13d) we have that

$$\mathrm{i}\gamma_0^2 p_1' = \gamma_0^2(\bar{\bar{u}}w_1 + \bar{\bar{v}}w_0)r^{(n-1)/(n+1)}.$$

Hence w_1 satisfies

$$\bar{\bar{u}}\left(w_1'' - \kappa_0^2 w_1\right) - \bar{\bar{u}}'' w_1 = 2\bar{\bar{u}}r^{2(n-1)/(n+1)}\left(\alpha_0\alpha_1 + \frac{\beta_0\beta_1}{r^2}\right)w_0 + \left(\bar{\bar{v}}'' - \frac{\bar{\bar{u}}''\bar{\bar{v}}}{\bar{\bar{u}}}\right)w_0. \quad (4.1.14)$$

By rewriting $\bar{\bar{v}}$ in such a way that

$$\bar{\bar{v}} = r\left(\alpha_1 - \frac{\alpha_0\beta_1}{\beta_0}\right)\bar{u} + \frac{\beta_1}{\beta_0}\bar{\bar{u}},$$

we find that w_1 satisfies the inhomogeneous form of Rayleigh's equation

$$\bar{\bar{u}}\left(w_1'' - \kappa_0^2 w_1\right) - \bar{\bar{u}}'' w_1 = 2\bar{\bar{u}}r^{2(n-1)/(n+1)}\left(\alpha_0\alpha_1 + \frac{\beta_0\beta_1}{r^2}\right)w_0 + r\left(\alpha_1 - \frac{\alpha_0\beta_1}{\beta_0}\right)\left(\bar{u}'' - \frac{\bar{u}\bar{\bar{u}}''}{\bar{\bar{u}}}\right)w_0. \quad (4.1.15)$$

Here we note that the second term on the right-hand side of (4.1.15) is singular at $\eta = \bar{\eta}$ due to the $\bar{u}\bar{\bar{u}}''/\bar{\bar{u}}$ term. We remove this singularity by placing a critical layer at $\eta = \bar{\eta}$. Henceforth $\bar{\eta}$ is referred to as the location of the critical layer. The critical layer exists in order to smooth out the singularities associated with the zeros of the effective velocity profile and its second derivative.

Gajjar (2007) completed the full non-linear analysis of the critical layer. Before considering the non-linear problem Gajjar solves the corresponding linear problem showing that the critical layer structure has thickness of $\mathcal{O}(\varepsilon^4)$ where in the Newtonian limit $\varepsilon = Re^{-1/[3(n+1)]}|_{n=1} = Re^{1/6}$. Here we find that the critical layer structure is much the same, having thickness of $\mathcal{O}(\varepsilon^4)$ with the critical layer coordinate given by

$\eta_{crit} = \varepsilon^{-1}(\eta - \bar{\eta})$.

Returning to the first-order inviscid analysis and dividing (4.1.15) by $\bar{\bar{u}}$ we find that

$$w_1'' - \kappa_0^2 w_1 - \frac{\bar{\bar{u}}''}{\bar{\bar{u}}} w_1 = 2r^{2(n-1)/(n+1)} \left(\alpha_0\alpha_1 + \frac{\beta_0\beta_1}{r^2} \right) w_0 + r \left(\alpha_1 - \frac{\alpha_0\beta_1}{\beta_0} \right) \left(\frac{\bar{u}''\bar{\bar{u}} - \bar{u}\bar{\bar{u}}''}{\bar{\bar{u}}^2} \right) w_0. \quad (4.1.16)$$

Now we let $w_1(\eta) = l(\eta)w_0(\eta)$ where $l(\eta)$ is unknown and $w_0(\eta)$ is the homogeneous solution and hence (4.1.16) becomes

$$l''w_0 + 2l'w_0' + lw_0'' - \kappa_0^2 l w_0 - \frac{\bar{\bar{u}}''}{\bar{\bar{u}}} l w_0 = 2r^{2(n-1)/(n+1)} \left(\alpha_0\alpha_1 + \frac{\beta_0\beta_1}{r^2} \right) w_0 + r \left(\alpha_1 - \frac{\alpha_0\beta_1}{\beta_0} \right) \left(\frac{\bar{u}''\bar{\bar{u}} - \bar{u}\bar{\bar{u}}''}{\bar{\bar{u}}^2} \right) w_0.$$

Multiplying the above by w_0 and using (4.1.11) yields

$$\left(l'w_0^2\right)' = 2r^{2(n-1)/(n+1)} \left(\alpha_0\alpha_1 + \frac{\beta_0\beta_1}{r^2} \right) w_0^2 + r \left(\alpha_1 - \frac{\alpha_0\beta_1}{\beta_0} \right) \left(\frac{\bar{u}''\bar{\bar{u}} - \bar{u}\bar{\bar{u}}''}{\bar{\bar{u}}^2} \right) w_0^2.$$

Hence we have that

$$\left(l'w_0^2\right) = 2r^{2(n-1)/(n+1)} \left(\alpha_0\alpha_1 + \frac{\beta_0\beta_1}{r^2} \right) \int^\eta w_0^2(\chi)\,\mathrm{d}\chi + r \left(\alpha_1 - \frac{\alpha_0\beta_1}{\beta_0} \right) \int^\eta w_0^2(\chi)\hat{U}(\chi)\,\mathrm{d}\chi,$$

where

$$\hat{U}(x) = \frac{\bar{u}''(x)\bar{\bar{u}}(x) - \bar{u}(x)\bar{\bar{u}}''(x)}{\bar{\bar{u}}^2(x)}. \quad (4.1.17)$$

Therefore l is given by

$$l = 2r^{2(n-1)/(n+1)}\left(\alpha_0\alpha_1 + \frac{\beta_0\beta_1}{r^2}\right)\int_{\bar{\bar{\eta}}}^{\eta}\frac{\mathrm{d}\chi}{w_0^2(\chi)}\int_{\infty}^{\chi} w_0^2(\theta)\,\mathrm{d}\theta + r\left(\alpha_1 - \frac{\alpha_0\beta_1}{\beta_0}\right)\int_{\bar{\bar{\eta}}}^{\eta}\frac{\mathrm{d}\chi}{w_0^2(\chi)}\int_{\infty}^{\chi} w_0^2(\theta)\hat{U}(\theta)\,\mathrm{d}\theta,$$

where $\bar{\bar{\eta}} > \bar{\eta}$. Thus the solution of (4.1.15) that satisfies $w_1 \to 0$ as $\eta \to \infty$ is

$$w_1 = 2r^{2(n-1)/(n+1)}\left(\alpha_0\alpha_1 + \frac{\beta_0\beta_1}{r^2}\right)w_0(\eta)\int_{\bar{\bar{\eta}}}^{\eta}\frac{\mathrm{d}\chi}{w_0^2(\chi)}\int_{\infty}^{\chi} w_0^2(\theta)\,\mathrm{d}\theta + r\left(\alpha_1 - \frac{\alpha_0\beta_1}{\beta_0}\right)w_0(\eta)\int_{\bar{\bar{\eta}}}^{\eta}\frac{\mathrm{d}\chi}{w_0^2(\chi)}\int_{\infty}^{\chi} w_0^2(\theta)\hat{U}(\theta)\,\mathrm{d}\theta. \quad (4.1.18)$$

Gajjar (2007) showed that if the derivative of the scaled effective velocity profile, evaluated at the critical layer, is less than zero, $\bar{\bar{u}}'(\bar{\eta})/\beta_0 < 0$, then the path of integration must be deformed above the singularity into the complex plane, whilst if $\bar{\bar{u}}'(\bar{\eta})/\beta_0 > 0$ the path of integration must be deformed below the singularity. We find that for $0.6 < n \leq 1$ the above solution is valid for $\eta < \bar{\eta}$ if the path of integration is deformed above the singularity, see table 4.2 and figure 4.5. By evaluating (4.1.18) at $\eta = 0$ we have that

$$w_1(0) = 2r^{2(n-1)/(n+1)}\left(\alpha_0\alpha_1 + \frac{\beta_0\beta_1}{r^2}\right)\frac{I_1}{w_0'(0)} + \left(\frac{\alpha_1}{\beta_0} - \frac{\alpha_0\beta_1}{\beta_0^2}\right)\frac{rI_2}{w_0'(0)}, \quad (4.1.19)$$

where

$$I_1 = \int_0^{\infty} w_0^2(\theta)\,\mathrm{d}\theta, \quad (4.1.20a)$$

$$I_2 = \beta_0\int_0^{\infty} w_0^2(\theta)\hat{U}(\theta)\,\mathrm{d}\theta. \quad (4.1.20b)$$

Trapezoidal numerical integration is used to evaluate I_1. This integral is relatively simple to compute as it depends on only the function w_0.

n	$\bar{\bar{u}}'_{\bar{\eta}}/\beta_0$
1	-0.5634
0.9	-0.5064
0.8	-0.4532
0.7	-0.4043
0.6	-0.3605

Table 4.2: Calculated values of the first derivative of the effective velocity profile evaluated at the critical layer for power-law fluids with $n = 1$, 0.9, 0.8, 0.7, 0.6.

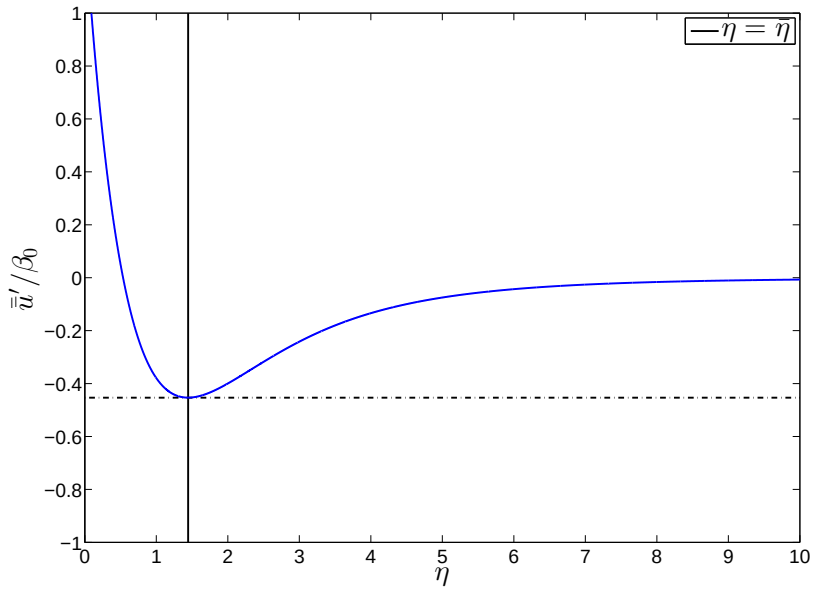

Figure 4.5: Plot of the first derivative of the scaled effective velocity profile $\bar{\bar{u}}'/\beta_0$ versus η for the case when $n = 0.8$. We see that $\bar{\bar{u}}'_{\bar{\eta}} < 0$.

In order to compute I_2 we use a fixed-step Simpson's rule numerical integration technique. Taking the singularity into account we integrate from $\eta = 0$ to below the singularity at $\eta = \bar{\eta} - \eta_s$ and then from above the singularity at $\eta = \bar{\eta} + \eta_s$ to a suitably large value of η. The value of η_s is chosen such that the real part of I_2 is maximised. For all of the following calculations $\eta_s = 0.0260$. In order to compute the contribution from the critical

n	I_1	I_2
1	0.0911	$0.0592 + 0.0299\mathrm{i}$
0.9	0.0848	$0.0619 + 0.0291\mathrm{i}$
0.8	0.0774	$0.0653 + 0.0281\mathrm{i}$
0.7	0.0689	$0.0671 + 0.0270\mathrm{i}$
0.6	0.0594	$0.0691 + 0.0255\mathrm{i}$

Table 4.3: Numerical values of the integrals I_1 and I_2 for power-law fluids with $n = 1,\ 0.9,\ 0.8,\ 0.7,\ 0.6$.

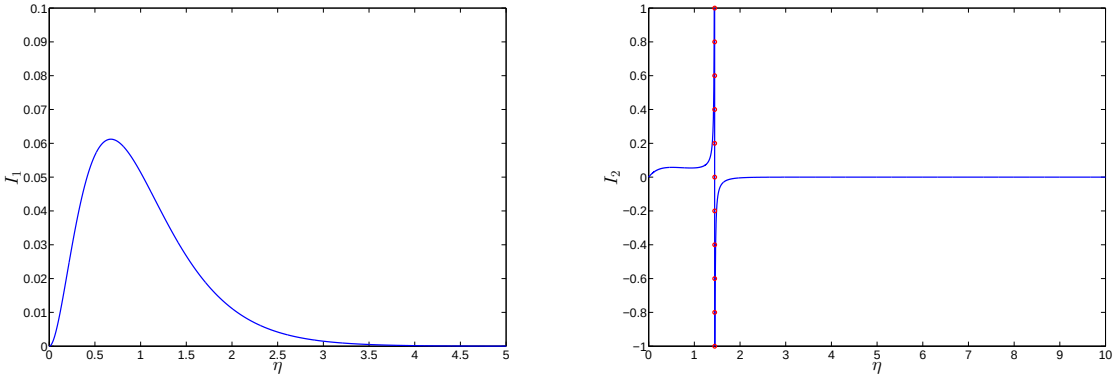

Figure 4.6: The integrands I_1 and I_2 versus η for the case when $n = 0.8$. The singularity is observed at the location of the critical layer $\eta = \bar{\eta}$.

layer we evaluate half the complex residue of the function

$$F(\eta) = \beta_0 w_0^2(\eta) \frac{\bar{u}''(\eta)\bar{\bar{u}}(\eta) - \bar{u}(\eta)\bar{\bar{u}}''(\eta)}{\bar{\bar{u}}^2(\eta)},$$

at $\eta = \bar{\eta}$, since I_2 has a simple pole at $\eta = \bar{\eta}$. After performing a Taylor expansion about $\eta = \bar{\eta}$ we find that

$$F(\bar{\eta}) = \beta_0 w_0^2 \frac{\bar{u}''\bar{\bar{u}}' - \bar{u}\bar{\bar{u}}'''}{(\eta - \bar{\eta})\bar{\bar{u}}'^2}\bigg|_{\eta=\bar{\eta}} = w_0^2 \frac{\bar{u}''(\lambda_0\bar{u}' + \bar{v}') - \bar{u}(\lambda_0\bar{u}''' + \bar{v}''')}{(\lambda_0\bar{u}' + \bar{v}')^2}\bigg|_{\eta=\bar{\eta}}.$$

By the residue theorem we have that $\mathrm{Res}(F, \bar{\eta}) = \lim_{\eta\to\bar{\eta}}(\eta - \bar{\eta})F(\eta)$ so that the contribution

from the singularity is given by

$$\mathrm{Im}(I_2) = -\pi \mathrm{Res}(F, \bar{\eta}) = -\pi w_0^2 \frac{\bar{u}''(\lambda_0 \bar{u}' + \bar{v}') - \bar{u}(\lambda_0 \bar{u}''' + \bar{v}''')}{(\lambda_0 \bar{u}' + \bar{v}')^2}\bigg|_{\eta=\bar{\eta}}.$$

Our numerical calculations for both the integrals I_1 and I_2 are displayed in table 4.3.

In order to satisfy the no-slip boundary condition at the wall a viscous wall layer must exist. We investigate the asymptotic structure of the solutions within this layer in the following subsection.

4.1.4 Wall layer analysis

Having calculated the zero-order and first-order solutions in the inviscid zone let us now go on to calculate the zero-order solution in the wall layer. The solution from this layer is required to match with the first-order solution in the inviscid zone, ensuring that the no-slip boundary condition on this disk is satisfied.

The wall layer is scaled by $Re^{-4/[3(n+1)]}$ so we define a new wall layer coordinate η_w by

$$\eta_w = r^{(1-n)/(n+1)} \varepsilon^{-4} z.$$

By performing a Taylor expansion of the base flow velocities as $\eta \to 0$ and noting that $\eta = \varepsilon \eta_w$ and $\bar{w}'(0) = 0$ we find that

$$\bar{u} = \varepsilon \eta_w \bar{u}_0 + \varepsilon^2 \eta_w^2 \bar{u}_1 + \cdots, \tag{4.1.21a}$$

$$\bar{v} = \varepsilon \eta_w \bar{v}_0 + \varepsilon^2 \eta_w^2 \bar{v}_1 + \cdots, \tag{4.1.21b}$$

$$\bar{w} = \varepsilon^2 \eta_w^2 \bar{w}_1 + \varepsilon^3 \eta_w^3 \bar{w}_2 + \cdots, \tag{4.1.21c}$$

where here

$$(\bar{u}_{j-1}, \bar{v}_{j-1}, \bar{w}_{j-1}) = \frac{[\bar{u}^j(0), \bar{v}^j(0), \bar{w}^j(0)]}{j!} \quad \text{for} \quad j = 1, 2, 3, \ldots.$$

As $\eta \to 0$ the disturbance velocities u_0 and v_0 are given respectively by

$$\begin{aligned}
u_0 &= \frac{\mathrm{i}r^{2/(n+1)}[w_0(0) + \varepsilon\eta_w w_0'(0) + \cdots]\bar{u}_0 - \alpha_0[p_0(0) + \varepsilon\eta_w p_0'(0) + \cdots]}{\varepsilon\eta_w \bar{\bar{u}}_0}, \\
&\sim \frac{\mathrm{i}r^{2/(n+1)} w_0'(0)\bar{u}_0}{\bar{\bar{u}}_0}, \\
v_0 &= \frac{\mathrm{i}r^{(n+3)/(n+1)}[w_0(0) + \varepsilon\eta_w w_0'(0) + \cdots]\bar{v}_0 - \beta_0[p_0(0) + \varepsilon\eta_w p_0'(0) + \cdots]}{r\varepsilon\eta_w \bar{\bar{u}}_0}, \\
&\sim \frac{\mathrm{i}r^{2/(n+1)} w_0'(0)\bar{v}_0}{\bar{\bar{u}}_0}.
\end{aligned}$$

Here we utilise the boundary condition $p_0 = 0$ at $\eta = 0$.

As in the Newtonian case we expand the disturbance velocity and pressure terms as

$$\tilde{u} = U_0(\eta_w) + \varepsilon U_1(\eta_w) + \cdots, \tag{4.1.22a}$$

$$\tilde{v} = V_0(\eta_w) + \varepsilon V_1(\eta_w) + \cdots, \tag{4.1.22b}$$

$$\tilde{w} = \varepsilon W_0(\eta_w) + \varepsilon^2 W_1(\eta_w) + \cdots, \tag{4.1.22c}$$

$$\tilde{p} = \varepsilon P_0(\eta_w) + \varepsilon^2 P_1(\eta_w) + \cdots. \tag{4.1.22d}$$

This ensures that the solution within the wall layer matches that in the inviscid zone. We note here that the axial velocity and pressure perturbation terms are both scaled by ε. The preceding expansions are then substituted into the linearised disturbance equations along with the following forms for the differential operators when applied to the disturbance quantities

$$\frac{\partial}{\partial r} = \frac{\eta_w(1-n)}{r(n+1)}\frac{\partial}{\partial \eta_w} + \left(\frac{\mathrm{i}}{\varepsilon^3}\right)(\alpha_0 + \varepsilon\alpha_1 + \cdots), \quad \frac{\partial}{\partial \theta} = \left(\frac{\mathrm{i}}{\varepsilon^3}\right)(\beta_0 + \varepsilon\beta_1 + \cdots).$$

Thus (4.1.4) yields

$$\left[\frac{\eta_w(1-n)}{r(n+1)}\frac{\partial}{\partial\eta_w}+\mathrm{i}\varepsilon^{-3}(\alpha_0+\varepsilon\alpha_1+\cdots)+\frac{1}{r}\right](U_0+\varepsilon U_1+\cdots)$$
$$+\frac{\mathrm{i}\varepsilon^{-3}(\beta_0+\varepsilon\beta_1+\cdots)(V_0+\varepsilon V_1+\cdots)}{r}+\varepsilon^{-4}r^{(1-n)/(n+1)}\frac{\partial(\varepsilon W_0+\varepsilon^2W_1+\cdots)}{\partial\eta_w}$$
$$=0, \tag{4.1.23a}$$

$$\left[\frac{\eta_w(\varepsilon\eta_w\bar{u}_0+\varepsilon^2\eta_w^2\bar{u}_1+\cdots)(1-n)}{(n+1)}\frac{\partial}{\partial\eta_w}+\mathrm{i}\varepsilon^{-3}r(\varepsilon\eta_w\bar{u}_0+\varepsilon^2\eta_w^2\bar{u}_1+\cdots)(\alpha_0+\varepsilon\alpha_1+\cdots)\right.$$
$$\left.+\mathrm{i}\varepsilon^{-3}(\varepsilon\eta_w\bar{v}_0+\varepsilon^2\eta_w^2\bar{v}_1+\cdots)(\beta_0+\varepsilon\beta_1+\cdots)+\varepsilon^{-1}(\varepsilon^2\eta_w^2\bar{w}_1+\varepsilon^3\eta_w^3\bar{w}_2+\cdots)\frac{\partial}{\partial\eta_w}\right]$$
$$\times(U_0+\varepsilon U_1+\cdots)+\frac{\varepsilon\eta_w(\bar{u}_0+2\varepsilon\eta_w\bar{u}_1+\cdots)(1-n)}{(n+1)}(U_0+\varepsilon U_1+\cdots)$$
$$+(\varepsilon\eta_w\bar{u}_0+\varepsilon^2\eta_w^2\bar{u}_1+\cdots)(U_0+\varepsilon U_1+\cdots)-2(\varepsilon\eta_w\bar{v}_0+\varepsilon^2\eta_w^2\bar{v}_1+\cdots+1)$$
$$\times(V_0+\varepsilon V_1+\cdots)+\varepsilon^{-3}r^{2/(n+1)}(\bar{u}_0+2\varepsilon\eta_w\bar{u}_1+\cdots)(\varepsilon W_0+\varepsilon^2W_1+\cdots)$$
$$=-\left[\frac{\eta_w(1-n)}{r(n+1)}\frac{\partial}{\partial\eta_w}+\mathrm{i}\varepsilon^{-3}(\alpha_0+\varepsilon\alpha_1+\cdots)\right](\varepsilon P_0+\varepsilon^2P_1+\cdots)$$
$$+\varepsilon^{-2}\frac{\partial}{\partial\eta_w}\left\{\bar{\mu}\frac{\partial(U_0+\varepsilon U_1+\cdots)}{\partial\eta_w}+\frac{(\bar{u}_0+2\varepsilon\eta_w\bar{u}_1+\cdots)\bar{\mu}(n-1)}{(\bar{u}_0^2+4\varepsilon\eta_w\bar{u}_0\bar{u}_1+\cdots)+(\bar{v}_0^2+4\varepsilon\eta_w\bar{v}_0\bar{v}_1+\cdots)}\right.$$
$$\times\left[(\bar{u}_0+2\varepsilon\eta_w\bar{u}_1+\cdots)\frac{\partial(U_0+\varepsilon U_1+\cdots)}{\partial\eta_w}\right.$$
$$\left.\left.+(\bar{v}_0+2\varepsilon\eta_w\bar{v}_1+\cdots)\frac{\partial(V_0+\varepsilon V_1+\cdots)}{\partial\eta_w}\right]\right\}, \tag{4.1.23b}$$

$$\left[\frac{\eta_w(\varepsilon\eta_w\bar{u}_0+\varepsilon^2\eta_w^2\bar{u}_1+\cdots)(1-n)}{(n+1)}\frac{\partial}{\partial\eta_w}+\mathrm{i}\varepsilon^{-3}r(\varepsilon\eta_w\bar{u}_0+\varepsilon^2\eta_w^2\bar{u}_1+\cdots)(\alpha_0+\varepsilon\alpha_1+\cdots)\right.$$
$$\left.+\mathrm{i}\varepsilon^{-3}(\varepsilon\eta_w\bar{v}_0+\varepsilon^2\eta_w^2\bar{v}_1+\cdots)(\beta_0+\varepsilon\beta_1+\cdots)+\varepsilon^{-1}(\varepsilon^2\eta_w^2\bar{w}_1+\varepsilon^3\eta_w^3\bar{w}_2+\cdots)\frac{\partial}{\partial\eta_w}\right]$$
$$\times(V_0+\varepsilon V_1+\cdots)+\frac{\varepsilon\eta_w(\bar{v}_0+2\varepsilon\eta_w\bar{v}_1+\cdots)(1-n)}{(n+1)}(U_0+\varepsilon U_1+\cdots)$$
$$+(\varepsilon\eta_w\bar{u}_0+\varepsilon^2\eta_w^2\bar{u}_1+\cdots)(V_0+\varepsilon V_1+\cdots)+2(\varepsilon\eta_w\bar{v}_0+\varepsilon^2\eta_w^2\bar{v}_1+\cdots+1)$$
$$\times(U_0+\varepsilon U_1+\cdots)+\varepsilon^{-3}r^{2/(n+1)}(\bar{v}_0+2\varepsilon\eta_w\bar{v}_1+\cdots)(\varepsilon W_0+\varepsilon^2W_1+\cdots)$$
$$=-\frac{\mathrm{i}\varepsilon^{-3}(\beta_0+\varepsilon\beta_1+\cdots)(\varepsilon P_0+\varepsilon^2P_1+\cdots)}{r}$$
$$+\varepsilon^{-2}\frac{\partial}{\partial\eta_w}\left\{\bar{\mu}\frac{\partial(V_0+\varepsilon V_1+\cdots)}{\partial\eta_w}+\frac{(\bar{v}_0+2\varepsilon\eta_w\bar{v}_1+\cdots)\bar{\mu}(n-1)}{(\bar{u}_0^2+4\varepsilon\eta_w\bar{u}_0\bar{u}_1+\cdots)+(\bar{v}_0^2+4\varepsilon\eta_w\bar{v}_0\bar{v}_1+\cdots)}\right.$$
$$\times\left[(\bar{u}_0+2\varepsilon\eta_w\bar{u}_1+\cdots)\frac{\partial(U_0+\varepsilon U_1+\cdots)}{\partial\eta_w}\right.$$
$$\left.\left.+(\bar{v}_0+2\varepsilon\eta_w\bar{v}_1+\cdots)\frac{\partial(V_0+\varepsilon V_1+\cdots)}{\partial\eta_w}\right]\right\},\tag{4.1.23c}$$

$$\left[\frac{\eta_w(\varepsilon\eta_w\bar{u}_0+\varepsilon^2\eta_w^2\bar{u}_1+\cdots)(1-n)}{(n+1)}\frac{\partial}{\partial\eta_w}+\mathrm{i}\varepsilon^{-3}r(\varepsilon\eta_w\bar{u}_0+\varepsilon^2\eta_w^2\bar{u}_1+\cdots)(\alpha_0+\varepsilon\alpha_1+\cdots)\right.$$
$$\left.+\mathrm{i}\varepsilon^{-3}(\varepsilon\eta_w\bar{v}_0+\varepsilon^2\eta_w^2\bar{v}_1+\cdots)(\beta_0+\varepsilon\beta_1+\cdots)+\varepsilon^{-1}(\varepsilon^2\eta_w^2\bar{w}_1+\varepsilon^3\eta_w^3\bar{w}_2+\cdots)\frac{\partial}{\partial\eta_w}\right]$$
$$\times(\varepsilon W_0+\varepsilon^2W_1+\cdots)+\varepsilon^3r^{-2/(n+1)}\frac{(1-n)}{(n+1)}(\varepsilon^2\eta_w^2\bar{w}_1+2\varepsilon^3\eta_w^3\bar{w}_2+\cdots)$$
$$\times(U_0+\varepsilon U_1+\cdots)+(2\varepsilon\eta_w\bar{w}_1+3\varepsilon^2\eta_w^2\bar{w}_2+\cdots)(\varepsilon W_0+\varepsilon^2W_1+\cdots)$$
$$=-\varepsilon^{-4}r^{(1-n)/(n+1)}\frac{\partial(\varepsilon P_0+\varepsilon^2P_1+\cdots)}{\partial\eta_w}+2\varepsilon^{-2}\frac{\partial}{\partial\eta_w}\left\{\bar{\mu}\frac{\partial(\varepsilon W_0+\varepsilon^2W_1+\cdots)}{\partial\eta_w}\right.$$
$$+\varepsilon^3r^{-2/(n+1)}\frac{(2\varepsilon\eta_w\bar{w}_1+3\varepsilon^2\eta_w^2\bar{w}_2+\cdots)\bar{\mu}(n-1)}{(\bar{u}_0^2+4\varepsilon\eta_w\bar{u}_0\bar{u}_1+\cdots)+(\bar{v}_0^2+4\varepsilon\eta_w\bar{v}_0\bar{v}_1+\cdots)}$$
$$\times\left[(\bar{u}_0+2\varepsilon\eta_w\bar{u}_1+\cdots)\frac{\partial(U_0+\varepsilon U_1+\cdots)}{\partial\eta_w}\right.$$
$$\left.\left.+(\bar{v}_0+2\varepsilon\eta_w\bar{v}_1+\cdots)\frac{\partial(V_0+\varepsilon V_1+\cdots)}{\partial\eta_w}\right]\right\}+\mathcal{O}(\varepsilon^2),\tag{4.1.23d}$$

where here $\bar{\mu}$ expands as

$$\bar{\mu} = [(\bar{u}_0^2 + 4\varepsilon\eta_w\bar{u}_0\bar{u}_1 + \cdots) + (\bar{v}_0^2 + 4\varepsilon\eta_w\bar{v}_0\bar{v}_1 + \cdots)]^{(n-1)/2}.$$

At $\mathcal{O}(\varepsilon^{-3})$ the continuity equation yields

$$\mathrm{i}\left(\alpha_0 U_0 + \frac{\beta_0 V_0}{r}\right) + r^{(1-n)/(n+1)}\frac{dW_0}{d\eta_w} = 0. \tag{4.1.24}$$

Equating terms of $\mathcal{O}(\varepsilon^{-2})$ in (4.1.23b) and (4.1.23c) we find that

$$\mathrm{i}\bar{\bar{u}}_0\eta_w U_0 + r^{2/(n+1)}W_0\bar{u}_0 = -\mathrm{i}\alpha_0 P_0 + \bar{\mu}_0\frac{d^2U_0}{d\eta_w^2} + \frac{\bar{u}_0\bar{\mu}_0(n-1)}{\bar{u}_0^2+\bar{v}_0^2}\left(\bar{u}_0\frac{d^2U_0}{d\eta_w^2} + \bar{v}_0\frac{d^2V_0}{d\eta_w^2}\right), \tag{4.1.25a}$$

$$\mathrm{i}\bar{\bar{u}}_0\eta_w V_0 + r^{2/(n+1)}W_0\bar{v}_0 = -\frac{\mathrm{i}\beta_0 P_0}{r} + \bar{\mu}_0\frac{d^2V_0}{d\eta_w^2} + \frac{\bar{v}_0\bar{\mu}_0(n-1)}{\bar{u}_0^2+\bar{v}_0^2}\left(\bar{u}_0\frac{d^2U_0}{d\eta_w^2} + \bar{v}_0\frac{d^2V_0}{d\eta_w^2}\right), \tag{4.1.25b}$$

respectively, where $\bar{\mu}_0 = [\bar{u}_0^2 + \bar{v}_0^2]^{(n-1)/2}$. By considering (4.1.23d) at $\mathcal{O}(\varepsilon^{-3})$ we find that P_0 is constant. Given the associated boundary condition at $\eta = 0$ then P_0 must be identically zero within the wall layer.

As expected, within the viscous wall layer, we see the emergence of additional terms associated with the introduction of the power-law viscosity model. For the case when $n = 1$ these terms vanish and we are left with the corresponding Newtonian relationships. However, when $n \neq 1$ we must consider these terms in our solution for W_0.

Let us start by firstly considering the Newtonian problem. By differentiating (4.1.25) in the Newtonian limit we find that

$$\mathrm{i}\bar{\bar{u}}_0\frac{d(\eta_w U_0)}{d\eta_w} + r\bar{u}_0\frac{dW_0}{d\eta_w} = \frac{d^3U_0}{d\eta_w^3}, \tag{4.1.26a}$$

$$\mathrm{i}\bar{\bar{u}}_0\frac{d(\eta_w V_0)}{d\eta_w} + r\bar{v}_0\frac{dW_0}{d\eta_w} = \frac{d^3V_0}{d\eta_w^3}. \tag{4.1.26b}$$

From (4.1.24) we can rewrite (4.1.26a) and (4.1.26b) as

$$\mathrm{i}\bar{\bar{u}}_0\frac{d(\eta_w U_0)}{d\eta_w} - \mathrm{i}r\bar{u}_0\left(\alpha_0 U_0 + \frac{\beta_0 V_0}{r}\right) = \frac{d^3 U_0}{d\eta_w^3}, \tag{4.1.27a}$$

$$\mathrm{i}\bar{\bar{u}}_0\frac{d(\eta_w V_0)}{d\eta_w} - \mathrm{i}r\bar{v}_0\left(\alpha_0 U_0 + \frac{\beta_0 V_0}{r}\right) = \frac{d^3 V_0}{d\eta_w^3}. \tag{4.1.27b}$$

Multiplying (4.1.27a) by α_0 and (4.1.27b) by β_0/r and adding the resulting equations yields

$$\frac{d^3}{d\eta_w^3}\left(\alpha_0 U_0 + \frac{\beta_0 V_0}{r}\right) - \mathrm{i}\bar{\bar{u}}_0\eta_w\frac{d}{d\eta_w}\left(\alpha_0 U_0 + \frac{\beta_0 V_0}{r}\right) = 0. \tag{4.1.28}$$

Now if we make the following substitutions

$$y = \frac{d}{d\eta_w}\left(\alpha_0 U_0 + \frac{\beta_0 V_0}{r}\right) \quad \text{with} \quad x = \gamma\eta_w \quad \text{where} \quad \gamma = (\mathrm{i}\bar{\bar{u}}_0)^{1/3},$$

then (4.1.28) reduces to the Airy equation

$$\frac{d^2 y}{dx^2} - xy = 0. \tag{4.1.29}$$

Thus we see that the solution of (4.1.28) is

$$\alpha_0 U_0 + \frac{\beta_0 V_0}{r} = C_0\int_0^{\eta_w}\mathrm{Ai}(\gamma s)\,\mathrm{d}s + C_1\int_0^{\eta_w}\mathrm{Bi}(\gamma s)\,\mathrm{d}s, \tag{4.1.30}$$

where C_0 and C_1 are constants of integration and Ai and Bi are the Airy functions of the first and second kind, respectively. We now apply the following two boundary conditions

$$\alpha_0 U_0 + \frac{\beta_0 V_0}{r} = 0 \quad \text{at} \quad \eta_w = 0, \tag{4.1.31a}$$

$$\alpha_0 U_0 + \frac{\beta_0 V_0}{r} \to \mathrm{i}w_0'(0) \quad \text{as} \quad \eta_w \to \infty. \tag{4.1.31b}$$

From the no-slip condition we have that $U_0(0) = V_0(0) = 0$, hence the first condition is implied and $C_1 = 0$. The second condition comes from noting that as $\eta \to 0$ in the inviscid zone we have that $\mathrm{i}(\alpha_0 u_0 + \beta_0 v_0/r) \to -r^{(1-n)/(n+1)} w_0'(0)$. Thus in the Newtonian limit we have that $\mathrm{i}(\alpha_0 u_0 + \beta_0 v_0/r) \to -w_0'(0)$. The solution of (4.1.30) that satisfies the boundary conditions is

$$\alpha_0 U_0 + \frac{\beta_0 V_0}{r} = \mathrm{i} w_0'(0) \frac{\int_0^{\eta_w} \mathrm{Ai}(\gamma s)\,\mathrm{d}s}{\int_0^{\infty} \mathrm{Ai}(\gamma s)\,\mathrm{d}s},$$

so that

$$\frac{dW_0}{d\eta_w} = w_0'(0) \frac{\int_0^{\eta_w} \mathrm{Ai}(\gamma s)\,\mathrm{d}s}{\int_0^{\infty} \mathrm{Ai}(\gamma s)\,\mathrm{d}s}. \tag{4.1.32}$$

Thus

$$W_0 = w_0'(0) \frac{\int_0^{\eta_w} \int_0^{t} \mathrm{Ai}(\gamma s)\,\mathrm{d}s\,\mathrm{d}t}{\int_0^{\infty} \mathrm{Ai}(\gamma s)\,\mathrm{d}s}. \tag{4.1.33}$$

Using integration by parts and Airy's equation, $\mathrm{Ai}''(\gamma\eta_w) - \gamma^3 \eta_w \mathrm{Ai}(\gamma\eta_w) = 0$, we have that

$$\begin{aligned}
\int_0^{\eta_w} \int_0^{t} \mathrm{Ai}(\gamma s)\,\mathrm{d}s\,\mathrm{d}t &= \eta_w \int_0^{\eta_w} \mathrm{Ai}(\gamma s)\,\mathrm{d}s - \int_0^{\eta_w} t\mathrm{Ai}(\gamma t)\,\mathrm{d}t, \\
&= \eta_w \int_0^{\eta_w} \mathrm{Ai}(\gamma s)\,\mathrm{d}s - \frac{1}{\gamma^3} \int_0^{\eta_w} \mathrm{Ai}''(\gamma t)\,\mathrm{d}t, \\
&= \eta_w \int_0^{\eta_w} \mathrm{Ai}(\gamma s)\,\mathrm{d}s + \frac{\mathrm{Ai}'(0) - \mathrm{Ai}'(\gamma\eta_w)}{\gamma^2}.
\end{aligned}$$

Now $\mathrm{Ai}'(\gamma\eta_w) \to 0$ as $\eta_w \to \infty$ and $\int_0^{\infty} \mathrm{Ai}(\gamma s)\,\mathrm{d}s = \gamma^{-1} \int_0^{\infty} \mathrm{Ai}(s)\,\mathrm{d}s$. Thus in the limit as $\eta_w \to \infty$ (4.1.33) becomes

$$W_0 \sim w_0'(0)\eta_w + \frac{w_0'(0)\mathrm{Ai}'(0)}{\gamma \int_0^{\infty} \mathrm{Ai}(s)\,\mathrm{d}s}.$$

Matching with the solution in the inviscid layer we find that

$$w_0(0) + \eta w_0'(0) + \varepsilon w_1 + \cdots = \varepsilon \left[w_0'(0)\eta_w + \frac{w_0'(0)\mathrm{Ai}'(0)}{\gamma \int_0^\infty \mathrm{Ai}(s)\,\mathrm{d}s} \right] + \varepsilon^2 W_1 + \cdots .$$

Therefore w_1, the order ε inviscid zone normal velocity component, must satisfy

$$w_1 \to \frac{w_0'(0)\mathrm{Ai}'(0)}{\gamma \int_0^\infty \mathrm{Ai}(s)\,\mathrm{d}s} \quad \text{as} \quad \eta \to 0.$$

This analytic solution to the Newtonian problem is relatively simple. This solution is achievable, in part, due to the symmetry of the viscous terms appearing in (4.1.26a) and (4.1.26b). We observe that these terms take the form AU_0''' and AV_0''', respectively, where in this case, $A = 1$. Clearly, from (4.1.25a) and (4.1.25b) this symmetry no longer exists when $n \neq 1$. Thus we need to provide an additional wall layer constraint, relating U_0 to V_0, in order to be able to obtain an analytic solution in the more general case. Matching with the solution in the inviscid zone we see that

$$\frac{U_0}{\bar{u}_0}, \quad \frac{V_0}{\bar{v}_0} \to \frac{\mathrm{i}r^{2/(n+1)}w_0'(0)}{\bar{\bar{u}}_0} \quad \text{as} \quad \eta_w \to \infty. \tag{4.1.34}$$

Again, differentiating (4.1.25a) and (4.1.25b) in the more general case we have that

$$\mathrm{i}\bar{\bar{u}}_0 \frac{d(\eta_w U_0)}{d\eta_w} + r^{2/(n+1)} \frac{dW_0}{d\eta_w}\bar{u}_0 = \bar{\mu}_0 \frac{d^3U_0}{d\eta_w^3} + \frac{\bar{u}_0\bar{\mu}_0(n-1)}{\bar{u}_0^2 + \bar{v}_0^2}\left(\bar{u}_0 \frac{d^3U_0}{d\eta_w^3} + \bar{v}_0 \frac{d^3V_0}{d\eta_w^3} \right), \tag{4.1.35a}$$

$$\mathrm{i}\bar{\bar{u}}_0 \frac{d(\eta_w V_0)}{d\eta_w} + r^{2/(n+1)} \frac{dW_0}{d\eta_w}\bar{v}_0 = \bar{\mu}_0 \frac{d^3V_0}{d\eta_w^3} + \frac{\bar{v}_0\bar{\mu}_0(n-1)}{\bar{u}_0^2 + \bar{v}_0^2}\left(\bar{u}_0 \frac{d^3U_0}{d\eta_w^3} + \bar{v}_0 \frac{d^3V_0}{d\eta_w^3} \right). \tag{4.1.35b}$$

We see that by replacing U_0 in (4.1.35a) with $\bar{u}_0V_0/\bar{v}_0$ we return (4.1.35b). Combining this fact with the form of the boundary conditions at $\eta_w = 0$ and as $\eta_w \to \infty$ indicates that inside the wall layer we have that $U_0 = (\bar{u}_0/\bar{v}_0)V_0$. Utilising this relationship simplifies

(4.1.35a) and (4.1.35b) such that

$$\mathrm{i}\bar{\bar{u}}_0\frac{d(\eta_w U_0)}{d\eta_w} + r^{2/(n+1)}\frac{dW_0}{d\eta_w}\bar{u}_0 = n\bar{\mu}_0\frac{d^3U_0}{d\eta_w^3}, \tag{4.1.36a}$$

$$\mathrm{i}\bar{\bar{u}}_0\frac{d(\eta_w U_0)}{d\eta_w} + r^{2/(n+1)}\frac{dW_0}{d\eta_w}\bar{v}_0 = n\bar{\mu}_0\frac{d^3V_0}{d\eta_w^3}. \tag{4.1.36b}$$

Hence the viscous terms are expressed in a symmetric fashion, with $A = n\bar{\mu}_0$. Thus an analytical solution for W_0 is once again obtainable. It is trivial to show that for any A the solution for W_0 is given by (4.1.33) where $\gamma = (\mathrm{i}\bar{\bar{u}}_0/A)^{1/3}$. Therefore for any value of the power-law index n we have that w_1 must satisfy

$$w_1 \to \frac{w_0'(0)\mathrm{Ai}'(0)}{\gamma\int_0^\infty \mathrm{Ai}(s)\,\mathrm{d}s} \quad \text{as} \quad \eta \to 0, \tag{4.1.37}$$

where now $\gamma = (\mathrm{i}\bar{\bar{u}}_0/n\bar{\mu}_0)^{1/3}$. It is important to note that here we have had to appeal to an additional matching constraint in order to be able to derive an analytical solution. This constraint holds in the Newtonian limit, although, in that case, W_0 is determinable independent of this result. To ensure a non-constant solution for W_0 it is imperative that $\lambda_0 \neq -\bar{v}_0/\bar{u}_0$. Results presented in tables 3.1 & 4.1 show that for values of n in the range of interest this requirement is indeed satisfied. We observe that substitution of $n = 1$ into (4.1.37) does return Hall's Newtonian result, as it should.

4.1.5 Asymptotic solutions

Matching the solution for w_1 from the inviscid zone (4.1.19) with the solution from the wall layer (4.1.37) produces the eigenrelation

$$\frac{[w_0'(0)]^2\mathrm{Ai}'(0)}{\gamma\int_0^\infty \mathrm{Ai}(s)\,\mathrm{d}s} = 2r^{2(n-1)/(n+1)}\left(\alpha_0\alpha_1 + \frac{\beta_0\beta_1}{r^2}\right)I_1 + \left(\frac{\alpha_1}{\beta_0} - \frac{\alpha_0\beta_1}{\beta_0^2}\right)rI_2. \tag{4.1.38}$$

Using the well-known values for $\mathrm{Ai}'(0)$ and $\int_0^\infty \mathrm{Ai}(s)\,\mathrm{d}s$ along with the previously calcul-

ated values for I_1 and I_2 we are able to solve the eigenrelation for the first order corrections to the effective wavenumber and wave angle for $0.6 \leq n \leq 1$.

For ease of notation we write

$$\left(\alpha_0\alpha_1 + \frac{\beta_0\beta_1}{r^2}\right) r^{2(n-1)/(n+1)} = \kappa_1 r^{-2/[3(n+1)]}\kappa_0, \tag{4.1.39a}$$

$$\left(\frac{\alpha_1}{\beta_0} - \frac{\alpha_0\beta_1}{\beta_0^2}\right) r = \lambda_1 r^{-2/[3(n+1)]}, \tag{4.1.39b}$$

where κ_1 and λ_1 are constants that are determined during the solution of the eigenrelation. Our solutions are given in table 4.4. Having calculated κ_1 and λ_1 we are able to determine the next terms in the asymptotic expansions of the effective wavenumber

$$\begin{aligned}\kappa = r^{(n-1)/(n+1)}\sqrt{\alpha^2 + \frac{\beta^2}{r^2}} &= \kappa_0 + r^{2(n-1)/(n+1)}\left(\alpha_0\alpha_1 + \frac{\beta_0\beta_1}{r^2}\right)\frac{\varepsilon}{\kappa_0} + \cdots, \\ &= \kappa_0 + \kappa_1 r^{-2/[3(n+1)]} Re^{-1/[3(n+1)]} + \cdots,\end{aligned} \tag{4.1.40a}$$

and the spiral wave angle

$$\begin{aligned}\tan\left(\frac{\pi}{2} - \phi\right) &= \lambda_0 + r\left(\frac{\alpha_1}{\beta_0} - \frac{\alpha_0\beta_1}{\beta_0^2}\right)\varepsilon + \cdots, \\ &= \lambda_0 + \lambda_1 r^{-2/[3(n+1)]} Re^{-1/[3(n+1)]} + \cdots.\end{aligned} \tag{4.1.40b}$$

By introducing the modified Reynolds number, $R = r^{2/(n+1)}Re^{1/(n+1)}$, based on the boundary-layer thickness and the local azimuthal velocity of the disk we are able to formulate expressions for the effective wavenumber and wave angle that have no explicit dependence on the radial variable r. From (4.1.40) we see that

$$\kappa = \kappa_0 + \kappa_1 R^{-1/3} + \cdots, \tag{4.1.41a}$$

$$\phi = \frac{\pi}{2} - \arctan(\lambda_0 + \lambda_1 R^{-1/3} + \cdots). \tag{4.1.41b}$$

n	$-\kappa_1$	λ_1
1	9.14	17.43
0.9	10.18	17.66
0.8	11.58	17.97
0.7	13.16	18.20
0.6	15.34	18.59

Table 4.4: First order corrections to the effective wavenumber and wave angle for power-law fluids with $n = 1$, 0.9, 0.8, 0.7, 0.6.

Having the solutions in this form allows us to plot κ and ϕ as functions of R for $Re \gg 1$. Solving for κ_1 and λ_1 allows us to determine α_1 and β_1/r. From the zero-order analysis we have that

$$\alpha_0 = r^{(1-n)/(n+1)} \frac{\lambda_0 \kappa_0}{\sqrt{1+\lambda_0^2}}, \quad \text{and} \quad \frac{\beta_0}{r} = \frac{\alpha_0}{\lambda_0}.$$

Substituting the above into (4.1.39a) and (4.1.39b) gives the next order terms in the radial and azimuthal wavenumber expansions

$$\alpha_1 = \alpha_0 \left[\frac{\kappa_1}{\kappa_0} + \frac{\lambda_1}{\lambda_0(1+\lambda_0^2)} \right],$$
$$\frac{\beta_1}{r} = \frac{\beta_0}{r} \left[\frac{\kappa_1}{\kappa_0} - \frac{\lambda_0 \lambda_1}{(1+\lambda_0^2)} \right].$$

So that the scaled radial and azimuthal wavenumbers are written as

$$\bar{\alpha} = \alpha r^{(n-1)/(n+1)} = \frac{\lambda_0 \kappa_0}{\sqrt{1+\lambda_0^2}} \left\{ 1 + \left[\frac{\kappa_1}{\kappa_0} + \frac{\lambda_1}{\lambda_0(1+\lambda_0^2)} \right] R^{-1/3} + \cdots \right\}, \tag{4.1.42a}$$

$$\bar{\beta} = \beta r^{-2/(n+1)} = \frac{\kappa_0}{\sqrt{1+\lambda_0^2}} \left\{ 1 + \left[\frac{\kappa_1}{\kappa_0} - \frac{\lambda_0 \lambda_1}{(1+\lambda_0^2)} \right] R^{-1/3} + \cdots \right\}. \tag{4.1.42b}$$

Again, having the solutions in this form allows us to plot the wavenumbers $\bar{\alpha}$ and $\bar{\beta}$ as functions of R for $Re \gg 1$.

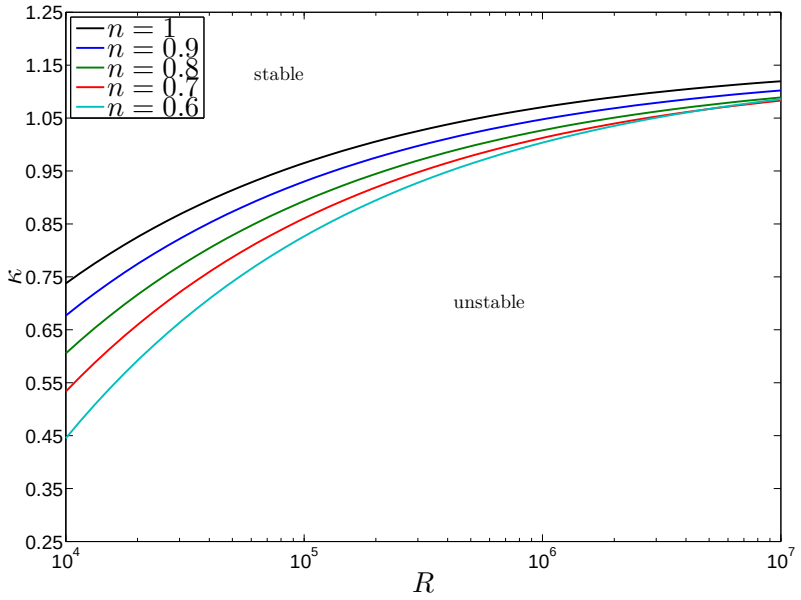

Figure 4.7: The two term asymptotic predictions of the neutral wavenumber κ versus the Reynolds number R for power-law fluids with $n = 1$, 0.9, 0.8, 0.7, 0.6.

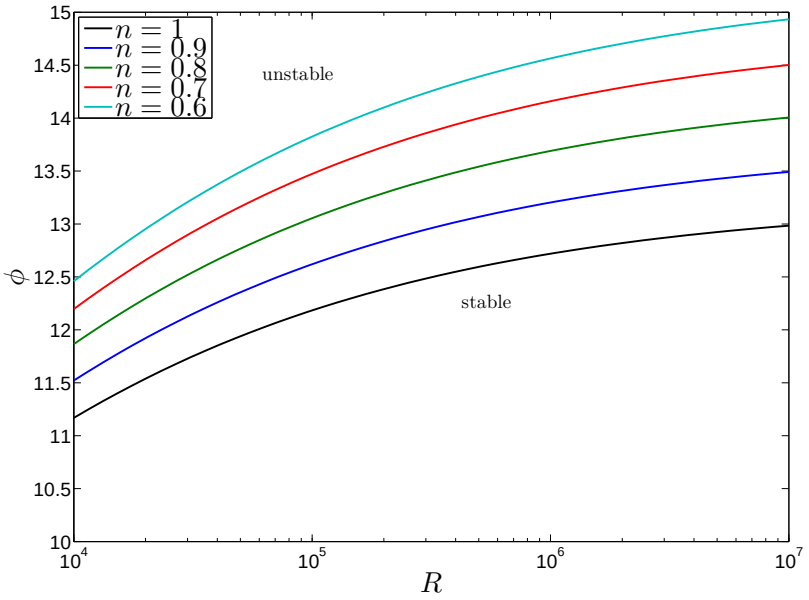

Figure 4.8: The two term asymptotic predictions of the neutral wave angle ϕ versus the Reynolds number R for power-law fluids with $n = 1$, 0.9, 0.8, 0.7, 0.6.

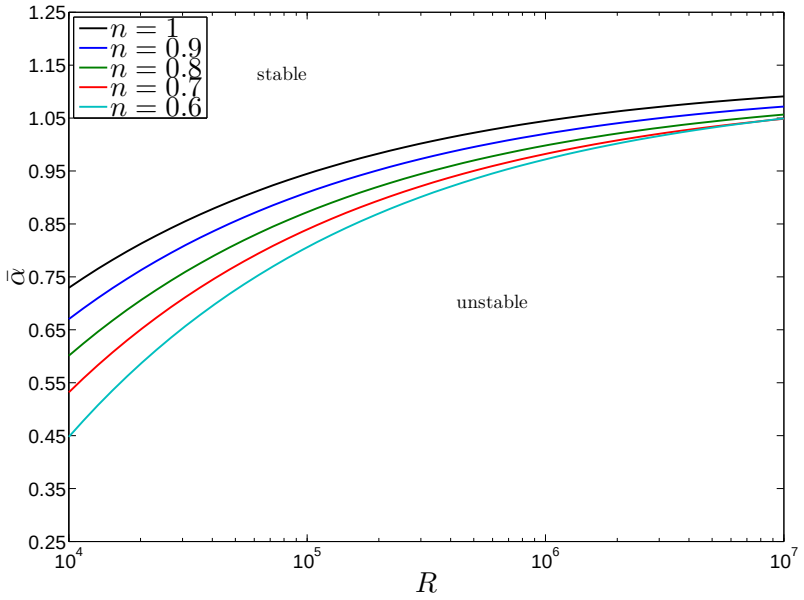

Figure 4.9: The two term asymptotic predictions of the neutral radial wavenumber $\bar{\alpha}$ versus the Reynolds number R for power-law fluids with $n = 1$, 0.9, 0.8, 0.7, 0.6.

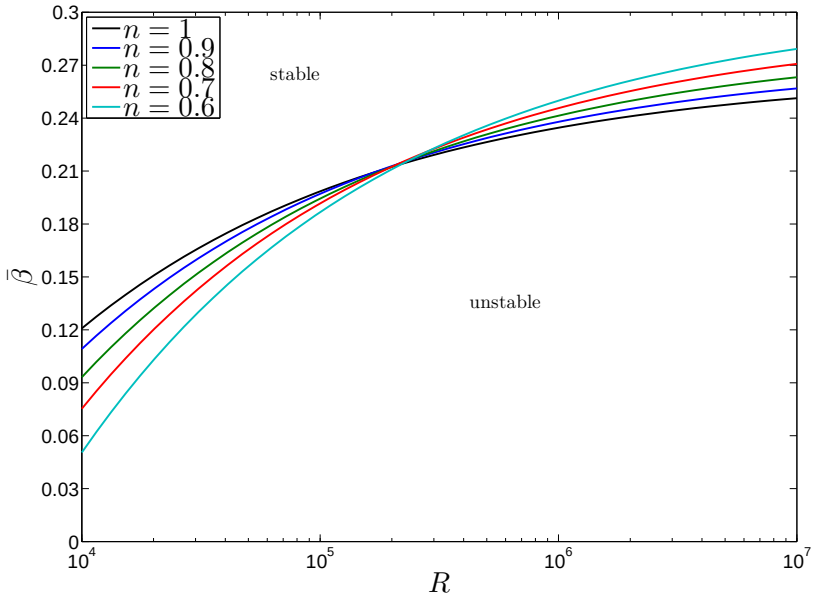

Figure 4.10: The two term asymptotic predictions of the neutral azimuthal wavenumber $\bar{\beta}$ versus the Reynolds number R for power-law fluids with $n = 1$, 0.9, 0.8, 0.7, 0.6.

4.1.6 Discussion

From the zero-order analysis we observe that reducing the power-law index has the effect of increasing the ratio of azimuthal to radial wavenumbers. Thus, λ_0 decreases, and the wave angle ϕ_0 increases for decreasing values of n. This analysis does not however reveal any clear trend regarding the effective wavenumber κ_0. Nevertheless, we do observe that the location of the critical layer, and hence the associated zeros of the effective velocity profile and its second derivative, moves slightly closer to the wall as the shear-thinning parameter increases.

We see that at the next order the correction terms appear to dominate in the expansion of the effective wavenumber and wave angle. Figure 4.7 shows that as n decreases so the κ plots are shifted uniformly down. The separation between each of the plots is larger for smaller values of the Reynolds number, whilst as $R \to \infty$ the plots tend to their respective limiting values, $\kappa \to \kappa_0$. This shifting of the wavenumber plots effectively reduces the area encompassed by the neutral curve, thus indicating a potentially stabilising effect on the flow. A similar trend can be seen in figure 4.8, here as the power-law index decreases so the ϕ plots are shifted up. In this case the area above the curves is unstable, see for example, figure 1.5. Therefore, as before, the area encompassed by the neutral curve is reduced which again implies stabilisation.

For completeness we have also included plots of the scaled radial and azimuthal wavenumbers. From figure 4.9 we see the strong dependence of κ on the radial wavenumber. We note that as $R \to \infty$ the value of $\bar{\beta}$ increases with n. However, the asymptotic theory predicts that at lower values of the Reynolds number the wavenumbers in the azimuthal direction will in fact be reduced as the shear-thinning properties of the fluid increases. Hence we observe the intersection of the curves in figure 4.10.

4.2 Case II: Bingham

In this section the linear, type I, asymptotic stability analysis is presented for fluids satisfying a Bingham constitutive relationship.

The linear disturbance equations are derived in a very similar manner. We recall the full scaled governing equations (2.2.11) and (2.2.23) and return to an unscaled frame of reference. By rewriting the velocity functions (U, V, W), pressure P and modified viscosity function $\tilde{\mu}$ in terms of the outer region coordinate z, whilst also removing the boundary-layer scaling on the axial velocity component we have that

$$[u(r,\theta,z), v(r,\theta,z), w(r,\theta,z)] = [U(r,\theta,Z), V(r,\theta,Z), Re^{-1/2}W(r,\theta,Z)], \tag{4.2.1a}$$

$$p(r,\theta,z) = P(r,\theta,Z), \quad \mu(r,\theta,z) = \tilde{\mu}(r,\theta,Z). \tag{4.2.1b}$$

Thus we return the dimensionless continuity and Navier-Stokes equations given by (4.1.2a)-(4.1.2d) where now

$$\mu = 1 + 2rRe^{1/2}B_n\left[\left(\frac{\partial u}{\partial z}\right)^2 + \left(\frac{\partial v}{\partial z}\right)^2 + \mathcal{T}_\mu\right]^{-1/2}. \tag{4.2.2}$$

Again, the form of the additional terms are outlined in the appendix B and are equivalent to the $\mathcal{O}(Re^{-1})$ and $\mathcal{O}(Re^{-2})$ terms given in (2.2.23).

The base flow is perturbed in a similar fashion

$$(u, v, w) = \boldsymbol{u} + [U_d(r,\theta,z), V_d(r,\theta,z), W_d(r,\theta,z)], \tag{4.2.3}$$

where U_d, V_d and W_d are the disturbance velocities. In this case the disturbance equations

are simplified somewhat and are given by

$$\frac{1}{r}\frac{\partial(rU_d)}{\partial r}+\frac{1}{r}\frac{\partial V_d}{\partial\theta}+\frac{\partial W_d}{\partial z}=0, \tag{4.2.4a}$$

$$\begin{aligned} r\bar{u}\frac{\partial U_d}{\partial r}+\bar{v}\frac{\partial U_d}{\partial\theta}+\bar{\bar{w}}\frac{\partial U_d}{\partial z}+rU_d\frac{\partial\bar{u}}{\partial r}+\bar{u}U_d-2(\bar{v}+1)V_d+rW_d\frac{\partial\bar{u}}{\partial z}&=-\frac{\partial P_d}{\partial r}\\ &+\frac{1}{Re}\frac{\partial}{\partial z}\left(\hat{\mu}\frac{\partial U_d}{\partial z}+r\hat{\hat{\mu}}\frac{\partial\bar{u}}{\partial z}\right), \end{aligned} \tag{4.2.4b}$$

$$\begin{aligned} r\bar{u}\frac{\partial V_d}{\partial r}+\bar{v}\frac{\partial V_d}{\partial\theta}+\bar{\bar{w}}\frac{\partial V_d}{\partial z}+rU_d\frac{\partial\bar{v}}{\partial r}+\bar{u}V_d+2(\bar{v}+1)U_d+rW_d\frac{\partial\bar{v}}{\partial z}&=-\frac{1}{r}\frac{\partial P_d}{\partial\theta}\\ &+\frac{1}{Re}\frac{\partial}{\partial z}\left(\hat{\mu}\frac{\partial V_d}{\partial z}+r\hat{\hat{\mu}}\frac{\partial\bar{v}}{\partial z}\right), \end{aligned} \tag{4.2.4c}$$

$$\begin{aligned} r\bar{u}\frac{\partial W_d}{\partial r}+\bar{v}\frac{\partial W_d}{\partial\theta}+\bar{\bar{w}}\frac{\partial W_d}{\partial z}+W_d\frac{\partial\bar{\bar{w}}}{\partial z}&=-\frac{\partial P_d}{\partial z}\\ &+\frac{1}{Re}\left\{\frac{1}{r}\frac{\partial}{\partial r}\left[r\left(\hat{\mu}\frac{\partial U_d}{\partial z}+r\hat{\hat{\mu}}\frac{\partial\bar{u}}{\partial z}\right)\right]\right.\\ &+\frac{1}{r}\frac{\partial}{\partial\theta}\left(\hat{\mu}\frac{\partial V_d}{\partial z}+r\hat{\hat{\mu}}\frac{\partial\bar{v}}{\partial z}\right)\\ &\left.+2\frac{\partial}{\partial z}\left(\hat{\mu}\frac{\partial W_d}{\partial z}+\hat{\hat{\mu}}\frac{\partial\bar{\bar{w}}}{\partial z}\right)\right\}, \end{aligned} \tag{4.2.4d}$$

where P_d is the non-dimensional pressure perturbation and $\bar{\bar{w}}=Re^{-1/2}\bar{w}$. The 'unperturbed' viscosity function $\hat{\mu}$ is given by

$$\hat{\mu}=1+2rRe^{-1/2}B_n\left[\left(r\frac{\partial\bar{u}}{\partial z}\right)^2+\left(r\frac{\partial\bar{v}}{\partial z}\right)^2\right]^{-1/2}. \tag{4.2.4e}$$

The 'perturbed' viscosity function $\hat{\hat{\mu}}$ takes the form

$$\hat{\hat{\mu}}=-2r^2Re^{1/2}B_n\left(\frac{\partial\bar{u}}{\partial z}\frac{\partial U_d}{\partial z}+\frac{\partial\bar{v}}{\partial z}\frac{\partial V_d}{\partial z}\right)\left[\left(r\frac{\partial\bar{u}}{\partial z}\right)^2+\left(r\frac{\partial\bar{v}}{\partial z}\right)^2\right]^{-3/2}. \tag{4.2.4f}$$

Here our small parameter ε is defined by $\varepsilon=\delta^{1/3}=Re^{-1/6}$ and the disturbance

velocities and pressure satisfy

$$U_d = \tilde{u}(z)E, \quad V_d = \tilde{v}(z)E, \quad W_d = \tilde{w}(z)E, \quad P_d = \tilde{p}(z)E,$$

where E is given by (4.1.5). The wavenumber expansions are identical to those stated in (4.1.7) and the inviscid zone velocity and pressure perturbations are expanded as

$$\tilde{u} = u_0(\zeta) + \varepsilon u_1(\zeta) + \cdots, \tag{4.2.5a}$$

$$\tilde{v} = v_0(\zeta) + \varepsilon v_1(\zeta) + \cdots, \tag{4.2.5b}$$

$$\tilde{w} = w_0(\zeta) + \varepsilon w_1(\zeta) + \cdots, \tag{4.2.5c}$$

$$\tilde{p} = p_0(\zeta) + \varepsilon p_1(\zeta) + \cdots, \tag{4.2.5d}$$

where $\zeta = \varepsilon^{-3}z$. The preceding expansions are then substituted into the linearised disturbance equations along with the following forms for the differential operators when applied to the disturbance quantities

$$\frac{\partial}{\partial r} = \frac{\partial}{\partial r} + \left(\frac{\mathrm{i}}{\varepsilon^3}\right)(\alpha_0 + \varepsilon\alpha_1 + \cdots), \quad \frac{\partial}{\partial \theta} = \left(\frac{\mathrm{i}}{\varepsilon^3}\right)(\beta_0 + \varepsilon\beta_1 + \cdots).$$

The asymptotic expansions of (4.2.4) are given in §B.1. Equating terms of $\mathcal{O}(\varepsilon^{-3})$ we have that

$$\mathrm{i}\alpha_0 u_0 + \frac{\mathrm{i}\beta_0 v_0}{r} + w_0' = 0, \tag{4.2.6a}$$

$$\mathrm{i}\bar{\bar{u}}u_0 + rw_0\bar{u}' + \mathrm{i}\alpha_0 p_0 = 0, \tag{4.2.6b}$$

$$\mathrm{i}\bar{\bar{u}}v_0 + rw_0\bar{v}' + \frac{\mathrm{i}\beta_0 p_0}{r} = 0, \tag{4.2.6c}$$

$$\mathrm{i}\bar{\bar{u}}w_0 + p_0' = 0, \tag{4.2.6d}$$

where, as before, $\bar{\bar{u}} = \alpha_0\bar{u}r + \beta_0\bar{v}$ and the primes denote differentiation with respect to ζ.

B_n	λ_0	$\bar{\zeta}$	γ_0	ϕ_0
0	4.256	1.458	1.162	13.22°
0.1	4.892	1.516	1.105	11.55°
0.2	5.558	1.586	1.046	10.20°
0.3	6.232	1.659	0.992	9.12°
0.4	6.900	1.732	0.946	8.25°
0.5	7.555	1.803	0.905	7.54°

Table 4.5: Calculated values for λ_0, $\bar{\zeta}$, γ_0 and ϕ_0 for Bingham plastic fluids with $B_n = 0,\ 0.1,\ 0.2,\ 0.3,\ 0.4,\ 0.5$.

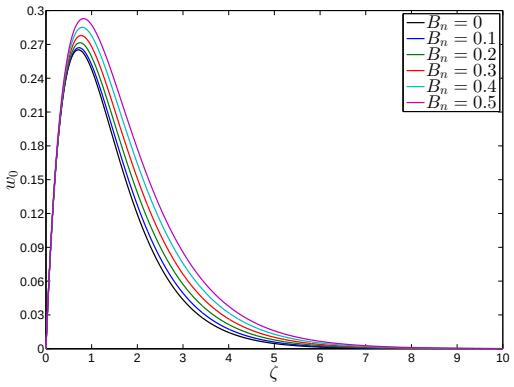

Figure 4.11: The inviscid eigenfunction w_0 versus ζ for Bingham plastic fluids with $B_n = 0,\ 0.1,\ 0.2,\ 0.3,\ 0.4,\ 0.5$.

Eliminating u_0, v_0 and p_0 we find that w_0 satisfies Rayleigh's equation

$$\bar{\bar{u}}(w_0'' - \gamma_0^2 w_0) - \bar{\bar{u}}'' w_0 = 0, \tag{4.2.7}$$

where $\gamma_0^2 = \alpha_0^2 + \beta_0^2/r^2$. Rayleigh's equation is solved subject to (4.1.12) with η being replaced by ζ.

Again, we ensure that (4.2.7) is not singular at the point where $\zeta = \bar{\zeta} > 0$ by choosing $\lambda_0 = \alpha_0 r/\beta_0$ such that $\bar{\bar{u}}$ and $\bar{\bar{u}}''$ vanish at $\zeta = \bar{\zeta}$. The eigenvalue problem is solved using the same methodology as before and the results are presented in table 4.5. The zero order eigenfunctions are plotted in figure 4.11.

At the next order in the inviscid zone we find that

$$\mathrm{i}(\alpha_0 u_1 + \alpha_1 u_0) + \frac{\mathrm{i}(\beta_0 v_1 + \beta_1 v_0)}{r} + w_1' = 0, \tag{4.2.8a}$$

$$\mathrm{i}\bar{\bar{u}} u_1 + \mathrm{i}\bar{\bar{v}} u_0 + r w_1 \bar{u}' + \mathrm{i}(\alpha_0 p_1 + \alpha_1 p_0) = 0, \tag{4.2.8b}$$

$$\mathrm{i}\bar{\bar{u}} v_1 + \mathrm{i}\bar{\bar{v}} v_0 + r w_1 \bar{v}' + \frac{\mathrm{i}(\beta_0 p_1 + \beta_1 p_0)}{r} = 0, \tag{4.2.8c}$$

$$\mathrm{i}\bar{\bar{u}} w_1 + \mathrm{i}\bar{\bar{v}} w_0 + p_1' = 0, \tag{4.2.8d}$$

where, as before, $\bar{\bar{v}} = \alpha_1 \bar{u} r + \beta_1 \bar{v}$. Eliminating u_0, v_0, p_0, u_1, v_1 and p_1 we find that w_1 satisfies the inhomogeneous form of Rayleigh's equation

$$\bar{\bar{u}}\left(w_1'' - \gamma_0^2 w_1\right) - \bar{\bar{u}}'' w_1 = 2\bar{\bar{u}}\left(\alpha_0\alpha_1 + \frac{\beta_0\beta_1}{r^2}\right) w_0 + r\left(\alpha_1 - \frac{\alpha_0\beta_1}{\beta_0}\right)\left(\bar{u}'' - \frac{\bar{u}\bar{\bar{u}}''}{\bar{\bar{u}}}\right) w_0. \tag{4.2.9}$$

The solution of (4.2.9) that satisfies $w_1 \to 0$ as $\zeta \to \infty$ is

$$w_1 = 2\left(\alpha_0\alpha_1 + \frac{\beta_0\beta_1}{r^2}\right) w_0(\zeta) \int_{\bar{\bar{\zeta}}}^{\zeta} \frac{\mathrm{d}\chi}{w_0^2(\chi)} \int_{\infty}^{\chi} w_0^2(\theta)\,\mathrm{d}\theta + r\left(\alpha_1 - \frac{\alpha_0\beta_1}{\beta_0}\right) w_0(\zeta) \int_{\bar{\bar{\zeta}}}^{\zeta} \frac{\mathrm{d}\chi}{w_0^2(\chi)} \int_{\infty}^{\chi} w_0^2(\theta)\hat{U}(\theta)\,\mathrm{d}\theta, \tag{4.2.10}$$

where $\bar{\bar{\zeta}}$ is such that $\bar{\bar{\zeta}} > \bar{\zeta}$ and $\hat{U}$ is as given by (4.1.17). By evaluating (4.2.10) at $\zeta = 0$ we have that

$$w_1(0) = 2\left(\alpha_0\alpha_1 + \frac{\beta_0\beta_1}{r^2}\right)\frac{I_1}{w_0'(0)} + \left(\frac{\alpha_1}{\beta_0} - \frac{\alpha_0\beta_1}{\beta_0^2}\right)\frac{rI_2}{w_0'(0)}, \tag{4.2.11}$$

where I_1 and I_2 are given by (4.1.20a) and (4.1.20b) respectively.

As with the power-law calculation, we find that the path of integration must be deformed above the singularity since $\bar{\bar{u}}'(\bar{\zeta})/\beta_0 < 0$ for $0 \le B_n \le 0.5$. The integrals I_1 and

B_n	I_1	I_2
0	0.0911	$0.0592 + 0.0299\mathrm{i}$
0.1	0.0956	$0.0494 + 0.0239\mathrm{i}$
0.2	0.1030	$0.0424 + 0.0199\mathrm{i}$
0.3	0.1126	$0.0369 + 0.0172\mathrm{i}$
0.4	0.1237	$0.0337 + 0.0153\mathrm{i}$
0.5	0.1356	$0.0311 + 0.0139\mathrm{i}$

Table 4.6: Numerical values of the integrals I_1 and I_2 for Bingham plastic fluids with $B_n = 0,\ 0.1,\ 0.2,\ 0.3,\ 0.4,\ 0.5$.

I_2 are computed in much the same way, where, for consistency, we take $\zeta_s = 0.0260 = \eta_s$. Our numerical calculations for both the integrals are displayed above.

In order to satisfy the no-slip boundary condition of the velocity components at the wall we again consider the viscous wall layer. The wall layer coordinate ζ_w is given by

$$\zeta_w = z\varepsilon^{-4}.$$

As $\zeta \to 0$ the basic flow solutions take the form

$$\bar{u} = \varepsilon\zeta_w\bar{u}_0 + \varepsilon^2\zeta_w^2\bar{u}_1 + \cdots, \tag{4.2.12a}$$

$$\bar{v} = \varepsilon\zeta_w\bar{v}_0 + \varepsilon^2\zeta_w^2\bar{v}_1 + \cdots, \tag{4.2.12b}$$

$$\bar{w} = \varepsilon^2\zeta_w^2\bar{w}_1 + \varepsilon^3\zeta_w^3\bar{w}_2 + \cdots, \tag{4.2.12c}$$

where the notation used here is consistent with that of the previous section. The disturbance quantities expand as

$$\tilde{u} = U_0(\zeta_w) + \varepsilon U_1(\zeta_w) + \cdots, \tag{4.2.13a}$$

$$\tilde{v} = V_0(\zeta_w) + \varepsilon V_1(\zeta_w) + \cdots, \tag{4.2.13b}$$

$$\tilde{w} = \varepsilon W_0(\zeta_w) + \varepsilon^2 W_1(\zeta_w) + \cdots, \tag{4.2.13c}$$

$$\tilde{p} = \varepsilon P_0(\zeta_w) + \varepsilon^2 P_1(\zeta_w) + \cdots . \tag{4.2.13d}$$

The asymptotic expansions of (4.2.4) are given in §B.2. At $\mathcal{O}(\varepsilon^{-3})$ the continuity equation yields

$$\mathrm{i}\left(\alpha_0 U_0 + \frac{\beta_0 V_0}{r}\right) + \frac{dW_0}{d\zeta_w} = 0. \tag{4.2.14}$$

Equating terms of $\mathcal{O}(\varepsilon^{-2})$ we find that

$$\mathrm{i}\bar{\bar{u}}_0\zeta_w U_0 + rW_0\bar{u}_0 = -\mathrm{i}\alpha_0 P_0 + \bar{\mu}_0\frac{d^2U_0}{d\zeta_w^2} + \frac{\bar{u}_0(1-\bar{\mu}_0)}{\bar{u}_0^2+\bar{v}_0^2}\left(\bar{u}_0\frac{d^2U_0}{d\zeta_w^2} + \bar{v}_0\frac{d^2V_0}{d\zeta_w^2}\right), \tag{4.2.15a}$$

$$\mathrm{i}\bar{\bar{u}}_0\zeta_w V_0 + rW_0\bar{v}_0 = -\frac{\mathrm{i}\beta_0 P_0}{r} + \bar{\mu}_0\frac{d^2V_0}{d\zeta_w^2} + \frac{\bar{v}_0(1-\bar{\mu}_0)}{\bar{u}_0^2+\bar{v}_0^2}\left(\bar{u}_0\frac{d^2U_0}{d\zeta_w^2} + \bar{v}_0\frac{d^2V_0}{d\zeta_w^2}\right), \tag{4.2.15b}$$

where $\bar{\mu}_0 = 1 + 2B_n[\bar{u}_0^2 + \bar{v}_0^2]^{-1/2}$. As before we find that $P_0 \equiv 0$ within the wall layer. Following the analysis of §4.1.3 we have that w_1 must satisfy

$$w_1 \to \frac{w_0'(0)\mathrm{Ai}'(0)}{\gamma\int_0^\infty \mathrm{Ai}(s)\,\mathrm{d}s} \quad \text{as} \quad \zeta \to 0, \tag{4.2.16}$$

for any value of the Bingham number B_n, where now $\gamma = (\mathrm{i}\bar{\bar{u}}_0)^{1/3}$. It is interesting to note here that the small ζ solution for w_1 has no specific dependence on B_n.

Matching the solution for w_1 from the inviscid zone (4.2.11) with the solution from the wall layer (4.2.16) produces the linear eigenrelation

$$\frac{[w_0'(0)]^2\mathrm{Ai}'(0)}{\gamma\int_0^\infty \mathrm{Ai}(s)\,\mathrm{d}s} = 2\left(\alpha_0\alpha_1 + \frac{\beta_0\beta_1}{r^2}\right)I_1 + \left(\frac{\alpha_1}{\beta_0} - \frac{\alpha_0\beta_1}{\beta_0^2}\right)rI_2. \tag{4.2.17}$$

We solve the eigenrelation for the first order corrections to the effective wavenumber and

B_n	$-\gamma_1$	λ_1
0	9.14	17.43
0.1	10.11	23.53
0.2	10.87	30.48
0.3	11.37	37.76
0.4	11.58	44.94
0.5	11.77	52.26

Table 4.7: First order corrections to the effective wavenumber and wave angle for Bingham plastic fluids with $B_n = 0,\ 0.1,\ 0.2,\ 0.3,\ 0.4,\ 0.5$.

wave angle for $0 \leq B_n \leq 0.5$. For ease of notation we write

$$\left(\alpha_0\alpha_1 + \frac{\beta_0\beta_1}{r^2}\right) = \gamma_1 r^{-1/3}\gamma_0, \tag{4.2.18a}$$

$$\left(\frac{\alpha_1}{\beta_0} - \frac{\alpha_0\beta_1}{\beta_0^2}\right) r = \lambda_1 r^{-1/3}, \tag{4.2.18b}$$

where γ_1 and λ_1 are constants that are determined during the solution of the eigenrelation. Our solutions are presented in table 4.7.

Thus we are able to determine the next order terms in the asymptotic expansions of the effective wavenumber

$$\begin{aligned}\gamma = \sqrt{\alpha^2 + \frac{\beta^2}{r^2}} &= \gamma_0 + \left(\alpha_0\alpha_1 + \frac{\beta_0\beta_1}{r^2}\right)\frac{\varepsilon}{\gamma_0} + \cdots, \\ &= \gamma_0 + \gamma_1 r^{-1/3} Re^{-1/6} + \cdots, \end{aligned} \tag{4.2.19a}$$

and the spiral wave angle

$$\begin{aligned}\tan\left(\frac{\pi}{2} - \phi\right) &= \lambda_0 + r\left(\frac{\alpha_1}{\beta_0} - \frac{\alpha_0\beta_1}{\beta_0^2}\right)\varepsilon + \cdots, \\ &= \lambda_0 + \lambda_1 r^{-1/3} Re^{-1/6} + \cdots. \end{aligned} \tag{4.2.19b}$$

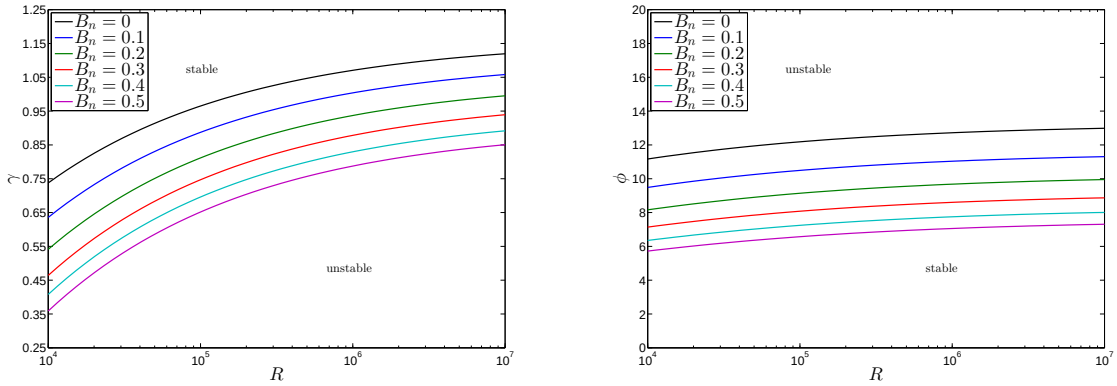

Figure 4.12: The two term asymptotic predictions of the neutral wavenumber γ and wave angle ϕ versus the Reynolds number R for Bingham plastic fluids with $B_n = 0,\ 0.1,\ 0.2,\ 0.3,\ 0.4,\ 0.5$.

From (4.2.19a) and (4.2.19b) we see that

$$\gamma = \gamma_0 + \gamma_1 R^{-1/3} + \cdots , \tag{4.2.20a}$$

$$\phi = \frac{\pi}{2} - \arctan(\lambda_0 + \lambda_1 R^{-1/3} + \cdots), \tag{4.2.20b}$$

where R is the modified Reynolds number defined in §2.2.2. Thus we are again able to plot γ and ϕ as functions of R for $Re \gg 1$. Having solved for γ_1 and λ_1 it is then possible to obtain solutions for $\bar{\alpha} = \alpha_0 + \alpha_1 R^{-1/3} + \cdots$ and $\bar{\beta} = (\beta_0/r) + (\beta_1/r)R^{-1/3} + \cdots$. In this case we find that

$$\bar{\alpha} = \frac{\lambda_0 \gamma_0}{\sqrt{1+\lambda_0^2}} \left\{ 1 + \left[\frac{\gamma_1}{\gamma_0} + \frac{\lambda_1}{\lambda_0(1+\lambda_0^2)} \right] R^{-1/3} + \cdots \right\}, \tag{4.2.21a}$$

$$\bar{\beta} = \frac{\gamma_0}{\sqrt{1+\lambda_0^2}} \left\{ 1 + \left[\frac{\gamma_1}{\gamma_0} - \frac{\lambda_0 \lambda_1}{(1+\lambda_0^2)} \right] R^{-1/3} + \cdots \right\}. \tag{4.2.21b}$$

Thus we are again able to plot $\bar{\alpha}$ and $\bar{\beta}$ as functions of R for $Re \gg 1$.

As before, we will firstly discuss the results from the zero-order analysis. From table 4.5 we observe the clear trend that as B_n increases from zero the zero order approxima-

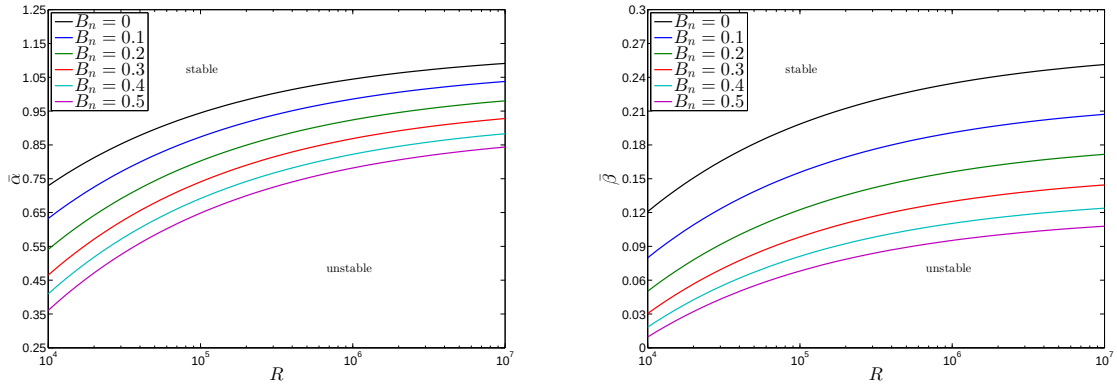

Figure 4.13: The two term asymptotic predictions of the neutral radial wavenumber $\bar{\alpha}$ and azimuthal wavenumber $\bar{\beta}$ versus the Reynolds number R for Bingham plastic fluids with $B_n = 0,\ 0.1,\ 0.2,\ 0.3,\ 0.4,\ 0.5$.

tion to the wave angle, ϕ_0, decreases. Thus, the ratio of radial to azimuthal wavenumbers increases in this case. A similar trend is observed when considering the zero order approximation to the wavenumber. We note the uniform decrease in the value of γ_0 as B_n increases. We also note that the location of the critical layer moves further from the wall as the yield stress is increased.

From figure 4.12 we see that as B_n increases so the γ plots are shifted uniformly down. The separation between each of the plots is seen to be relatively uniform as $R \to \infty$. We note that this is in part due to the linear decrease in the value of γ_0 as B_n increases. Again, this shifting of the wavenumber plots effectively reduces the area encompassed by the neutral curve indicating a potentially stabilising effect. We also observe that as the Bingham number is increased so the ϕ plots are shifted down. This downward shifting of the plots increases the area encompassed by the neutral curve suggesting a destabilising effect. Physically, we interpret the wavenumber as being the primary indicator of stability. Independent of the wave angle, if at a fixed Reynolds number, the flow exhibits a greater number of spiral vortices, it would be considered to be less stable, suggesting an advanced onset of turbulent flow.

4.3 Case III: Carreau

The formulation here is almost identical to that of §4.2. After returning to an unscaled frame of reference we recover the dimensionless continuity and Navier-Stokes equations, (4.1.2a)-(4.1.2d). In this case the viscosity function is given by

$$\mu = 1 + c_0\left\{1 + \left(\frac{k}{rRe^{1/2}}\right)^2\left[\left(\frac{\partial u}{\partial z}\right)^2 + \left(\frac{\partial v}{\partial z}\right)^2 + \mathcal{T}_\mu\right]\right\}^{(n-1)/2}. \tag{4.3.1}$$

The additional terms here are equivalent to the $\mathcal{O}(Re^{-1})$ and $\mathcal{O}(Re^{-2})$ terms given in (2.2.29).

Having perturbed the flow in the usual fashion we arrive at the disturbance equations, (4.2.4a)-(4.2.4b), the 'unperturbed' viscosity function $\hat{\mu}$ takes the form

$$\hat{\mu} = 1 + c_0\left\{1 + \left(\frac{k}{rRe^{1/2}}\right)^2\left[\left(r\frac{\partial \bar{u}}{\partial z}\right)^2 + \left(r\frac{\partial \bar{v}}{\partial z}\right)^2\right]\right\}^{(n-1)/2}, \tag{4.3.2a}$$

whilst the 'perturbed' viscosity function $\hat{\hat{\mu}}$ is given by

$$\hat{\hat{\mu}} = \frac{k^2 c_0(n-1)}{rRe}\left(\frac{\partial \bar{u}}{\partial z}\frac{\partial U_d}{\partial z} + \frac{\partial \bar{v}}{\partial z}\frac{\partial V_d}{\partial z}\right) \times\left\{1 + \left(\frac{k}{rRe^{1/2}}\right)^2\left[\left(r\frac{\partial \bar{u}}{\partial z}\right)^2 + \left(r\frac{\partial \bar{v}}{\partial z}\right)^2\right]\right\}^{(n-3)/2}. \tag{4.3.2b}$$

Again our small parameter ε is defined by $\varepsilon = \delta^{1/3} = Re^{-1/6}$ and the disturbance velocities and pressure are defined in the usual manner. The wavenumber expansions are identical to those stated in (4.1.7) and the inviscid zone velocity and pressure perturbations are expanded in the form

n	λ_0	$\bar{\xi}$	γ_0	ϕ_0
0.25	4.182	1.459	1.154	13.45°
0.5	4.135	1.502	1.112	13.59°
0.75	4.126	1.657	1.004	13.62°
0.95	4.215	1.954	0.862	13.35°
1	4.256	2.062	0.822	13.22°
1.05	4.304	2.185	0.781	13.08°
1.25	4.551	2.821	0.626	12.39°
1.5	4.922	3.894	0.472	11.48°
1.75	5.296	5.195	0.366	10.69°

Table 4.8: Calculated values for λ_0, $\bar{\xi}$, γ_0 and ϕ_0 for shear-thinning and shear-thickening Carreau fluids.

$$\tilde{u} = u_0(\xi) + \varepsilon u_1(\xi) + \cdots , \tag{4.3.3a}$$

$$\tilde{v} = v_0(\xi) + \varepsilon v_1(\xi) + \cdots , \tag{4.3.3b}$$

$$\tilde{w} = w_0(\xi) + \varepsilon w_1(\xi) + \cdots , \tag{4.3.3c}$$

$$\tilde{p} = p_0(\xi) + \varepsilon p_1(\xi) + \cdots . \tag{4.3.3d}$$

where $\xi = \varepsilon^{-3} z$. The preceding expansions are then substituted into the linearised disturbance equations along with the following forms for the differential operators when applied to the disturbance quantities

$$\frac{\partial}{\partial r} = \frac{\partial}{\partial r} + \left(\frac{\mathrm{i}}{\varepsilon^3}\right)(\alpha_0 + \varepsilon\alpha_1 + \cdots), \quad \frac{\partial}{\partial \theta} = \left(\frac{\mathrm{i}}{\varepsilon^3}\right)(\beta_0 + \varepsilon\beta_1 + \cdots).$$

The asymptotic expansions of the disturbance equations are given in §B.3. Equating terms of $\mathcal{O}(\varepsilon^{-3})$ we find that w_0 satisfies Rayleigh's equation given by (4.2.7). This is again solved subject to (4.1.12) with η being replaced by ξ. By choosing $\lambda_0 = \alpha_0 r/\beta_0$ such that $\bar{\bar{u}}$ and $\bar{\bar{u}}''$ vanish at $\xi = \bar{\xi}$ we ensure Rayleigh's equation is not singular at the critical layer. Our numerical calculations are presented in table 4.8 and the zero order eigenfunctions are plotted in figure 4.14.

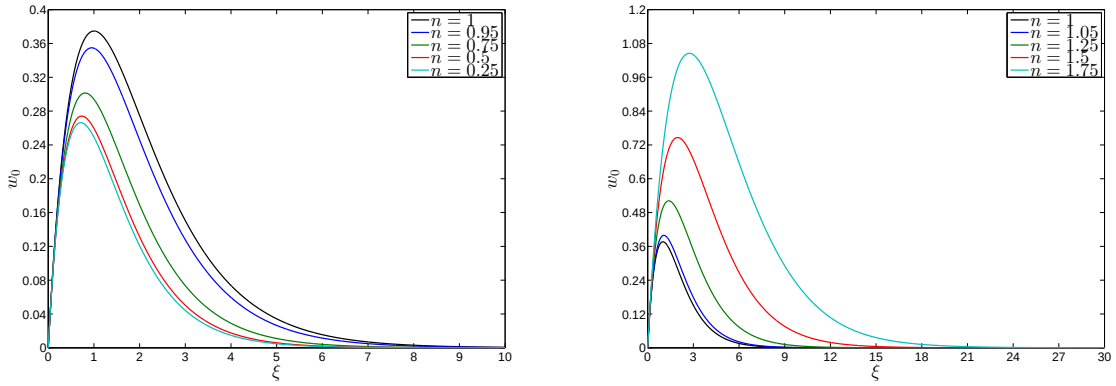

Figure 4.14: The inviscid eigenfunction w_0 versus ξ for shear-thinning and shear-thickening Carreau fluids.

At the next order in the inviscid zone we find that $w_1(0)$ satisfies (4.2.11) where I_1 and I_2 are given by (4.1.20a) and (4.1.20b) respectively.

As with the previous calculations, we find that the path of integration must be deformed above the singularity. The integrals I_1 and I_2 are computed in much the same way, where, for consistency, we take $\xi_s = 0.0260 = \eta_s = \zeta_s$. Our numerical calculations for both the integrals are displayed in table 4.9.

As before we consider the structure of the wall layer solution in order to solve for the first order correction terms to the effective wavenumber and wave angle. The wall layer coordinate $\xi_w = z\varepsilon^{-4}$. In the limit as $\xi \to 0$ the basic flow solutions take the form

$$\bar{u} = \varepsilon\xi_w\bar{u}_0 + \varepsilon^2\xi_w^2\bar{u}_1 + \cdots , \tag{4.3.4a}$$

$$\bar{v} = \varepsilon\xi_w\bar{v}_0 + \varepsilon^2\xi_w^2\bar{v}_1 + \cdots , \tag{4.3.4b}$$

$$\bar{w} = \varepsilon^2\xi_w^2\bar{w}_1 + \varepsilon^3\xi_w^3\bar{w}_2 + \cdots , \tag{4.3.4c}$$

where the notation used here is consistent with that of the previous section. The disturbance quantities expand as

n	I_1	I_2
0.25	0.0922	$0.0622 + 0.0318\mathrm{i}$
0.5	0.1008	$0.0651 + 0.0321\mathrm{i}$
0.75	0.1344	$0.0712 + 0.0359\mathrm{i}$
0.95	0.2190	$0.0804 + 0.0405\mathrm{i}$
1	0.2573	$0.0835 + 0.0422\mathrm{i}$
1.05	0.3087	$0.0867 + 0.0445\mathrm{i}$
1.25	0.6800	$0.1065 + 0.0557\mathrm{i}$
1.5	1.9397	$0.1383 + 0.0786\mathrm{i}$
1.75	5.1699	$0.1759 + 0.1123\mathrm{i}$

Table 4.9: Numerical values of the integrals I_1 and I_2 for shear-thinning and shear-thickening Carreau fluids.

$$\tilde{u} = U_0(\xi_w) + \varepsilon U_1(\xi_w) + \cdots , \tag{4.3.5a}$$

$$\tilde{v} = V_0(\xi_w) + \varepsilon V_1(\xi_w) + \cdots , \tag{4.3.5b}$$

$$\tilde{w} = \varepsilon W_0(\xi_w) + \varepsilon^2 W_1(\xi_w) + \cdots , \tag{4.3.5c}$$

$$\tilde{p} = \varepsilon P_0(\xi_w) + \varepsilon^2 P_1(\xi_w) + \cdots . \tag{4.3.5d}$$

The asymptotic expansions of the disturbance equations are given in §B.4. Equating terms of $\mathcal{O}(\varepsilon^{-2})$ and noting that $P_0 \equiv 0$ we find that

$$\mathrm{i}\bar{\bar{u}}_0\xi_w U_0 + rW_0\bar{u}_0 = \bar{\mu}_0\frac{d^2U_0}{d\xi_w^2} + \frac{\bar{u}_0k^2(\bar{\mu}_0-1)(n-1)}{1+k^2(\bar{u}_0^2+\bar{v}_0^2)}\left(\bar{u}_0\frac{d^2U_0}{d\xi_w^2} + \bar{v}_0\frac{d^2V_0}{d\xi_w^2}\right), \tag{4.3.6a}$$

$$\mathrm{i}\bar{\bar{u}}_0\xi_w V_0 + rW_0\bar{v}_0 = \bar{\mu}_0\frac{d^2V_0}{d\xi_w^2} + \frac{\bar{v}_0k^2(\bar{\mu}_0-1)(n-1)}{1+k^2(\bar{u}_0^2+\bar{v}_0^2)}\left(\bar{u}_0\frac{d^2U_0}{d\xi_w^2} + \bar{v}_0\frac{d^2V_0}{d\xi_w^2}\right), \tag{4.3.6b}$$

where $\bar{\mu}_0 = 1 + c_0[1 + k^2(\bar{u}_0^2 + \bar{v}_0^2)]^{(n-1)/2}$. Following the analysis of §4.1.3 we find that w_1 must satisfy

$$w_1 \to \frac{w_0'(0)\mathrm{Ai}'(0)}{\gamma\int_0^\infty \mathrm{Ai}(s)\,\mathrm{d}s} \quad \text{as} \quad \xi \to 0, \tag{4.3.7}$$

n	$-\gamma_1$	λ_1
0.25	9.16	16.63
0.5	9.06	16.56
0.75	8.57	17.34
0.95	7.58	19.00
1	7.25	19.59
1.05	6.82	20.08
1.25	5.49	22.89
1.5	3.88	25.87
1.75	2.73	27.85

Table 4.10: First order corrections to the effective wavenumber and wave angle for shear-thinning and shear-thickening Carreau fluids.

where

$$\gamma = \left\{ \frac{\mathrm{i}\bar{\bar{u}}_0[1 + k^2(\bar{u}_0^2 + \bar{v}_0^2)]}{\bar{\mu}_0[1 + k^2(\bar{u}_0^2 + \bar{v}_0^2)] + k^2(\bar{\mu}_0 - 1)(n-1)(\bar{u}_0^2 + \bar{v}_0^2)} \right\}^{1/3}.$$

Matching the solution from the inviscid zone with the wall layer solution produces the linear eigenrelation given by (4.2.17), where γ is as given above. Solving the eigenrelation we determine the constants γ_1 and λ_1, defined by (4.2.18a) and (4.2.18b), respectively; the resulted are tabulated above.

Thus, as before, we are able to determine the next order terms in the asymptotic expansions of the effective wavenumber and wave angle

$$\gamma = \gamma_0 + \gamma_1 R^{-1/3} + \cdots, \tag{4.3.8a}$$

$$\phi = \frac{\pi}{2} - \arctan(\lambda_0 + \lambda_1 R^{-1/3} + \cdots), \tag{4.3.8b}$$

where R is the modified Reynolds number defined in §2.2.3. For brevity we choose to exclude the detail regarding the radial and azimuthal wavenumbers. Expressions for $\bar{\alpha}$ and $\bar{\beta}$ are easily inferred from §4.2. It is sufficient to note that the $\bar{\alpha}$ and $\bar{\beta}$ plots are qualitatively similar to the combined wavenumber plots in both the shear-thinning and

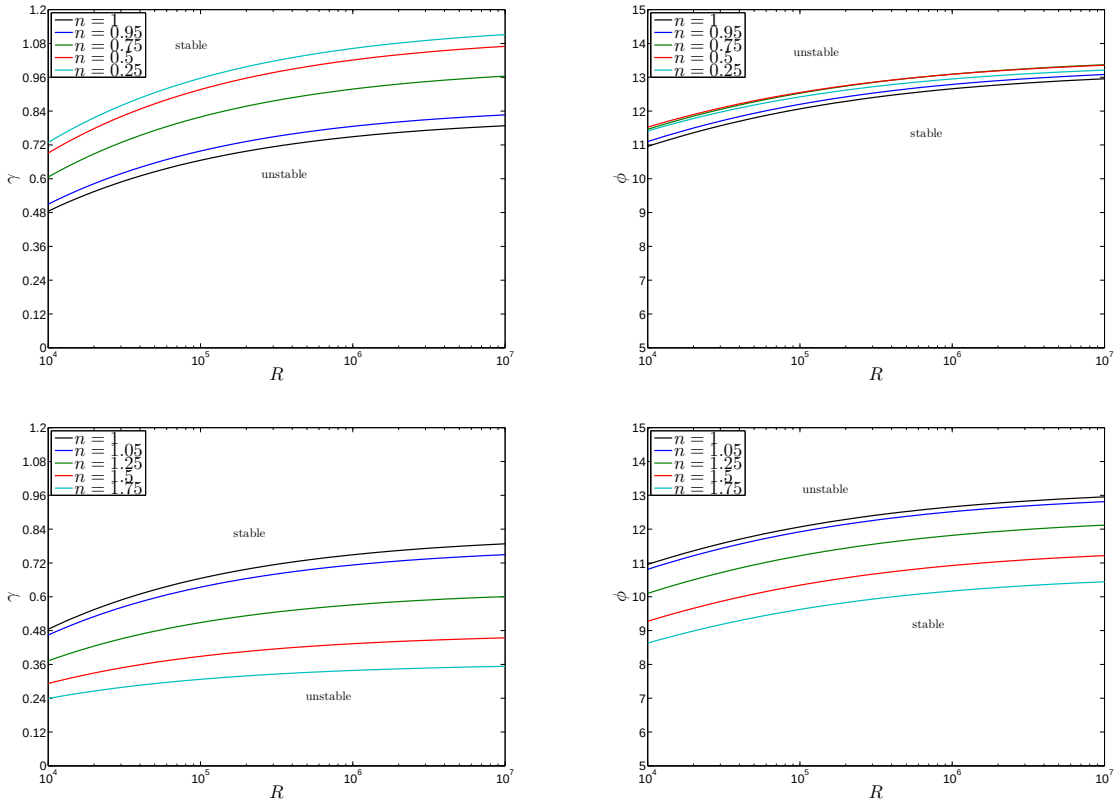

Figure 4.15: The two term asymptotic predictions of the neutral wavenumber γ and wave angle ϕ versus the Reynolds number R for shear-thinning and shear-thickening Carreau fluids.

shear-thickening cases.

The zero-order analysis reveals that increasing the shear-thinning parameter has little effect on the wave angle of the disturbances. This is contrary to the shear-thickening results where increasing n clearly decreases the wave angle ϕ_0. The effective wavenumber also decreases with increasing n. This provides the first indication that shear-thinning may have a destabilising effect on the boundary-layer flow. This is in direct contrast to the power-law results presented in §4.1. It is very interesting to note that when $n = 1$ the zero order prediction for the wave angle is identical to that of Hall (1986), this is not immediately obvious as here the viscosity function is set to $\bar{\mu} = 1 + c_0$, rather than unity. This suggests that in the large Reynolds number limit the angle of the spiral vortices is

independent of the viscosity, in the Newtonian case at least.

These primary results are reinforced at the next order. Figure 4.15 shows that increasing the power-law index effectively reduces the area encompassed by the wavenumber neutral curve, therefore predicting that shear-thickening has a potentially stabilising effect. We observe that the angle of the spiral vortices is not greatly effected by shear-thinning but is significantly reduced in the shear-thickening case. This would suggest a destabilising effect with respect to the wave angle.

4.4 Concluding Remarks

In this chapter we have shown that the inviscid stability analysis used to describe the upper-branch stationary neutral modes of the von Kármán flow (for $Re \gg 1$) can be extended to incorporate the rheology of power-law, Bingham plastic and Carreau fluids. As one might expect the solutions in the respective inviscid zones are not dissimilar to Hall's Newtonian results. It is within the viscous wall layer where we observe the emergence of additional non-Newtonian terms. Despite the appearance of these additional viscous terms in our leading order equations we find that analytic results are still obtainable. By appealing to an additional matched solution and noting $\lambda_0 \neq -\bar{v}_0/\bar{u}_0$, we determine the wall layer solutions in terms of the decaying Airy function Ai. Matching these solutions with the solutions in the inviscid zone we obtain a set of linear eigenrelations which we then solve for the first order correction terms to the effective wavenumber and wave angle.

The results for shear-thinning power-law fluids suggest that decreasing n has a stabilising effect on the flow, as noted by Griffiths *et al.* (2014*a*). A similar conclusion is drawn in §4.2 where we predict that an increase in fluid yield stress will also produce favourable stabilising behaviour, with fewer spiral vortices predicted as B_n increases from zero. Interestingly, our results for shear-thinning Carreau fluids are in disagreement with the power-law results. Although decreasing n below one has little effect on the wave angle,

our analysis predicts that a greater number of spiral vortices will be shed from the disk in this case, indicating destabilisation. Correspondingly, we observe that shear-thickening fluids have the opposite effect on the boundary-layer flow.

To further explore, and hopefully justify this contradictory conclusion we will proceed by presenting a numerical investigation, akin to that of Malik (1986) and Lingwood (1995*a*). It is hoped that results from this study will validate our exact asymptotic predictions. Unlike the asymptotic analysis, this investigation will not be entirely mathematically rigorous but will provide a better description of the physics, especially at lower Reynolds numbers. Indeed, the aim will be to determine values for the critical Reynolds number at which the onset of convective instability is first predicted. It is expected that in the large Reynolds number limit the asymptotics will provided a good approximation to the numerical solutions.

Chapter 5

Numerical Analysis - The Convective Instabilities

In this chapter we reformulate our system of linear disturbance equations with the aim of studying, numerically, the linear convective instability associated with generalised Newtonian boundary-layer flow on a rotating disk. Following the approach of Malik (1986) and Lingwood (1995*a*) we compute curves of neutral stability that can then be directly compared to our asymptotic predictions. Numerous other studies have utilised and modified the numerical scheme employed by Lingwood (1995*a*). Garrett & Peake (2002) consider the stability and transition of the boundary-layer on a rotating sphere whilst Garrett *et al.* (2009) investigate the cross-flow instability of the boundary-layer on a rotating cone. One particularly interesting extension, with respect to the von Kármán boundary-layer, is the temperature dependent viscosity study of Jasmine & Gajjar (2005). The authors introduce a viscosity model based on an inverse linear function of temperature, controlled by the small parameter ϵ (not to be confused with our boundary-layer scaling ε). They conclude that the stability of the flow is particularly sensitive to changes in viscosity and even for small positive values of ϵ the flow is much more unstable compared to the constant viscosity case defined by $\epsilon = 0$.

As with the previous chapter a detailed analysis is presented firstly for case I. It transpires that the numerical solution of the reformulated stability equations relies heavily on the far-field form of the viscosity function. As we will see, the numerical integration starts at the outer-edge of the boundary-layer, moving down towards the surface of the disk. Thus, in order to initiate, the scheme requires data from the base flow velocity and velocity components at the boundary-layer edge. It is this requirement that eliminates the possibility of a numerical investigation for case II, as noted by Griffiths (2015). We have seen that for case II the viscosity profiles grow exponentially in the far-field and thus the scheme will fail to initiate. It is sufficient for the viscosity profiles to exhibit constant gradient behaviour at the outer-edge of the boundary-layer hence we find that numerical solutions are achievable for cases I and III.

The power-law analysis presented within this chapter appears in the literature as Griffiths *et al.* (2014*b*). We note that the notation used within this chapter is self-contained and therefore shouldn't be confused with that of the preceding chapters.

5.1 Case I: Power-law

As before we begin by perturbing the base flow velocity and pressure profiles to determine a new set of linear disturbance equations dependent on the power-law index. By assuming the perturbations quantities have the normal-mode form we are then able to derive a sixth-order system of ODEs, from which we compute the curves of neutral stability. Akin to previous Newtonian studies we find that the neutral curves have two critical values associated with the type I, upper-branch, and type II lower-branch modes. In the limit of large Reynolds number we are able to compare our solutions with the asymptotic predictions.

5.1.1 Derivation of the perturbation equations

Here the problem formulation differs somewhat from that of the asymptotic study. For completeness we begin by introducing the dimensional governing boundary-layer equations, easily obtained from (2.2.19)

$$\frac{1}{r^*}\frac{\partial(r^*\tilde{U}_0^*)}{\partial r^*}+\frac{1}{r^*}\frac{\partial\tilde{V}_0^*}{\partial\theta}+\frac{\partial\tilde{W}_0^*}{\partial z^*}=0, \tag{5.1.1a}$$

$$\tilde{\mathcal{L}}_0^*\tilde{U}_0^*-\frac{(\tilde{V}_0^*+r^*\Omega^*)^2}{r^*}=\frac{1}{\rho^*}\frac{\partial}{\partial z^*}\left(\tilde{\mu}_0^*\frac{\partial\tilde{U}_0^*}{\partial z^*}\right), \tag{5.1.1b}$$

$$\tilde{\mathcal{L}}_0^*\tilde{V}_0^*+\frac{\tilde{U}_0^*\tilde{V}_0^*}{r^*}+2\Omega^*\tilde{U}_0^*=\frac{1}{\rho^*}\frac{\partial}{\partial z^*}\left(\tilde{\mu}_0^*\frac{\partial\tilde{V}_0^*}{\partial z^*}\right), \tag{5.1.1c}$$

$$\begin{aligned}\tilde{\mathcal{L}}_0^*\tilde{W}_0^*=\frac{1}{\rho^*}\Bigg[&-\frac{\partial\tilde{P}_1^*}{\partial z^*}+\frac{1}{r^*}\frac{\partial}{\partial r^*}\left(\tilde{\mu}_0^* r^*\frac{\partial\tilde{U}_0^*}{\partial z^*}\right)\\&+\frac{1}{r^*}\frac{\partial}{\partial\theta}\left(\tilde{\mu}_0^*\frac{\partial\tilde{V}_0^*}{\partial z^*}\right)+2\frac{\partial}{\partial z^*}\left(\tilde{\mu}_0^*\frac{\partial\tilde{W}_0^*}{\partial z^*}\right)\Bigg],\end{aligned} \tag{5.1.1d}$$

where

$$\tilde{\mathcal{L}}_0^*=\frac{\partial}{\partial t^*}+\tilde{U}_0^*\frac{\partial}{\partial r^*}+\frac{\tilde{V}_0^*}{r^*}\frac{\partial}{\partial\theta}+\tilde{W}_0^*\frac{\partial}{\partial z^*}.$$

The viscosity function $\tilde{\mu}_0^*$ is given by

$$\tilde{\mu}_0^*=m^*\left[\left(\frac{\partial\tilde{U}_0^*}{\partial z^*}\right)^2+\left(\frac{\partial\tilde{V}_0^*}{\partial z^*}\right)^2\right]^{(n-1)/2}. \tag{5.1.1e}$$

Here $(\tilde{U}_0^*,\tilde{V}_0^*,\tilde{W}_0^*)$ are the leading order velocity components and $\tilde{P}_1^*$ is the leading order fluid pressure term.

We introduce the generalisation of the classic Newtonian similarity solution in order to solve for the steady mean flow relative to the disk. The dimensionless similarity variables

are defined by

$$U(\eta) = \frac{\tilde{U}_0^*}{r^*\Omega^*}, \quad V(\eta) = \frac{\tilde{V}_0^*}{r^*\Omega^*}, \quad W(\eta) = \frac{\tilde{W}_0^*}{\sigma^*}, \quad P(\eta) = \frac{\tilde{P}_1^*}{\rho^*{\sigma^*}^2}, \tag{5.1.2}$$

where

$$\sigma^* = \left[\frac{\nu^*}{{r^*}^{1-n}{\Omega^*}^{1-2n}}\right]^{1/(n+1)}.$$

Here (U, V, W) are the dimensionless radial, azimuthal and axial base flow velocities, respectively, P is the pressure and $\nu^* = m^*/\rho^*$ is the kinematic viscosity. The dimensionless similarity coordinate is

$$\eta = \frac{{r^*}^{(1-n)/(n+1)} z^*}{{L^*}^{2/(n+1)}} \quad \text{where} \quad L^* = \sqrt{\frac{\nu^*}{{\Omega^*}^{2-n}}},$$

is the non-dimensionalising lengthscale. Substitution of the similarity variables into (5.1.1) yields exactly the base flow equations derived in §3.2, albeit with a slight change of notation.

The stability analysis, applied at a radius r_a^*, involves imposing infinitesimally small disturbances on the steady mean flow. The local Reynolds number is defined as

$$R = {r_a^*}^{2/(n+1)}\left[\frac{{\Omega^*}^{2-n}L^*}{\nu^*}\right]^{2/(n+1)} = \left[\frac{r_a^*}{L^*}\right]^{2/(n+1)} = r_a^{2/(n+1)}. \tag{5.1.3}$$

We note that this R is identical to the modified Reynolds number outlined in the asymptotic analysis. Thus we are able to provide direct comparisons between our numerical and asymptotic results. The non-dimensionalising velocity, pressure and time-scales are $r_a^*\Omega^*$, $\rho^*{r_a^*}^2{\Omega^*}^2$ and $L^*/(\Omega^* r_a^*)$, respectively. The leading order pressure terms in the radial and azimuthal momentum equations are retained, allowing for the inclusion of the distur-

bance pressure terms in the respective linear disturbance equations. The instantaneous non-dimensional velocities and pressure are given by

$$\tilde{U}_0(\eta, r, \theta, t) = \frac{r}{R^{(n+1)/2}} U(\eta) + u(r, \theta, \eta, t), \tag{5.1.4a}$$

$$\tilde{V}_0(\eta, r, \theta, t) = \frac{r}{R^{(n+1)/2}} V(\eta) + v(r, \theta, \eta, t), \tag{5.1.4b}$$

$$\tilde{W}_0(\eta, r, \theta, t) = \frac{r^{(n-1)/(n+1)}}{R^{(n+1)/2}} W(\eta) + w(r, \theta, \eta, t), \tag{5.1.4c}$$

$$\tilde{P}_1(\eta, r, \theta, t) = \frac{r^{2(n-1)/(n+1)}}{R^{(n+1)}} P(\eta) + p(r, \theta, \eta, t), \tag{5.1.4d}$$

where $\eta = \eta(r, z) = r^{(1-n)/(n+1)} z$ and u, v, w and p are small perturbation quantities.

The dimensionless Navier-Stokes equations are linearised with respect to the perturbation quantities. In much the same way as Lingwood (1995*a*) we utilise a parallel-flow approximation in order to make the linearised perturbation equations separable in r, θ and t. This so called 'parallel-flow' approximation is commonplace in the analysis of growing boundary layers, where the variation of the Reynolds number in the streamwise direction is often ignored. In order to be consistent with preceding studies we use the same terminology here. Ignoring variations in the Reynolds number with radius we replace the variable r with $R^{(n+1)/2}$. Thus the linear disturbance equations take the form

$$R^{(n-1)/2} \frac{\partial u}{\partial r} + \frac{u}{R} + \frac{\eta(1-n)}{R(n+1)} \frac{\partial u}{\partial \eta} + \frac{1}{R} \frac{\partial v}{\partial \theta} + \frac{\partial w}{\partial \eta} = 0, \tag{5.1.5a}$$

$$\begin{aligned} R^{(n-1)/2} \left(\frac{\partial u}{\partial t} + U \frac{\partial u}{\partial r} \right) + \frac{V}{R} \frac{\partial u}{\partial \theta} + \frac{W}{R} \frac{\partial u}{\partial \eta} + \frac{Uu}{R} - \frac{2(V+1)v}{R} + U'w \\ + \frac{\eta(1-n)}{R(n+1)} \left(U'u + U \frac{\partial u}{\partial \eta} + \frac{\partial p}{\partial \eta} \right) = -R^{(n-1)/2} \frac{\partial p}{\partial r} + \frac{1}{R} \frac{\partial}{\partial \eta} \left(\mu \frac{\partial u}{\partial \eta} + \hat{\mu} U' \right), \end{aligned} \tag{5.1.5b}$$

$$R^{(n-1)/2}\left(\frac{\partial v}{\partial t}+U\frac{\partial v}{\partial r}\right)+\frac{V}{R}\frac{\partial v}{\partial\theta}+\frac{W}{R}\frac{\partial v}{\partial\eta}+\frac{Uv}{R}+\frac{2(V+1)u}{R}+V'w$$
$$+\frac{\eta(1-n)}{R(n+1)}\left(V'u+U\frac{\partial v}{\partial\eta}\right)=-\frac{1}{R}\frac{\partial p}{\partial\theta}+\frac{1}{R}\frac{\partial}{\partial\eta}\left(\mu\frac{\partial v}{\partial\eta}+\hat{\mu}V'\right), \quad (5.1.5c)$$

$$R^{(n-1)/2}\left(\frac{\partial w}{\partial t}+U\frac{\partial w}{\partial r}\right)+\frac{V}{R}\frac{\partial w}{\partial\theta}+\frac{W}{R}\frac{\partial w}{\partial\eta}+\frac{W'w}{R}+\frac{\eta(1-n)}{R(n+1)}U\frac{\partial w}{\partial\eta}$$
$$=-\frac{\partial p}{\partial\eta}+\frac{1}{R}\frac{\partial}{\partial\eta}\left(\mu\frac{\partial w}{\partial\eta}\right)+\mathcal{O}(R^{-2}), \quad (5.1.5d)$$

where $\mu=[U'^2+V'^2]^{(n-1)/2}$ and the disturbance viscosity function is given by

$$\hat{\mu}=\frac{(n-1)\mu}{U'^2+V'^2}\left(U'\frac{\partial u}{\partial\eta}+V'\frac{\partial v}{\partial\eta}\right).$$

The above is directly equivalent to (4.1.4f) given in the formulation of the linear disturbance equations for the corresponding asymptotic analysis. The additional viscous terms associated with the generalised binomial expansion of the perturbed viscosity function do not appear in (5.1.5d) as these are found to be $\mathcal{O}(R^{-2})$.

The $\mathcal{O}(R^{-2})$ terms are neglected, and as in the rotating cone study of Garrett *et al.* (2009), we assume that the boundary-layer coordinate scaled by the Reynolds number is small, so that $\eta/R\ll 1$. The aforementioned viscous terms are also removed from this analysis. We appeal to the preceding asymptotic investigation for justification of this simplification. We have already determined exact analytical solutions for the upper-branch neutral modes, inclusive of the disturbance viscosity terms $R^{-1}[\hat{\mu}(U',V')]'$. Thus it is with relative ease that we are able to make direct comparisons between solutions, both with, and without these additional terms, although we omit the full details here. It transpires that the solutions obtained from the reduced system of equations do provide an excellent approximation to those presented in §4.1.5. Comparative plots of the asymptotic neutral wavenumber and wave angle are presented in figure 5.1. Indeed, for every n within

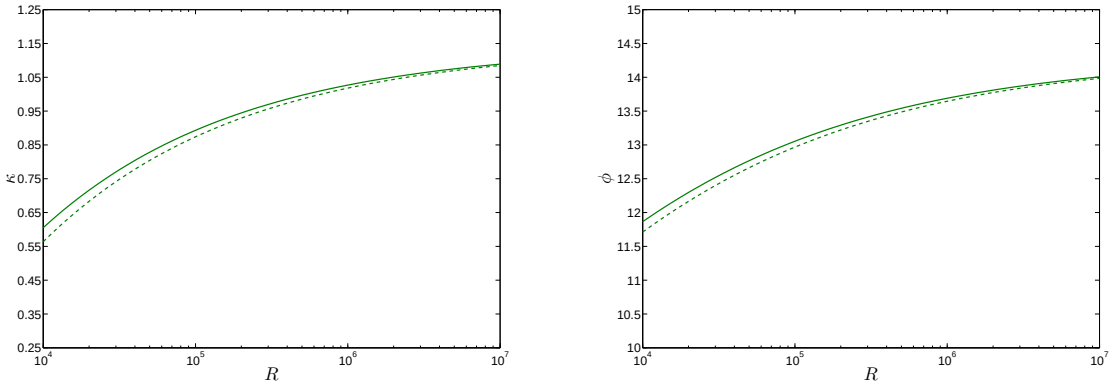

Figure 5.1: The neutral wavenumber and wave angle predictions for power-law fluids with $n = 0.8$. The solid lines are the exact solutions obtained in §4.1.5, the dashed lines represent the approximate solutions.

our scope of interest there is a good agreement between the two sets of solutions, with the limiting asymptotic values being recovered by the approximate results as $R \to \infty$.

Having simplified the linear disturbance equations we assume that the perturbation quantities have the normal-mode form

$$u = \hat{u}(\eta; \alpha, \beta, \omega; R, n) e^{\mathrm{i}(\alpha r + \beta\theta - \omega t)}, \tag{5.1.6a}$$

$$v = \hat{v}(\eta; \alpha, \beta, \omega; R, n) e^{\mathrm{i}(\alpha r + \beta\theta - \omega t)}, \tag{5.1.6b}$$

$$w = \hat{w}(\eta; \alpha, \beta, \omega; R, n) e^{\mathrm{i}(\alpha r + \beta\theta - \omega t)}, \tag{5.1.6c}$$

$$p = \hat{p}(\eta; \alpha, \beta, \omega; R, n) e^{\mathrm{i}(\alpha r + \beta\theta - \omega t)}, \tag{5.1.6d}$$

where $\hat{u}$, $\hat{v}$ and $\hat{w}$ are the spectral representations of the perturbation velocities and $\hat{p}$ is the spectral representation of the perturbation pressure. The complex frequency of the disturbance in the rotating frame is $\omega = \omega_r + \mathrm{i}\omega_i$, the complex radial wavenumber is $\alpha = \alpha_r + \mathrm{i}\alpha_i$ and β is the real azimuthal wavenumber.

The perturbation equations may be written as a set of six first order ordinary differential equations in the following transformed variables:

$$\eta_1(\eta;\alpha,\beta,\omega;R,n) = (\bar{\alpha} - \mathrm{i}/R)\hat{u} + \bar{\beta}\hat{v}, \tag{5.1.7a}$$

$$\eta_2(\eta;\alpha,\beta,\omega;R,n) = (\bar{\alpha} - \mathrm{i}/R)\hat{u}' + \bar{\beta}\hat{v}', \tag{5.1.7b}$$

$$\eta_3(\eta;\alpha,\beta,\omega;R,n) = \hat{w}, \tag{5.1.7c}$$

$$\eta_4(\eta;\alpha,\beta,\omega;R,n) = \hat{p}, \tag{5.1.7d}$$

$$\eta_5(\eta;\alpha,\beta,\omega;R,n) = (\bar{\alpha} - \mathrm{i}/R)\hat{v} - \bar{\beta}\hat{u}, \tag{5.1.7e}$$

$$\eta_6(\eta;\alpha,\beta,\omega;R,n) = (\bar{\alpha} - \mathrm{i}/R)\hat{v}' - \bar{\beta}\hat{u}', \tag{5.1.7f}$$

where $\bar{\alpha} = R^{(n-1)/2}\alpha$, $\bar{\beta} = \beta/R$ and the primes denote differentiation with respect to η. These equations are

$$\eta_1' = \eta_2, \tag{5.1.8a}$$

$$\left[\frac{\mu\eta_2'}{R}\right]_v = \frac{\eta_2(W_s - \mu_v')}{R} + \frac{[\mathrm{i}R\left(\bar{\alpha}U + \bar{\beta}V - \bar{\omega}\right) + U_s]\eta_1}{R} - \frac{2(1_c + V_s)\eta_5}{R} + (\bar{\alpha}_1 U' + \bar{\beta}V')\eta_3 + \mathrm{i}\left[\kappa^2 - \left(\frac{\bar{\alpha}\mathrm{i}}{R}\right)_s\right]\eta_4, \tag{5.1.8b}$$

$$\eta_3' = -\mathrm{i}\eta_1, \tag{5.1.8c}$$

$$\eta_4' = \frac{\mathrm{i}[\eta_1 W_s - (\eta_1\mu)_v']}{R} - \frac{[\mathrm{i}R\left(\bar{\alpha}U + \bar{\beta}V - \bar{\omega}\right) + W_s']\eta_3}{R}, \tag{5.1.8d}$$

$$\eta_5' = \eta_6, \tag{5.1.8e}$$

$$\left[\frac{\mu\eta_6'}{R}\right]_v = \frac{\eta_6(W_s - \mu_v')}{R} + \frac{[\mathrm{i}R\left(\bar{\alpha}U + \bar{\beta}V - \bar{\omega}\right) + U_s]\eta_5}{R} + \frac{2(1_c + V_s)\eta_1}{R} + (\bar{\alpha}_1 V' - \bar{\beta}U')\eta_3 + \left[\frac{\bar{\beta}\eta_4}{R}\right]_s, \tag{5.1.8f}$$

where $\bar{\omega} = R^{(n-1)/2}\omega$, $\bar{\alpha}_1 = \bar{\alpha} - (\mathrm{i}/R)_s$, $\kappa^2 = \bar{\alpha}^2 + \bar{\beta}^2$ and the subscripts v, c and s indicate which of the $\mathcal{O}(R^{-1})$ terms are the viscous, Coriolis and streamline curvature terms, respectively.

If the Coriolis and streamline curvature effects are neglected, the result can be written

as the fourth-order Orr-Sommerfeld equation for the rotating disk

$$\mathrm{i}[\mu(\eta_3''' - \kappa^2\eta_3') + \mu'\eta_3'']' + R(\bar{\alpha}U + \bar{\beta}V - \bar{\omega})(\eta_3'' - \kappa^2\eta_3) - R(\bar{\alpha}U'' + \bar{\beta}V'')\eta_3 = 0. \quad (5.1.9)$$

Neglecting all the viscous terms the Orr-Sommerfeld equation reduces to the Rayleigh equation

$$(\bar{\alpha}U + \bar{\beta}V - \bar{\omega})(\eta_3'' - \kappa^2\eta_3) - (\bar{\alpha}U'' + \bar{\beta}V'')\eta_3 = 0. \quad (5.1.10)$$

We note here that

$$\kappa = \sqrt{\bar{\alpha}^2 + \bar{\beta}^2} = r^{(n-1)/(n+1)}\sqrt{\alpha^2 + \frac{\beta^2}{r^2}},$$

and

$$\phi = \arctan\left(\frac{\bar{\beta}}{\bar{\alpha}}\right) = \frac{\pi}{2} - \arctan\left(\frac{\alpha r}{\beta}\right).$$

Thus the definitions of the neutral wavenumber and wave angle are consistent with that of the asymptotic study.

Substitution of $n = 1$ into (5.1.8) does not admit the Newtonian set of perturbation equations derived by Lingwood (1995*a*). This is because of the boundary-layer approximation used in the formulation of this problem. In order to construct the steady mean flow solutions we removed the higher order viscous terms (see chapters 2 & 3). Thus we observe this slight departure from the expected Newtonian results. A comparison between the exact, Newtonian, perturbation equations and this system of boundary-layer equations is provided in the appendix C. We do note however, that (5.1.8) does indeed reduce to the corresponding Newtonian system when considered in the frame of a boundary-layer

approximation, as expected.

5.1.2 Solution of the perturbation equations

We solve the eigenvalue problem defined by system (5.1.8) subject to the homogenous boundary conditions

$$\eta_i = 0 \quad \text{at} \quad \eta = 0, \tag{5.1.11a}$$

$$\eta_i \to 0 \quad \text{as} \quad \eta \to \infty, \tag{5.1.11b}$$

for $i = 1, 2, \ldots, 6$. The sixth-order ordinary differential equation system (5.1.8) permits six independent solutions for each of the six transformed variables. We denote these by $\eta_i^j(\eta; \alpha, \beta, \omega; R, n)$, where the subscript i denotes one of the transformed variables and the superscript j indicates one of the corresponding six independent solutions. We find that the $j = 2$, 4 and 6 solutions grow exponentially as $\eta \to \infty$, whereas the $j = 1$, 3 and 5 solutions decay exponentially. From (5.1.11b) we have that solutions must decay in the far-field, thus we need only consider these decaying solutions. Each transformed variable solution is formed from a linear combination of these solutions with corresponding coefficients A_1, A_3 and A_5. These coefficients are determined from (5.1.11a) and so we write

$$\begin{bmatrix} \eta_1(0) \\ \eta_3(0) \\ \eta_5(0) \end{bmatrix} = \begin{bmatrix} \eta_1^1(0) & \eta_1^3(0) & \eta_1^5(0) \\ \eta_3^1(0) & \eta_3^3(0) & \eta_3^5(0) \\ \eta_5^1(0) & \eta_5^3(0) & \eta_5^5(0) \end{bmatrix} \begin{bmatrix} A_1 \\ A_3 \\ A_5 \end{bmatrix} = \begin{bmatrix} 0 \\ 0 \\ 0 \end{bmatrix}. \tag{5.1.12}$$

The above has non-trivial solutions when the determinant D, of the 3×3 matrix is zero

$$D(\alpha, \beta, \omega; R, n) = 0. \tag{5.1.13}$$

This is the dispersion relation for a rotating disk with fluid index n. At each R we are able to calculate α, β or ω, given the other two. Clearly when the dispersion relation is satisfied the 3×3 matrix is singular and so A_1, A_3 and A_5 are determined from singular value decomposition, which in turn allows for the eigenfunctions $\eta_i(\eta; \alpha, \beta, \omega; R, n)$ to be calculated.

The solution of (5.1.8) is dependent on the form of the far-field form of the steady mean flow quantities. From §3.2 we note that

$$U \to 0, \quad V \to -1, \quad W \to W_\infty = -\frac{(3n+1)}{(n+1)} \int_0^\infty U \, \mathrm{d}\eta,$$
$$U' \to 0, \quad V' \to 0, \quad W' \to 0, \quad \mu' \to \frac{(n-1)W_\infty}{n} = \frac{(1-n)(3n+1)}{n(n+1)} \int_0^\infty U \, \mathrm{d}\eta,$$

as $\eta \to \infty$. Substituting the above into (5.1.8) gives

$$\eta_1' = \eta_2, \tag{5.1.14a}$$
$$\eta_2' = \frac{\eta_2 W_\infty - \mathrm{i}nR(\bar{\beta} + \bar{\omega})\eta_1 + n(\mathrm{i}R\kappa^2 + \bar{\alpha})\eta_4}{n\mu_\infty}, \tag{5.1.14b}$$
$$\eta_3' = -\mathrm{i}\eta_1, \tag{5.1.14c}$$
$$\eta_4' = \frac{\mathrm{i}[\eta_1 W_\infty - \eta_2 n\mu_\infty + nR(\bar{\beta} + \bar{\omega})\eta_3]}{nR}, \tag{5.1.14d}$$
$$\eta_5' = \eta_6, \tag{5.1.14e}$$
$$\eta_6' = \frac{\eta_6 W_\infty - \mathrm{i}nR(\bar{\beta} + \bar{\omega})\eta_5 + n\bar{\beta}\eta_4}{n\mu_\infty}, \tag{5.1.14f}$$

where μ_∞ denotes evaluation of the function μ at some suitably large value of $\eta = \eta_\infty$. These have exact closed form solutions

$$\eta_i^j(\eta \to \infty; \alpha, \beta, \omega; R, n) = a_i^j e^{\gamma_j \eta}, \tag{5.1.15}$$

with the coefficients a_i^j and exponents γ_j being constants. By substituting (5.1.15) into

(5.1.14) we obtain

$$\gamma_1, \gamma_2 = \frac{W_\infty}{2n\mu_\infty} \mp \sqrt{\left(\frac{W_\infty}{2n\mu_\infty}\right)^2 - \frac{\mathrm{i}R(\bar{\beta}+\bar{\omega})}{\mu_\infty}}, \tag{5.1.16a}$$

$$\gamma_3, \gamma_4 = \frac{W_\infty}{2n\mu_\infty} \mp \sqrt{\left(\frac{W_\infty}{2n\mu_\infty}\right)^2 - \frac{\mathrm{i}R(\bar{\beta}+\bar{\omega})}{\mu_\infty}}, \tag{5.1.16b}$$

$$\gamma_5, \gamma_6 = \mp\sqrt{\kappa^2 - \frac{\bar{\alpha}\mathrm{i}}{R}}. \tag{5.1.16c}$$

The sign preceding the square-root terms shows why only the $j = 1$, 3 and 5 solutions are relevant here. The a_i^j terms for $i = 1$, 3 and 5 are

$$\begin{aligned}
&a_1^1 = 1, && a_1^3 = 0, && a_1^5 = \mathrm{i}\gamma_5,\\
&a_2^1 = \gamma_1, && a_2^3 = 0, && a_2^5 = \mathrm{i}\gamma_5^2,\\
&a_3^1 = -\mathrm{i}/\gamma_1, && a_3^3 = 0, && a_3^5 = 1,\\
&a_4^1 = 0, && a_4^3 = 0, && a_4^5 = [\mathrm{i}nR(\bar{\beta}+\bar{\omega}) - W_\infty\gamma_5 + n\mu_\infty(\kappa^2 - \bar{\alpha}\mathrm{i}/R)]/n\gamma_5 R,\\
&a_5^1 = 0, && a_5^3 = 1, && a_5^5 = 0,\\
&a_6^1 = 0, && a_6^3 = \gamma_3, && a_6^5 = 0.
\end{aligned}$$

The perturbation equations (5.1.8) are integrated from each of the initial solutions at the outer-edge of the boundary-layer down towards the surface of the disk. Here the boundary-layer is approximated by the region $0 \leq \eta \leq 20$, thus we find that generally the axial velocity component will not have converged to its constant limiting value within the confines of the boundary-layer region. This is due to the strong dependence the function W has on the fluid index n as it decays to the far-field, as noted in §3.2. Indeed, the computational boundary-layer thickness could be extended to ensure the use of fully converged steady mean flow results when solving system (5.1.8). However, this proves to be computationally very expensive. The step size in η was reduced and the value of infinity increased until there were no discernible differences in the numerical results. The

values taken were such that the boundary-layer was approximated by 2000 equally spaced data points between $\eta = 0$ and $\eta = 20$. This discretisation is known to be consistent with Lingwood (1995*a*) and Garrett & Peake (2004), for example, and represents an appropriate balance between accuracy and computational effort for each n. We find that increasing η_∞ beyond $\eta_\infty = 20$ does not serve to provide any significantly more accurate results. Thus, in much the same way as the study of Garrett & Peake (2004), we conclude that in this case, the cramping of the boundary-layer does not cause major inaccuracies when solving (5.1.8) subject to (5.1.11).

The spatial and temporal branches are calculated using a double-precision fixed-step-size, fourth-order Runge-Kutta integrator with Gram-Schmidt orthonormalisation and a Newton-Raphson linear search procedure, using a modification of the numerical code discussed in Garrett & Peake (2002). To calculate the spatial branches for each n and R for a given frequency ω, the wavenumber β is varied and the value of α that satisfies the dispersion relation is calculated. To calculate the temporal branches for each n and R for a given wavenumber β and imaginary part of the frequency ω_i, the real part of the frequency ω_r is varied and α is calculated in the same way. Comprehensive details on the implementation of the code are given in Lingwood (1995*b*)

5.1.3 Results

Here we solve (5.1.8) with the aim of studying the occurrence of convective instabilities. For each n in the particular range of interest two spatial branches determine the convective instability characteristics of the system. Figures 5.2 & 5.3 show the structure of these two branches in the complex α-plane when $n = 0.8$ for $R = 700$ and $R = 745$, we note that these plots have been constructed in the unscaled α axes as opposed to the scaled $\bar{\alpha}$ axes. A branch lying below the line $\alpha_i = 0$ indicates convective instability. Branch 2 ceases to exist when analysing the Orr-Sommerfeld equation (5.1.9), indicating that it has to arise

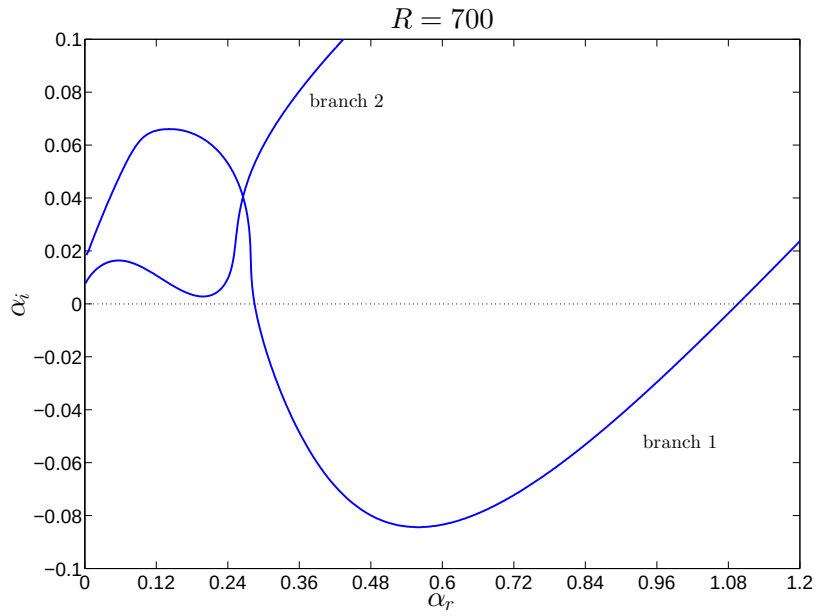

Figure 5.2: The two spatial branches determined from the governing dispersion relation for the case when $n = 0.8$, showing the type I instability from branch 1 only at $R = 700$. A branch lying below the line $\alpha_i = 0$ indicates a region of convective instability.

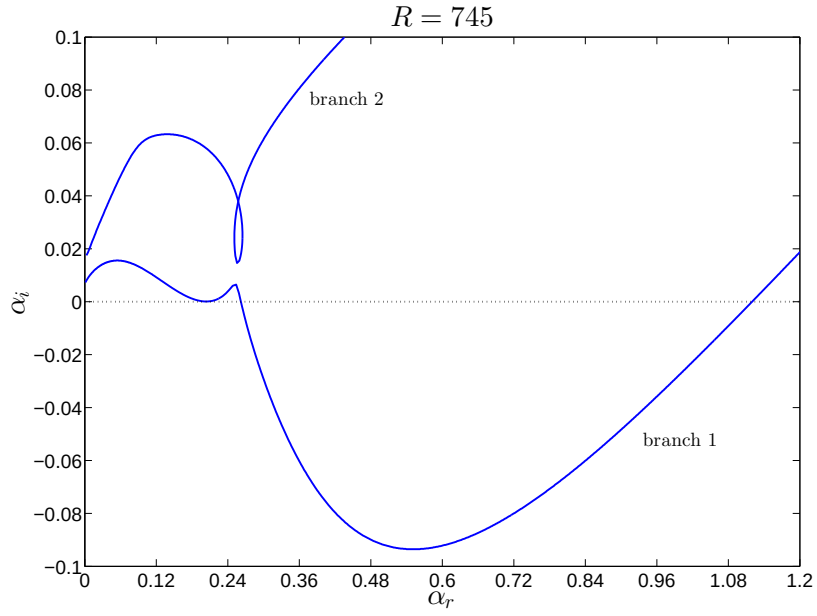

Figure 5.3: The two spatial branches showing the type I and type II instabilities from the modified branch 1 at $R = 745$. Here we see that there has been an exchange of modes.

n	R_c	$\bar{\alpha}$	$\bar{\beta}$	κ	ϕ
1	272.90	0.4033	0.0802	0.4112	11.25°
0.9	334.01	0.3767	0.0780	0.3847	11.69°
0.8	417.49	0.3522	0.0759	0.3603	12.17°
0.7	534.55	0.3311	0.0743	0.3394	12.64°
0.6	703.77	0.3132	0.0729	0.3216	13.10°

Table 5.1: The values of the critical Reynolds number R_c, wavenumbers $\bar{\alpha}$, $\bar{\beta}$ and κ, and wave angle ϕ corresponding to decreasing values of n on the upper-branch for stationary waves.

from streamline curvature effects. We observe from the figure 5.3 that at $R = 745$ there has been an exchange of modes.

The modified branch 1 now determines the region of convective instability. Increasing the value of R causes the peak between the two minima on branch 1 to move downwards and the points where the branch crosses the line $\alpha_i = 0$ move apart, thereby widening the regions of instability and mapping out two lobes on the neutral curve. Above a certain value of R the peak moves below the line $\alpha_i = 0$ and further increases in R change the region of instability, producing the upper and lower branches of the neutral curve.

This spatial branch behaviour is typical for each n. The neutral curves, defined by $\alpha_i = 0$, have been calculated for values of the power-law index ranging from $n = 0.6 - 1$ in increments of 0.1. Figures 5.4 & 5.5 show in detail the characteristic two-lobed structure synonymous with flows of this nature, an upper lobe due to the cross-flow instability and a lower lobe attributed to external streamline curvature. Each curve encloses a region that is convectively unstable. The neutral curves show that decreasing n, in the power-law regime, has the effect of stabilising the boundary-layer flow. The value of the critical Reynolds number is increased on both the upper and lower lobes as n decreases, as shown in tables 5.1 & 5.2, respectively. We note a slight discrepancy between our boundary-layer results for the case when $n = 1$ and the exact Newtonian results ($\epsilon = 0$) of Jasmine & Gajjar (2005). On the upper-branch Jasmine & Gajjar (2005)

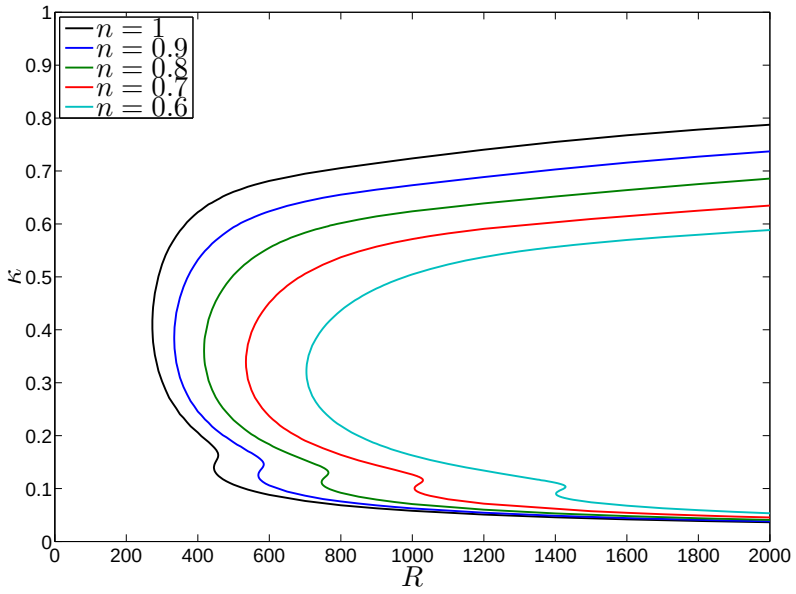

Figure 5.4: Neutral stability curves for decreasing values of n. The neutral wavenumber κ is plotted against the Reynolds number. The R-axis has been truncated at $R = 2000$.

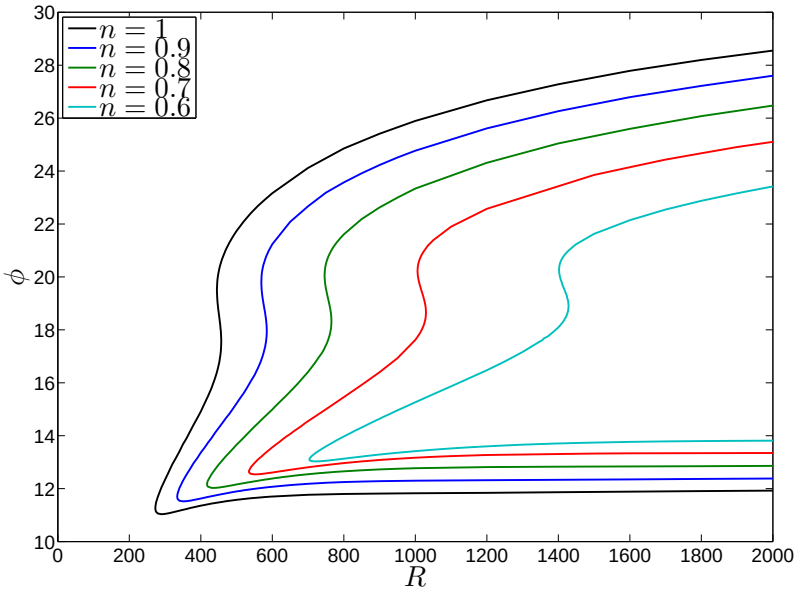

Figure 5.5: Neutral stability curves for decreasing values of n. The neutral wave angle ϕ is plotted against the Reynolds number. The R-axis has been truncated at $R = 2000$.

n	R_c	$\bar{\alpha}$	$\bar{\beta}$	κ	ϕ
1	445.22	0.1322	0.0467	0.1402	19.46°
0.9	569.27	0.1183	0.0425	0.1257	19.77°
0.8	746.23	0.1054	0.0385	0.1122	20.04°
0.7	1006.3	0.0941	0.0347	0.1003	20.23°
0.6	1402.0	0.0845	0.0312	0.0901	20.28°

Table 5.2: The values of the critical Reynolds number R_c, wavenumbers $\bar{\alpha}$, $\bar{\beta}$ and κ, and wave angle ϕ corresponding to decreasing values of n on the lower-branch for stationary waves.

report critical values of $R_c = 287.2$ with $\kappa = 0.3927$ and $\phi = 11.40°$ whilst on the lower-branch the critical values are given as $R_c = 451.4$ with $\kappa = 0.1402$ and $\phi = 19.50°$. In both cases the value of the critical Reynolds number presented here is marginally reduced due to the inaccuracies associated with the boundary-layer approximation at these relatively small Reynolds numbers. As mentioned previously this boundary-layer approximation is necessary in order to construct steady mean flow solutions when $n \neq 1$. We observe that although the critical Reynolds numbers have been reduced the values of the wavenumber and wave angle at these Reynolds numbers is not greatly affected when compared to the exact Newtonian results of Jasmine & Gajjar (2005)

Figures 5.6 & 5.7 show a comparison between the large Reynolds number neutral stability curves and the asymptotic results determined in §4.1.5. An excellent quantitative agreement is found between the two sets of solutions for each n in the range of interest, results for the cases when $n = 0.9$, 0.7 and 0.6 are given in the appendix C. As expected, in the large Reynolds number limit, the asymptotic predictions are indeed very good. However, as the Reynolds number decreases we find that the asymptotic predictions stray somewhat from the numerical results. A necessary asymptotic assumption is that $\varepsilon = Re^{-1/[3(n+1)]} \ll 1$ which is equivalent to $R \gg 1$. Thus the validity of these results diminishes somewhat as R decreases, hence we observe the slight departure from the numerical solutions in this case.

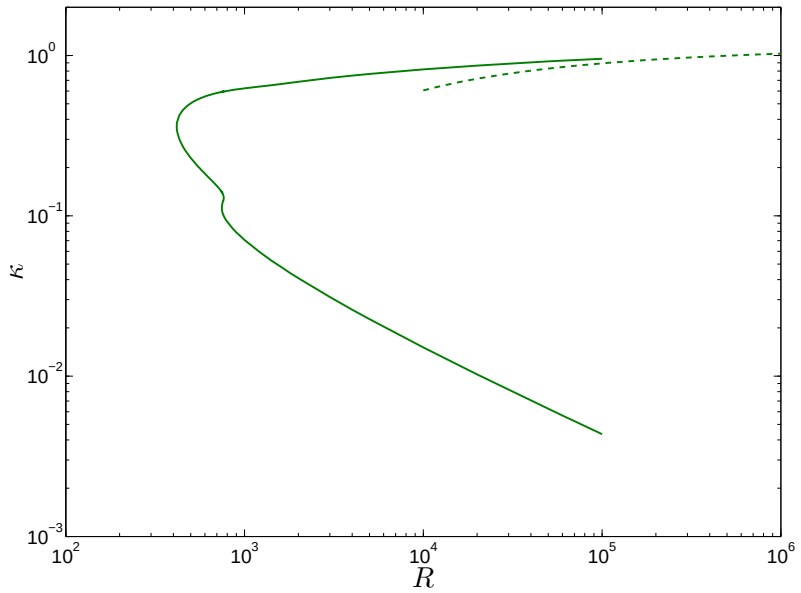

Figure 5.6: Neutral wavenumber stability curve for power-law fluids with $n = 0.8$. The type I asymptotic solutions are given by the dashed line.

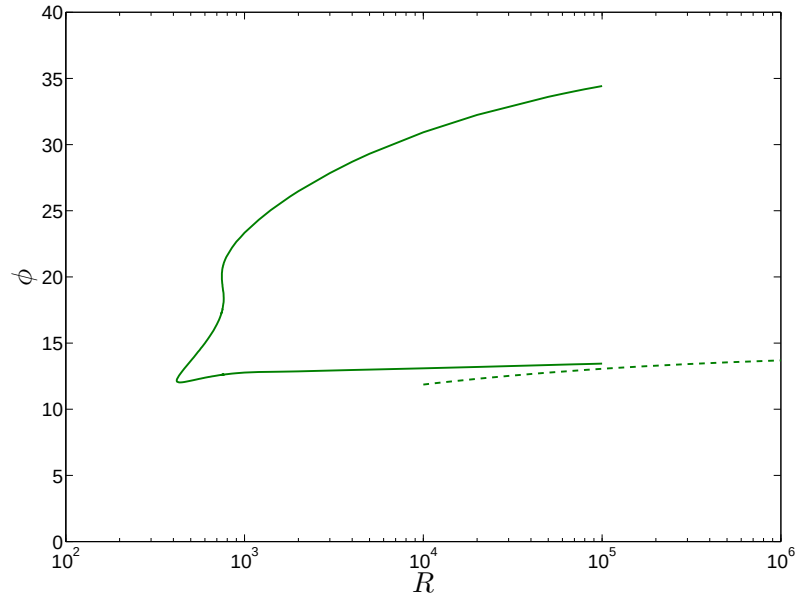

Figure 5.7: Neutral wave angle stability curve for power-law fluids with $n = 0.8$. The type I asymptotic solutions are given by the dashed line.

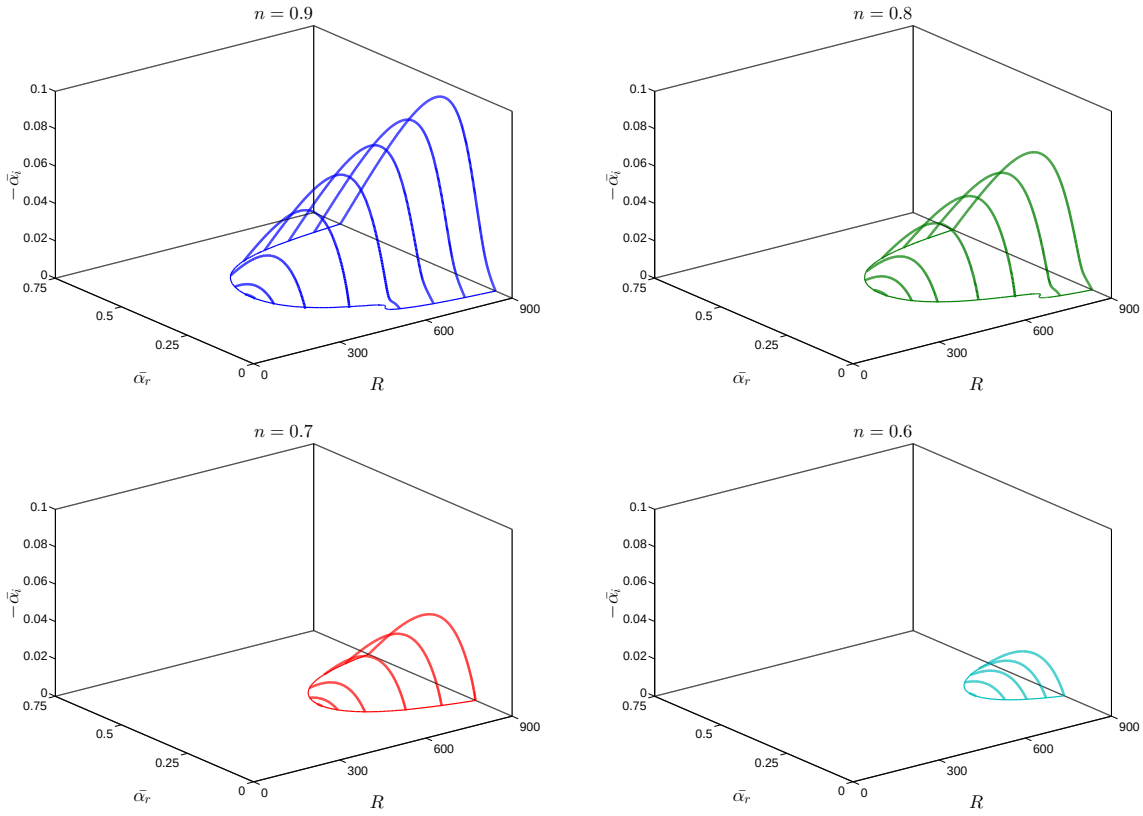

Figure 5.8: Linear convective growth rates for stationary mode disturbances of type I through the convectively unstable region for power-law fluids with $n = 0.9$, 0.8, 0.7, 0.6.

Figure 5.8 plots the spatial branches of the type I mode though the convectively unstable region for decreasing values of n in order to visualize the growth rates. In concordance with rotating cone study of Garrett (2010) we denote $-\bar{\alpha}_i$ as the spatial growth rate. For clarity and brevity the type II growth rates are not included here. These are found to be comparatively very small. However, we find that on both the upper and lower branches, as n decreases the growth rates are significantly reduced whilst also being pushed to a higher critical Reynolds number.

5.2 Case III: Carreau

We begin by recalling the governing boundary-layer equations (5.1.1a)-(5.1.1d), in this case the viscosity function $\tilde{\mu}_0^*$ is given by

$$\tilde{\mu}_0^* = \mu_\infty^* + (\mu_0^* - \mu_\infty^*)\left\{1 + \lambda^{*^2}\left[\left(\frac{\partial \tilde{U}_0^*}{\partial z^*}\right)^2 + \left(\frac{\partial \tilde{V}_0^*}{\partial z^*}\right)^2\right]\right\}^{(n-1)/2}. \tag{5.2.1}$$

The steady mean flow relative to the disk is solved for via the introduction of the classic Newtonian similarity solution. The dimensionless similarity variables are defined by

$$U(z) = \frac{\tilde{U}_0^*}{r^*\Omega^*}, \quad V(z) = \frac{\tilde{V}_0^*}{r^*\Omega^*}, \quad W(z) = \frac{\tilde{W}_0^*}{\sqrt{\nu^*\Omega^*}}, \quad P(z) = \frac{\tilde{P}_1^*}{\rho^*\nu^*\Omega^*}, \tag{5.2.2}$$

Here (U, V, W) are the dimensionless radial, azimuthal and axial base flow velocities, respectively, P is the pressure and $\nu^* = \mu_\infty^*/\rho^*$ is the kinematic viscosity. The dimensionless similarity coordinate is $z = z^*/L^*$ where $L^* = \sqrt{\nu^*/\Omega^*}$ is the non-dimensionalising length-scale. The dimensionless relaxation time is $k = \lambda^* r^* \Omega^* \sqrt{\Omega^*/\nu^*}$ and $c_0 = (\mu_0^* - \mu_\infty^*)/\mu_\infty^*$ is the dimensionless viscosity index. Substitution of the similarity variables into the dimensional boundary-layer equations yields the base flow ODEs obtained in §3.4.

Having already determined our steady mean flow profiles we begin by constructing our stability analysis about a specified radius r_s^*. The local Reynolds number is defined as $R = (r_s \Omega^* L^*)/\nu^* = r_s^*/L^* = r_s = rRe^{1/2}$. The non-dimensionalising velocity, pressure and time-scales are $r_s^*\Omega^*$, $\rho^* r_s^{*^2}\Omega^{*^2}$ and $L^*/(\Omega^* r_s^*)$, respectively. As before, we retain the leading order pressure terms in the radial and azimuthal momentum equations. The instantaneous non-dimensional velocities and pressure are given by

$$\tilde{U}_0(z, r, \theta, t) = \frac{r}{R}U(z) + u(r, \theta, z, t), \tag{5.2.3a}$$

$$\tilde{V}_0(z, r, \theta, t) = \frac{r}{R}V(z) + v(r, \theta, z, t), \tag{5.2.3b}$$

$$\tilde{W}_0(z,r,\theta,t) = \frac{1}{R}W(z) + w(r,\theta,z,t), \tag{5.2.3c}$$

$$\tilde{P}_1(z,r,\theta,t) = \frac{1}{R^2}P(z) + p(r,\theta,z,t), \tag{5.2.3d}$$

where u, v, w and p are the small perturbation quantities.

As in §5.1.1 we linearise the Navier-Stokes equations with respect to the perturbation quantities and ignore variations in the Reynolds number with radius, replacing the variable r with R. This is our parallel-flow approximation. Hence we find that the linear disturbance equations are simplified somewhat and are given by

$$\frac{\partial u}{\partial r} + \frac{u}{R} + \frac{1}{R}\frac{\partial v}{\partial \theta} + \frac{\partial w}{\partial z} = 0, \tag{5.2.4a}$$

$$\begin{aligned}\frac{\partial u}{\partial t} + U\frac{\partial u}{\partial r} + \frac{V}{R}\frac{\partial u}{\partial \theta} + \frac{W}{R}\frac{\partial u}{\partial z} + \frac{Uu}{R} - \frac{2(V+1)v}{R} + U'w &= -\frac{\partial p}{\partial r} \\ &\quad + \frac{1}{R}\frac{\partial}{\partial z}\left(\mu\frac{\partial u}{\partial z} + \hat{\hat{\mu}}U'\right),\end{aligned} \tag{5.2.4b}$$

$$\begin{aligned}\frac{\partial v}{\partial t} + U\frac{\partial v}{\partial r} + \frac{V}{R}\frac{\partial v}{\partial \theta} + \frac{W}{R}\frac{\partial v}{\partial z} + \frac{Uv}{R} + \frac{2(V+1)u}{R} + V'w &= -\frac{1}{R}\frac{\partial p}{\partial \theta} \\ &\quad + \frac{1}{R}\frac{\partial}{\partial z}\left(\mu\frac{\partial v}{\partial z} + \hat{\hat{\mu}}V'\right),\end{aligned} \tag{5.2.4c}$$

$$\begin{aligned}\frac{\partial w}{\partial t} + U\frac{\partial w}{\partial r} + \frac{V}{R}\frac{\partial w}{\partial \theta} + \frac{W}{R}\frac{\partial w}{\partial z} + \frac{W'w}{R} &= -\frac{\partial p}{\partial z} \\ &\quad + \frac{1}{R}\frac{\partial}{\partial z}\left(\mu\frac{\partial w}{\partial z}\right),\end{aligned} \tag{5.2.4d}$$

where $\mu = 1 + c_0[1 + k^2(U'^2 + V'^2)]^{(n-1)/2}$, the disturbance viscosity function is given by

$$\hat{\hat{\mu}} = \frac{k^2(\mu-1)(n-1)}{1 + k^2(U'^2 + V'^2)}\left(U'\frac{\partial u}{\partial z} + V'\frac{\partial v}{\partial z}\right),$$

and, as before, the $\mathcal{O}(R^{-2})$ terms associated with (5.2.4d) have been neglected.

We proceed by noting that the argument made in §5.1.1, regarding the dominant nature of the unperturbed viscous terms, again holds in this case. Having made this consideration we are able to write the perturbation equations as a set of six first order

ordinary differential equations in the following transformed variables:

$$z_1(z;\alpha,\beta,\omega;R,c_0,k,n) = (\alpha - \mathrm{i}/R)\hat{u} + \bar{\beta}\hat{v}, \tag{5.2.5a}$$

$$z_2(z;\alpha,\beta,\omega;R,c_0,k,n) = (\alpha - \mathrm{i}/R)\hat{u}' + \bar{\beta}\hat{v}', \tag{5.2.5b}$$

$$z_3(z;\alpha,\beta,\omega;R,c_0,k,n) = \hat{w}, \tag{5.2.5c}$$

$$z_4(z;\alpha,\beta,\omega;R,c_0,k,n) = \hat{p}, \tag{5.2.5d}$$

$$z_5(z;\alpha,\beta,\omega;R,c_0,k,n) = (\alpha - \mathrm{i}/R)\hat{v} - \bar{\beta}\hat{u}, \tag{5.2.5e}$$

$$z_6(z;\alpha,\beta,\omega;R,c_0,k,n) = (\alpha - \mathrm{i}/R)\hat{v}' - \bar{\beta}\hat{u}', \tag{5.2.5f}$$

where $\hat{u}$, $\hat{v}$, $\hat{w}$ and $\hat{p}$ are the corresponding normal-mode forms of the perturbations quantities, $\bar{\beta} = \beta/R$ and the primes denote differentiation with respect to z. These equations are

$$z_1' = z_2, \tag{5.2.6a}$$

$$\left[\frac{\mu z_2'}{R}\right]_v = \frac{z_2(W_s - \mu_v')}{R} + \frac{[\mathrm{i}R\left(\alpha U + \bar{\beta}V - \omega\right) + U_s]z_1}{R} - \frac{2(1_c + V_s)z_5}{R} + (\alpha_1 U' + \bar{\beta}V')z_3 + \mathrm{i}\left[\gamma^2 - \left(\frac{\alpha \mathrm{i}}{R}\right)_s\right]z_4, \tag{5.2.6b}$$

$$z_3' = -\mathrm{i}z_1, \tag{5.2.6c}$$

$$z_4' = \frac{\mathrm{i}[z_1 W_s - (z_1\mu)_v']}{R} - \frac{[\mathrm{i}R\left(\alpha U + \bar{\beta}V - \omega\right) + W_s']z_3}{R}, \tag{5.2.6d}$$

$$z_5' = z_6, \tag{5.2.6e}$$

$$\left[\frac{\mu z_6'}{R}\right]_v = \frac{z_6(W_s - \mu_v')}{R} + \frac{[\mathrm{i}R\left(\alpha U + \bar{\beta}V - \omega\right) + U_s]z_5}{R} + \frac{2(1_c + V_s)z_1}{R} + (\alpha_1 V' - \bar{\beta}U')z_3 + \left[\frac{\bar{\beta}z_4}{R}\right]_s, \tag{5.2.6f}$$

where $\alpha_1 = \alpha - (\mathrm{i}/R)_s$ and $\gamma^2 = \alpha^2 + \bar{\beta}^2 = \alpha^2 + \beta^2/r^2$. Corresponding Orr-Sommerfeld and Rayleigh equations are easily derived from this system, although we omit that detail here.

The perturbation equations are solved using the methodology of §5.1.2. However, here, it is important to note that the behaviour of the steady mean flow solutions is markedly different in the far-field, as $z \to \infty$ we have that

$$U \to 0, \quad V \to -1, \quad W \to W_\infty = -2\int_0^\infty U \,\mathrm{d}z, \quad \mu \to 1 + c_0$$
$$U' \to 0, \quad V' \to 0, \quad W' \to 0, \quad \mu' \to 0.$$

Substituting the above into (5.2.6) gives

$$z_1' = z_2, \tag{5.2.7a}$$
$$z_2' = \frac{z_2 W_\infty - \mathrm{i}R(\bar{\beta}+\omega)z_1 + (\mathrm{i}R\gamma^2 + \alpha)z_4}{1+c_0}, \tag{5.2.7b}$$
$$z_3' = -\mathrm{i}z_1, \tag{5.2.7c}$$
$$z_4' = \frac{\mathrm{i}[z_1 W_\infty - z_2(1+c_0) + R(\bar{\beta}+\omega)z_3]}{R}, \tag{5.2.7d}$$
$$z_5' = z_6, \tag{5.2.7e}$$
$$z_6' = \frac{z_6 W_\infty - \mathrm{i}R(\bar{\beta}+\omega)z_5 + \bar{\beta}z_4}{1+c_0}. \tag{5.2.7f}$$

These have exact closed form solutions, $z_i^j(z \to \infty; \alpha, \beta, \omega; R, c_0, k, n) = b_i^j e^{\kappa_j z}$, with constants

$$\kappa_1, \kappa_2 = \frac{W_\infty}{2(1+c_0)} \mp \sqrt{\left[\frac{W_\infty}{2(1+c_0)}\right]^2 - \frac{\mathrm{i}R(\bar{\beta}+\omega)}{(1+c_0)}}, \tag{5.2.8a}$$
$$\kappa_3, \kappa_4 = \frac{W_\infty}{2(1+c_0)} \mp \sqrt{\left[\frac{W_\infty}{2(1+c_0)}\right]^2 - \frac{\mathrm{i}R(\bar{\beta}+\omega)}{(1+c_0)}}, \tag{5.2.8b}$$
$$\kappa_5, \kappa_6 = \mp\sqrt{\gamma^2 - \frac{\alpha\mathrm{i}}{R}}. \tag{5.2.8c}$$

n	R_c	α	$\bar{\beta}$	γ	ϕ
0.25	301.11	0.3999	0.0815	0.4081	11.52°
0.5	328.80	0.3805	0.0784	0.3885	11.64°
0.75	364.51	0.3403	0.0700	0.3475	11.62°
0.95	383.93	0.2961	0.0595	0.3020	11.36°
1	385.93	0.2846	0.0567	0.2902	11.26°
1.05	386.77	0.2733	0.0538	0.2786	11.14°
1.25	381.53	0.2321	0.0434	0.2362	10.59°
1.5	367.95	0.1923	0.0337	0.1953	9.926°
1.75	355.97	0.1632	0.0271	0.1655	9.420°

Table 5.3: The values of the critical Reynolds number R_c, wavenumbers α, $\bar{\beta}$ and γ, and wave angle ϕ for Carreau fluids on the upper-branch for stationary waves.

The non-zero b_i^j terms for $i = 1$, 3 and 5 are

$$b_1^1 = 1, \quad b_2^1 = \kappa_1, \quad b_3^1 = -\mathrm{i}/\kappa_1, \quad b_5^3 = 1, \quad b_6^3 = \kappa_3, \quad b_1^5 = \mathrm{i}\kappa_5, \quad b_2^5 = \mathrm{i}\kappa_5^2,$$
$$b_3^5 = 1, \quad b_4^5 = [\mathrm{i}R(\bar{\beta} + \omega) - W_\infty\kappa_5 + (1 + c_0)(\gamma^2 - \alpha\mathrm{i}/R)]/\kappa_5 R.$$

As before, the perturbation equations (5.2.6) are integrated from each of the initial solutions at the outer-edge of the boundary-layer down towards the surface of the disk and the boundary-layer is approximated by the region $0 \leq z \leq 20$. Consequently, our base flow solutions have fully converged within the confines of the boundary-layer region. This is in stark contrast to the preceding power-law analysis.

The spatial branches are calculated in much the same way, with modified initial conditions and governing ODEs (5.2.6). As with the asymptotic analysis we fix $c_0 = 1$ and $k = 100$ whilst varying n. A quantitative comparison between numerical studies is not achievable, even in the Newtonian limit, due to the modified form of the Carreau viscosity function. We can, however, make qualitative comparisons between the two sets of shear-thinning solutions.

The neutral curves presented in figures 5.9 & 5.10 are strikingly different to the

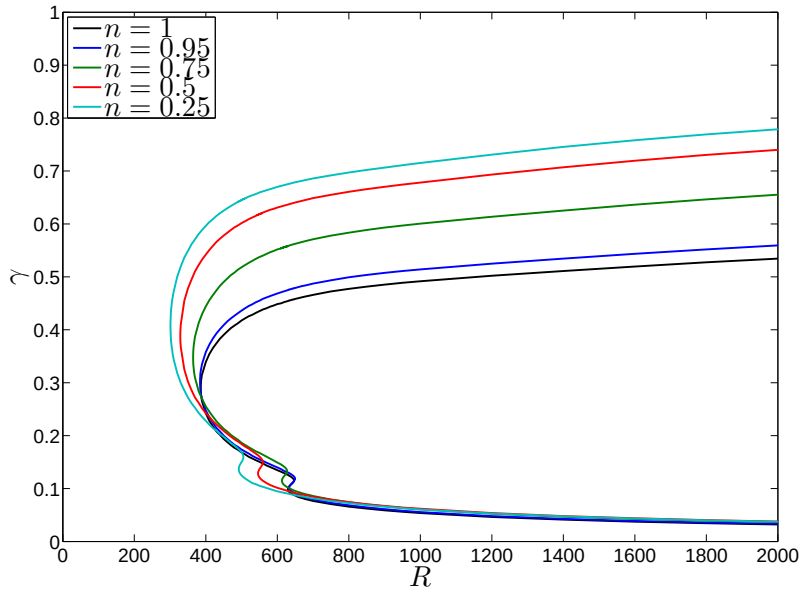

Figure 5.9: Neutral stability curves for shear-thinning Carreau fluids. The neutral wavenumber γ is plotted against the Reynolds number.

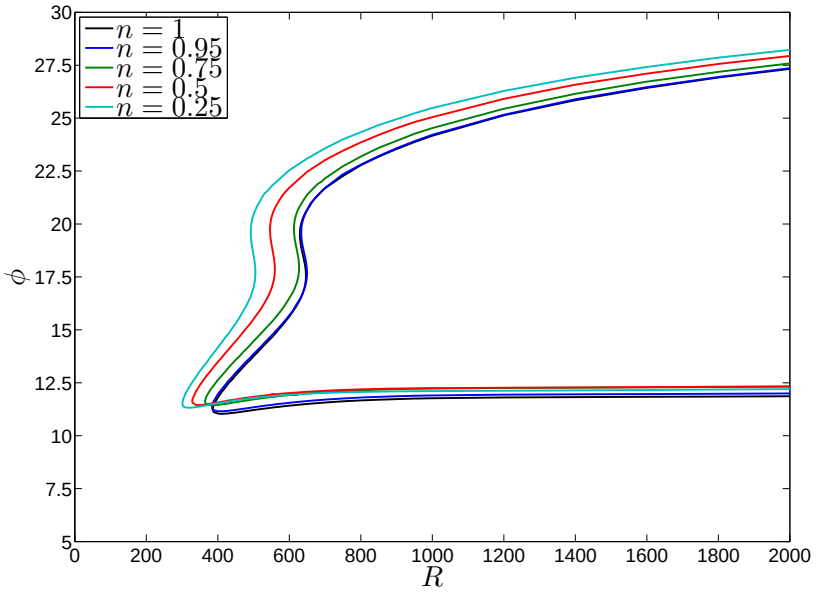

Figure 5.10: Neutral stability curves for shear-thinning Carreau fluids. The neutral wave angle ϕ is plotted against the Reynolds number.

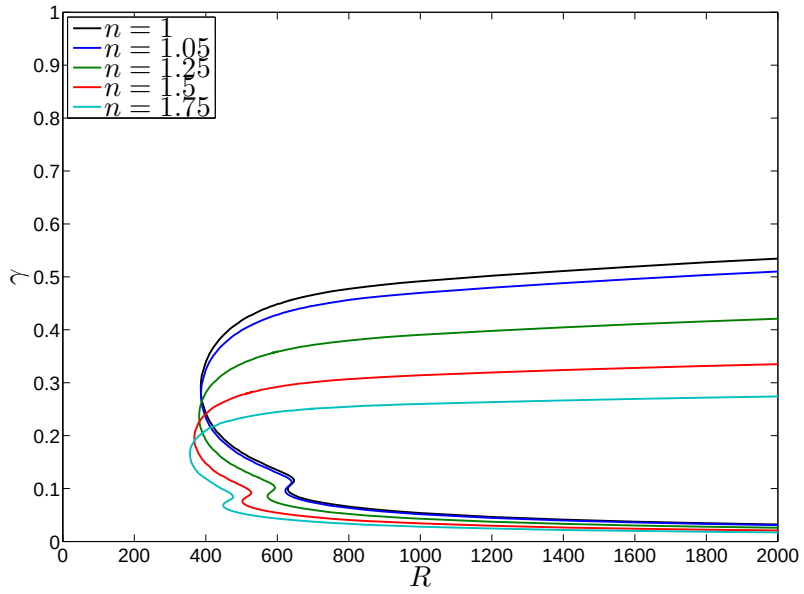

Figure 5.11: Neutral stability curves for shear-thickening Carreau fluids. The neutral wavenumber γ is plotted against the Reynolds number.

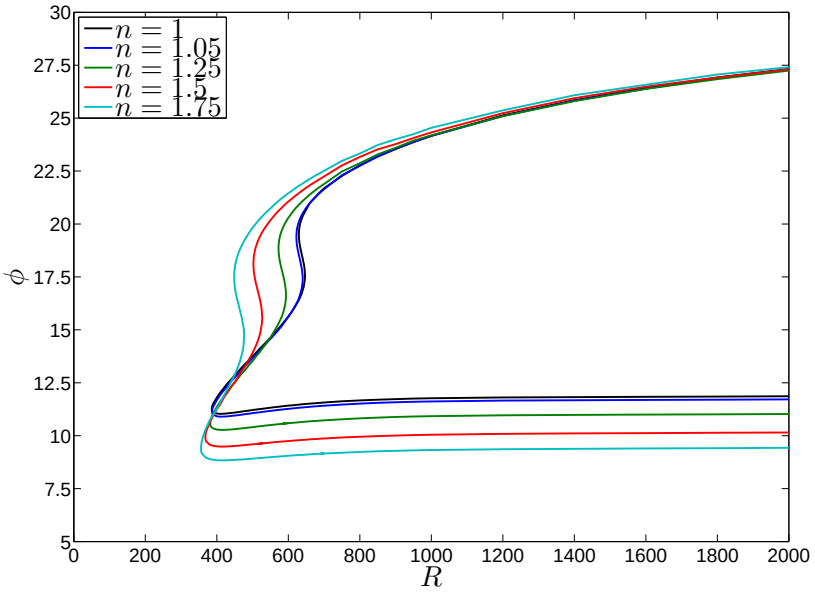

Figure 5.12: Neutral stability curves for shear-thickening Carreau fluids. The neutral wave angle ϕ is plotted against the Reynolds number.

n	R_c	α	$\bar{\beta}$	γ	ϕ
0.25	492.11	0.1288	0.0459	0.1367	19.61°
0.5	546.03	0.1209	0.0434	0.1285	19.72°
0.75	612.90	0.1079	0.0388	0.1147	19.77°
0.95	633.34	0.0960	0.0342	0.1019	19.59°
1	629.61	0.0931	0.0330	0.0988	19.50°
1.05	622.53	0.0904	0.0318	0.0958	19.40°
1.25	572.67	0.0811	0.0277	0.0856	18.85°
1.5	502.39	0.0721	0.0236	0.0758	18.12°
1.75	448.68	0.0653	0.0205	0.0685	17.47°

Table 5.4: The values of the critical Reynolds number R_c, wavenumbers α, $\bar{\beta}$ and γ, and wave angle ϕ for Carreau fluids on the lower-branch for stationary waves.

equivalent power-law results. We see that decreasing the power-law index has the effect of increasing the convectively unstable region enclosed by the wavenumber neutral curve. Interestingly, we note that increasing the shear-thinning parameter has little effect on the lower-branch results. This mode has its structure fixed by a balance between viscous and Coriolis forces, therefore one might expect that this mode would be most greatly effected as n varies. However, this appears not to be the case, with the destabilising nature of shear-thinning emanating from the type I mode. As the asymptotic theory predicts the wave angle is only marginally effected by the power-law index.

Figures 5.11 & 5.12 clearly indicate that as the shear-thickening parameter increases so the type II critical Reynolds numbers decrease. The gulf between the upper and lower-branch critical Reynolds numbers diminishes for increasing n, suggesting that the type II modes would begin to dominate the stability characteristics of the flow for some $n > 1.75$. More generally, we would consider the effect of shear-thickening to be stabilising as the area enclosed by the wavenumber neutral curves is reduced in this case, although we note that the critical Reynolds numbers are not greatly altered.

We again observe excellent agreement between our asymptotic predictions and numerical solutions. Examples in both the shear-thinning and shear-thickening regimes are

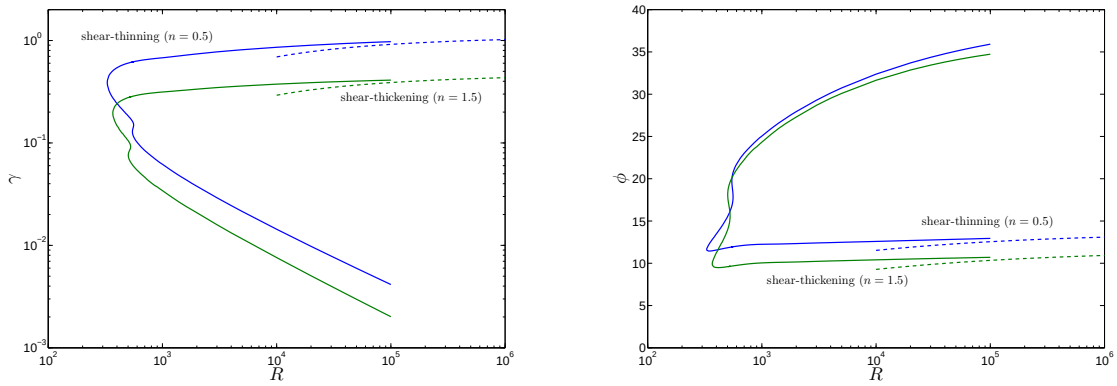

Figure 5.13: Neutral wavenumber and wave angle stability curves for shear-thinning and shear-thickening Carreau fluids. The type I asymptotic solutions are given by the dashed line.

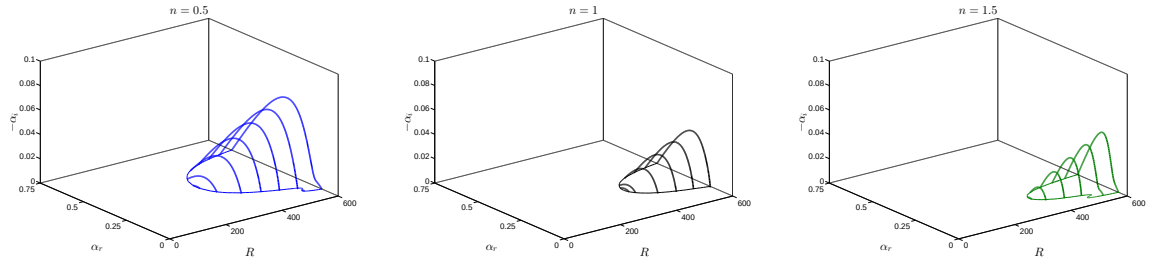

Figure 5.14: A comparison between the type I spatial growth rates for shear-thinning and shear-thickening Carreau fluids and Newtonian fluids with $\mu = 1 + c_0$.

provided in figure 5.13. The spatial branches for the cases when $n < 1$, $n = 1$ and $n > 1$ are plotted in figure 5.14. The growth rates are generally reduced as n increases, another indication of stabilisation. Again, we find that the type II growth rates are comparatively small. It is perhaps easier here to visualise the dramatic shrinking of the wavenumber neutral curve for increasing n. It may appear from figure 5.13 that the γ neutral curves are simply being shifted downwards, this misconception is due to the non-linear y-axis scale.

As a point of interest we also investigate the effect of the parameter k on the local stability characteristics. We expect that for shear-thinning fluids any effect will be marginal, due to the largely unperturbed base flow velocities in this case, as noted in §3.4. In the

shear-thickening case the velocity and viscosity profiles are significantly altered thus we expect that increasing k will have a more noticeable effect when $n > 1$. Indeed, this is the case. Increasing k with $n < 1$ has a marginal destabilising effect, although this is very slight. Whilst when $n > 1$ increasing k has substantial effect on both the type I and type II modes, resulting in smaller growth rates and decreased upper and lower-branch critical Reynolds numbers. In order to visualise this the low Reynolds number neutral curves are plotted in the appendix C.

5.3 Concluding Remarks

Malik (1986) was the first to compute the curves of neutral stability for stationary disturbances in Newtonian rotating disk flow. In this chapter we have shown that these results can be extended to incorporate the rheology of power-law and Carreau fluids. Importantly, both sets of results help to confirm the asymptotic predictions made previously. For power-law fluids we find that on both the type I and II modes the onset of linear convective instability is delayed as n decreases, the critical Reynolds number, R_c, is increased and the linear convective growth rates are significantly reduced. Furthermore, a decrease in n results in the wavenumber and wave angle neutral curves undergoing a shift from the left to the right, effectively expanding the region of stable flow. Direct comparison with the asymptotic predictions reveals an excellent agreement for all n in the large Reynolds number limit.

We observe qualitatively different results for Carreau fluids. As the shear-thinning index increases so the type I and type II critical Reynolds numbers decrease, indicating an advanced onset of convective instability. The area encompassed by the neutral curves is increased, however, the lower-branch structure appears to be largely unaffected. The effect of reducing n is much more noticeable on the upper-branch modes. In direct contrast to the shear-thinning power-law results we see that the linear convective growth rates are

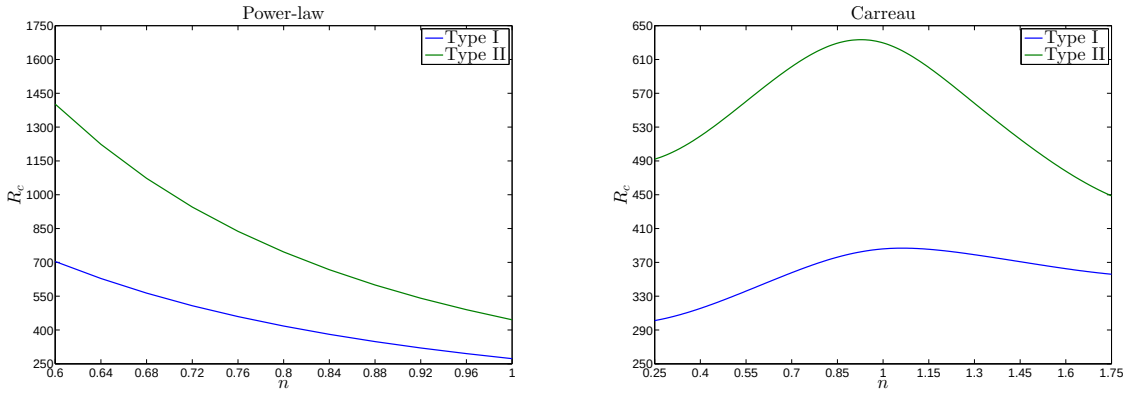

Figure 5.15: Variation of the type I and type II critical Reynolds number with n for power-law and Carreau fluids.

significantly increased as n reduces below one. For shear-thickening fluids we note that although the type I and type II critical Reynolds numbers are generally decreased as n increases above unity, the area encompassed by the neutral curves is significantly reduced. Also, we observe that the type II 'viscous bump' becomes more prominent with increasing n, suggesting that for sufficiently large n this mode will determine the onset of convective instability.

The stark differences between the results from the two viscous models is perhaps best visualised in figure 5.15. Here we have plotted the variation of the two critical Reynolds numbers with n for both power-law and Carreau fluids. The power-law model predicts ever increasing values of R_c with decreasing n. Conversely, and more interestingly, predictions from the Carreau model show that R_c is maximised in a region near to $n = 1$, the requirement for Newtonian flow.

As noted in §4.4 the analysis presented in this chapter is not entirely rigorous, here we will discuss, and provided some justification for, the necessary assumptions we have made. Two important approximations have been made during the completion of this work. Firstly, instead of considering the full-field equations we have appealed to the boundary-layer approximation in order to obtain steady mean flow solutions. This has

an effect on the ensuing derivation of the sixth-order system of linear stability equations. Consequently, we find that reduction of our systems to Newtonian form does not admit the governing equations stated by Lingwood (1995*a*), instead a number of minor simplifications are observed. As a result the formulation of the respective Orr-Sommerfeld equations is also modified. However, when solving for the cases when $n = 1$ and $c_0 = 0$ we find that the results are comparable to those of previous Newtonian studies. Essentially use of the boundary-layer approximation decreases the critical Reynolds number on the type I and II modes predicting an advancement of the onset of linear convective instability. Thus, in the Newtonian case at least, the results presented here are considered to be less stable than those derived from the system of full-field equations. Secondly, in order to simplify the linear disturbance equations a parallel-flow approximation was made and the perturbed viscosity terms were removed. Having appealed to the asymptotic investigation, in the power-law regime, we demonstrated that at high Reynolds number the type I neutral modes are not greatly effected by the removal of these additional viscous terms. This is also the case for Carreau fluids although the detail was omitted. Because of this, and the parallel-flow approximation, the perturbation equations solved in this analysis are not rigorous at $\mathcal{O}(R^{-1})$. Although it is acknowledged that these approximations will lead to inaccuracies at the predicted critical Reynolds numbers, it is expected that these will be small. Indeed, this approximation has been used in numerous studies previously. The excellent agreement obtained between the numerical and exact asymptotic results shows that the affects of these approximations are negligible at high Reynolds number.

This numerical investigation has given us a great deal of insight into the effect fluid viscosity can have on the upper and lower-branch neutral modes of convective instability. Most importantly these results have helped to justify our upper-branch asymptotic predictions. It remains for us to investigate, asymptotically, the structure of the lower-branch modes. We consider exactly this in the penultimate chapter.

Chapter 6

The Type II Viscous Modes - A Preliminary Investigation

Here we consider the stability of the stationary viscous modes for cases I, II & III, following the structure presented by Hall (1986). This asymptotic analysis gives predictions for the wavenumber and wave angle of the disturbances. However, unlike the type I investigation, only the first term in the wavenumber expansion is calculated. As noted by Hall (1986) the lower-branch modes are governed by a triple deck structure, analogous to that found for the Blasius boundary-layer over a flat plate, as was first described by Smith (1979). In the upper-branch analysis we required that both the effective velocity profile and its second derivative vanished at the critical layer. Here, we require that the effective wall shear, $\alpha\bar{u}'r + \beta\bar{v}'$, vanishes at leading order. This ensures that the type II modes are time-independent, and therefore stationary, within our rotating frame of reference.

The triple deck structure consists of an upper deck, a main deck and a lower deck. This is shown schematically in figure 6.1. Our solutions are matched between each of the decks, with the no-slip condition being satisfied within the lower deck. It is here that we determine a leading order eigenrelation that can be solved for the zero order solution for the wavenumber and first order corrections to the effective wave angle. This type of

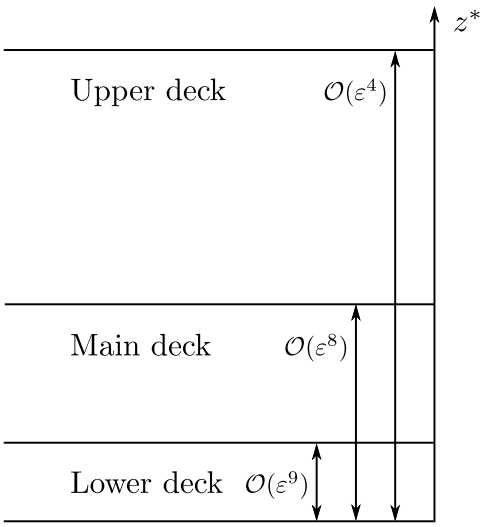

Figure 6.1: Schematic diagram showing the triple deck structure inside the rotating disk boundary-layer. The small parameter ε, scaled in the boundary-layer thickness δ, will be defined subsequently.

analysis has been extended previously, namely to rotating cone investigations; such as that of Garrett *et al.* (2009) and Towers (2013), who present incompressible and compressible studies, respectively. The corresponding non-linear analysis was completed by MacKerrell (1987).

It is expected that these results will agree well with our numerical predictions in the large Reynolds number limit. Clearly this is not achievable for case II, however, we hope to support our claim that an increase in fluid yield stress has a stabilising effect by producing qualitatively similar results to those presented in §4.2.

6.1 Case I: Power-law

Having already determined our linear disturbance equations in §4.1.1 we begin by redefining our small parameter ε such that $\varepsilon = \delta^{1/8} = Re^{-1/[8(n+1)]}$. Following Hall (1986) we stipulate that the disturbance velocities and pressure take the from

$$U_d = \tilde{u}(r,z)F, \quad V_d = \tilde{v}(r,z)F, \quad W_d = \tilde{w}(r,z)F, \quad P_d = \tilde{p}(r,z)F,$$

where the exponential F is given by

$$F = \exp\left[\frac{\mathrm{i}}{\varepsilon^4}\left(\int^r \alpha(r,\varepsilon)\,\mathrm{d}r + \theta\beta(\varepsilon)\right)\right]. \tag{6.1.1}$$

Hence we are considering modes with a lengthscale of order $Re^{-1/[2(n+1)]}$ in the radial and azimuthal directions. We expand the radial and azimuthal wavenumbers α and β as such

$$\alpha = \alpha_0 + \varepsilon^2\alpha_1 + \varepsilon^3\alpha_2 + \cdots, \tag{6.1.2a}$$

$$\beta = \beta_0 + \varepsilon^2\beta_1 + \varepsilon^3\beta_2 + \cdots, \tag{6.1.2b}$$

and seek neutrally stable disturbances, thus $\alpha, \beta \in \mathbb{R}$. We note that the order ε terms are zero here.

The upper deck has thickness $\mathcal{O}(\varepsilon^4)$ therefore we define our upper deck coordinate as

$$\eta_u = r^{(1-n)/(n+1)}Re^{1/[2(n+1)]}z = r^{(1-n)/(n+1)}\varepsilon^{-4}z.$$

Inside the upper deck the velocity and pressure perturbations are expanded in the form

$$\tilde{u} = \varepsilon^3 U_0^u(\eta_u) + \varepsilon^4 U_1^u(\eta_u) + \cdots, \tag{6.1.3a}$$

$$\tilde{v} = \varepsilon^3 V_0^u(\eta_u) + \varepsilon^4 V_1(\eta_u) + \cdots, \tag{6.1.3b}$$

$$\tilde{w} = \varepsilon^3 W_0^u(\eta_u) + \varepsilon^4 W_1^u(\eta_u) + \cdots, \tag{6.1.3c}$$

$$\tilde{p} = \varepsilon^3 P_0^u(\eta_u) + \varepsilon^4 P_1^u(\eta_u) + \cdots. \tag{6.1.3d}$$

The preceding expansions are then substituted into the linearised disturbance equations, given in §4.1.1, along with the following forms for the differential operators when applied

to the disturbance quantities

$$\frac{\partial}{\partial r}=\frac{\eta_u(1-n)}{r(n+1)}\frac{\partial}{\partial \eta_u}+\left(\frac{\mathrm{i}}{\varepsilon^4}\right)(\alpha_0+\varepsilon^2\alpha_1+\varepsilon^3\alpha_2+\cdots),\quad \frac{\partial}{\partial\theta}=\left(\frac{\mathrm{i}}{\varepsilon^4}\right)(\beta_0+\varepsilon^2\beta_1+\varepsilon^3\beta_2+\cdots).$$

In the upper deck $\bar{u}=0$, $\bar{v}=-1$, $\bar{w}=\bar{w}_\infty\neq 0$ and $\bar{\mu}=\bar{\mu}_\infty\neq 0$. Thus the expansion equations in the upper deck are written as

$$\begin{aligned}
&\left[\frac{\eta_u(1-n)}{r(n+1)}\frac{\partial}{\partial\eta_u}+\mathrm{i}\varepsilon^{-4}(\alpha_0+\varepsilon^2\alpha_1+\varepsilon^3\alpha_2+\cdots)+\frac{1}{r}\right](\varepsilon^3U_0^u+\varepsilon^4U_1^u+\cdots)\\
&+\frac{\mathrm{i}\varepsilon^{-4}(\beta_0+\varepsilon^2\beta_1+\varepsilon^3\beta_2+\cdots)(\varepsilon^3V_0^u+\varepsilon^4V_1^u+\cdots)}{r}\\
&+\varepsilon^{-4}r^{(1-n)/(n+1)}\frac{\partial(\varepsilon^3W_0^u+\varepsilon^4W_1^u+\cdots)}{\partial\eta_u}=0,
\end{aligned}\tag{6.1.4a}$$

$$\begin{aligned}
&-\mathrm{i}\varepsilon^{-4}(\beta_0+\varepsilon^2\beta_1+\varepsilon^3\beta_2+\cdots)(\varepsilon^3U_0^u+\varepsilon^4U_1^u+\cdots)+\varepsilon^4\bar{w}_\infty\frac{\partial(\varepsilon^3U_0^u+\varepsilon^4U_1^u+\cdots)}{\partial\eta_u}\\
&=-\left[\frac{\eta_u(1-n)}{r(n+1)}+\mathrm{i}\varepsilon^{-4}(\alpha_0+\varepsilon^2\alpha_1+\varepsilon^3\alpha_2+\cdots)\right]\frac{\partial(\varepsilon^3P_0^u+\varepsilon^4P_1^u+\cdots)}{\partial\eta_u}\\
&+\varepsilon^8\left\{\bar{\mu}_\infty\frac{\partial^2(\varepsilon^3U_0^u+\varepsilon^4U_1^u+\cdots)}{\partial\eta_u^2}+(n-1)\left[\bar{\mu}_\infty^{\bar{u}'\bar{u}'}\frac{\partial^2(\varepsilon^3U_0^u+\varepsilon^4U_1^u+\cdots)}{\partial\eta_u^2}\right.\right.\\
&\left.\left.+\bar{\mu}_\infty^{\bar{v}'\bar{v}'}\frac{\partial^2(\varepsilon^3V_0^u+\varepsilon^4V_1^u+\cdots)}{\partial\eta_u^2}\right]\right\},
\end{aligned}\tag{6.1.4b}$$

$$\begin{aligned}
&-\mathrm{i}\varepsilon^{-4}(\beta_0+\varepsilon^2\beta_1+\varepsilon^3\beta_2+\cdots)(\varepsilon^3V_0^u+\varepsilon^4V_1^u+\cdots)+\varepsilon^4\bar{w}_\infty\frac{\partial(\varepsilon^3V_0^u+\varepsilon^4V_1^u+\cdots)}{\partial\eta_u}\\
&=-\frac{\mathrm{i}\varepsilon^{-4}(\beta_0+\varepsilon^2\beta_1+\varepsilon^3\beta_2+\cdots)(\varepsilon^3P_0^u+\varepsilon^4P_1^u+\cdots)}{r}\\
&+\varepsilon^8\left\{\bar{\mu}_\infty\frac{\partial^2(\varepsilon^3V_0^u+\varepsilon^4V_1^u+\cdots)}{\partial\eta_u^2}+(n-1)\left[\bar{\mu}_\infty^{\bar{v}'\bar{u}'}\frac{\partial^2(\varepsilon^3U_0^u+\varepsilon^4U_1^u+\cdots)}{\partial\eta_u^2}\right.\right.\\
&\left.\left.+\bar{\mu}_\infty^{\bar{v}'\bar{v}'}\frac{\partial^2(\varepsilon^3V_0^u+\varepsilon^4V_1^u+\cdots)}{\partial\eta_u^2}\right]\right\},
\end{aligned}\tag{6.1.4c}$$

$$
\begin{aligned}
&- \mathrm{i}\varepsilon^{-4}(\beta_0 + \varepsilon^2\beta_1 + \varepsilon^3\beta_2 + \cdots)(\varepsilon^3 W_0^u + \varepsilon^4 W_1^u + \cdots) + \varepsilon^4 \bar{w}_\infty \frac{\partial(\varepsilon^3 W_0^u + \varepsilon^4 W_1^u + \cdots)}{\partial \eta_u} \\
&+ \varepsilon^8 r^{-2/(n+1)} \frac{(n-1)}{(n+1)} \bar{w}_\infty (\varepsilon^3 U_0^u + \varepsilon^4 U_1^u + \cdots) \\
&= -\varepsilon^{-4} r^{(1-n)/(n+1)} \frac{\partial(\varepsilon^3 P_0^u + \varepsilon^4 P_1^u + \cdots)}{\partial \eta_u} \\
&+ 2\varepsilon^8 \Bigg\{ \bar{\mu}_\infty \frac{\partial^2(\varepsilon^3 W_0^u + \varepsilon^4 W_1^u + \cdots)}{\partial \eta_u^2} + \varepsilon^8 r^{-2/(n+1)}(n-1) \\
&\times \left[\bar{\mu}_\infty^{\bar{w}'\bar{u}'} \frac{\partial^2(\varepsilon^3 U_0^u + \varepsilon^4 U_1^u + \cdots)}{\partial \eta_u^2} + \bar{\mu}_\infty^{\bar{w}'\bar{v}'} \frac{\partial^2(\varepsilon^3 V_0^u + \varepsilon^4 V_1^u + \cdots)}{\partial \eta_u^2} \right] \Bigg\} + \mathcal{O}(\varepsilon^{16}),
\end{aligned}
\tag{6.1.4d}
$$

where

$$
\bar{\mu}_\infty^{xy} = \left. \frac{\bar{\mu} x y}{\bar{u}'^2 + \bar{v}'^2} \right|_{\eta = \eta_\infty}, \quad \text{with} \quad x = \bar{u}', \bar{v}', \bar{w}' \quad \text{and} \quad y = \bar{u}', \bar{v}'.
$$

For $n \neq 1$ these quantities are non-zero in the upper deck.

Equating terms of $\mathcal{O}(\varepsilon^{-1})$ we have that

$$
\mathrm{i}\alpha_0 U_0^u + \frac{\mathrm{i}\beta_0 V_0^u}{r} + r^{(1-n)/(n+1)} \frac{dW_0^u}{d\eta_u} = 0, \tag{6.1.5a}
$$

$$
-\beta_0 U_0^u + \alpha_0 P_0^u = 0, \tag{6.1.5b}
$$

$$
-V_0 + \frac{P_0^u}{r} = 0, \tag{6.1.5c}
$$

$$
-\mathrm{i}\beta_0 W_0^u + r^{(1-n)/(n+1)} \frac{dP_0^u}{d\eta_u} = 0. \tag{6.1.5d}
$$

Eliminating U_0^u, V_0^u and W_0^u gives

$$
\frac{d^2 P_0^u}{d\eta_u^2} - \kappa_0^2 \frac{dP_0^u}{d\eta_u} = 0,
$$

where, as before, $\kappa_0 = r^{(n-1)/(n+1)} \sqrt{\alpha_0^2 + \beta_0^2/r^2}$. Therefore the solution of this system

that decays to zero as $\eta_u \to \infty$ is

$$U_0^u = \frac{\alpha_0 C e^{-\kappa_0 \eta_u}}{\beta_0}, \tag{6.1.6a}$$

$$V_0^u = \frac{C e^{-\kappa_0 \eta_u}}{r}, \tag{6.1.6b}$$

$$W_0^u = \mathrm{i} r^{(1-n)/(n+1)} \frac{\kappa_0 C e^{-\kappa_0 \eta_u}}{\beta_0}, \tag{6.1.6c}$$

$$P_0^u = C e^{-\kappa_0 \eta_u}, \tag{6.1.6d}$$

where C is an unknown function of r.

In the main deck we scale the radial and azimuthal disturbances by the difference in powers of ε between the upper and main deck. Our upper deck leading order solutions are $\mathcal{O}(\varepsilon^3)$, whilst the difference between decks is $\mathcal{O}(\varepsilon^4)$, thus we see the ε^{-1} terms appearing in the $\tilde{u}$ and $\tilde{v}$ expansions. In order to match with the solutions in the upper deck, the axial and pressure perturbations are expanded at the same leading order. So that

$$\tilde{u} = \varepsilon^{-1} u_0^m(\eta) + u_1^m(\eta) + \cdots, \tag{6.1.7a}$$

$$\tilde{v} = \varepsilon^{-1} v_0^m(\eta) + v_1^m(\eta) + \cdots, \tag{6.1.7b}$$

$$\tilde{w} = \varepsilon^{3} w_0^m(\eta) + \varepsilon^{4} w_1^m(\eta) + \cdots, \tag{6.1.7c}$$

$$\tilde{p} = \varepsilon^{3} p_0^m(\eta) + \varepsilon^{4} p_1^m(\eta) + \cdots, \tag{6.1.7d}$$

where $\eta = r^{(1-n)/(n+1)} \varepsilon^{-8} z$. Thus the expansion equations in the main deck are written as

$$\begin{aligned}
&\left[\frac{\eta(1-n)}{r(n+1)}\frac{\partial}{\partial \eta} + \mathrm{i}\varepsilon^{-4}(\alpha_0 + \varepsilon^2\alpha_1 + \varepsilon^3\alpha_2 + \cdots) + \frac{1}{r}\right](\varepsilon^{-1}u_0^m + u_1^m + \cdots) \\
&+ \frac{\mathrm{i}\varepsilon^{-4}(\beta_0 + \varepsilon^2\beta_1 + \varepsilon^3\beta_2 + \cdots)(\varepsilon^{-1}v_0^m + v_1^m + \cdots)}{r} \\
&+ \varepsilon^{-8} r^{(1-n)/(n+1)} \frac{\partial(\varepsilon^3 w_0^m + \varepsilon^4 w_1^m + \cdots)}{\partial \eta} = 0,
\end{aligned} \tag{6.1.8a}$$

$$\left[\frac{\eta\bar{u}(1-n)}{(n+1)}\frac{\partial}{\partial\eta}+\mathrm{i}\varepsilon^{-4}r\bar{u}(\alpha_0+\varepsilon^2\alpha_1+\varepsilon^3\alpha_2+\cdots)+\mathrm{i}\varepsilon^{-4}\bar{v}(\beta_0+\varepsilon^2\beta_1+\varepsilon^3\beta_2+\cdots)+\bar{w}\frac{\partial}{\partial\eta}\right]$$
$$\times(\varepsilon^{-1}u_0^m+u_1^m+\cdots)+\frac{\eta\bar{u}'(1-n)}{(n+1)}(\varepsilon^{-1}u_0^m+u_1^m+\cdots)+\bar{u}(\varepsilon^{-1}u_0^m+u_1^m+\cdots)$$
$$-2(\bar{v}+1)(\varepsilon^{-1}v_0^m+v_1^m+\cdots)+\varepsilon^{-8}r^{2/(n+1)}\bar{u}'(\varepsilon^3w_0^m+\varepsilon^4w_1^m+\cdots)$$
$$=-\left[\frac{\eta(1-n)}{r(n+1)}\frac{\partial}{\partial\eta}+\mathrm{i}\varepsilon^{-4}(\alpha_0+\varepsilon^2\alpha_1+\varepsilon^3\alpha_2+\cdots)\right](\varepsilon^3p_0^m+\varepsilon^4p_1^m+\cdots)$$
$$+\frac{\partial}{\partial\eta}\left\{\bar{\mu}\frac{\partial(\varepsilon^{-1}u_0^m+u_1^m+\cdots)}{\partial\eta}+\frac{\bar{u}'\bar{\mu}(n-1)}{\bar{u}'^2+\bar{v}'^2}\left[\bar{u}'\frac{\partial(\varepsilon^{-1}u_0^m+u_1^m+\cdots)}{\partial\eta}\right.\right.$$
$$\left.\left.+\bar{v}'\frac{\partial(\varepsilon^{-1}v_0^m+v_1^m+\cdots)}{\partial\eta}\right]\right\},\tag{6.1.8b}$$

$$\left[\frac{\eta\bar{u}(1-n)}{(n+1)}\frac{\partial}{\partial\eta}+\mathrm{i}\varepsilon^{-4}r\bar{u}(\alpha_0+\varepsilon^2\alpha_1+\varepsilon^3\alpha_2+\cdots)+\mathrm{i}\varepsilon^{-4}\bar{v}(\beta_0+\varepsilon^2\beta_1+\varepsilon^3\beta_2+\cdots)+\bar{w}\frac{\partial}{\partial\eta}\right]$$
$$\times(\varepsilon^{-1}v_0^m+v_1^m+\cdots)+\frac{\eta\bar{v}'(1-n)}{(n+1)}(\varepsilon^{-1}u_0^m+u_1^m+\cdots)+\bar{u}(\varepsilon^{-1}v_0^m+v_1^m+\cdots)$$
$$+2(\bar{v}+1)(\varepsilon^{-1}u_0^m+u_1^m+\cdots)+\varepsilon^{-8}r^{2/(n+1)}\bar{v}'(\varepsilon^3w_0^m+\varepsilon^4w_1^m+\cdots)$$
$$=-\frac{\mathrm{i}\varepsilon^{-4}(\beta_0+\varepsilon^2\beta_1+\varepsilon^3\beta_2+\cdots)(\varepsilon^3p_0^m+\varepsilon^4p_1^m+\cdots)}{r}$$
$$+\frac{\partial}{\partial\eta}\left\{\bar{\mu}\frac{\partial(\varepsilon^{-1}v_0^m+v_1^m+\cdots)}{\partial\eta}+\frac{\bar{v}'\bar{\mu}(n-1)}{\bar{u}'^2+\bar{v}'^2}\left[\bar{u}'\frac{\partial(\varepsilon^{-1}u_0^m+u_1^m+\cdots)}{\partial\eta}\right.\right.$$
$$\left.\left.+\bar{v}'\frac{\partial(\varepsilon^{-1}v_0^m+v_1^m+\cdots)}{\partial\eta}\right]\right\},\tag{6.1.8c}$$

$$\left[\frac{\eta\bar{u}(1-n)}{(n+1)}\frac{\partial}{\partial\eta}+\mathrm{i}\varepsilon^{-4}r\bar{u}(\alpha_0+\varepsilon^2\alpha_1+\varepsilon^3\alpha_2+\cdots)+\mathrm{i}\varepsilon^{-4}\bar{v}(\beta_0+\varepsilon^2\beta_1+\varepsilon^3\beta_2+\cdots)+\bar{w}\frac{\partial}{\partial\eta}\right]$$
$$\times(\varepsilon^3w_0^m+\varepsilon^4w_1^m+\cdots)+\varepsilon^8r^{-2/(n+1)}\frac{(n-1)}{(n+1)}(\bar{w}-\eta\bar{w}')(\varepsilon^{-1}u_0^m+u_1^m+\cdots)$$
$$+\bar{w}'(\varepsilon^3w_0^m+\varepsilon^4w_1^m+\cdots)=-\varepsilon^{-8}r^{(1-n)/(n+1)}\frac{\partial(\varepsilon^3p_0^m+\varepsilon^4p_1^m+\cdots)}{\partial\eta}$$
$$+2\frac{\partial}{\partial\eta}\left\{\bar{\mu}\frac{\partial(\varepsilon^3w_0^m+\varepsilon^4w_1^m+\cdots)}{\partial\eta}+\varepsilon^8r^{-2/(n+1)}\frac{\bar{w}'\bar{\mu}(n-1)}{\bar{u}'^2+\bar{v}'^2}\left[\bar{u}'\frac{\partial(\varepsilon^{-1}u_0^m+u_1^m+\cdots)}{\partial\eta}\right.\right.$$
$$\left.\left.+\bar{v}'\frac{\partial(\varepsilon^{-1}v_0^m+v_1^m+\cdots)}{\partial\eta}\right]\right\}+\mathcal{O}(\varepsilon^8).\tag{6.1.8d}$$

Equating terms of $\mathcal{O}(\varepsilon^{-5})$ we have that

$$\mathrm{i}\alpha_0 u_0^m + \frac{\mathrm{i}\beta_0^m v_0}{r} + r^{(1-n)/(n+1)}(w_0^m)' = 0, \tag{6.1.9a}$$

$$\mathrm{i}\bar{\bar{u}} u_0^m + r^{2/(n+1)} w_0^m \bar{u}' = 0, \tag{6.1.9b}$$

$$\mathrm{i}\bar{\bar{u}} v_0^m + r^{2/(n+1)} w_0^m \bar{v}' = 0, \tag{6.1.9c}$$

$$r^{(1-n)/(n+1)}(p_0^m)' = 0, \tag{6.1.9d}$$

where, in accordance with the notation used in chapter 4, $\bar{\bar{u}} = \alpha_0 \bar{u} r + \beta_0 \bar{v}$ and the primes denote differentiation with respect to η. Eliminating u_0^m and v_0^m we have that

$$\frac{(w_0^m)'}{w_0^m} = \frac{\bar{\bar{u}}'}{\bar{\bar{u}}} \implies w_0^m = A\bar{\bar{u}},$$

where A is a constant. We have that

$$W_0^u = \mathrm{i} r^{(1-n)/(n+1)} \frac{\kappa_0 C}{\beta_0} \quad \text{at} \quad \eta_u = 0, \quad \text{and} \quad w_0^m \to -A\beta_0 \quad \text{as} \quad \eta \to \infty,$$

thus $A = -\mathrm{i} r^{(1-n)/(n+1)} \kappa_0 C/\beta_0^2$. Therefore

$$u_0^m = r^{2(1-n)/(n+1)} \frac{C r \kappa_0 \bar{u}'}{\beta_0^2}, \tag{6.1.10a}$$

$$v_0^m = r^{2(1-n)/(n+1)} \frac{C r \kappa_0 \bar{v}'}{\beta_0^2}, \tag{6.1.10b}$$

$$w_0^m = -\mathrm{i} r^{(1-n)/(n+1)} \frac{\kappa_0 C \bar{\bar{u}}}{\beta_0^2}, \tag{6.1.10c}$$

$$p_0^m = C. \tag{6.1.10d}$$

Now w_0^m satisfies the no-slip condition at $\eta = 0$, however, u_0^m and v_0^m do not. Therefore

n	λ_0	ϕ_0
1	1.2072	39.64°
0.9	1.2316	39.07°
0.8	1.2626	38.38°
0.7	1.3020	37.53°
0.6	1.3542	36.44°

Table 6.1: Calculated values of λ_0 and ϕ_0 for power-law fluids with $n = 1,\ 0.9,\ 0.8,\ 0.7,\ 0.6$.

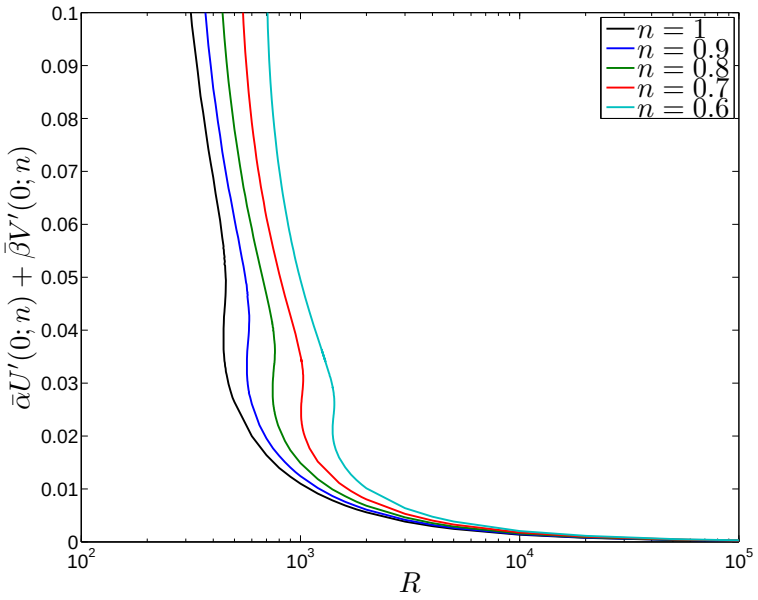

Figure 6.2: Numerical predictions of the effective wall shear along the type II mode for power-law fluids with $n = 1,\ 0.9,\ 0.8,\ 0.7,\ 0.6$. The y-axis notation is consistent with the numerical study and is equivalent to $r^{(n-1)/(n+1)}(\alpha_0\bar{u}_0 + \beta_0\bar{v}_0/r)$.

we impose the following constraint

$$\alpha_0\bar{u}_0 + \frac{\beta_0\bar{v}_0}{r} = 0 \implies \frac{\alpha_0 r}{\beta_0} = -\frac{\bar{v}_0}{\bar{u}_0} = \lambda_0, \tag{6.1.11}$$

then $\alpha_0 u_0^m + \beta_0 v_0^m/r \to 0$ as $\eta \to 0$. It is this imposition that forces us to consider only stationary disturbances. In our rotating frame of reference these modes remain fixed on the disk surface. Here we assume that the effective wall shear is zero along the lower-

branch. This can be quantified using our numerical solutions obtain previously. Figure 6.2 plots the effective wall shear profiles for moderately shear-thinning power-law fluids. We note that for every n in the range of interest this quantity does indeed tend to zero as $R \to \infty$. Having calculated λ_0 we determine the zero order approximation to the wave angle, $\phi_0 = \pi/2 - \arctan \lambda_0$. These values are tabulated in table 6.1.

The lower deck has thickness $\mathcal{O}(\varepsilon^9)$ therefore we define our lower deck coordinate as

$$\eta_l = r^{(1-n)/(n+1)} Re^{9/[8(n+1)]} z = r^{(1-n)/(n+1)} \varepsilon^{-9} z.$$

By expanding the base flow for small η and noting that $\eta = \varepsilon \eta_l$ and $\bar{w}'(0) = 0$ we find that

$$\bar{u} = \varepsilon \eta_l \bar{u}_0 + \varepsilon^2 \bar{u}_1 \eta_l^2 + \varepsilon^3 \bar{v}_2 \eta_l^3 + \cdots , \tag{6.1.12a}$$

$$\bar{v} = \varepsilon \eta_l \bar{v}_0 + \varepsilon^2 \bar{v}_1 \eta_l^2 + \varepsilon^3 \bar{v}_2 \eta_l^3 + \cdots , \tag{6.1.12b}$$

$$\bar{w} = \varepsilon^2 \bar{w}_1 \eta_l^2 + \varepsilon^3 \bar{w}_2 \eta_l^3 + \cdots , \tag{6.1.12c}$$

where, as before,

$$(\bar{u}_{j-1}, \bar{v}_{j-1}, \bar{w}_{j-1}) = \frac{[\bar{u}^j(0), \bar{v}^j(0), \bar{w}^j(0)]}{j!} \quad \text{for} \quad j = 1, 2, 3, \ldots .$$

Now the lower deck disturbances are expressed in the form $\tilde{u} = \varepsilon^{-1} U_{-1}^l(\eta_l) + U_0^l(\eta_l) + \cdots$, with a similar expression for $\tilde{v}$, and $\tilde{w} = \varepsilon^3 W_0^l(\eta_l) + \varepsilon^4 W_1^l(\eta_l) + \cdots$, with a similar expression for $\tilde{p}$. These expansions are then matched with the main deck solutions where we utilise the base flow expansions (6.1.12) to express the disturbance quantities solely in terms of the lower deck coordinate. This effectively ensures that the matching criterion is satisfied prior to the evaluation of our lower deck leading order solutions. Similarly to Hall (1986)

we determine that

$$\tilde{u} = \varepsilon^{-1} r^{(3-n)/(n+1)} \frac{\kappa_0 C(\bar{u}_0 + 2\varepsilon\bar{u}_1\eta_l + 3\varepsilon^2\bar{u}_2\eta_l^2 + \cdots)}{\beta_0^2}$$
$$+ \varepsilon^{-1}U_{-1}^l(\eta_l) + U_0^l(\eta_l) + \varepsilon U_1^l(\eta_l) + \varepsilon^2 U_2^l(\eta_l) + \cdots, \tag{6.1.13a}$$
$$\tilde{v} = \varepsilon^{-1} r^{(3-n)/(n+1)} \frac{\kappa_0 C(\bar{v}_0 + 2\varepsilon\bar{v}_1\eta_l + 3\varepsilon^2\bar{v}_2\eta_l^2 + \cdots)}{\beta_0^2}$$
$$+ \varepsilon^{-1}V_{-1}^l(\eta_l) + V_0^l(\eta_l) + \varepsilon V_1^l(\eta_l) + \varepsilon^2 V_2^l(\eta_l) + \cdots, \tag{6.1.13b}$$
$$\tilde{w} = -\varepsilon^5 \mathrm{i} r^{(1-n)/(n+1)} \frac{\kappa_0 C(\bar{\bar{u}}_1\eta_l^2 + \varepsilon\bar{\bar{u}}_2\eta_l^3 + \varepsilon^2\bar{\bar{u}}_3\eta_l^4 + \cdots)}{\beta_0^2}$$
$$+ \varepsilon^6 W_1^l(\eta_l) + \varepsilon^7 W_2^l(\eta_l) + \cdots, \tag{6.1.13c}$$
$$\tilde{p} = \varepsilon^3 P_1^l(\eta_l) + \cdots, \tag{6.1.13d}$$

where $\bar{\bar{u}}_k = \alpha_0\bar{u}_k r + \beta_0\bar{v}_k$ for $k = 0, 1, 2, \ldots$. Thus the expansion equations in the lower deck are written as

$$\left[\frac{\eta_l(1-n)}{r(n+1)}\frac{\partial}{\partial\eta_l} + \mathrm{i}\varepsilon^{-4}(\alpha_0 + \varepsilon^2\alpha_1 + \varepsilon^3\alpha_2 + \cdots) + \frac{1}{r}\right]\left[\frac{r^{(3-n)/(n+1)}\kappa_0 C}{\varepsilon\beta_0^2}\right.$$
$$\left.\times\,(\bar{u}_0 + 2\varepsilon\bar{u}_1\eta_l + 3\varepsilon^2\bar{u}_2\eta_l^2 + \cdots) + \varepsilon^{-1}U_{-1}^l + U_0^l + \varepsilon U_1^l + \varepsilon^2 U_2^l + \cdots\right]$$
$$+\,\frac{\mathrm{i}\varepsilon^{-4}(\beta_0 + \varepsilon^2\beta_1 + \varepsilon^3\beta_2 + \cdots)}{r}\left[\frac{r^{(3-n)/(n+1)}\kappa_0 C}{\varepsilon\beta_0^2}(\bar{v}_0 + 2\varepsilon\bar{v}_1\eta_l + 3\varepsilon^2\bar{v}_2\eta_l^2 + \cdots)\right.$$
$$\left.+\,\varepsilon^{-1}V_{-1}^l + V_0^l + \varepsilon V_1^l + \varepsilon^2 V_2^l + \cdots\right]$$
$$+\,\varepsilon^{-9}r^{(1-n)/(n+1)}\frac{\partial}{\partial\eta_l}\left[-\frac{\varepsilon^5\mathrm{i}r^{(1-n)/(n+1)}\kappa_0 C}{\beta_0^2}(\bar{\bar{u}}_1\eta_l^2 + \varepsilon\bar{\bar{u}}_2\eta_l^3 + \varepsilon^2\bar{\bar{u}}_3\eta_l^4 + \cdots)\right.$$
$$\left.+\,\varepsilon^6 W_1^l + \varepsilon^7 W_2^l + \cdots\right] = 0, \tag{6.1.14a}$$

$$\Bigg[\frac{\eta_l(\varepsilon\bar{u}_0\eta_l+\varepsilon^2\bar{u}_1\eta_l^2+\varepsilon^3\bar{u}_2\eta_l^3+\cdots)(1-n)}{(n+1)}\frac{\partial}{\partial\eta_l}+\mathrm{i}\varepsilon^{-4}r(\varepsilon\bar{u}_0\eta_l+\varepsilon^2\bar{u}_1\eta_l^2+\varepsilon^3\bar{u}_2\eta_l^3+\cdots)$$
$$\times(\alpha_0+\varepsilon^2\alpha_1+\varepsilon^3\alpha_2+\cdots)+\mathrm{i}\varepsilon^{-4}(\beta_0+\varepsilon^2\beta_1+\varepsilon^3\beta_2+\cdots)$$
$$+\varepsilon^{-1}(\varepsilon^2\bar{w}_1\eta_l^2+\varepsilon^3\bar{w}_2\eta_l^3+\cdots)\frac{\partial}{\partial\eta_l}\Bigg]\Bigg[\frac{r^{(3-n)/(n+1)}\kappa_0 C}{\varepsilon\beta_0^2}(\bar{u}_0+2\varepsilon\bar{u}_1\eta_l+3\varepsilon^2\bar{u}_2\eta_l^2+\cdots)$$
$$+\varepsilon^{-1}U_{-1}^l+U_0^l+\varepsilon U_1^l+\varepsilon^2U_2^l+\cdots\Bigg]+\frac{\varepsilon\eta_l(\bar{u}_0+2\varepsilon\bar{u}_1\eta_l+3\varepsilon^2\bar{u}_2\eta_l^2+\cdots)(1-n)}{(n+1)}$$
$$\times\Bigg[\frac{r^{(3-n)/(n+1)}\kappa_0 C}{\varepsilon\beta_0^2}(\bar{u}_0+2\varepsilon\bar{u}_1\eta_l+3\varepsilon^2\bar{u}_2\eta_l^2+\cdots)+\varepsilon^{-1}U_{-1}^l+U_0^l+\varepsilon U_1^l+\varepsilon^2U_2^l+\cdots\Bigg]$$
$$+(\varepsilon\bar{u}_0\eta_l+\varepsilon^2\bar{u}_1\eta_l^2+\varepsilon^3\bar{u}_2\eta_l^3+\cdots)\Bigg[\frac{r^{(3-n)/(n+1)}\kappa_0 C}{\varepsilon\beta_0^2}(\bar{u}_0+2\varepsilon\bar{u}_1\eta_l+3\varepsilon^2\bar{u}_2\eta_l^2+\cdots)$$
$$+\varepsilon^{-1}U_{-1}^l+U_0^l+\varepsilon U_1^l+\varepsilon^2U_2^l+\cdots\Bigg]-2(\varepsilon\bar{v}_0\eta_l+\varepsilon^2\bar{v}_1\eta_l^2+\varepsilon^3\bar{v}_2\eta_l^3+\cdots+1)$$
$$\times\Bigg[\frac{r^{(3-n)/(n+1)}\kappa_0 C}{\varepsilon\beta_0^2}(\bar{v}_0+2\varepsilon\bar{v}_1\eta_l+3\varepsilon^2\bar{v}_2\eta_l^2+\cdots)+\varepsilon^{-1}V_{-1}^l+V_0^l+\varepsilon V_1^l+\varepsilon^2V_2^l+\cdots\Bigg]$$
$$+\varepsilon^{-8}r^{2/(n+1)}(\bar{u}_0+2\varepsilon\bar{u}_1\eta_l+3\varepsilon^2\bar{u}_2\eta_l^2+\cdots)\Bigg[-\frac{\varepsilon^5\mathrm{i}r^{(1-n)/(n+1)}\kappa_0 C}{\beta_0^2}$$
$$\times(\bar{\bar{u}}_1\eta_l^2+\varepsilon\bar{\bar{u}}_2\eta_l^3+\varepsilon^2\bar{\bar{u}}_3\eta_l^4+\cdots)+\varepsilon^6W_1^l+\varepsilon^7W_2^l+\cdots\Bigg]$$
$$=-\Bigg[\frac{\eta_l(1-n)}{r(n+1)}\frac{\partial}{\partial\eta_l}+\mathrm{i}\varepsilon^{-4}(\alpha_0+\varepsilon^2\alpha_1+\varepsilon^3\alpha_2+\cdots)\Bigg](\varepsilon^3P_1^l+\cdots)$$
$$+\varepsilon^{-2}\frac{\partial}{\partial\eta_l}\Bigg\{(\bar{\mu}_0+\varepsilon\bar{\mu}_1\eta_l+\varepsilon^2\bar{\mu}_2\eta_l^2+\cdots)\frac{\partial}{\partial\eta_l}\Bigg[\frac{r^{(3-n)/(n+1)}\kappa_0 C}{\varepsilon\beta_0^2}$$
$$\times(\bar{u}_0+2\varepsilon\bar{u}_1\eta_l+3\varepsilon^2\bar{u}_2\eta_l^2+\cdots)+\varepsilon^{-1}U_{-1}^l+U_0^l+\varepsilon U_1^l+\varepsilon^2U_2^l+\cdots\Bigg]\Bigg\}$$
$$+\varepsilon^{-2}\frac{\partial}{\partial\eta_l}\Bigg\{(\bar{u}_0+2\varepsilon\bar{u}_1\eta_l+3\varepsilon^2\bar{u}_2\eta_l^2+\cdots)(\bar{u}_0+2\varepsilon\bar{u}_1\eta_l+3\varepsilon^2\bar{u}_2\eta_l^2+\cdots)$$
$$\times(\bar{\nu}_0+\varepsilon\bar{\nu}_1\eta_l+\varepsilon^2\bar{\nu}_2\eta_l^2+\cdots)\frac{\partial}{\partial\eta_l}\Bigg[\frac{r^{(3-n)/(n+1)}\kappa_0 C}{\varepsilon\beta_0^2}(\bar{u}_0+2\varepsilon\bar{u}_1\eta_l+3\varepsilon^2\bar{u}_2\eta_l^2+\cdots)$$
$$+\varepsilon^{-1}U_{-1}^l+U_0^l+\varepsilon U_1^l+\varepsilon^2U_2^l+\cdots\Bigg]\Bigg\}$$
$$+\varepsilon^{-2}\frac{\partial}{\partial\eta_l}\Bigg\{(\bar{u}_0+2\varepsilon\bar{u}_1\eta_l+3\varepsilon^2\bar{u}_2\eta_l^2+\cdots)(\bar{v}_0+2\varepsilon\bar{v}_1\eta_l+3\varepsilon^2\bar{v}_2\eta_l^2+\cdots)$$
$$\times(\bar{\nu}_0+\varepsilon\bar{\nu}_1\eta_l+\varepsilon^2\bar{\nu}_2\eta_l^2+\cdots)\frac{\partial}{\partial\eta_l}\Bigg[\frac{r^{(3-n)/(n+1)}\kappa_0 C}{\varepsilon\beta_0^2}(\bar{v}_0+2\varepsilon\bar{v}_1\eta_l+3\varepsilon^2\bar{v}_2\eta_l^2+\cdots)$$
$$+\varepsilon^{-1}V_{-1}^l+V_0^l+\varepsilon V_1^l+\varepsilon^2V_2^l+\cdots\Bigg]\Bigg\},\qquad(6.1.14b)$$

$$\Bigg[\frac{\eta_l(\varepsilon\bar{u}_0\eta_l+\varepsilon^2\bar{u}_1\eta_l^2+\varepsilon^3\bar{u}_2\eta_l^3+\cdots)(1-n)}{(n+1)}\frac{\partial}{\partial\eta_l}+\mathrm{i}\varepsilon^{-4}r(\varepsilon\bar{u}_0\eta_l+\varepsilon^2\bar{u}_1\eta_l^2+\varepsilon^3\bar{u}_2\eta_l^3+\cdots)$$
$$\times(\alpha_0+\varepsilon^2\alpha_1+\varepsilon^3\alpha_2+\cdots)+\mathrm{i}\varepsilon^{-4}(\beta_0+\varepsilon^2\beta_1+\varepsilon^3\beta_2+\cdots)$$
$$+\varepsilon^{-1}(\varepsilon^2\bar{w}_1\eta_l^2+\varepsilon^3\bar{w}_2\eta_l^3+\cdots)\frac{\partial}{\partial\eta_l}\Bigg]\Bigg[\frac{r^{(3-n)/(n+1)}\kappa_0 C}{\varepsilon\beta_0^2}(\bar{v}_0+2\varepsilon\bar{v}_1\eta_l+3\varepsilon^2\bar{v}_2\eta_l^2+\cdots)$$
$$+\varepsilon^{-1}V_{-1}^l+V_0^l+\varepsilon V_1^l+\varepsilon^2V_2^l+\cdots\Bigg]+\frac{\varepsilon\eta_l(\bar{v}_0+2\varepsilon\bar{v}_1\eta_l+3\varepsilon^2\bar{v}_2\eta_l^2+\cdots)(1-n)}{(n+1)}$$
$$\times\Bigg[\frac{r^{(3-n)/(n+1)}\kappa_0 C}{\varepsilon\beta_0^2}(\bar{u}_0+2\varepsilon\bar{u}_1\eta_l+3\varepsilon^2\bar{u}_2\eta_l^2+\cdots)+\varepsilon^{-1}U_{-1}^l+U_0^l+\varepsilon U_1^l+\varepsilon^2U_2^l+\cdots\Bigg]$$
$$+(\varepsilon\bar{u}_0\eta_l+\varepsilon^2\bar{u}_1\eta_l^2+\varepsilon^3\bar{u}_2\eta_l^3+\cdots)\Bigg[\frac{r^{(3-n)/(n+1)}\kappa_0 C}{\varepsilon\beta_0^2}(\bar{v}_0+2\varepsilon\bar{v}_1\eta_l+3\varepsilon^2\bar{v}_2\eta_l^2+\cdots)$$
$$+\varepsilon^{-1}V_{-1}^l+V_0^l+\varepsilon V_1^l+\varepsilon^2V_2^l+\cdots\Bigg]+2(\varepsilon\bar{v}_0\eta_l+\varepsilon^2\bar{v}_1\eta_l^2+\varepsilon^3\bar{v}_2\eta_l^3+\cdots+1)$$
$$\times\Bigg[\frac{r^{(3-n)/(n+1)}\kappa_0 C}{\varepsilon\beta_0^2}(\bar{u}_0+2\varepsilon\bar{u}_1\eta_l+3\varepsilon^2\bar{u}_2\eta_l^2+\cdots)+\varepsilon^{-1}U_{-1}^l+U_0^l+\varepsilon U_1^l+\varepsilon^2U_2^l+\cdots\Bigg]$$
$$+\varepsilon^{-8}r^{2/(n+1)}(\bar{v}_0+2\varepsilon\bar{v}_1\eta_l+3\varepsilon^2\bar{v}_2\eta_l^2+\cdots)\Bigg[-\frac{\varepsilon^5\mathrm{i}r^{(1-n)/(n+1)}\kappa_0 C}{\beta_0^2}$$
$$\times(\bar{\bar{u}}_1\eta_l^2+\varepsilon\bar{\bar{u}}_2\eta_l^3+\varepsilon^2\bar{\bar{u}}_3\eta_l^4+\cdots)+\varepsilon^6W_1^l+\varepsilon^7W_2^l+\cdots\Bigg]$$
$$=-\frac{\mathrm{i}\varepsilon^{-4}(\beta_0+\varepsilon^2\beta_1+\varepsilon^3\beta_2+\cdots)(\varepsilon^3P_1^l+\cdots)}{r}$$
$$+\varepsilon^{-2}\frac{\partial}{\partial\eta_l}\Bigg\{(\bar{\mu}_0+\varepsilon\bar{\mu}_1\eta_l+\varepsilon^2\bar{\mu}_2\eta_l^2+\cdots)\frac{\partial}{\partial\eta_l}\Bigg[\frac{r^{(3-n)/(n+1)}\kappa_0 C}{\varepsilon\beta_0^2}$$
$$\times(\bar{v}_0+2\varepsilon\bar{v}_1\eta_l+3\varepsilon^2\bar{v}_2\eta_l^2+\cdots)+\varepsilon^{-1}V_{-1}^l+V_0^l+\varepsilon V_1^l+\varepsilon^2V_2^l+\cdots\Bigg]\Bigg\}$$
$$+\varepsilon^{-2}\frac{\partial}{\partial\eta_l}\Bigg\{(\bar{v}_0+2\varepsilon\bar{v}_1\eta_l+3\varepsilon^2\bar{v}_2\eta_l^2+\cdots)(\bar{u}_0+2\varepsilon\bar{u}_1\eta_l+3\varepsilon^2\bar{u}_2\eta_l^2+\cdots)$$
$$\times(\bar{\nu}_0+\varepsilon\bar{\nu}_1\eta_l+\varepsilon^2\bar{\nu}_2\eta_l^2+\cdots)\frac{\partial}{\partial\eta_l}\Bigg[\frac{r^{(3-n)/(n+1)}\kappa_0 C}{\varepsilon\beta_0^2}(\bar{u}_0+2\varepsilon\bar{u}_1\eta_l+3\varepsilon^2\bar{u}_2\eta_l^2+\cdots)$$
$$+\varepsilon^{-1}U_{-1}^l+U_0^l+\varepsilon U_1^l+\varepsilon^2U_2^l+\cdots\Bigg]\Bigg\}$$
$$+\varepsilon^{-2}\frac{\partial}{\partial\eta_l}\Bigg\{(\bar{v}_0+2\varepsilon\bar{v}_1\eta_l+3\varepsilon^2\bar{v}_2\eta_l^2+\cdots)(\bar{v}_0+2\varepsilon\bar{v}_1\eta_l+3\varepsilon^2\bar{v}_2\eta_l^2+\cdots)$$
$$\times(\bar{\nu}_0+\varepsilon\bar{\nu}_1\eta_l+\varepsilon^2\bar{\nu}_2\eta_l^2+\cdots)\frac{\partial}{\partial\eta_l}\Bigg[\frac{r^{(3-n)/(n+1)}\kappa_0 C}{\varepsilon\beta_0^2}(\bar{v}_0+2\varepsilon\bar{v}_1\eta_l+3\varepsilon^2\bar{v}_2\eta_l^2+\cdots)$$
$$+\varepsilon^{-1}V_{-1}^l+V_0^l+\varepsilon V_1^l+\varepsilon^2V_2^l+\cdots\Bigg]\Bigg\},\qquad(6.1.14c)$$

$$\Bigg[\frac{\eta_l(\varepsilon\bar{u}_0\eta_l+\varepsilon^2\bar{u}_1\eta_l^2+\varepsilon^3\bar{u}_2\eta_l^3+\cdots)(1-n)}{(n+1)}\frac{\partial}{\partial\eta_l}+\mathrm{i}\varepsilon^{-4}r(\varepsilon\bar{u}_0\eta_l+\varepsilon^2\bar{u}_1\eta_l^2+\varepsilon^3\bar{u}_2\eta_l^3+\cdots)$$
$$\times(\alpha_0+\varepsilon^2\alpha_1+\varepsilon^3\alpha_2+\cdots)+\mathrm{i}\varepsilon^{-4}(\beta_0+\varepsilon^2\beta_1+\varepsilon^3\beta_2+\cdots)$$
$$+\varepsilon^{-1}(\varepsilon^2\bar{w}_1\eta_l^2+\varepsilon^3\bar{w}_2\eta_l^3+\cdots)\frac{\partial}{\partial\eta_l}\Bigg]\Bigg[-\frac{\varepsilon^5\mathrm{i}r^{(1-n)/(n+1)}\kappa_0 C}{\beta_0^2}$$
$$\times(\bar{\bar{u}}_1\eta_l^2+\varepsilon\bar{\bar{u}}_2\eta_l^3+\varepsilon^2\bar{\bar{u}}_3\eta_l^4+\cdots)+\varepsilon^6W_1^l+\varepsilon^7W_2^l+\cdots\Bigg]$$
$$+\varepsilon^8r^{-2/(n+1)}\frac{(1-n)}{(n-1)}(\varepsilon^2\bar{w}_1\eta_l^2+2\varepsilon^3\bar{w}_2\eta_l^3+\cdots)$$
$$\times\left[\frac{r^{(3-n)/(n+1)}\kappa_0 C}{\varepsilon\beta_0^2}(\bar{u}_0+2\varepsilon\bar{u}_1\eta_l+3\varepsilon^2\bar{u}_2\eta_l^2+\cdots)+\varepsilon^{-1}U_{-1}^l+U_0^l+\varepsilon U_1^l+\varepsilon^2U_2^l+\cdots\right]$$
$$+(2\varepsilon\bar{w}_1\eta_l+3\varepsilon^2\bar{w}_2\eta_l^2+\cdots)\Bigg[-\frac{\varepsilon^5\mathrm{i}r^{(1-n)/(n+1)}\kappa_0 C}{\beta_0^2}(\bar{\bar{u}}_1\eta_l^2+\varepsilon\bar{\bar{u}}_2\eta_l^3+\varepsilon^2\bar{\bar{u}}_3\eta_l^4+\cdots)$$
$$+\varepsilon^6W_1^l+\varepsilon^7W_2^l+\cdots\Bigg]=-\varepsilon^{-9}r^{(1-n)/(n+1)}\frac{\partial(\varepsilon^3P_1^l+\cdots)}{\partial\eta_l}$$
$$+2\varepsilon^{-2}\frac{\partial}{\partial\eta_l}\Bigg\{(\bar{\mu}_0+\varepsilon\bar{\mu}_1\eta_l+\varepsilon^2\bar{\mu}_2\eta_l^2+\cdots)\frac{\partial}{\partial\eta_l}\Bigg[-\frac{\varepsilon^5\mathrm{i}r^{(1-n)/(n+1)}\kappa_0 C}{\beta_0^2}$$
$$\times(\bar{\bar{u}}_1\eta_l^2+\varepsilon\bar{\bar{u}}_2\eta_l^3+\varepsilon^2\bar{\bar{u}}_3\eta_l^4+\cdots)+\varepsilon^6W_1^l+\varepsilon^7W_2^l+\cdots\Bigg]\Bigg\}$$
$$+2\varepsilon^6r^{-2/(n+1)}\frac{\partial}{\partial\eta_l}\Bigg\{(2\varepsilon\bar{w}_1\eta_l+3\varepsilon^2\bar{w}_2\eta_l^2+\cdots)(\bar{u}_0+2\varepsilon\bar{u}_1\eta_l+3\varepsilon^2\bar{u}_2\eta_l^2+\cdots)$$
$$\times(\bar{\nu}_0+\varepsilon\bar{\nu}_1\eta_l+\varepsilon^2\bar{\nu}_2\eta_l^2+\cdots)\frac{\partial}{\partial\eta_l}\left[\frac{r^{(3-n)/(n+1)}\kappa_0 C}{\varepsilon\beta_0^2}(\bar{u}_0+2\varepsilon\bar{u}_1\eta_l+3\varepsilon^2\bar{u}_2\eta_l^2+\cdots)\right.$$
$$\left.+\varepsilon^{-1}U_{-1}^l+U_0^l+\varepsilon U_1^l+\varepsilon^2U_2^l+\cdots\right]\Bigg\}$$
$$+2\varepsilon^6r^{-2/(n+1)}\frac{\partial}{\partial\eta_l}\Bigg\{(2\varepsilon\bar{w}_1\eta_l+3\varepsilon^2\bar{w}_2\eta_l^2+\cdots)(\bar{v}_0+2\varepsilon\bar{v}_1\eta_l+3\varepsilon^2\bar{v}_2\eta_l^2+\cdots)$$
$$\times(\bar{\nu}_0+\varepsilon\bar{\nu}_1\eta_l+\varepsilon^2\bar{\nu}_2\eta_l^2+\cdots)\frac{\partial}{\partial\eta_l}\left[\frac{r^{(3-n)/(n+1)}\kappa_0 C}{\varepsilon\beta_0^2}(\bar{v}_0+2\varepsilon\bar{v}_1\eta_l+3\varepsilon^2\bar{v}_2\eta_l^2+\cdots)\right.$$
$$\left.+\varepsilon^{-1}V_{-1}^l+V_0^l+\varepsilon V_1^l+\varepsilon^2V_2^l+\cdots\right]\Bigg\}+\mathcal{O}(\varepsilon^6). \tag{6.1.14d}$$

The expansions of the viscosity function are given by

$$
\begin{aligned}
\bar{\mu}_0 &= [\bar{u}_0^2 + \bar{v}_0^2]^{(n-1)/2}, \\
\bar{\mu}_1 &= \frac{2(n-1)\bar{\mu}_0(\bar{u}_0\bar{u}_1 + \bar{v}_0\bar{v}_1)}{\bar{u}_0^2 + \bar{v}_0^2}, \\
\bar{\mu}_2 &= \frac{2(n-1)(n-3)\bar{\mu}_0(\bar{u}_0\bar{u}_1 + \bar{v}_0\bar{v}_1)^2}{(\bar{u}_0^2 + \bar{v}_0^2)^2} + \frac{(n-1)\bar{\mu}_0[2(\bar{u}_1^2 + \bar{v}_1^2) + 3(\bar{u}_0\bar{u}_2 + \bar{v}_0\bar{v}_2)]}{\bar{u}_0^2 + \bar{v}_0^2}, \\
\bar{\nu}_0 &= \frac{(n-1)\bar{\mu}_0}{\bar{u}_0^2 + \bar{v}_0^2}, \\
\bar{\nu}_1 &= \frac{2(n-3)\bar{\nu}_0(\bar{u}_0\bar{u}_1 + \bar{v}_0\bar{v}_1)}{\bar{u}_0^2 + \bar{v}_0^2}, \\
\bar{\nu}_2 &= \frac{2(n-3)(n-5)\bar{\nu}_0(\bar{u}_0\bar{u}_1 + \bar{v}_0\bar{v}_1)^2}{(\bar{u}_0^2 + \bar{v}_0^2)^2} + \frac{(n-3)\bar{\nu}_0[2(\bar{u}_1^2 + \bar{v}_1^2) + 3(\bar{u}_0\bar{u}_2 + \bar{v}_0\bar{v}_2)]}{\bar{u}_0^2 + \bar{v}_0^2},
\end{aligned}
$$

and, after some lengthy algebra, we find that

$$
\begin{aligned}
\bar{u}_1 &= \frac{-1}{2n\bar{\mu}_0}\left[1 + \frac{(n-1)\bar{v}_0^2}{\bar{u}_0^2 + \bar{v}_0^2}\right], \\
\bar{v}_1 &= \frac{1}{2n\bar{\mu}_0}\left[\frac{(n-1)\bar{u}_0\bar{v}_0}{\bar{u}_0^2 + \bar{v}_0^2}\right], \\
\bar{u}_2 &= \frac{-\bar{v}_0}{3\bar{\mu}_0} + \frac{\bar{u}_0(1-n)}{6n^2\bar{\mu}_0^2(\bar{u}_0^2 + \bar{v}_0^2)}\left[1 + \frac{(3n-1)\bar{v}_0^2}{\bar{u}_0^2 + \bar{v}_0^2}\right], \\
\bar{v}_2 &= \frac{\bar{u}_0}{3\bar{\mu}_0} + \frac{\bar{v}_0(1-n)}{6n^2\bar{\mu}_0^2(\bar{u}_0^2 + \bar{v}_0^2)}\left[1 + \frac{(n-1)\bar{v}_0^2 - 2n\bar{u}_0^2}{\bar{u}_0^2 + \bar{v}_0^2}\right].
\end{aligned}
$$

Now at $\mathcal{O}(\varepsilon^{-5})$ the continuity equation reduces to

$$
\mathrm{i}\bar{\bar{u}}_0\frac{r^{2(1-n)/(n+1)}\kappa_0 C}{\beta_0^2} + \mathrm{i}(\alpha_0 U_{-1}^l + \beta_0 V_{-1}^l/r) = 0.
$$

Given that $\bar{\bar{u}}_0 = 0$ then clearly

$$
V_{-1}^l = -(\alpha_0 r/\beta_0)U_{-1}^l. \tag{6.1.15}
$$

Similarly we find that

$$V_0^l = -(\alpha_0 r/\beta_0)U_0^l. \tag{6.1.16}$$

After suitable simplification the next order yields

$$\mathrm{i}(\alpha_0 U_1^l + \beta_0 V_1^l/r) + \mathrm{i}(\alpha_1 \bar{u}_0 r + \beta_1 \bar{v}_0)\left[\frac{r^{2(1-n)/(n+1)}\kappa_0 C}{\beta_0^2}\right] + \mathrm{i}(\alpha_1 U_{-1}^l + \beta_1 V_{-1}^l/r) + r^{(1-n)/(n+1)}\frac{dW_1^l}{d\eta_l} = 0. \tag{6.1.17}$$

We note that at leading order $P_1 = C$. At $\mathcal{O}(\varepsilon^{-3})$ the r-momentum equation reduces to

$$\mathrm{i}\bar{\bar{u}}_0\eta_l\left[\frac{2r^{(3-n)/(n+1)}\kappa_0 C\bar{u}_1\eta_l}{\beta_0^2} + U_0^l\right] + \mathrm{i}\bar{\bar{u}}_1\eta_l^2\left[\frac{r^{(3-n)/(n+1)}\kappa_0 C\bar{u}_0}{\beta_0^2} + U_{-1}^l\right] - \mathrm{i}\bar{\bar{u}}_1\eta_l^2\left[\frac{r^{(3-n)/(n+1)}\kappa_0 C\bar{u}_0}{\beta_0^2}\right] = \bar{\mu}_0\frac{d^2U_{-1}^l}{d\eta_l^2} + \bar{u}_0\bar{\nu}_0\left(\bar{u}_0\frac{d^2U_{-1}^l}{d\eta_l^2} + \bar{v}_0\frac{d^2V_{-1}^l}{d\eta_l^2}\right),$$

which can be simplified to give

$$\frac{d^2U_{-1}^l}{d\eta_l^2} - \frac{\mathrm{i}\bar{\bar{u}}_1\eta_l^2 U_{-1}^l}{n\bar{\mu}_0} = 0.$$

By writing

$$z = \sqrt{2}\Lambda^{1/4}\eta_l, \quad \text{where} \quad \Lambda = \frac{\mathrm{i}\bar{\bar{u}}_1}{n\bar{\mu}_0},$$

we obtain the standard parabolic cylinder equation with $y = U_{-1}^l$ and $a = 0$

$$\frac{d^2U_{-1}^l}{dz^2} - \left(\frac{z^2}{4}\right)U_{-1}^l = 0. \tag{6.1.18}$$

Thus, $U_{-1}^l = C_1U(0,z) + C_2V(0,z)$, where C_1 and C_2 are constants of integration, and

$U(0,z)$ and $V(0,z)$ are the exponentially decaying and growing parabolic cylinder functions, respectively. Now at $\mathcal{O}(\varepsilon^{-1})$ we have that $u_0^m = r^{3(1-n)/(n+1)}(\kappa_0/\beta_0^2)C\bar{u}_0$ at $\eta = 0$, thus from (6.1.13a) we require that $U_{-1}^l \to 0$ as $\eta_l \to \infty$. Satisfying the no-slip boundary condition we further require that $U_{-1}^l = -r^{(3-n)/(n+1)}(\kappa_0/\beta_0^2)C\bar{u}_0$ at $\eta_l = 0$. Whilst at $\mathcal{O}(\varepsilon^i)$ we have that $U_i^l = 0$ at $\eta_l = 0$ for $i = 0, 1, 2, \ldots$. Hence the solution of (6.1.18) that matches with the main deck is

$$U_{-1}^l = -\frac{r^{(3-n)/(n+1)}\kappa_0 C\bar{u}_0}{\beta_0^2}\frac{U(0,\sqrt{2}\Lambda^{1/4}\eta_l)}{U(0,0)}.$$

Equivalently, from the θ-momentum equation and associated boundary conditions

$$V_{-1}^l = -\frac{r^{(3-n)/(n+1)}\kappa_0 C\bar{v}_0}{\beta_0^2}\frac{U(0,\sqrt{2}\Lambda^{1/4}\eta_l)}{U(0,0)}.$$

At $\mathcal{O}(\varepsilon^{-2})$ the r-momentum equation reduces to

$$\begin{aligned}
&\mathrm{i}\bar{\bar{u}}_0\eta_l\left[\frac{3r^{(3-n)/(n+1)}\kappa_0 C\bar{u}_2\eta_l^2}{\beta_0^2} + U_1^l\right] + \mathrm{i}\bar{\bar{u}}_1\eta_l^2\left[\frac{2r^{(3-n)/(n+1)}\kappa_0 C\bar{u}_1\eta_l}{\beta_0^2} + U_0^l\right] \\
&+ \mathrm{i}\eta_l[\bar{\bar{u}}_2\eta_l^2 + (\alpha_1\bar{u}_0 r + \beta_1\bar{v}_0)]\left[\frac{r^{(3-n)/(n+1)}\kappa_0 C\bar{u}_0}{\beta_0^2} + U_{-1}^l\right] - \mathrm{i}\bar{\bar{u}}_2\eta_l^3\left[\frac{r^{(3-n)/(n+1)}\kappa_0 C\bar{u}_0}{\beta_0^2}\right] \\
&- \mathrm{i}\bar{\bar{u}}_1\eta_l^2\left[\frac{2r^{(3-n)/(n+1)}\kappa_0 C\bar{u}_1\eta_l}{\beta_0^2}\right] + r^{2/(n+1)}\bar{u}_0 W_1^l = \bar{\mu}_0\frac{d^2U_0^l}{d\eta_l^2} \\
&+ \bar{\nu}_0\bar{u}_0\left(\bar{u}_0\frac{d^2U_0^l}{d\eta_l^2} + \bar{v}_0\frac{d^2V_0^l}{d\eta_l^2}\right) + [\bar{\mu}_1 + (\bar{\nu}_1\bar{u}_0^2 + 4\bar{\nu}_0\bar{u}_0\bar{u}_1)]\frac{d}{d\eta_l}\left(\eta_l\frac{dU_{-1}^l}{d\eta_l}\right) \\
&+ [\bar{\nu}_1\bar{u}_0\bar{v}_0 + 2\bar{\nu}_0(\bar{u}_0\bar{v}_1 + \bar{u}_1\bar{v}_0)]\frac{d}{d\eta_l}\left(\eta_l\frac{dV_{-1}^l}{d\eta_l}\right).
\end{aligned}$$

This can be simplified to give

$$\begin{aligned}
\mathrm{i}\bar{\bar{u}}_1\eta_l^2 U_0^l + \mathrm{i}\bar{\bar{u}}_2\eta_l^3 U_{-1}^l + \mathrm{i}(\alpha_1\bar{u}_0 r + \beta_1\bar{v}_0)\eta_l\left[\frac{r^{(3-n)/(n+1)}\kappa_0 C\bar{u}_0}{\beta_0^2} + U_{-1}^l\right] \\
+ r^{2/(n+1)}\bar{u}_0 W_1^l = n\bar{\mu}_0\frac{d^2U_0^l}{d\eta_l^2} + \frac{(1-n)}{\bar{u}_0}\frac{d}{d\eta_l}\left(\eta_l\frac{dU_{-1}^l}{d\eta_l}\right).
\end{aligned}$$

Correspondingly, after simplification, the θ-momentum equation yields

$$\mathrm{i}\bar{\bar{u}}_1\eta_l^2 V_0^l + \mathrm{i}\bar{\bar{u}}_2\eta_l^3 V_{-1}^l + \mathrm{i}(\alpha_1\bar{u}_0 r + \beta_1\bar{v}_0)\eta_l\left[\frac{r^{(3-n)/(n+1)}\kappa_0 C\bar{v}_0}{\beta_0^2} + V_{-1}^l\right] + r^{2/(n+1)}\bar{v}_0 W_1^l = n\bar{\mu}_0\frac{d^2V_0^l}{d\eta_l^2}.$$

Thus we see that $V_0^l = -(\alpha_0 r/\beta_0)U_0^l$ only in the case when $n = 1$. In order to continue we appeal to the upper-branch analysis and assume that the terms owing from the perturbed viscosity function are sufficiently small when compared to the unperturbed viscous terms. We have shown in §5.1.1 that this is certainly the case for the type I modes in the large Reynolds number limit. Essentially, the $\bar{\nu}_i$ for $i = 0, 1, 2, \ldots$ are ignored throughout the remainder of this analysis.

In this case the upper deck and main deck equations remain unchanged, as do the equations determined from the continuity and z-momentum equations in the lower deck. At $\mathcal{O}(\varepsilon^{-3})$ the r and θ-momentum equations become

$$\frac{d^2U_{-1}^l}{d\eta_l^2} - \frac{\mathrm{i}\bar{\bar{u}}_1\eta_l^2 U_{-1}^l}{\bar{\mu}_0} = 0, \tag{6.1.19a}$$

$$\frac{d^2V_{-1}^l}{d\eta_l^2} - \frac{\mathrm{i}\bar{\bar{u}}_1\eta_l^2 V_{-1}^l}{\bar{\mu}_0} = 0, \tag{6.1.19b}$$

respectively, hence

$$(U_{-1}^l, V_{-1}^l) = -\frac{r^{(3-n)/(n+1)}\kappa_0 C(\bar{u}_0, \bar{v}_0)}{\beta_0^2}\frac{U(0, \sqrt{2}\Delta^{1/4}\eta_l)}{U(0,0)}, \tag{6.1.20}$$

where $\Delta = \mathrm{i}\bar{\bar{u}}_1/\bar{\mu}_0$. At $\mathcal{O}(\varepsilon^{-2})$ the r and θ-momentum equations become

$$\mathrm{i}\bar{\bar{u}}_1\eta_l^2 U_0^l + \mathrm{i}\bar{\bar{u}}_2\eta_l^3 U_{-1}^l + \mathrm{i}(\alpha_1\bar{u}_0 r + \beta_1\bar{v}_0)\eta_l\left[\frac{r^{(3-n)/(n+1)}\kappa_0 C\bar{u}_0}{\beta_0^2} + U_{-1}^l\right] + r^{2/(n+1)}\bar{u}_0 W_1^l = \bar{\mu}_0\frac{d^2U_0^l}{d\eta_l^2} + \bar{\mu}_1\frac{d}{d\eta_l}\left(\eta_l\frac{dU_{-1}^l}{d\eta_l}\right), \tag{6.1.21a}$$

$$\mathrm{i}\bar{\bar{u}}_1\eta_l^2 V_0^l + \mathrm{i}\bar{\bar{u}}_2\eta_l^3 V_{-1}^l + \mathrm{i}(\alpha_1\bar{u}_0 r + \beta_1\bar{v}_0)\eta_l\left[\frac{r^{(3-n)/(n+1)}\kappa_0 C\bar{v}_0}{\beta_0^2} + V_{-1}^l\right] + r^{2/(n+1)}\bar{v}_0 W_1^l = \bar{\mu}_0\frac{d^2V_0^l}{d\eta_l^2} + \bar{\mu}_1\frac{d}{d\eta_l}\left(\eta_l\frac{dV_{-1}^l}{d\eta_l}\right), \quad (6.1.21b)$$

respectively. So that now the continuity equation at $\mathcal{O}(\varepsilon^{-4})$ is indeed satisfied. At $\mathcal{O}(\varepsilon^{-1})$ the r-momentum equation reduces to

$$\begin{aligned}
&\mathrm{i}\bar{\bar{u}}_0\eta_l\left[\frac{4r^{(3-n)/(n+1)}\kappa_0 C\bar{u}_3\eta_l^3}{\beta_0^2} + U_2^l\right] + \mathrm{i}\bar{\bar{u}}_1\eta_l^2\left[\frac{3r^{(3-n)/(n+1)}\kappa_0 C\bar{u}_2\eta_l^2}{\beta_0^2} + U_1^l\right] \\
&+ \mathrm{i}\eta_l[\bar{\bar{u}}_2\eta_l^2 + (\alpha_1\bar{u}_0 r + \beta_1\bar{v}_0)]\left[\frac{2r^{(3-n)/(n+1)}\kappa_0 C\bar{u}_1\eta_l}{\beta_0^2} + U_0^l\right] \\
&+ \mathrm{i}\eta_l[\bar{\bar{u}}_3\eta_l^3 + (\alpha_1\bar{u}_1 r + \beta_1\bar{v}_1)\eta_l + (\alpha_2\bar{u}_0 r + \beta_2\bar{v}_0)]\left[\frac{r^{(3-n)/(n+1)}\kappa_0 C\bar{u}_0}{\beta_0^2} + U_{-1}^l\right] \\
&- 2\left[\frac{r^{(3-n)/(n+1)}\kappa_0 C\bar{v}_0}{\beta_0^2} + V_{-1}^l\right] - \mathrm{i}\bar{\bar{u}}_3\eta_l^4\left[\frac{r^{(3-n)/(n+1)}\kappa_0 C\bar{u}_0}{\beta_0^2}\right] \\
&- \mathrm{i}\bar{\bar{u}}_2\eta_l^3\left[\frac{2r^{(3-n)/(n+1)}\kappa_0 C\bar{u}_1\eta_l}{\beta_0^2}\right] - \mathrm{i}\bar{\bar{u}}_1\eta_l^2\left[\frac{3r^{(3-n)/(n+1)}\kappa_0 C\bar{u}_2\eta_l^2}{\beta_0^2}\right] \\
&+ r^{2/(n+1)}(\bar{u}_0 W_2^l + 2\bar{u}_1\eta_l W_1^l) = -\mathrm{i}\alpha_0 P_1^l + \bar{\mu}_0\left[\frac{d^2U_1^l}{d\eta_l^2} + \frac{6r^{(3-n)/(n+1)}\kappa_0 C\bar{u}_2}{\beta_0^2}\right] \\
&+ \bar{\mu}_1\frac{d}{d\eta_l}\left(\eta_l\frac{dU_0^l}{d\eta_l}\right) + \bar{\mu}_2\frac{d}{d\eta_l}\left(\eta_l^2\frac{dU_{-1}^l}{d\eta_l}\right). \qquad (6.1.22)
\end{aligned}$$

This can be simplified to give

$$\begin{aligned}
&\mathrm{i}\bar{\bar{u}}_1\eta_l^2 U_1^l + \mathrm{i}\bar{\bar{u}}_2\eta_l^3 U_0^l + \mathrm{i}\bar{\bar{u}}_3\eta_l^4 U_{-1}^l + \mathrm{i}(\alpha_1\bar{u}_0 r + \beta_1\bar{v}_0)\eta_l\left[\frac{2r^{(3-n)/(n+1)}\kappa_0 C\bar{u}_1\eta_l}{\beta_0^2} + U_0^l\right] \\
&+ \mathrm{i}\eta_l[(\alpha_1\bar{u}_1 r + \beta_1\bar{v}_1)\eta_l + (\alpha_2\bar{u}_0 r + \beta_2\bar{v}_0)]\left[\frac{r^{(3-n)/(n+1)}\kappa_0 C\bar{u}_0}{\beta_0^2} + U_{-1}^l\right] \\
&- 2\left[\frac{r^{(3-n)/(n+1)}\kappa_0 C\bar{v}_0}{\beta_0^2} + V_{-1}^l\right] + r^{2/(n+1)}(\bar{u}_0 W_2^l + 2\bar{u}_1\eta_l W_1^l) = -\mathrm{i}\alpha_0 P_1^l \\
&+ \bar{\mu}_0\left[\frac{d^2U_1^l}{d\eta_l^2} + \frac{6r^{(3-n)/(n+1)}\kappa_0 C\bar{u}_2}{\beta_0^2}\right] + \bar{\mu}_1\frac{d}{d\eta_l}\left(\eta_l\frac{dU_0^l}{d\eta_l}\right) + \bar{\mu}_2\frac{d}{d\eta_l}\left(\eta_l^2\frac{dU_{-1}^l}{d\eta_l}\right). \qquad (6.1.23a)
\end{aligned}$$

It is here that we observe the first occurrence of Coriolis terms owing from the choice of

our rotating coordinate system. The θ-momentum equation at the same order reduces to

$$\begin{aligned}
&\mathrm{i}\bar{\bar{u}}_1\eta_l^2 V_1^l + \mathrm{i}\bar{\bar{u}}_2\eta_l^3 V_0^l + \mathrm{i}\bar{\bar{u}}_3\eta_l^4 V_{-1}^l + \mathrm{i}(\alpha_1\bar{u}_0 r + \beta_1\bar{v}_0)\eta_l\left[\frac{2r^{(3-n)/(n+1)}\kappa_0 C\bar{v}_1\eta_l}{\beta_0^2} + V_0^l\right] \\
&+ \mathrm{i}\eta_l[(\alpha_1\bar{u}_1 r + \beta_1\bar{v}_1)\eta_l + (\alpha_2\bar{u}_0 r + \beta_2\bar{v}_0)]\left[\frac{r^{(3-n)/(n+1)}\kappa_0 C\bar{v}_0}{\beta_0^2} + V_{-1}^l\right] \\
&+ 2\left[\frac{r^{(3-n)/(n+1)}\kappa_0 C\bar{u}_0}{\beta_0^2} + U_{-1}^l\right] + r^{2/(n+1)}(\bar{v}_0 W_2^l + 2\bar{v}_1\eta_l W_1^l) = -\frac{\mathrm{i}\beta_0 P_1^l}{r} \\
&+ \bar{\mu}_0\left[\frac{d^2V_1^l}{d\eta_l^2} + \frac{6r^{(3-n)/(n+1)}\kappa_0 C\bar{v}_2}{\beta_0^2}\right] + \bar{\mu}_1\frac{d}{d\eta_l}\left(\eta_l\frac{dV_0^l}{d\eta_l}\right) + \bar{\mu}_2\frac{d}{d\eta_l}\left(\eta_l^2\frac{dV_{-1}^l}{d\eta_l}\right). \qquad (6.1.23b)
\end{aligned}$$

Taking the linear combination $\mathrm{i}\alpha_0\times$(6.1.23a)+$\mathrm{i}(\beta_0/r)\times$(6.1.23b) produces the following

$$\begin{aligned}
&\mathrm{i}\bar{\mu}_0\left[\alpha_0\frac{d^2U_1^l}{d\eta_l^2} + \frac{\beta_0}{r}\frac{d^2V_1^l}{d\eta_l^2}\right] + r^{2(1-n)/(n+1)}\kappa_0^2 P_1^l + 2\mathrm{i}(\alpha_0 V_{-1}^l - \beta_0 U_{-1}^l/r) \\
&\quad + \mathrm{i}[\alpha_0(\bar{v}_0 + 3\bar{\mu}_0\bar{u}_2)r + \beta_0(3\bar{\mu}_0\bar{v}_2 - \bar{u}_0) - \mathrm{i}\bar{\bar{u}}_1(\alpha_1\bar{u}_0 r + \beta_1\bar{v}_0)\eta_l^2]\left[\frac{2r^{2(1-n)/(n+1)}\kappa_0 C}{\beta_0^2}\right] \\
&\qquad = \bar{\bar{u}}_1\eta_l\big[2\mathrm{i}r^{(1-n)/(n+1)}W_1^l - (\alpha_0 U_1^l + \beta_0 V_1^l/r)\eta_l\big].
\end{aligned}$$

We observe the balance between the viscous and Coriolis terms. This indicates that the structure of the type II neutral curve is dependent on both viscous and Coriolis effects. Using (6.1.17) we eliminate U_1^l and V_1^l from the above. Utilising the form of (6.1.15), (6.1.17) and (6.1.20) and recalling the expressions for $\bar{u}_2$ and $\bar{v}_2$ we obtain

$$\begin{aligned}
\bar{\mu}_0 r^{(n-1)/(n+1)}\left[\frac{d^3W_1^l}{d\eta_l^3} - \Delta\eta_l^2\frac{dW_1^l}{d\eta_l} + 2\Delta\eta_l W_1^l\right] &= \kappa_0^2 C - \mathrm{i}\Delta(\alpha_1\bar{u}_0 r + \beta_1\bar{v}_0) \\
\times\frac{\kappa_0 C\bar{\mu}_0\eta_l^2}{\beta_0^2} + \frac{2\mathrm{i}\kappa_0 C}{\beta_0}\left[\bar{u}_0\left(1 + \frac{\bar{v}_0^2}{\bar{u}_0^2}\right)\frac{U(0,\sqrt{2}\Delta^{1/4}\eta_l)}{U(0,0)} + \frac{(n-1)\bar{v}_0}{n\bar{\mu}_0(\bar{u}_0^2 + \bar{v}_0^2)}\right]. \qquad (6.1.24)
\end{aligned}$$

Following Hall (1986) the solution of this equation that matches with the main deck is given by

$$\bar{\mu}_0 r^{(n-1)/(n+1)} W_1^l = -\mathrm{i}(\alpha_1 \bar{u}_0 r + \beta_1 \bar{v}_0)\frac{\kappa_0 C \bar{\mu}_0 \eta_l}{\beta_0^2}$$
$$+ \Delta^{-3/4}\left\{\kappa_0^2 C F_1(s) + \frac{2\mathrm{i}\kappa_0 C}{\beta_0}\left[\bar{u}_0\left(1+\frac{\bar{v}_0^2}{\bar{u}_0^2}\right)\frac{F_2(s)}{U(0,0)} + \frac{(n-1)\bar{v}_0 F_1(s)}{n\bar{\mu}_0(\bar{u}_0^2+\bar{v}_0^2)}\right]\right\} + D\eta_l^2, \quad (6.1.25)$$

where D is a constant, $s = \Delta^{1/4}\eta_l$ and F_1 and F_2 satisfy

$$F_1''' - s^2 F_1' + 2sF_1 = 1, \quad (6.1.26a)$$
$$F_2''' - s^2 F_2' + 2sF_2 = U(0, \sqrt{2}s), \quad (6.1.26b)$$

respectively, with boundary conditions

$$F_1, F_2 = 0 \quad \text{at} \quad \eta_l = 0, \quad (6.1.27a)$$
$$F_1, F_2 \to 0 \quad \text{as} \quad \eta_l \to \infty. \quad (6.1.27b)$$

Thus, substituting (6.1.25) into (6.1.17) and evaluating at $\eta_l = 0$ produces the eigenrelation

$$\kappa_0^3 I_3 + \frac{2\mathrm{i}\kappa_0}{\beta_0}\left[\bar{u}_0\left(1+\frac{\bar{v}_0^2}{\bar{u}_0^2}\right)I_4 + \frac{(n-1)\bar{v}_0 I_3}{n\bar{\mu}_0(\bar{u}_0^2+\bar{v}_0^2)}\right] = \mathrm{i}\Delta^{1/2}(\alpha_1\bar{u}_0 r + \beta_1\bar{v}_0)\frac{\kappa_0\bar{\mu}_0}{\beta_0^2}, \quad (6.1.28)$$

where

$$I_3 = F_1'(0) = \frac{1}{2U(0,0)}\int_0^\infty xU(0,x)\,\mathrm{d}x = 0.5991,$$
$$I_4 = \frac{F_2'(0)}{U(0,0)} = \frac{1}{2U^2(0,0)}\int_0^\infty xU^2(0,x)\,\mathrm{d}x = 0.2285.$$

Solutions for the functions F_1 and F_2 can be expressed in terms of exponentially decaying parabolic cylinder functions, thus it is possible to write I_3 and I_4 as above. For brevity we do not include the detail of these calculations here as they prove to be quite lengthy.

n	$\bar{\kappa}_0$	λ_1
1	1.2244	2.3130
0.9	1.3700	2.7117
0.8	1.5336	3.1669
0.7	1.7238	3.6973
0.6	1.9551	4.3346

Table 6.2: Zero order solutions for the effective wavenumber and first order corrections to the effective wave angle for power-law fluids with $n = 1$, 0.9, 0.8, 0.7, 0.6.

The interested reader is referred to Hussain (2010) who outlines the computations in his rotating cone study. We note that application of $n = 1$ in (6.1.28) returns Hall's simplified Newtonian solution, as required.

Solving (6.1.28) gives

$$\begin{aligned}\kappa_0 &= \frac{2}{\beta_0}\left[\bar{u}_0\left(1+\frac{\bar{v}_0^2}{\bar{u}_0^2}\right)\frac{I_4}{I_3}+\frac{(n-1)\bar{v}_0}{n\bar{\mu}_0(\bar{u}_0^2+\bar{v}_0^2)}\right]\\ &= \frac{\sqrt{2}}{r^{1/(n+1)}}\left(1+\frac{\bar{v}_0^2}{\bar{u}_0^2}\right)^{1/4}\left[\bar{u}_0\left(1+\frac{\bar{v}_0^2}{\bar{u}_0^2}\right)\frac{I_4}{I_3}+\frac{(n-1)\bar{v}_0}{n\bar{\mu}_0(\bar{u}_0^2+\bar{v}_0^2)}\right]^{1/2}, \qquad (6.1.29a)\end{aligned}$$

$$\frac{\alpha_1}{\beta_0}-\frac{\beta_1\alpha_0}{\beta_0^2} = \frac{2\kappa_0^{3/2}I_3}{r^{n/(n+1)}|\bar{u}_0\bar{v}_0|^{1/2}}\left(1+\frac{\bar{v}_0^2}{\bar{u}_0^2}\right)^{-1/4}. \qquad (6.1.29b)$$

For convenience we write

$$\kappa_0 = \frac{\bar{\kappa}_0}{r^{1/(n+1)}}, \quad \frac{\alpha_1}{\beta_0}-\frac{\beta_1\alpha_0}{\beta_0^2} = \frac{\lambda_1}{r^{(2n+3)/[2(n+1)]}},$$

so that the effective wavenumber scaled on the viscous mode wavelength is given by

$$\begin{aligned}\kappa = r^{(n-1)/(n+1)}Re^{-1/[2(n+1)]}\sqrt{\alpha^2+\frac{\beta^2}{r^2}} &= \bar{\kappa}_0 r^{-1/(n+1)}\varepsilon^4+\cdots,\\ &= \bar{\kappa}_0 r^{-1/(n+1)}Re^{-1/[2(n+1)]}+\cdots, \qquad (6.1.30a)\end{aligned}$$

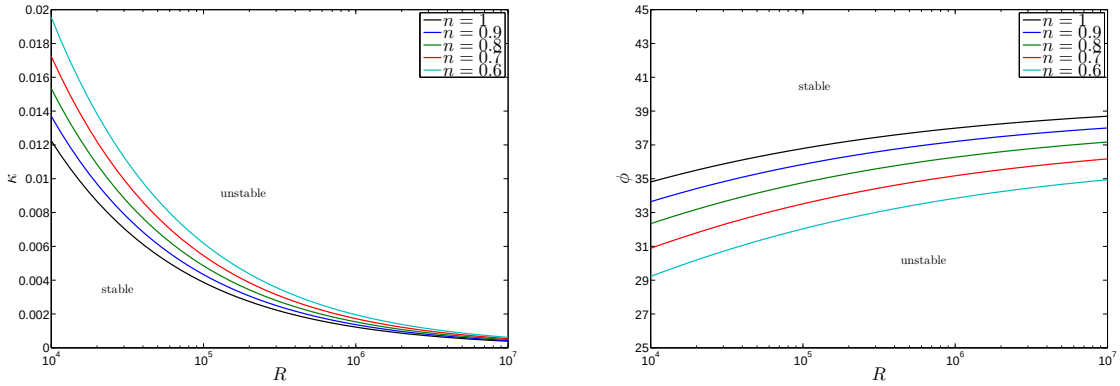

Figure 6.3: The viscous neutral wavenumber and wave angle predictions for power-law fluids with $n = 1$, 0.9, 0.8, 0.7, 0.6.

and the spiral wave angle expands as

$$\tan\left(\frac{\pi}{2} - \phi\right) = \lambda_0 + \lambda_1 r^{-1/[2(n+1)]}\varepsilon^2 + \cdots,$$
$$= \lambda_0 + \lambda_1 r^{-1/[2(n+1)]} Re^{-1/[4(n+1)]} + \cdots. \tag{6.1.30b}$$

By recalling the modified Reynolds number, $R = r^{2/(n+1)}Re^{1/(n+1)}$, we are again able to formulate expressions for the effective wavenumber and wave angle that have no explicit dependence on the radial variable r. From (6.1.30) we see that

$$\kappa = \bar{\kappa}_0 R^{-1/2} + \cdots, \tag{6.1.31a}$$
$$\phi = \frac{\pi}{2} - \arctan(\lambda_0 + \lambda_1 R^{-1/4} + \cdots). \tag{6.1.31b}$$

Having the solutions in this form again allows us to plot κ and ϕ as functions of R for $Re \gg 1$. However, here we are unable to plot $\bar{\alpha}$ and $\bar{\beta}$ as we are unable to determine the first order expressions for the radial and azimuthal wavenumbers. To do so we would need to determine the solution for W_2^l. This is beyond the scope of the current investigation, although we note that any stabilising/destabilising claims are inferred simply from our

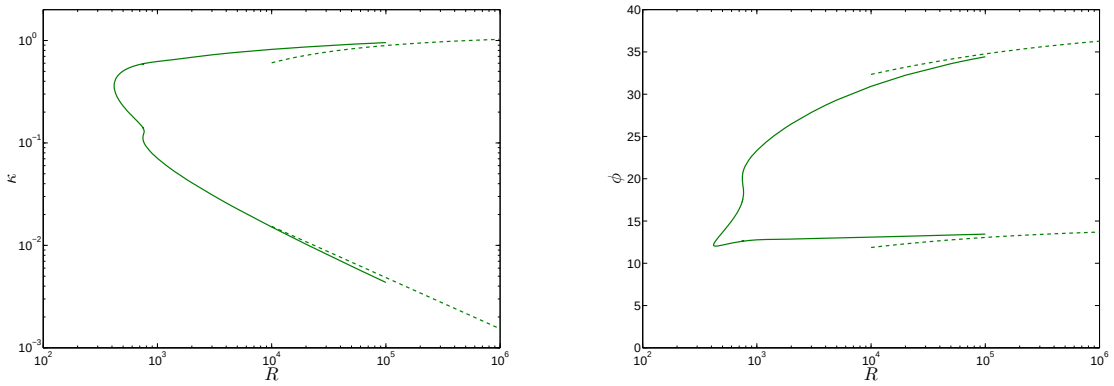

Figure 6.4: Neutral wavenumber and wave angle stability curves for power-law fluids with $n = 0.8$. The upper and lower-branch asymptotic solutions are given by the dashed lines.

solutions for κ and ϕ.

The zero order approximation to the wave angle shows that decreasing the power-law index has the effect of decreasing the wave angle of the disturbances. This is reaffirmed at the next order. We see from figure 6.3 that the ϕ plots are shifted uniformly down into the unstable region as n decreases, indicating stabilisation. A similar phenomenon is observed in the wavenumber plots.

Figure 6.4 demonstrates the excellent agreement between these results and our numerical solutions, this is indeed the case for each n in the range of interest, the remaining cases are plotted in the appendix C. The results from this study are consistent with those of our previous two, indicating that shear-thinning has a stabilising effect on the boundary-layer flow on a rotating disk, at least in the context of the power-law model.

6.2 Case II: Bingham

Here our small parameter ε is defined by $\varepsilon = \delta^{1/8} = Re^{-1/16}$ and the disturbance velocities and pressure satisfy

$$U_d = \tilde{u}(r,z)F, \quad V_d = \tilde{v}(r,z)F, \quad W_d = \tilde{w}(r,z)F, \quad P_d = \tilde{p}(r,z)F,$$

where F is given by (6.1.1). The wavenumber expansions are identical to those stated in (6.1.2), and the upper, main and lower deck coordinates are defined by

$$\zeta_u = Re^{1/4}z = \varepsilon^{-4}z,$$
$$\zeta = Re^{1/2}z = \varepsilon^{-8}z,$$
$$\zeta_l = Re^{9/16} = \varepsilon^{-9}z,$$

respectively. Inside the upper deck the disturbance perturbations are expanded as such

$$\tilde{u} = \varepsilon^3 U_0^u(\zeta_u) + \varepsilon^4 U_1^u(\zeta_u) + \cdots, \tag{6.2.1a}$$
$$\tilde{v} = \varepsilon^3 V_0^u(\zeta_u) + \varepsilon^4 V_1(\zeta_u) + \cdots, \tag{6.2.1b}$$
$$\tilde{w} = \varepsilon^3 W_0^u(\zeta_u) + \varepsilon^4 W_1^u(\zeta_u) + \cdots, \tag{6.2.1c}$$
$$\tilde{p} = \varepsilon^3 P_0^u(\zeta_u) + \varepsilon^4 P_1^u(\zeta_u) + \cdots. \tag{6.2.1d}$$

The preceding expansions are then substituted into the linearised disturbance equations, given in §4.2, along with the following forms for the differential operators when applied to the disturbance quantities

$$\frac{\partial}{\partial r} = \frac{\partial}{\partial r} + \left(\frac{\mathrm{i}}{\varepsilon^4}\right)(\alpha_0 + \varepsilon^2\alpha_1 + \varepsilon^3\alpha_2 + \cdots), \quad \frac{\partial}{\partial \theta} = \left(\frac{\mathrm{i}}{\varepsilon^4}\right)(\beta_0 + \varepsilon^2\beta_1 + \varepsilon^3\beta_2 + \cdots).$$

Equating terms of $\mathcal{O}(\varepsilon^{-1})$ we find that

$$\mathrm{i}\alpha_0 U_0^u + \frac{\mathrm{i}\beta_0 V_0^u}{r} + \frac{dW_0^u}{d\zeta_u} = 0, \tag{6.2.2a}$$
$$-\beta_0 U_0^u + \alpha_0 P_0^u = 0, \tag{6.2.2b}$$
$$-V_0 + \frac{P_0^u}{r} = 0, \tag{6.2.2c}$$
$$-\mathrm{i}\beta_0 W_0^u + \frac{dP_0^u}{d\zeta_u} = 0. \tag{6.2.2d}$$

Therefore the solution of this system that decays to zero as $\zeta_u \to \infty$ is

$$U_0^u = \frac{\alpha_0 C e^{-\gamma_0 \zeta_u}}{\beta_0}, \tag{6.2.3a}$$

$$V_0^u = \frac{C e^{-\gamma_0 \zeta_u}}{r}, \tag{6.2.3b}$$

$$W_0^u = \mathrm{i}\frac{\gamma_0 C e^{-\gamma_0 \zeta_u}}{\beta_0}, \tag{6.2.3c}$$

$$P_0^u = C e^{-\gamma_0 \zeta_u}, \tag{6.2.3d}$$

where, as before, $\gamma_0 = \sqrt{\alpha_0^2 + \beta_0^2/r^2}$ and C is an unknown function of r.

In order to match with the solutions in the upper deck, the main deck velocity and pressure perturbations are expanded in the form

$$\tilde{u} = \varepsilon^{-1} u_0^m(\zeta) + u_1^m(\zeta) + \cdots, \tag{6.2.4a}$$

$$\tilde{v} = \varepsilon^{-1} v_0^m(\zeta) + v_1^m(\zeta) + \cdots, \tag{6.2.4b}$$

$$\tilde{w} = \varepsilon^{3} w_0^m(\zeta) + \varepsilon^{4} w_1^m(\zeta) + \cdots, \tag{6.2.4c}$$

$$\tilde{p} = \varepsilon^{3} p_0^m(\zeta) + \varepsilon^{4} p_1^m(\zeta) + \cdots. \tag{6.2.4d}$$

At $\mathcal{O}(\varepsilon^{-5})$ we have that

$$\mathrm{i}\alpha_0 u_0^m + \frac{\mathrm{i}\beta_0^m v_0}{r} + (w_0^m)' = 0, \tag{6.2.5a}$$

$$\mathrm{i}\bar{\bar{u}} u_0^m + r w_0^m \bar{u}' = 0, \tag{6.2.5b}$$

$$\mathrm{i}\bar{\bar{u}} v_0^m + r w_0^m \bar{v}' = 0, \tag{6.2.5c}$$

$$(p_0^m)' = 0. \tag{6.2.5d}$$

B_n	λ_0	ϕ_0
0	1.2072	39.64°
0.1	1.3892	35.75°
0.2	1.5853	32.24°
0.3	1.7839	29.27°
0.4	1.9799	26.80°
0.5	2.1790	24.65°

Table 6.3: Calculated values of λ_0 and ϕ_0 for Bingham plastic fluids with $B_n = 0,\ 0.1,\ 0.2,\ 0.3,\ 0.4,\ 0.5$.

Matching with the solution in the upper deck we find that

$$u_0^m = \frac{Cr\gamma_0\bar{u}'}{\beta_0^2}, \tag{6.2.6a}$$

$$v_0^m = \frac{Cr\gamma_0\bar{v}'}{\beta_0^2}, \tag{6.2.6b}$$

$$w_0^m = -\mathrm{i}\frac{\gamma_0 C\bar{\bar{u}}}{\beta_0^2}, \tag{6.2.6c}$$

$$p_0^m = C. \tag{6.2.6d}$$

Again, to ensure that the no-slip condition is satisfied we set $\alpha_0 r/\beta_0 = -\bar{v}_0/\bar{u}_0 = \lambda_0$. Values of λ_0 and therefore ϕ_0 for B_n in the range of interest are tabulated above.

After expanding the base flow velocities in the usual manner we find that, in order to match with the solutions in the main deck, the lower deck disturbance velocities and pressure must take the form

$$\tilde{u} = \frac{r\gamma_0 C(\bar{u}_0 + 2\varepsilon\bar{u}_1\zeta_l + 3\varepsilon^2\bar{u}_2\zeta_l^2 + \cdots)}{\varepsilon\beta_0^2} + \frac{U_{-1}(\zeta_l)}{\varepsilon} + U_0(\zeta_l) + \varepsilon U_1(\zeta_l) + \cdots, \tag{6.2.7a}$$

$$\tilde{v} = \frac{r\gamma_0 C(\bar{v}_0 + 2\varepsilon\bar{v}_1\zeta_l + 3\varepsilon^2\bar{v}_2\zeta_l^2 + \cdots)}{\varepsilon\beta_0^2} + \frac{V_{-1}(\zeta_l)}{\varepsilon} + V_0(\zeta_l) + \varepsilon V_1(\zeta_l) + \cdots, \tag{6.2.7b}$$

$$\tilde{w} = -\frac{\varepsilon^5\mathrm{i}\gamma_0 C(\bar{\bar{u}}_1\zeta_l^2 + \varepsilon\bar{\bar{u}}_2\zeta_l^3 + \varepsilon^2\bar{\bar{u}}_3\zeta_l^4 + \cdots)}{\beta_0^2} + \varepsilon^6 W_1(\zeta_l) + \varepsilon^7 W_2(\zeta_l) + \cdots, \tag{6.2.7c}$$

$$\tilde{p} = \varepsilon^3 P_1(\zeta_l) + \cdots. \tag{6.2.7d}$$

B_n	$\bar{\gamma}_0$	λ_1
0	1.2244	2.3130
0.1	1.5650	3.5821
0.2	1.8871	5.0250
0.3	2.1852	6.5855
0.4	2.4599	8.2283
0.5	2.7139	9.9309

Table 6.4: Zero order solutions for the effective wavenumber and first order corrections to the effective wave angle for Bingham plastic fluids with $B_n = 0,\ 0.1,\ 0.2,\ 0.3,\ 0.4,\ 0.5$.

We forgo the lengthy analysis associated with the solution in the lower deck and simply state the equivalent eigenrelation. The methodology employed is largely the same, although the expansion equations are somewhat simplified in this case. Expressions for the expansions of the viscosity function and base flow velocities are given in the appendix D. It is important to note that we again need to assume that the perturbed viscous terms are negligible when compared to the unperturbed terms. This is an additional constraint that we must impose. After considerable work we find that

$$\gamma_0^3 I_3 + \frac{2\mathrm{i}\gamma_0}{\beta_0}\left[\bar{u}_0\left(1+\frac{\bar{v}_0^2}{\bar{u}_0^2}\right)I_4 + \frac{(1-\bar{\mu}_0)\bar{v}_0 I_3}{\bar{\mu}_0(\bar{u}_0^2+\bar{v}_0^2)}\right] = \mathrm{i}\Delta^{1/2}(\alpha_1\bar{u}_0 r + \beta_1\bar{v}_0)\frac{\gamma_0\bar{\mu}_0}{\beta_0^2}, \tag{6.2.8}$$

where I_3 and I_4 are as before. Solving (6.2.8) gives

$$\begin{aligned}\gamma_0 &= \frac{2}{\beta_0}\left[\bar{u}_0\left(1+\frac{\bar{v}_0^2}{\bar{u}_0^2}\right)\frac{I_4}{I_3} + \frac{(1-\bar{\mu}_0)\bar{v}_0}{\bar{\mu}_0(\bar{u}_0^2+\bar{v}_0^2)}\right] \\ &= \frac{\sqrt{2}}{r^{1/2}}\left(1+\frac{\bar{v}_0^2}{\bar{u}_0^2}\right)^{1/4}\left[\bar{u}_0\left(1+\frac{\bar{v}_0^2}{\bar{u}_0^2}\right)\frac{I_4}{I_3} + \frac{(1-\bar{\mu}_0)\bar{v}_0}{\bar{\mu}_0(\bar{u}_0^2+\bar{v}_0^2)}\right]^{1/2}, \qquad (6.2.9a)\end{aligned}$$

$$\frac{\alpha_1}{\beta_0} - \frac{\beta_1\alpha_0}{\beta_0^2} = \frac{2\gamma_0^{3/2} I_3}{r^{1/2}|\bar{u}_0\bar{v}_0|^{1/2}}\left(1+\frac{\bar{v}_0^2}{\bar{u}_0^2}\right)^{-1/4}. \tag{6.2.9b}$$

For convenience we write

$$\gamma_0 = \frac{\bar{\gamma}_0}{r^{1/2}}, \quad \frac{\alpha_1}{\beta_0} - \frac{\beta_1\alpha_0}{\beta_0^2} = \frac{\lambda_1}{r^{5/4}}.$$

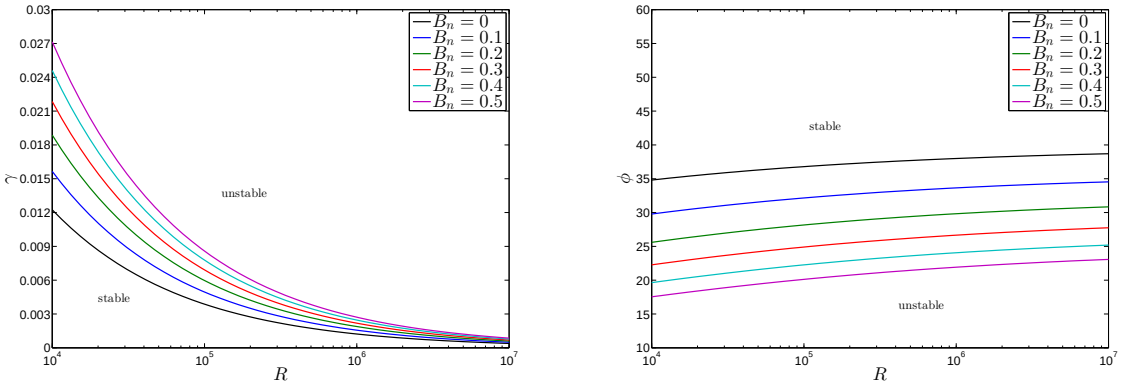

Figure 6.5: The viscous neutral wavenumber and wave angle predictions for Bingham plastic fluids with $B_n = 0$, 0.1, 0.2, 0.3, 0.4, 0.5.

So that the effective wavenumber scaled on the viscous mode wavelength is given by

$$\gamma = Re^{-1/4}\sqrt{\alpha^2 + \frac{\beta^2}{r^2}} = \bar{\gamma}_0 r^{-1/2}\varepsilon^4 + \cdots, \\ = \bar{\gamma}_0 r^{-1/2} Re^{-1/4} + \cdots, \tag{6.2.10a}$$

and the spiral wave angle expands as

$$\tan\left(\frac{\pi}{2} - \phi\right) = \lambda_0 + \lambda_1 r^{-1/4}\varepsilon^2 + \cdots, \\ = \lambda_0 + \lambda_1 r^{-1/4} Re^{-1/8} + \cdots. \tag{6.2.10b}$$

We recall the modified Reynolds number, $R = rRe^{1/2}$, and express the effective wavenumber and wave angle as such

$$\gamma = \bar{\gamma}_0 R^{-1/2} + \cdots, \tag{6.2.11a}$$

$$\phi = \frac{\pi}{2} - \arctan(\lambda_0 + \lambda_1 R^{-1/4} + \cdots). \tag{6.2.11b}$$

Clearly we see that increasing the fluid yield stress has a very significant effect on the boundary-layer stability. Previously, in §4.2, we stated that the downward shifting of

the wave angle plots indicated destabilisation as the area encompassed by neutral curve was increasing. However, this is only the case if the lower-branch modes are held fixed or shift upwards. We see from the zero-order analysis and figure 6.5 that the wave angle decreases enormously as B_n increases. This suggests that the area encompassed by the neutral curve is significantly decreased as the yield stress increases. Stabilising behaviour is also observed from the wavenumber plots, both here and in figure 4.12.

These results are consistent with those of §4.2. We postulate that the onset of convective instability will be significantly delayed as the fluid yield stress is increased. However, without a corresponding numerical investigation we are unable to provide details on the effect of the Bingham number on the critical Reynolds number or the linear convective growth rates. Having said that, we have already seen that there exists an excellent agreement between our asymptotic and numerical results for other generalised Newtonian models, leading us to believe that this would also be the case here. We reiterate that constructing a numerical study in this case will provide somewhat more of a challenge.

6.3 Case III: Carreau

Here the details of the analysis and calculations can easily be inferred from the previous two sections. The upper, and main deck solutions are essentially unchanged. The lower deck solutions take a very similar form with the exception of the additional viscous terms that are model dependent. Here we simply state the results and the governing eigenrelation

$$\gamma_0^3 I_3 + \frac{2\mathrm{i}\gamma_0}{\beta_0}\left[\bar{u}_0\left(1+\frac{\bar{v}_0^2}{\bar{u}_0^2}\right)I_4 + \frac{k^2(\bar{\mu}_0-1)(n-1)\bar{v}_0 I_3}{\bar{\mu}_0\bar{\sigma}_0}\right] = \mathrm{i}\Delta^{1/2}(\alpha_1\bar{u}_0 r + \beta_1\bar{v}_0)\frac{\gamma_0\bar{\mu}_0}{\beta_0^2}, \quad (6.3.1)$$

where $\bar{\sigma}_0 = \bar{\mu}_0[1+k^2(\bar{u}_0^2+\bar{v}_0^2)] + k^2(\bar{\mu}_0-1)(n-1)(\bar{u}_0^2+\bar{v}_0^2)$. Expression for the expansions of the viscosity function and base flow velocities are stated in the appendix D. The

n	λ_0	ϕ_0	$\bar{\gamma}_0$	λ_1
0.25	1.2035	39.72°	1.2302	2.3793
0.50	1.1956	39.91°	1.2212	2.4462
0.75	1.1891	40.06°	1.1702	2.5275
0.95	1.2006	39.79°	1.0651	2.5353
1.00	1.2070	39.64°	1.0295	2.5221
1.05	1.2150	39.46°	0.9917	2.5036
1.25	1.2577	38.49°	0.8352	2.4025
1.50	1.3138	37.28°	0.6717	2.2968
1.75	1.3631	36.26°	0.5596	2.2681

Table 6.5: Zero order solutions for the effective wavenumber and wave angle, and first order corrections to the effective wave angle for shear-thinning and shear-thickening Carreau fluids.

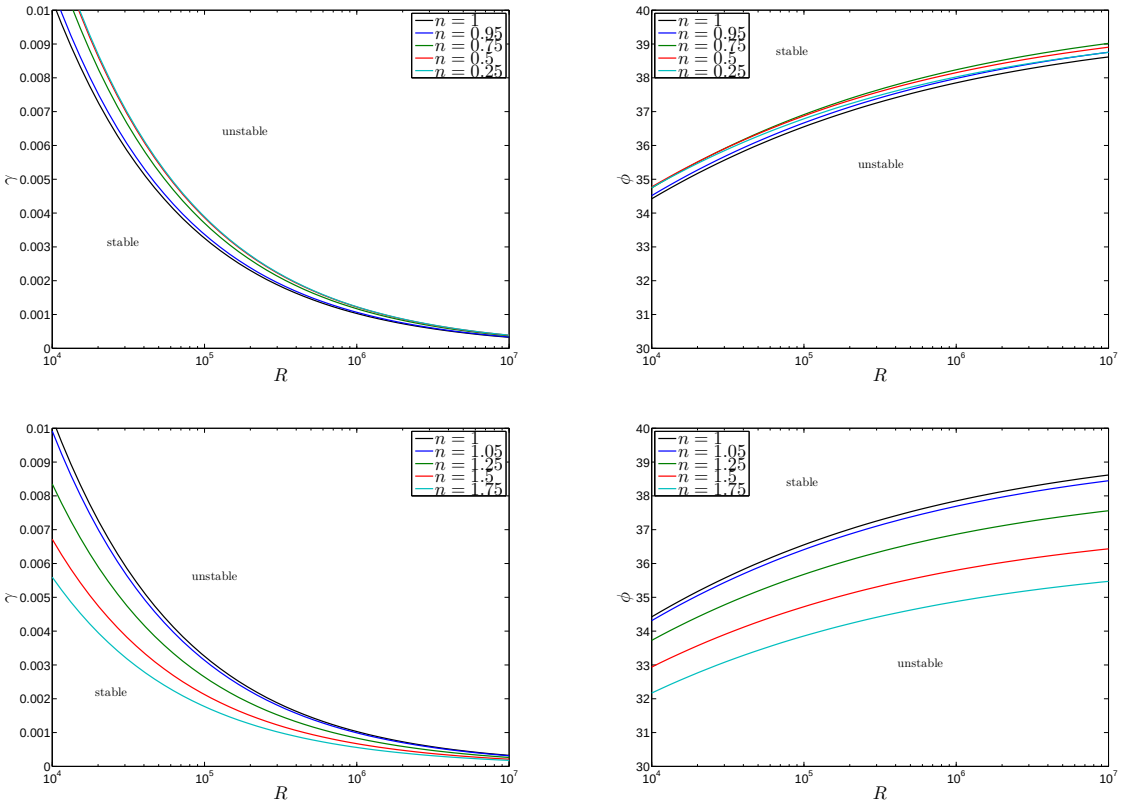

Figure 6.6: The neutral type II wavenumber and wave angle predictions for shear-thinning and shear-thickening Carreau fluids.

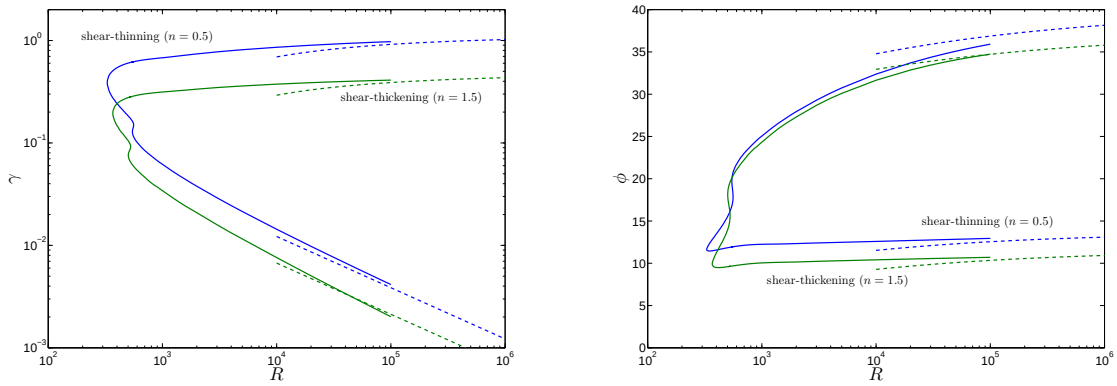

Figure 6.7: Neutral wavenumber and wave angle stability curves for shear-thinning and shear-thickening Carreau fluids. The upper and lower-branch asymptotic solutions are given by the dashed lines.

asymptotic expansions of the wavenumber and wave angle are identical to those given in (6.2.10) & (6.2.11), where now the modified Reynolds number is scaled by the infinite-shear-rate viscosity.

Figure 6.6 reveals that the wave angle is largely unaffected for shear-thinning flows, as was the case for the type I modes, whereas the wavenumber is very marginally stabilised. The results for $n = 1$ again show that in the large Reynolds number limit the angle of the spiral vortices is independent of the fluid viscosity, in the Newtonian limit at least. Our result for ϕ_0 is identical to Hall's even though we stipulated a different Newtonian viscosity function ($\bar{\mu} = 1 + c_0$ rather than $\bar{\mu} = 1$). The shear-thickening results would be considered stabilising with respect to the wave angle and destabilising with respect to the wavenumber. However, we note that these effects are slight. Interestingly, it is in fact the upper-branch modes that are most greatly effected with variations in the power-law index. Again we observe the excellent agreement between our asymptotic and numerical solutions. As noted in §5.2 the non-linear y-axis scale has the effect of distorting the wavenumber neutral curves so that it appears as though the plots are simply being shifted downwards, clearly this is not the case. We plot the results in this fashion in order to be consistent with convention.

6.4 Concluding Remarks

In this chapter we have presented an initial lower-branch instability investigation for power-law, Bingham and Carreau fluid models. The solutions in the respective upper and main decks are independent of the fluid viscosity and thus, in these cases, our solutions are largely similar to those of Hall (1986). It is within the lower deck where we observe the appearance of additional non-Newtonian terms. When considering the type I modes we were able to obtain analytic solutions inclusive of the perturbed viscous terms. For the type II modes we find that this no longer achievable. In each of the three cases we must assume that perturbed terms have a negligible effect. Certainly near to the limiting Newtonian cases when $n \approx 1$ or $B_n \approx 0$ this condition will be satisfied, however, as n and B_n diverge from one and zero respectively, this will not always be so. Therefore this study *must* be considered as a preliminary investigation only.

The results for cases I & III agree well with our numerical investigations and again outline the marked difference between shear-thinning results owing from the power-law model and those obtain from the Carreau model. We hypothesised in §4.2 that an increase in fluid yield stress has a stabilising effect on the boundary-layer flow. This claim is supported by the type II results where we see that increasing B_n dramatically reduces the area encompassed by the neutral curve.

Over the course of the last three chapters we have determined the convective stability characteristics for a number of generalised Newtonian fluid models in the context of the rotating disk boundary-layer. However, we are yet to provide a physical interpretation of these results or indeed explain the contrasting behaviour we have observed for two shear-thinning fluid models. We address these issue and others in the final chapter.

Chapter 7

Conclusions, Summary & Future Work

This thesis focuses on the boundary-layer flow induced by the rotation of an infinite impermeable plane; here we have presented both base flow solutions and linear stability analyses for three generalised Newtonian fluid models. In each of the cases (I, II & III) we have non-dimensionalised the governing continuity and Navier-Stokes equations, and applied suitable boundary-layer approximations in order to determine the respective leading order equations. For case I (power-law) we find that the viscosity characteristics of the flow are governed by the power-law index n, in case II (Bingham) the controlling parameter is the Bingham number $B_n = \tau_y^*/(2r^*\Omega^*\sqrt{\mu_p^*\rho^*\Omega^*})$, whilst for case III (Carreau) we have the need to stipulate three constants, the viscosity ratio $c_0 = (\mu_0^* - \mu_\infty^*)/\mu_\infty^*$, n and the dimensionless form of the relaxation parameter $k = r^*\lambda^*\Omega^*\sqrt{\rho^*\Omega^*/\mu_\infty^*}$.

Unsurprisingly, in the case of non-constant viscosity, an exact solution of the Navier-Stokes equations is no longer realisable. However, in the large Reynolds number limit, where the boundary-layer equations are applicable, we find that the base flow can be determined via von Kármán's classical similarity solution, albeit with some minor modifications. This boundary-layer flow must be matched to the exterior, thus in much the

same way as Denier & Hewitt (2004), we determine large similarity coordinate forms for all of our solutions. Results owing from the power-law model exhibit algebraic decay whilst for cases II & III we note an exponential decay of the velocity functions. Our shear-thinning power-law solutions are identical to those of Denier & Hewitt (2004) and our solutions for Bingham plastic fluids agree excellently with Ahmadpour & Sadeghy (2013). The Carreau fluid model had not previously been considered within the context of the rotating disk boundary-layer; we have done so here. Solutions are presented for both shear-thinning and shear-thickening fluids and, most importantly, we find that the viscosity function tends to a well-defined limit within the boundary-layer region. This is in stark contrast to the shear-thinning power-law results that predict an unbounded fluid viscosity at the outer-edge of the boundary-layer. This leads us to suggest that the results owing from the Carreau model do indeed provide a much better representation of the nature of the boundary-layer flow for shear-thickening and shear-thinning non-Newtonian fluids, as noted by Griffiths (2015).

We determined the linear stability characteristics of the boundary-layer flow using both asymptotic and numerical methods. Firstly, we will discuss the type I asymptotic analysis, the detail of which is the subject matter of chapter 4. Having perturbed the basic flow we derived three new sets of linear disturbance equations dependent on the relevant non-Newtonian parameters. Notably we observe the appearance of additional viscous terms due to the generalised Newtonian formulation of the problem, these unperturbed and perturbed viscous terms are found to be of the same order. Following the methodology of Hall (1986), and assuming high Reynolds number flow, we investigate the inviscid (type I) modes of instability. At leading order the disturbances satisfy the two-dimensional Rayleigh equation. In all cases we solve the resulting equation using a finite difference scheme and present solutions for the location of the critical layer, and the leading order terms in the expansions of the wavenumber and wave angle. Considering the next order

in the analysis we see that for each case the resulting inhomogeneous form of Rayleigh's equation is similar to that derived by Hall (1986). The solution of the non-singular integral I_1, is trivial as it is a function of the zero-order eigenfunction only. When computing the singular integral I_2, a great deal of care has been taken to ensure accurate results. Using a fixed-step Simpson's integration scheme we obtain results for both the real and imaginary parts of the integral. Gajjar (2007) reports $I_1 = 0.091$ and $\Re(I_2) = 0.0596$, clearly our results in the Newtonian limit are in excellent agreement with those[1]. We note here that the sign of $\Im(I_2)$ in Hall (1986) is incorrect due to the incorrect deformation of the path of integration with respect to the singularity.

The wall layer analysis is of particular interest as it is here where the leading order viscous terms first appear. We find that analytic solutions are obtainable provided that we appeal to an additional matching constraint. This constraint imposes the condition that $\lambda_0 \neq -\bar{v}_0/\bar{u}_0$, which certainly holds for every case considered within this study. Indeed, the lower-branch analysis requires that $\lambda_0 = -\bar{v}_0/\bar{u}_0$, given that these modes are distinct and have differing asymptotic structures the aforementioned condition will always be satisfied for the upper-branch neutral modes. Matching between the inviscid zone and the wall layer produces a model dependent eigenrelation. This is solved for the first order correction terms for the effective wavenumber and wave angle, and, in the Newtonian limit our solutions are in good agreement with those reported by Gajjar (2007). Our results show comparatively different behaviour for shear-thinning fluids described by the power-law model and those described by the Carreau model. The power-law results indicate boundary-layer stabilisation whilst the results owing from the Carreau model predict destabilisation. In fact the Carreau model predicts that shear-thickening will have a stabilising effect on the inviscid modes. We know that viscosity dissipates energy and, intuitively, we would expect that at a fixed Reynolds number the onset of instability

[1]Gajjar (2007) does not report a value for $\Im(I_2)$ as in his formulation the inviscid zone disturbances are assumed to have a non-complex form.

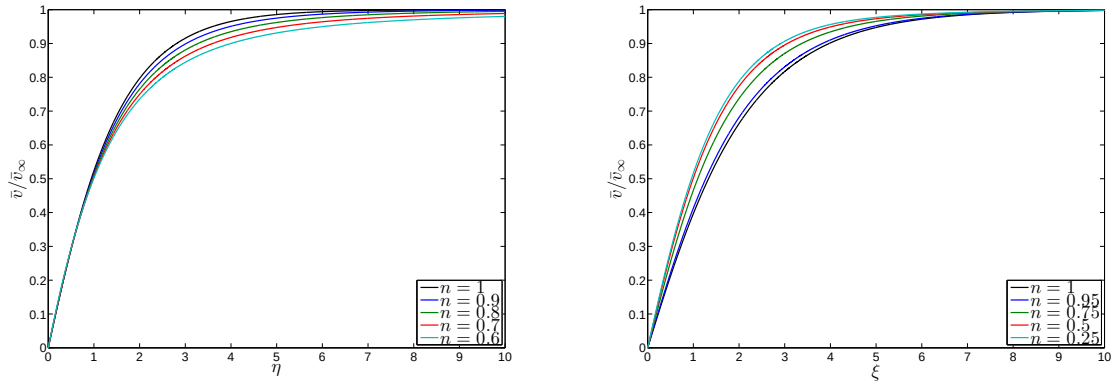

Figure 7.1: Comparative normalised azimuthal velocity profiles for shear-thinning power-law and Carreau fluids. In accordance with other rotating disk studies the boundary-layer thickness is taken to be 99% of the normalised azimuthal velocity.

will be advanced for less viscous fluids; the more viscous a fluid is the less susceptible it is to breakup. However, in the context of the rotating disk model there are currently no experimental investigations that would support this claim. The numerical study of Lashgari, Pralits, Giannetti & Brandt (2012) is of particular interest here, the authors investigate the instability of the flow past a circular cylinder using the Carreau fluid model scaled by the zero-shear-rate. They conclude that it is indeed the effect of shear-thinning that is destabilising, noting that the shear-thickening effect stabilises the cylinder flow dramatically. Although the geometry and base flow for this problem are clearly very different to this study, the results do go some way in supporting our claims.

The opposing results for our two shear-thinning models are indeed quite striking. At first glance it may appear as though something has gone drastically wrong. However, this is unlikely to be the case as we have shown in chapter 5 that both sets of results are consistent with their corresponding and independent numerical solutions. The explanation for these puzzling results does in fact come from the form of our base flow solutions, which, in turn, stems from the characteristic traits of both the models. In §2.1 we noted that for shear-thinning power-law fluids $\mu(\dot{\gamma} \to 0) \to \infty$, which is exemplified by our base flow solutions where we see that the viscosity function grows without bound as we move away

from the surface of the disk, or equivalently move towards a region of low shear-rate. This essentially has the effect of increasing the predicted boundary-layer thickness, see figure 7.1. Contrastingly, we have that $\mu(\dot{\gamma} \to 0) \to \mu_0$ for shear-thinning Carreau fluids. Thus, far from the disk, in regions of low shear-rate, we find that $\bar{\mu} \to 1 + c_0$, and in this case the boundary-layer thickness is reduced. It is this failing of the power-law model in regions of low shear rates that dramatically affects the predicted velocity profiles and therefore our linear stability results.

The process of computing the type I asymptotic solutions is the same in all cases. We can therefore view this computation as an 'operator' where we input initial data, the results from our base flow calculations, and output predictions for the wavenumber and wave angle of the disturbances. If the input is different then we should expect the 'operator' to output different results. This is exactly what is being observed here. The inability of the power-law model to accurately describe shear-thinning flows in the limit as $\dot{\gamma}^* \to 0$ has such a significant effect on the base flow profiles that it in turn effects the predicted stability characteristics. Therefore it is with relative confidence that we can say that the results owing from the Carreau model do indeed provide a much better description of the observed cross-flow instabilities.

Returning now to case II we see that an increase in the fluid yield stress will have a significantly stabilising effect on the boundary-layer flow. This is consistent with previous studies concerning Poiseuille flow (see Frigaard, Howison & Sobey 1994 and Nouar, Kabouya, Dusek & Mamou 2007*a*) and also Couette flow (see Peng & Zhu 2004). Physically this is what we would expect to see, as the disk spins the shear-rate increases. However, this effect is more difficult to overcome as the fluid yield stress is increased. We know that Bingham plastic fluids behave in a Newtonian fashion in the yielded region, see figure 2.3, and therefore we would expect that instability will be induced at a higher critical Reynolds number. This Newtonian behaviour of Bingham plastic fluids in the

yielded region is also predicted by, firstly, our base flow solutions, where we observe the 'Newtonian' decay of the velocity functions and secondly, in our wall layer solution where we see that the solution has no specific dependence on the Bingham number whatsoever.

A rather lengthy summary of the numerical study is provided in §5.3 and so we keep our discussion here brief. By reformulating the derivation of our linear disturbance equations we determined new sets of perturbation equations that are amenable to numerical investigation. Following the methodology of Lingwood (1995*a*) we arrive at systems of sixth-order ODEs from which we compute curves of neutral stability. During this process we make two important approximations, which are discussed in detail in §5.3. Despite our boundary-layer formulation of the problem, our results in the Newtonian limit are in good agreement with the exact solutions of Jasmine & Gajjar (2005). In our case both the critical Reynolds numbers are slightly reduced suggesting that results owing from the boundary-layer approximation are marginally less stable than those determined from the full-field equations.

We again determine opposing results for our two shear-thinning models. In all cases the agreement with our asymptotic predictions is excellent; this provides some justification for the conclusions made previously. If anything, the failings of the power-law model will be more noticeable in this study. The asymptotic solutions essentially hinge on the values of the velocity components at the disk surface; however, the numerical scheme integrates from the outer-edge of the boundary-layer down towards the surface of the disk. Thus the scheme initiates using the far-field data, which will be largely inaccurate in the power-law regime. Hence, as before, we suggest that it is the Carreau fluid model that provides a more physical representation of the non-Newtonian boundary-layer stability characteristics. Interestingly, in this case, we predict that the largest critical Reynolds numbers will be observed in a region near to $n = 1$, the requirement for Newtonian flow.

We have been unable to determine curves of neutral stability in case II. This is due

to the exponential growth of the viscosity functions for fluids with non-zero yield stress. In this case the numerical scheme fails to initiate. It is interesting to note that this effect is not noticeable in the upper-branch asymptotic analysis. Despite this unphysical prediction for the variation of viscosity within the boundary-layer we find that the velocity solutions behave in a 'Newtonian' fashion, suggesting that there is an $\mathcal{O}(1)$ balance between the decaying velocity functions and the growing viscosity function. Indeed, our type I asymptotic predictions are independent of the viscosity function and depend only on the values of the velocity components evaluated at the disk surface. This is a neat example of where an exact asymptotic analysis can reveal important information whereas the corresponding numerical investigation will breakdown.

Finally, we discuss the preliminary type II asymptotic analysis, the detail of which is the subject matter of chapter 6. Using the triple deck structure first described by Hall (1986) we investigate the viscous (type II) modes of instability. The solution of the leading order equations in the upper and main decks is relatively simple. In the main deck we impose the condition that the effective wall shear is zero at leading order, which is consistent with Hall (1986). Our own numerical investigations show that this criterion certainly is satisfied for cases I & III, and we assume this to be the case for fluids satisfying the Bingham constitutive relationship. It is within the lower deck where the generalised Newtonian terms first appear. In order to maintain the consistency of the leading order equations we require that the perturbed viscous terms are negligible when compared to the unperturbed terms. Close to the Newtonian limit this is a valid approximation. Following Hall (1986) we determine a third order ODE for the first order axial disturbance W_1^l, and, having determined this quantity we arrive at a leading order eigenrelation dependent on the respective non-Newtonian parameters and two standard integrals of parabolic cylinder functions. For each of the three cases our results are in keeping with those of our previous investigations and so help to support the conclusions made therein. We reiterate that this

study *must* be considered as preliminary as our approximation in the lower deck is only truly applicable in regions close to $n = 1$ or $B_n = 0$.

In summary, we have shown that it is possible to model the instability mechanisms associated with the boundary-layer flow due to a rotating disk when considering non-Newtonian fluids. We have further shown that the observed non-Newtonian fluid properties can produce differing stability results. In fact even between models that predict the same qualitative fluid behaviour we can arrive at quantitatively different results. This body of work clearly emphasises the importance of using the correct non-Newtonian model in the correct context. Certainly in regions of moderate shear-rate the power-law model can be sufficient, hence its widespread use in both industrial and academic environments. However, one must proceed with caution when applying this model in regions of very high or very low shear rates, as we have shown here; doing so can have very significant effects. It is even possible to determine differing stability results from within the same non-Newtonian model. Nouar, Bottaro & Brancher (2007*b*) note in their Carreau fluid channel flow study that shear-thinning can in fact be shown to be stabilising or destabilising depending on simply the choice of the reference viscosity used for non-dimensionalisation. The one-dimensional theoretical coating investigation of Jenekhe & Schuldt (1984) is of particular interest here. In this study results are presented for film thickness profiles on a rotating disk for Newtonian, power-law and Carreau fluids. The authors conclude that the breakdown of the power-law model at vanishing shear-rates has a significant effect on the predicted film thickness. As with this study the results for power-law and Carreau fluids are in stark contrast to each other. This further suggests that the applicability of the power-law model must be questioned in the context of rotating flows of this nature.

There is a great deal of scope for future work with regards to this research. Here we will discuss some, but not all, of the many possible extensions. Firstly we address the shortcomings of the current investigation. As noted previously we have been unable to

solve our numerical scheme when considering fluids that exhibit a yield stress. We find that the Bingham model is entirely inadequate in regions of low shear, so much so that the numerical procedure fails to initiate. However, other popular viscoplastic schemes including the Herschel-Bulkley and Casson models are defined in a similar manner and exhibit $\dot{\gamma}^{-1}$ dependence. One possible solution to this problem would be to stipulate Newtonian-like viscosity behaviour across the whole of the boundary-layer region. Certainly near to the disk in the high shear-rate yielded region this approximation is valid. Having already obtained asymptotic predictions for case II it would be interesting to see if an approximate boundary-layer viscosity profile could be used to provide suitably accurate results.

In both the numerical and type II asymptotic calculations we have ignored the contribution from the perturbed viscous terms. We have shown asymptotically that for the type I modes the effect of including these terms is negligible; this fact helped us to simplify our perturbations equations and hence solve them numerically. It was hoped that we would arrive at a similar conclusion when considering an asymptotic investigation of the type II modes. However, we have been unable to satisfy the leading order wall shear criterion whilst retaining these additional terms. It is not yet clear how best to continue with our preliminary investigation. Perhaps the non-Newtonian viscous modes satisfy a slightly modified asymptotic structure? Even if this is the case the unperturbed and perturbed viscous terms will still always appear at the same order. Certainly there is a considerable amount of work remaining in this very interesting problem. Attempting to retain these terms in our numerical scheme would prove to be significantly more difficult. In this case we will no longer be able to determine a sixth order set of ODEs in six transformed variables, and instead would be required to solve the complete set of governing PDEs. This presents an incredibly challenging numerical task and is way beyond the scope of the current investigation. We reiterate that the agreement between our exact type I solutions and our numerical results provides some suggestion that attempting this rather daunting

investigation may not be of any further worth, given the complexity of the challenge.

Within this body of work we introduced the Carreau model and showed that the viscosity profile is controlled by three dimensionless parameters. We have investigated the effect of varying both the power-law index and the relaxation parameter but have done so at a fixed viscosity ratio. It would be an interesting extension to consider what effect altering c_0 would have on the predicted boundary-layer flow profiles and the resulting neutral stability curves. Another possible extension would be to reformulate our problem so that the Reynolds number is scaled by the zero-shear-rate viscosity rather than the infinite-shear-rate viscosity. This would align our investigation with that of Nouar *et al.* (2007*b*) and Alibenyahia, Lemaitre, Nouar & Ait-Messaoudene (2012), amongst others. In these studies the authors take the limit as $\mu^*_\infty/\mu^*_0 \to 0$, stating that infinite-shear-rate viscosity is often much smaller than zero-shear-rate viscosity. In our case this would mean that the viscosity function would take the form

$$\bar{\mu} = [1 + k^2(\bar{u}'^2 + \bar{v}'^2)]^{(n-1)/2},$$

where k would now also be scaled by μ^*_0, so that in the Newtonian limit this reduces to $\bar{\mu} = 1$ and hence we would be able to make direct, quantitative comparisons between our power-law and modified Carreau fluid results. Indeed initial investigations into this problem have begun; we hope to report on this study in due course.

This work clearly motivates the need for detailed experimental results with which to compare our theoretical analysis. To the best of the author's knowledge no such experiments have yet taken place. Certainly in the Newtonian regime a wealth of literature exists, and this is currently a topic of particular interest, see Imayama, Alfredsson & Lingwood (2012, 2013, 2014), for example. Personal communication with these authors has revealed the difficulty of obtaining consistently accurate experimental results; therefore

we can only envisage the introduction of non-Newtonian fluids would serve to significantly complicate any experimental procedure. In fact, for the experiments mentioned here, the Newtonian fluid used is air, thus there is no need to submerge the disk in liquid. As noted by Colley, Carpenter & Thomas (2006) even submerging the disk in say, water, makes the experimental task even more demanding. Nevertheless, this is an area of further study that needs to be addressed in order to improve our understanding of the stability and transition of non-Newtonian fluids in the context of three-dimensional boundary layers.

There are other natural extensions of this work; we will close by mentioning a few of them here. For Newtonian rotating disk flows it has been shown both experimentally (see Corke & Knasiak 1998) and theoretically (see Hussain, Garrett & Stephen 2011) that non-stationary travelling disturbances are the most unstable modes. With relative ease the analysis of chapters 4, 5 & 6 could be extended to include non-stationary modes ($\omega \neq 0$) of instability. In addition to this chapter 5 could also be extended to incorporate an absolute instability analysis, akin to that of Lingwood (1995*a*). Lastly, it would be particularly interesting to compare our stability results to those of other non-Newtonian boundary-layer studies. Dabrowski (2004) gives a detailed insight into the solutions of the flat plate boundary-layer equations for power-law and Carreau fluids. The author notes that the decay of the shear-thinning power-law solutions is strongly algebraic, which is consistent with our findings. It would be insightful to see if a corresponding linear stability analysis predicts differing behaviour for shear-thinning power-law and Carreau fluids, as we have done here.

Appendix A

Determining The Shear Rate Function

Firstly, we show that $I = 0$ for incompressible fluids. In component form $\dot{\boldsymbol{\gamma}}$ is given by

$$\dot{\gamma}_{ij} = \frac{\partial u_i}{\partial x_j} + \frac{\partial u_j}{\partial x_i} = u_{i,j} + u_{j,i},$$

for any arbitrary flow field $\boldsymbol{u} = \boldsymbol{u}(x_1, x_2, x_3, t)$, in an arbitrary coordinate system. Thus

$$I = \operatorname{tr} \dot{\boldsymbol{\gamma}} = \sum_i \dot{\gamma}_{ii} = 2 \sum_i u_{i,i} = 2(\boldsymbol{\nabla} \cdot \boldsymbol{u}) = 0.$$

Working in cylindrical coordinates (r^*, θ, z^*) the rate-of-strain tensor $\dot{\boldsymbol{\gamma}}^* = \boldsymbol{\nabla} \boldsymbol{u}^* + (\boldsymbol{\nabla} \boldsymbol{u}^*)^{\mathrm{T}}$ takes the form

$$\dot{\boldsymbol{\gamma}}^* = \dot{\gamma}^*_{ij} = \begin{bmatrix} \dot{\gamma}^*_{r^*r^*} & \dot{\gamma}^*_{r^*\theta} & \dot{\gamma}^*_{r^*z^*} \\ \dot{\gamma}^*_{\theta r^*} & \dot{\gamma}^*_{\theta\theta} & \dot{\gamma}^*_{\theta z^*} \\ \dot{\gamma}^*_{z^*r^*} & \dot{\gamma}^*_{z^*\theta} & \dot{\gamma}^*_{z^*z^*} \end{bmatrix}, \tag{A.0.1}$$

where in cylindrical coordinates

$$\dot{\gamma}^*_{r^*r^*} = 2\left(\frac{\partial u^*}{\partial r^*}\right), \tag{A.0.2a}$$

$$\dot{\gamma}^*_{\theta\theta} = 2\left(\frac{1}{r^*}\frac{\partial v^*}{\partial \theta} + \frac{u^*}{r^*}\right), \tag{A.0.2b}$$

$$\dot{\gamma}^*_{z^*z^*} = 2\left(\frac{\partial w^*}{\partial z^*}\right), \tag{A.0.2c}$$

$$\dot{\gamma}^*_{r^*\theta} = r^*\frac{\partial}{\partial r^*}\left(\frac{v^*}{r^*}\right) + \frac{1}{r^*}\frac{\partial u^*}{\partial \theta} = \dot{\gamma}^*_{\theta r^*}, \tag{A.0.2d}$$

$$\dot{\gamma}^*_{r^*z^*} = \frac{\partial u^*}{\partial z^*} + \frac{\partial w^*}{\partial r^*} \qquad = \dot{\gamma}^*_{z^*r^*}, \tag{A.0.2e}$$

$$\dot{\gamma}^*_{\theta z^*} = \frac{\partial v^*}{\partial z^*} + \frac{1}{r^*}\frac{\partial w^*}{\partial \theta} \qquad = \dot{\gamma}^*_{z^*\theta}, \tag{A.0.2f}$$

and (u^*, v^*, w^*) are the radial, azimuthal and axial velocity components, respectively. Thus

$$II = \sum_i \sum_j \dot{\gamma}^{*^2}_{ij} = \dot{\gamma}^{*^2}_{r^*r^*} + \dot{\gamma}^{*^2}_{\theta\theta} + \dot{\gamma}^{*^2}_{z^*z^*} + 2(\dot{\gamma}^{*^2}_{r^*\theta} + \dot{\gamma}^{*^2}_{r^*z^*} + \dot{\gamma}^{*^2}_{\theta z^*}),$$

is given by

$$\begin{aligned} II = 4&\left[\left(\frac{\partial u^*}{\partial r^*}\right)^2 + \left(\frac{1}{r^*}\frac{\partial v^*}{\partial \theta} + \frac{u^*}{r^*}\right)^2 + \left(\frac{\partial w^*}{\partial z^*}\right)^2\right] \\ &+ 2\left\{\left[r^*\frac{\partial}{\partial r^*}\left(\frac{v^*}{r^*}\right) + \frac{1}{r^*}\frac{\partial u^*}{\partial \theta}\right]^2 + \left(\frac{\partial u^*}{\partial z^*} + \frac{\partial w^*}{\partial r^*}\right)^2 + \left(\frac{\partial v^*}{\partial z^*} + \frac{1}{r^*}\frac{\partial w^*}{\partial \theta}\right)^2\right\}. \end{aligned} \tag{A.0.3}$$

So that

$$\begin{aligned} \dot{\gamma}^* = \sqrt{\frac{II}{2}} = \Bigg\{&2\left[\left(\frac{\partial u^*}{\partial r^*}\right)^2 + \left(\frac{1}{r^*}\frac{\partial v^*}{\partial \theta} + \frac{u^*}{r^*}\right)^2 + \left(\frac{\partial w^*}{\partial z^*}\right)^2\right] \\ &+ \left[r^*\frac{\partial}{\partial r^*}\left(\frac{v^*}{r^*}\right) + \frac{1}{r^*}\frac{\partial u^*}{\partial \theta}\right]^2 + \left(\frac{\partial u^*}{\partial z^*} + \frac{\partial w^*}{\partial r^*}\right)^2 + \left(\frac{\partial v^*}{\partial z^*} + \frac{1}{r^*}\frac{\partial w^*}{\partial \theta}\right)^2\Bigg\}^{1/2}. \end{aligned} \tag{A.0.4}$$

The components of the stress tensor $\boldsymbol{\tau}^* = \mu^*(\dot{\gamma}^*)\dot{\boldsymbol{\gamma}}^*$ can therefore be inferred from (A.0.4), once the specific form of μ^* is known.

It is more common to define the invariants of the rate-of-strain tensor in the following way

$$I_1 = I = \operatorname{tr}\dot{\boldsymbol{\gamma}}, \tag{A.0.5a}$$

$$2I_2 = I^2 - II = (\operatorname{tr}\dot{\boldsymbol{\gamma}})^2 - \operatorname{tr}\dot{\boldsymbol{\gamma}}^2, \tag{A.0.5b}$$

$$6I_3 = I^3 - 3I \cdot II + 2III = (\operatorname{tr}\dot{\boldsymbol{\gamma}})^3 - 3\operatorname{tr}\dot{\boldsymbol{\gamma}} \cdot \operatorname{tr}\dot{\boldsymbol{\gamma}}^2 + 2\operatorname{tr}\dot{\boldsymbol{\gamma}}^3 = 6\det\dot{\boldsymbol{\gamma}}. \tag{A.0.5c}$$

These are included here for completeness.

Working within our boundary-layer formulation of the rotating disk problem it is relatively simple to show that the third invariant III is identically zero, as noted by Bird *et al.* (1977). By non-dimensionalising $\dot{\boldsymbol{\gamma}}^*$ in a manner that is consistent with that of chapter 2 we find that the components of the rate-of-strain tensor take the form

$$\dot{\boldsymbol{\gamma}} = \dot{\gamma}_{ij} = \begin{Bmatrix} 2\delta U_r & \delta[r(V/r)_r + U_\theta/r] & U_Z + \delta^2 W_r \\ \delta[r(V/r)_r + U_\theta/r] & 2\delta(V_\theta + U)/r & V_Z + \delta^2 W_\theta/r \\ U_Z + \delta^2 W_r & V_Z + \delta^2 W_\theta/r & 2\delta W_Z \end{Bmatrix}, \tag{A.0.6}$$

where δ is the non-dimensional boundary-layer thickness and the subscripts denote partial differentiation. Therefore, after making our boundary-layer approximation, at leading order, we find that $III = \operatorname{tr}\dot{\boldsymbol{\gamma}}^3 = 0$.

Appendix B

Additional Viscous Terms & Type I Asymptotic Expansions

The additional viscous terms that do not appear in that stability analysis of chapter 4 are presented here

$$\mathcal{T}_r = \frac{2}{r}\frac{\partial}{\partial r}\left(\mu r\frac{\partial u}{\partial r}\right) + \frac{1}{r}\frac{\partial}{\partial \theta}\left\{\mu\left[r\frac{\partial}{\partial r}\left(\frac{v}{r}\right) + \frac{1}{r}\frac{\partial u}{\partial \theta}\right]\right\} + \frac{\partial}{\partial z}\left(\mu\frac{\partial w}{\partial r}\right) - \frac{2\mu}{r^2}\left(\frac{\partial v}{\partial \theta} + u\right), \tag{B.0.1}$$

$$\mathcal{T}_\theta = \frac{1}{r^2}\frac{\partial}{\partial r}\left\{\mu\left[r^3\frac{\partial}{\partial r}\left(\frac{v}{r}\right) + r\frac{\partial u}{\partial \theta}\right]\right\} + \frac{2}{r}\frac{\partial}{\partial \theta}\left[\mu\left(\frac{1}{r}\frac{\partial v}{\partial \theta} + \frac{u}{r}\right)\right] + \frac{\partial}{\partial z}\left(\frac{\mu}{r}\frac{\partial w}{\partial \theta}\right), \tag{B.0.2}$$

$$\mathcal{T}_z = \frac{1}{r}\frac{\partial}{\partial r}\left(\mu r\frac{\partial w}{\partial r}\right) + \frac{1}{r}\frac{\partial}{\partial \theta}\left(\frac{\mu}{r}\frac{\partial w}{\partial \theta}\right), \tag{B.0.3}$$

$$\mathcal{T}_\mu = 2\left(\frac{\partial u}{\partial r}\right)^2 + 2\left(\frac{1}{r}\frac{\partial v}{\partial \theta} + \frac{u}{r}\right)^2 + 2\left(\frac{\partial w}{\partial z}\right)^2 + \left[r\frac{\partial}{\partial r}\left(\frac{v}{r}\right) + \frac{1}{r}\frac{\partial u}{\partial \theta}\right]^2 + 2\frac{\partial u}{\partial z}\frac{\partial w}{\partial r} + \left(\frac{\partial w}{\partial r}\right)^2 + \frac{2}{r}\frac{\partial v}{\partial z}\frac{\partial w}{\partial \theta} + \left(\frac{1}{r}\frac{\partial w}{\partial \theta}\right)^2. \tag{B.0.4}$$

B.1 Case II: Inviscid zone expansions

The linear inviscid zone asymptotic expansions of the continuity and Navier-Stokes equations are provided here as a point of reference.

$$\left[\frac{\partial}{\partial r}+\mathrm{i}\varepsilon^{-3}(\alpha_0+\varepsilon\alpha_1+\cdots)+\frac{1}{r}\right](u_0+\varepsilon u_1+\cdots)$$
$$+\frac{\mathrm{i}\varepsilon^{-3}(\beta_0+\varepsilon\beta_1+\cdots)(v_0+\varepsilon v_1+\cdots)}{r}+\varepsilon^{-3}\frac{\partial(w_0+\varepsilon w_1+\cdots)}{\partial\zeta}=0, \tag{B.1.1a}$$

$$\left[r\bar{u}\frac{\partial}{\partial r}+\mathrm{i}\varepsilon^{-3}r\bar{u}(\alpha_0+\varepsilon\alpha_1+\cdots)+\mathrm{i}\varepsilon^{-3}\bar{v}(\beta_0+\varepsilon\beta_1+\cdots)+\bar{w}\frac{\partial}{\partial\zeta}\right]$$
$$\times(u_0+\varepsilon u_1+\cdots)+\bar{u}(u_0+\varepsilon u_1+\cdots)-2(\bar{v}+1)(v_0+\varepsilon v_1+\cdots)$$
$$+\varepsilon^{-3}r\bar{u}'(w_0+\varepsilon w_1+\cdots)=-\left[\frac{\partial}{\partial r}+\mathrm{i}\varepsilon^{-3}(\alpha_0+\varepsilon\alpha_1+\cdots)\right](p_0+\varepsilon p_1+\cdots)$$
$$+\frac{\partial}{\partial\zeta}\left\{\bar{\mu}\frac{\partial(u_0+\varepsilon u_1+\cdots)}{\partial\zeta}+\frac{\bar{u}'(1-\bar{\mu})}{\bar{u}'^2+\bar{v}'^2}\left[\bar{u}'\frac{\partial(u_0+\varepsilon u_1+\cdots)}{\partial\zeta}\right.\right.$$
$$\left.\left.+\bar{v}'\frac{\partial(v_0+\varepsilon v_1+\cdots)}{\partial\zeta}\right]\right\}, \tag{B.1.1b}$$

$$\left[r\bar{u}\frac{\partial}{\partial r}+\mathrm{i}\varepsilon^{-3}r\bar{u}(\alpha_0+\varepsilon\alpha_1+\cdots)+\mathrm{i}\varepsilon^{-3}\bar{v}(\beta_0+\varepsilon\beta_1+\cdots)+\bar{w}\frac{\partial}{\partial\zeta}\right]$$
$$\times(v_0+\varepsilon v_1+\cdots)+\bar{u}(v_0+\varepsilon v_1+\cdots)+2(\bar{v}+1)(u_0+\varepsilon u_1+\cdots)$$
$$+\varepsilon^{-3}r\bar{v}'(w_0+\varepsilon w_1+\cdots)=-\frac{\mathrm{i}\varepsilon^{-3}(\beta_0+\varepsilon\beta_1+\cdots)(p_0+\varepsilon p_1+\cdots)}{r}$$
$$+\frac{\partial}{\partial\zeta}\left\{\bar{\mu}\frac{\partial(v_0+\varepsilon v_1+\cdots)}{\partial\zeta}+\frac{\bar{v}'(1-\bar{\mu})}{\bar{u}'^2+\bar{v}'^2}\left[\bar{u}'\frac{\partial(u_0+\varepsilon u_1+\cdots)}{\partial\zeta}\right.\right.$$
$$\left.\left.+\bar{v}'\frac{\partial(v_0+\varepsilon v_1+\cdots)}{\partial\zeta}\right]\right\}, \tag{B.1.1c}$$

$$\left[r\bar{u}\frac{\partial}{\partial r}+\mathrm{i}r\bar{u}\varepsilon^{-3}(\alpha_0+\varepsilon\alpha_1+\cdots)+\mathrm{i}\bar{v}\varepsilon^{-3}(\beta_0+\varepsilon\beta_1+\cdots)+\bar{w}\frac{\partial}{\partial\zeta}\right]$$
$$\times(w_0+\varepsilon w_1+\cdots)+\bar{w}'(w_0+\varepsilon w_1+\cdots)=-\varepsilon^{-3}\frac{\partial(p_0+\varepsilon p_1+\cdots)}{\partial\zeta}$$
$$+2\frac{\partial}{\partial\zeta}\left\{\bar{\mu}\frac{\partial(w_0+\varepsilon w_1+\cdots)}{\partial\zeta}+\varepsilon^3 r^{-1}\frac{\bar{w}'(1-\bar{\mu})}{\bar{u}'^2+\bar{v}'^2}\left[\bar{u}'\frac{\partial(u_0+\varepsilon u_1+\cdots)}{\partial\zeta}\right.\right.$$
$$\left.\left.+\bar{v}'\frac{\partial(v_0+\varepsilon v_1+\cdots)}{\partial\zeta}\right]\right\}+\mathcal{O}(\varepsilon^3). \tag{B.1.1d}$$

B.2 Case II: Wall layer expansions

The linear wall layer asymptotic expansions of the continuity and Navier-Stokes equations are provided here as a point of reference.

$$\left[\frac{\partial}{\partial r}+\mathrm{i}\varepsilon^{-3}(\alpha_0+\varepsilon\alpha_1+\cdots)+\frac{1}{r}\right](U_0+\varepsilon U_1+\cdots)$$
$$+\frac{\mathrm{i}\varepsilon^{-3}(\beta_0+\varepsilon\beta_1+\cdots)(V_0+\varepsilon V_1+\cdots)}{r}+\varepsilon^{-4}\frac{\partial(\varepsilon W_0+\varepsilon^2 W_1+\cdots)}{\partial\zeta_w}=0, \tag{B.2.1a}$$

$$\left[r(\varepsilon\zeta_w\bar{u}_0+\varepsilon^2\zeta_w^2\bar{u}_1+\cdots)\frac{\partial}{\partial r}+\mathrm{i}\varepsilon^{-3}r(\varepsilon\zeta_w\bar{u}_0+\varepsilon^2\zeta_w^2\bar{u}_1+\cdots)(\alpha_0+\varepsilon\alpha_1+\cdots)\right.$$
$$\left.+\mathrm{i}\varepsilon^{-3}(\varepsilon\zeta_w\bar{v}_0+\varepsilon^2\zeta_w^2\bar{v}_1+\cdots)(\beta_0+\varepsilon\beta_1+\cdots)+\varepsilon^{-1}(\varepsilon^2\zeta_w^2\bar{w}_1+\varepsilon^3\zeta_w^3\bar{w}_2+\cdots)\frac{\partial}{\partial\zeta_w}\right]$$
$$\times(U_0+\varepsilon U_1+\cdots)+(\varepsilon\zeta_w\bar{u}_0+\varepsilon^2\zeta_w^2\bar{u}_1+\cdots)(U_0+\varepsilon U_1+\cdots)$$
$$-2(\varepsilon\zeta_w\bar{v}_0+\varepsilon^2\zeta_w^2\bar{v}_1+\cdots+1)(V_0+\varepsilon V_1+\cdots)+\varepsilon^{-3}r(\bar{u}_0+2\varepsilon\zeta_w\bar{u}_1+\cdots)$$
$$\times(\varepsilon W_0+\varepsilon^2 W_1+\cdots)=-\left[\frac{\partial}{\partial r}+\mathrm{i}\varepsilon^{-3}(\alpha_0+\varepsilon\alpha_1+\cdots)\right](\varepsilon P_0+\varepsilon^2 P_1+\cdots)$$
$$+\varepsilon^{-2}\frac{\partial}{\partial\zeta_w}\left\{\bar{\mu}\frac{\partial(U_0+\varepsilon U_1+\cdots)}{\partial\zeta_w}+\frac{(\bar{u}_0+2\varepsilon\zeta_w\bar{u}_1+\cdots)(1-\bar{\mu})}{(\bar{u}_0^2+4\varepsilon\zeta_w\bar{u}_0\bar{u}_1+\cdots)+(\bar{v}_0^2+4\varepsilon\zeta_w\bar{v}_0\bar{v}_1+\cdots)}\right.$$
$$\times\left[(\bar{u}_0+2\varepsilon\zeta_w\bar{u}_1+\cdots)\frac{\partial(U_0+\varepsilon U_1+\cdots)}{\partial\zeta_w}\right.$$
$$\left.\left.+(\bar{v}_0+2\varepsilon\zeta_w\bar{v}_1+\cdots)\frac{\partial(V_0+\varepsilon V_1+\cdots)}{\partial\zeta_w}\right]\right\}, \tag{B.2.1b}$$

$$\Big[r(\varepsilon\zeta_w\bar{u}_0+\varepsilon^2\zeta_w^2\bar{u}_1+\cdots)\frac{\partial}{\partial r}+\mathrm{i}\varepsilon^{-3}r(\varepsilon\zeta_w\bar{u}_0+\varepsilon^2\zeta_w^2\bar{u}_1+\cdots)(\alpha_0+\varepsilon\alpha_1+\cdots)$$
$$+\mathrm{i}\varepsilon^{-3}(\varepsilon\zeta_w\bar{v}_0+\varepsilon^2\zeta_w^2\bar{v}_1+\cdots)(\beta_0+\varepsilon\beta_1+\cdots)+\varepsilon^{-1}(\varepsilon^2\zeta_w^2\bar{w}_1+\varepsilon^3\zeta_w^3\bar{w}_2+\cdots)\frac{\partial}{\partial\zeta_w}\Big]$$
$$\times(V_0+\varepsilon V_1+\cdots)+(\varepsilon\zeta_w\bar{u}_0+\varepsilon^2\zeta_w^2\bar{u}_1+\cdots)(V_0+\varepsilon V_1+\cdots)$$
$$+2(\varepsilon\zeta_w\bar{v}_0+\varepsilon^2\zeta_w^2\bar{v}_1+\cdots+1)(U_0+\varepsilon U_1+\cdots)+\varepsilon^{-3}r(\bar{v}_0+2\varepsilon\zeta_w\bar{v}_1+\cdots)$$
$$\times(\varepsilon W_0+\varepsilon^2W_1+\cdots)=-\frac{\mathrm{i}\varepsilon^{-3}(\beta_0+\varepsilon\beta_1+\cdots)(\varepsilon P_0+\varepsilon^2P_1+\cdots)}{r}$$
$$+\varepsilon^{-2}\frac{\partial}{\partial\zeta_w}\Bigg\{\bar{\mu}\frac{\partial(V_0+\varepsilon V_1+\cdots)}{\partial\zeta_w}+\frac{(\bar{v}_0+2\varepsilon\zeta_w\bar{v}_1+\cdots)(1-\bar{\mu})}{(\bar{u}_0^2+4\varepsilon\zeta_w\bar{u}_0\bar{u}_1+\cdots)+(\bar{v}_0^2+4\varepsilon\zeta_w\bar{v}_0\bar{v}_1+\cdots)}$$
$$\times\Big[(\bar{u}_0+2\varepsilon\zeta_w\bar{u}_1+\cdots)\frac{\partial(U_0+\varepsilon U_1+\cdots)}{\partial\zeta_w}$$
$$+(\bar{v}_0+2\varepsilon\zeta_w\bar{v}_1+\cdots)\frac{\partial(V_0+\varepsilon V_1+\cdots)}{\partial\zeta_w}\Big]\Bigg\},\tag{B.2.1c}$$

$$\Big[r(\varepsilon\zeta_w\bar{u}_0+\varepsilon^2\zeta_w^2\bar{u}_1+\cdots)\frac{\partial}{\partial r}+\mathrm{i}\varepsilon^{-3}r(\varepsilon\zeta_w\bar{u}_0+\varepsilon^2\zeta_w^2\bar{u}_1+\cdots)(\alpha_0+\varepsilon\alpha_1+\cdots)$$
$$+\mathrm{i}\varepsilon^{-3}(\varepsilon\zeta_w\bar{v}_0+\varepsilon^2\zeta_w^2\bar{v}_1+\cdots)(\beta_0+\varepsilon\beta_1+\cdots)+\varepsilon^{-1}(\varepsilon^2\zeta_w^2\bar{w}_1+\varepsilon^3\zeta_w^3\bar{w}_2+\cdots)\frac{\partial}{\partial\zeta_w}\Big]$$
$$\times(\varepsilon W_0+\varepsilon^2W_1+\cdots)+(2\varepsilon\zeta_w\bar{w}_1+3\varepsilon^2\zeta_w^2\bar{w}_2+\cdots)(\varepsilon W_0+\varepsilon^2W_1+\cdots)$$
$$=-\varepsilon^{-4}\frac{\partial(\varepsilon P_0+\varepsilon^2P_1+\cdots)}{\partial\zeta_w}+2\varepsilon^{-2}\frac{\partial}{\partial\zeta_w}\Bigg\{\bar{\mu}\frac{\partial(\varepsilon W_0+\varepsilon^2W_1+\cdots)}{\partial\zeta_w}$$
$$+\varepsilon^3r^{-1}\frac{(2\varepsilon\zeta_w\bar{w}_1+3\varepsilon^2\zeta_w^2\bar{w}_2+\cdots)(1-\bar{\mu})}{(\bar{u}_0^2+4\varepsilon\zeta_w\bar{u}_0\bar{u}_1+\cdots)+(\bar{v}_0^2+4\varepsilon\zeta_w\bar{v}_0\bar{v}_1+\cdots)}$$
$$\times\Big[(\bar{u}_0+2\varepsilon\zeta_w\bar{u}_1+\cdots)\frac{\partial(U_0+\varepsilon U_1+\cdots)}{\partial\zeta_w}$$
$$+(\bar{v}_0+2\varepsilon\zeta_w\bar{v}_1+\cdots)\frac{\partial(V_0+\varepsilon V_1+\cdots)}{\partial\zeta_w}\Big]\Bigg\}+\mathcal{O}(\varepsilon^2),\tag{B.2.1d}$$

where here $\bar{\mu}$ expands as

$$\bar{\mu}=1+\frac{2B_n}{\sqrt{(\bar{u}_0^2+4\varepsilon\zeta_w\bar{u}_0\bar{u}_1+\cdots)+(\bar{v}_0^2+4\varepsilon\zeta_w\bar{v}_0\bar{v}_1+\cdots)}}.\tag{B.2.1e}$$

B.3 Case III: Inviscid zone expansions

The linear inviscid zone asymptotic expansions of the continuity and Navier-Stokes equations are provided here as a point of reference.

$$\left[\frac{\partial}{\partial r}+\mathrm{i}\varepsilon^{-3}(\alpha_0+\varepsilon\alpha_1+\cdots)+\frac{1}{r}\right](u_0+\varepsilon u_1+\cdots)$$
$$+\frac{\mathrm{i}\varepsilon^{-3}(\beta_0+\varepsilon\beta_1+\cdots)(v_0+\varepsilon v_1+\cdots)}{r}+\varepsilon^{-3}\frac{\partial(w_0+\varepsilon w_1+\cdots)}{\partial\xi}=0, \tag{B.3.1a}$$

$$\left[r\bar{u}\frac{\partial}{\partial r}+\mathrm{i}\varepsilon^{-3}r\bar{u}(\alpha_0+\varepsilon\alpha_1+\cdots)+\mathrm{i}\varepsilon^{-3}\bar{v}(\beta_0+\varepsilon\beta_1+\cdots)+\bar{w}\frac{\partial}{\partial\xi}\right]$$
$$\times(u_0+\varepsilon u_1+\cdots)+\bar{u}(u_0+\varepsilon u_1+\cdots)-2(\bar{v}+1)(v_0+\varepsilon v_1+\cdots)$$
$$+\varepsilon^{-3}r\bar{u}'(w_0+\varepsilon w_1+\cdots)=-\left[\frac{\partial}{\partial r}+\mathrm{i}\varepsilon^{-3}(\alpha_0+\varepsilon\alpha_1+\cdots)\right](p_0+\varepsilon p_1+\cdots)$$
$$+\frac{\partial}{\partial\xi}\left\{\bar{\mu}\frac{\partial(u_0+\varepsilon u_1+\cdots)}{\partial\xi}+\frac{\bar{u}'k^2(\bar{\mu}-1)(n-1)}{1+k^2(\bar{u}'^2+\bar{v}'^2)}\left[\bar{u}'\frac{\partial(u_0+\varepsilon u_1+\cdots)}{\partial\xi}\right.\right.$$
$$\left.\left.+\bar{v}'\frac{\partial(v_0+\varepsilon v_1+\cdots)}{\partial\xi}\right]\right\}, \tag{B.3.1b}$$

$$\left[r\bar{u}\frac{\partial}{\partial r}+\mathrm{i}\varepsilon^{-3}r\bar{u}(\alpha_0+\varepsilon\alpha_1+\cdots)+\mathrm{i}\varepsilon^{-3}\bar{v}(\beta_0+\varepsilon\beta_1+\cdots)+\bar{w}\frac{\partial}{\partial\xi}\right]$$
$$\times(v_0+\varepsilon v_1+\cdots)+\bar{u}(v_0+\varepsilon v_1+\cdots)+2(\bar{v}+1)(u_0+\varepsilon u_1+\cdots)$$
$$+\varepsilon^{-3}r\bar{v}'(w_0+\varepsilon w_1+\cdots)=-\frac{\mathrm{i}\varepsilon^{-3}(\beta_0+\varepsilon\beta_1+\cdots)(p_0+\varepsilon p_1+\cdots)}{r}$$
$$+\frac{\partial}{\partial\xi}\left\{\bar{\mu}\frac{\partial(v_0+\varepsilon v_1+\cdots)}{\partial\xi}+\frac{\bar{v}'k^2(\bar{\mu}-1)(n-1)}{1+k^2(\bar{u}'^2+\bar{v}'^2)}\left[\bar{u}'\frac{\partial(u_0+\varepsilon u_1+\cdots)}{\partial\xi}\right.\right.$$
$$\left.\left.+\bar{v}'\frac{\partial(v_0+\varepsilon v_1+\cdots)}{\partial\xi}\right]\right\}, \tag{B.3.1c}$$

$$\left[r\bar{u}\frac{\partial}{\partial r}+\mathrm{i}r\bar{u}\varepsilon^{-3}(\alpha_0+\varepsilon\alpha_1+\cdots)+\mathrm{i}\bar{v}\varepsilon^{-3}(\beta_0+\varepsilon\beta_1+\cdots)+\bar{w}\frac{\partial}{\partial\xi}\right]$$
$$\times(w_0+\varepsilon w_1+\cdots)+\bar{w}'(w_0+\varepsilon w_1+\cdots)=-\varepsilon^{-3}\frac{\partial(p_0+\varepsilon p_1+\cdots)}{\partial\xi}$$
$$+2\frac{\partial}{\partial\xi}\left\{\bar{\mu}\frac{\partial(w_0+\varepsilon w_1+\cdots)}{\partial\xi}+\varepsilon^3 r^{-1}\frac{\bar{w}'k^2(\bar{\mu}-1)(n-1)}{1+k^2(\bar{u}'^2+\bar{v}'^2)}\left[\bar{u}'\frac{\partial(u_0+\varepsilon u_1+\cdots)}{\partial\xi}\right.\right.$$
$$\left.\left.+\bar{v}'\frac{\partial(v_0+\varepsilon v_1+\cdots)}{\partial\xi}\right]\right\}+\mathcal{O}(\varepsilon^3). \tag{B.3.1d}$$

B.4 Case III: Wall layer expansions

The linear wall layer asymptotic expansions of the continuity and Navier-Stokes equations are provided here as a point of reference.

$$\left[\frac{\partial}{\partial r}+\mathrm{i}\varepsilon^{-3}(\alpha_0+\varepsilon\alpha_1+\cdots)+\frac{1}{r}\right](U_0+\varepsilon U_1+\cdots)$$
$$+\frac{\mathrm{i}\varepsilon^{-3}(\beta_0+\varepsilon\beta_1+\cdots)(V_0+\varepsilon V_1+\cdots)}{r}+\varepsilon^{-4}\frac{\partial(\varepsilon W_0+\varepsilon^2W_1+\cdots)}{\partial\xi_w}=0, \tag{B.4.1a}$$

$$\left[r(\varepsilon\xi_w\bar{u}_0+\varepsilon^2\xi_w^2\bar{u}_1+\cdots)\frac{\partial}{\partial r}+\mathrm{i}\varepsilon^{-3}r(\varepsilon\xi_w\bar{u}_0+\varepsilon^2\xi_w^2\bar{u}_1+\cdots)(\alpha_0+\varepsilon\alpha_1+\cdots)\right.$$
$$\left.+\mathrm{i}\varepsilon^{-3}(\varepsilon\xi_w\bar{v}_0+\varepsilon^2\xi_w^2\bar{v}_1+\cdots)(\beta_0+\varepsilon\beta_1+\cdots)+\varepsilon^{-1}(\varepsilon^2\xi_w^2\bar{w}_1+\varepsilon^3\xi_w^3\bar{w}_2+\cdots)\frac{\partial}{\partial\xi_w}\right]$$
$$\times(U_0+\varepsilon U_1+\cdots)+(\varepsilon\xi_w\bar{u}_0+\varepsilon^2\xi_w^2\bar{u}_1+\cdots)(U_0+\varepsilon U_1+\cdots)$$
$$-2(\varepsilon\xi_w\bar{v}_0+\varepsilon^2\xi_w^2\bar{v}_1+\cdots+1)(V_0+\varepsilon V_1+\cdots)+\varepsilon^{-3}r(\bar{u}_0+2\varepsilon\xi_w\bar{u}_1+\cdots)$$
$$\times(\varepsilon W_0+\varepsilon^2W_1+\cdots)=-\left[\frac{\partial}{\partial r}+\mathrm{i}\varepsilon^{-3}(\alpha_0+\varepsilon\alpha_1+\cdots)\right](\varepsilon P_0+\varepsilon^2P_1+\cdots)$$
$$+\varepsilon^{-2}\frac{\partial}{\partial\xi_w}\left\{\bar{\mu}\frac{\partial(U_0+\varepsilon U_1+\cdots)}{\partial\xi_w}+\frac{(\bar{u}_0+2\varepsilon\xi_w\bar{u}_1+\cdots)k^2(\bar{\mu}-1)(n-1)}{1+k^2[(\bar{u}_0^2+4\varepsilon\xi_w\bar{u}_0\bar{u}_1+\cdots)+(\bar{v}_0^2+4\varepsilon\xi_w\bar{v}_0\bar{v}_1+\cdots)]}\right.$$
$$\times\left[(\bar{u}_0+2\varepsilon\xi_w\bar{u}_1+\cdots)\frac{\partial(U_0+\varepsilon U_1+\cdots)}{\partial\xi_w}\right.$$
$$\left.\left.+(\bar{v}_0+2\varepsilon\xi_w\bar{v}_1+\cdots)\frac{\partial(V_0+\varepsilon V_1+\cdots)}{\partial\xi_w}\right]\right\}, \tag{B.4.1b}$$

$$\Big[r(\varepsilon\xi_w\bar{u}_0+\varepsilon^2\xi_w^2\bar{u}_1+\cdots)\frac{\partial}{\partial r}+\mathrm{i}\varepsilon^{-3}r(\varepsilon\xi_w\bar{u}_0+\varepsilon^2\xi_w^2\bar{u}_1+\cdots)(\alpha_0+\varepsilon\alpha_1+\cdots)$$
$$+\mathrm{i}\varepsilon^{-3}(\varepsilon\xi_w\bar{v}_0+\varepsilon^2\xi_w^2\bar{v}_1+\cdots)(\beta_0+\varepsilon\beta_1+\cdots)+\varepsilon^{-1}(\varepsilon^2\xi_w^2\bar{w}_1+\varepsilon^3\xi_w^3\bar{w}_2+\cdots)\frac{\partial}{\partial\xi_w}\Big]$$
$$\times(V_0+\varepsilon V_1+\cdots)+(\varepsilon\xi_w\bar{u}_0+\varepsilon^2\xi_w^2\bar{u}_1+\cdots)(V_0+\varepsilon V_1+\cdots)$$
$$+2(\varepsilon\xi_w\bar{v}_0+\varepsilon^2\xi_w^2\bar{v}_1+\cdots+1)(U_0+\varepsilon U_1+\cdots)+\varepsilon^{-3}r(\bar{v}_0+2\varepsilon\xi_w\bar{v}_1+\cdots)$$
$$\times(\varepsilon W_0+\varepsilon^2W_1+\cdots)=-\frac{\mathrm{i}\varepsilon^{-3}(\beta_0+\varepsilon\beta_1+\cdots)(\varepsilon P_0+\varepsilon^2P_1+\cdots)}{r}$$
$$+\varepsilon^{-2}\frac{\partial}{\partial\xi_w}\Bigg\{\bar{\mu}\frac{\partial(V_0+\varepsilon V_1+\cdots)}{\partial\xi_w}+\frac{(\bar{v}_0+2\varepsilon\xi_w\bar{v}_1+\cdots)k^2(\bar{\mu}-1)(n-1)}{1+k^2[(\bar{u}_0^2+4\varepsilon\xi_w\bar{u}_0\bar{u}_1+\cdots)+(\bar{v}_0^2+4\varepsilon\xi_w\bar{v}_0\bar{v}_1+\cdots)]}$$
$$\times\Big[(\bar{u}_0+2\varepsilon\xi_w\bar{u}_1+\cdots)\frac{\partial(U_0+\varepsilon U_1+\cdots)}{\partial\xi_w}$$
$$+(\bar{v}_0+2\varepsilon\xi_w\bar{v}_1+\cdots)\frac{\partial(V_0+\varepsilon V_1+\cdots)}{\partial\xi_w}\Big]\Bigg\},\tag{B.4.1c}$$

$$\Big[r(\varepsilon\xi_w\bar{u}_0+\varepsilon^2\xi_w^2\bar{u}_1+\cdots)\frac{\partial}{\partial r}+\mathrm{i}\varepsilon^{-3}r(\varepsilon\xi_w\bar{u}_0+\varepsilon^2\xi_w^2\bar{u}_1+\cdots)(\alpha_0+\varepsilon\alpha_1+\cdots)$$
$$+\mathrm{i}\varepsilon^{-3}(\varepsilon\xi_w\bar{v}_0+\varepsilon^2\xi_w^2\bar{v}_1+\cdots)(\beta_0+\varepsilon\beta_1+\cdots)+\varepsilon^{-1}(\varepsilon^2\xi_w^2\bar{w}_1+\varepsilon^3\xi_w^3\bar{w}_2+\cdots)\frac{\partial}{\partial\xi_w}\Big]$$
$$\times(\varepsilon W_0+\varepsilon^2W_1+\cdots)+(2\varepsilon\xi_w\bar{w}_1+3\varepsilon^2\xi_w^2\bar{w}_2+\cdots)(\varepsilon W_0+\varepsilon^2W_1+\cdots)$$
$$=-\varepsilon^{-4}\frac{\partial(\varepsilon P_0+\varepsilon^2P_1+\cdots)}{\partial\xi_w}+2\varepsilon^{-2}\frac{\partial}{\partial\xi_w}\Bigg\{\bar{\mu}\frac{\partial(\varepsilon W_0+\varepsilon^2W_1+\cdots)}{\partial\xi_w}$$
$$+\varepsilon^3r^{-1}\frac{(2\varepsilon\xi_w\bar{w}_1+3\varepsilon^2\xi_w^2\bar{w}_2+\cdots)k^2(\bar{\mu}-1)(n-1)}{1+k^2[(\bar{u}_0^2+4\varepsilon\xi_w\bar{u}_0\bar{u}_1+\cdots)+(\bar{v}_0^2+4\varepsilon\xi_w\bar{v}_0\bar{v}_1+\cdots)]}$$
$$\times\Big[(\bar{u}_0+2\varepsilon\xi_w\bar{u}_1+\cdots)\frac{\partial(U_0+\varepsilon U_1+\cdots)}{\partial\xi_w}$$
$$+(\bar{v}_0+2\varepsilon\xi_w\bar{v}_1+\cdots)\frac{\partial(V_0+\varepsilon V_1+\cdots)}{\partial\xi_w}\Big]\Bigg\}+\mathcal{O}(\varepsilon^2),\tag{B.4.1d}$$

where here $\bar{\mu}$ expands as

$$\bar{\mu}=1+c_0\{1+k^2[(\bar{u}_0^2+4\varepsilon\xi_w\bar{u}_0\bar{u}_1+\cdots)+(\bar{v}_0^2+4\varepsilon\xi_w\bar{v}_0\bar{v}_1+\cdots)]\}^{(n-1)/2}.\tag{B.4.1e}$$

Appendix C

Newtonian Perturbation Equations & Non-Newtonian Neutral Curves

Lingwood (1995*a*) gives the exact Newtonian perturbation equations as

$$\eta_1' = \eta_2, \tag{C.0.1}$$

$$\left[\frac{\eta_2'}{R}\right]_v = \frac{\eta_2 W_s}{R} + \frac{[\kappa_v^2 + \mathrm{i}R\left(\bar{\alpha}U + \bar{\beta}V - \bar{\omega}\right) + U_s]\eta_1}{R} - \frac{2(1_c + V_s)\eta_5}{R} + (\bar{\alpha}_1 U' + \bar{\beta}V')\eta_3 + \mathrm{i}\left[\kappa^2 - \left(\frac{\bar{\alpha}\mathrm{i}}{R}\right)_s\right]\eta_4, \tag{C.0.2}$$

$$\eta_3' = -\mathrm{i}\eta_1, \tag{C.0.3}$$

$$\eta_4' = \frac{\mathrm{i}[\eta_1 W_s - (\eta_1)_v']}{R} - \frac{[\kappa_v^2 + \mathrm{i}R\left(\bar{\alpha}U + \bar{\beta}V - \bar{\omega}\right) + W_s']\eta_3}{R}, \tag{C.0.4}$$

$$\eta_5' = \eta_6, \tag{C.0.5}$$

$$\left[\frac{\eta_6'}{R}\right]_v = \frac{\eta_6 W_s}{R} + \frac{[\kappa_v^2 + \mathrm{i}R\left(\bar{\alpha}U + \bar{\beta}V - \bar{\omega}\right) + U_s]\eta_5}{R} + \frac{2(1_c + V_s)\eta_1}{R} + (\bar{\alpha}_1 V' - \bar{\beta}U')\eta_3 + \left[\frac{\bar{\beta}\eta_4}{R}\right]_s. \tag{C.0.6}$$

The κ_v^2 terms vanish when appealing to a boundary-layer approximation. Thus we see that substitution of $n = 1$ into (5.1.8) does admit the corresponding Newtonian boundary-layer set of perturbation equations.

The additional large Reynolds number neutral stability curves are plotted below

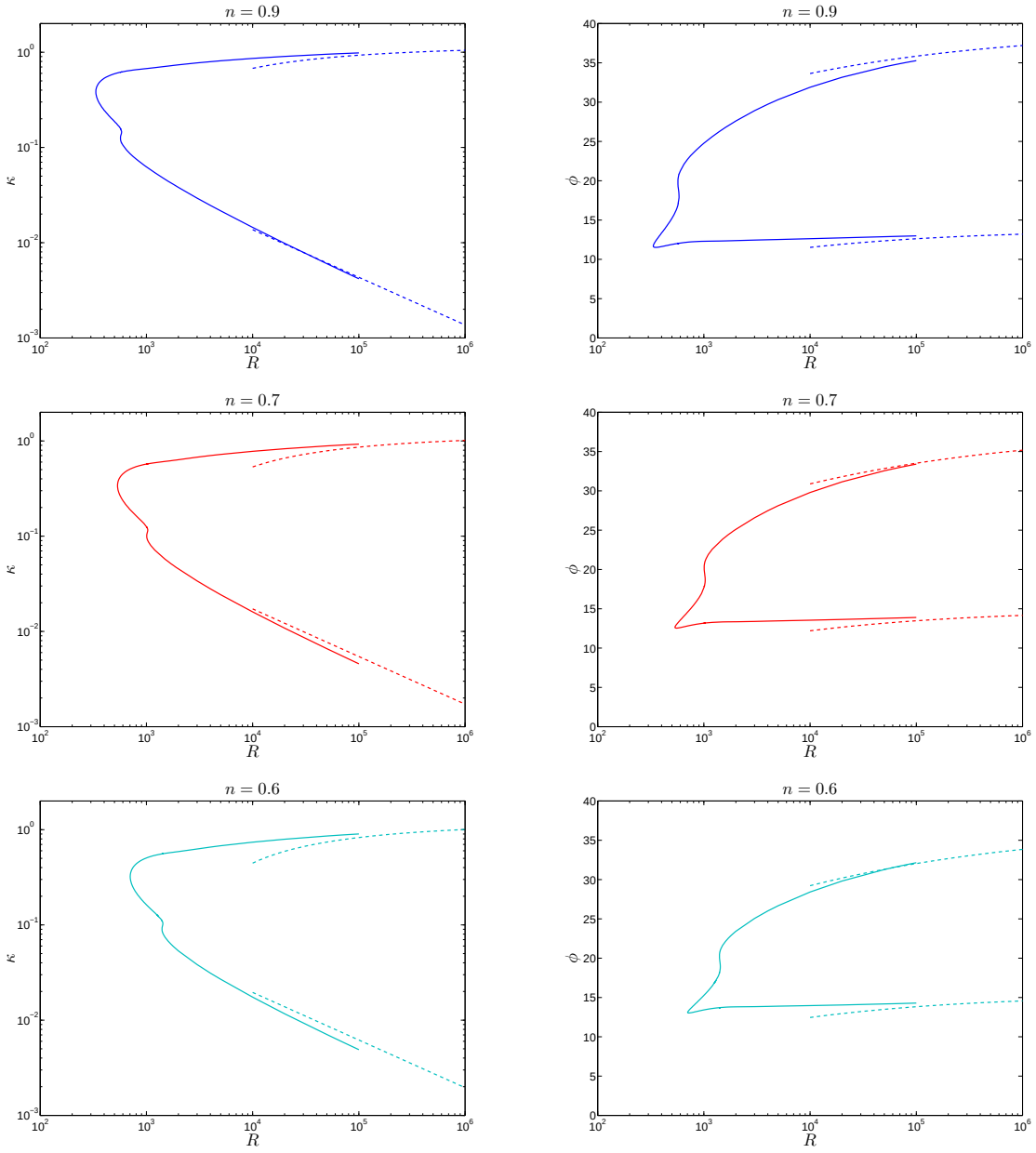

Figure C.1: Neutral stability curves for power-law fluids with $n = 0.9$, 0.7, 0.6. The type I asymptotic solutions are given by the dashed lines.

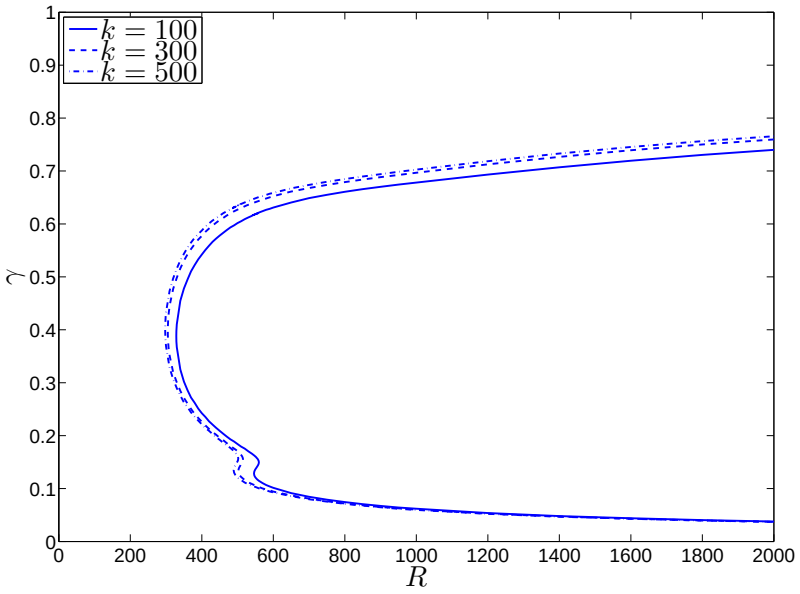

Figure C.2: Neutral wavenumber stability curves for shear-thinning Carreau fluids with $n = 0.5$ and $k = 100$, 300, 500.

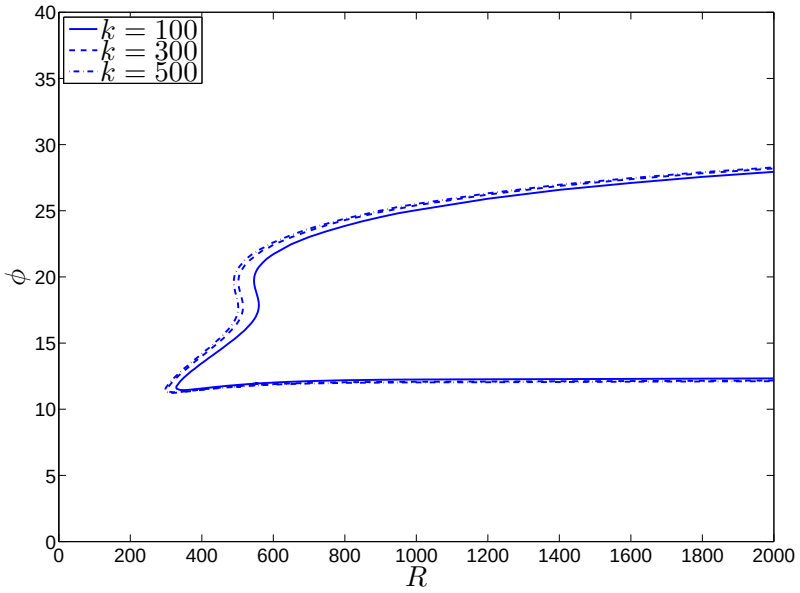

Figure C.3: Neutral wave angle stability curves for shear-thinning Carreau fluids with $n = 0.5$ and $k = 100$, 300, 500.

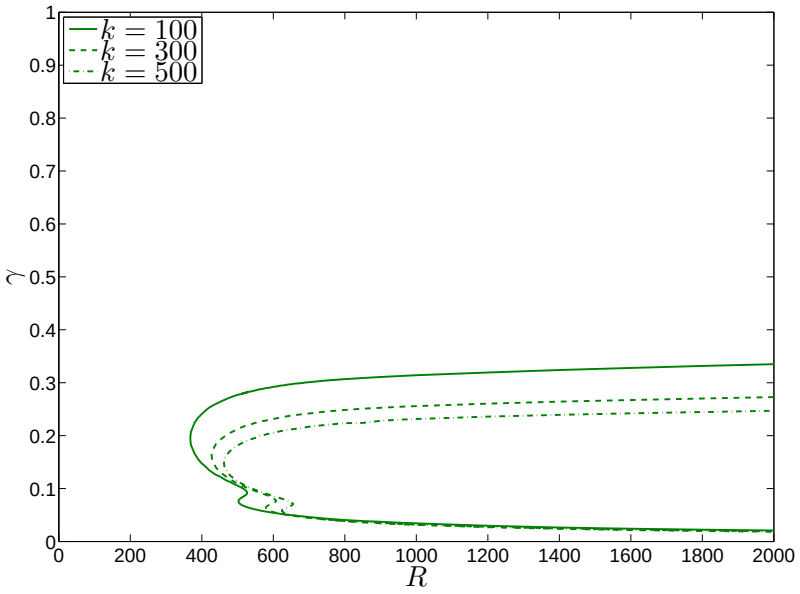

Figure C.4: Neutral wavenumber stability curves for shear-thickening Carreau fluids with $n = 1.5$ and $k = 100$, 300, 500.

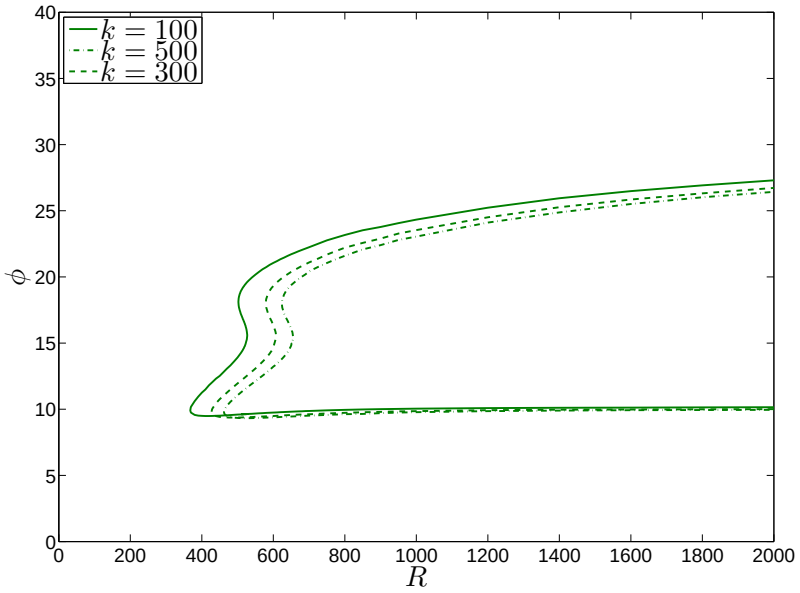

Figure C.5: Neutral wave angler stability curves for shear-thickening Carreau fluids with $n = 1.5$ and $k = 100$, 300, 500.

Appendix D

Type II Asymptotic Expansions

Here we provide the expansions of the viscosity function and base flow velocities for cases II & III, these are utilised in the analysis of chapter 6. We note that in both cases we set the $\bar{\nu}_i$ terms to be zero for $i = 0, 1, 2, \ldots$. For Bingham plastic fluids we find that

$$\bar{\mu}_0 = 1 + 2B_n[\bar{u}_0^2 + \bar{v}_0^2]^{-1/2}, \tag{D.0.1a}$$

$$\bar{\mu}_1 = \frac{2(1-\bar{\mu}_0)(\bar{u}_0\bar{u}_1 + \bar{v}_0\bar{v}_1)}{\bar{u}_0^2 + \bar{v}_0^2}, \tag{D.0.1b}$$

$$\bar{\mu}_2 = -\frac{6(1-\bar{\mu}_0)(\bar{u}_0\bar{u}_1 + \bar{v}_0\bar{v}_1)^2}{(\bar{u}_0^2 + \bar{v}_0^2)^2} + \frac{(1-\bar{\mu}_0)[2(\bar{u}_1^2 + \bar{v}_1^2) + 3(\bar{u}_0\bar{u}_2 + \bar{v}_0\bar{v}_2)]}{\bar{u}_0^2 + \bar{v}_0^2}, \tag{D.0.1c}$$

where

$$\bar{u}_1 = \frac{-1}{2\bar{\mu}_0}\left[1 - \frac{(1-\bar{\mu}_0)\bar{u}_0^2}{\bar{u}_0^2 + \bar{v}_0^2}\right], \tag{D.0.2a}$$

$$\bar{v}_1 = \frac{1}{2\bar{\mu}_0}\left[\frac{(1-\bar{\mu}_0)\bar{u}_0\bar{v}_0}{\bar{u}_0^2 + \bar{v}_0^2}\right], \tag{D.0.2b}$$

$$\bar{u}_2 = \frac{-\bar{v}_0}{3\bar{\mu}_0} + \frac{\bar{u}_0(1-\bar{\mu}_0)}{6\bar{\mu}_0^2(\bar{u}_0^2 + \bar{v}_0^2)}\left[-1 + \frac{\bar{u}_0^2 - 2\bar{v}_0^2}{\bar{u}_0^2 + \bar{v}_0^2}\right], \tag{D.0.2c}$$

$$\bar{v}_2 = \frac{\bar{u}_0}{3\bar{\mu}_0} + \frac{\bar{v}_0(1-\bar{\mu}_0)}{6\bar{\mu}_0^2(\bar{u}_0^2 + \bar{v}_0^2)}\left[-1 + \frac{3\bar{u}_0^2}{\bar{u}_0^2 + \bar{v}_0^2}\right]. \tag{D.0.2d}$$

The corresponding expressions for Carreau fluids are given by

$$\bar{\mu}_0 = 1 + c_0[1 + k^2(\bar{u}_0^2 + \bar{v}_0^2)]^{(n-1)/2}, \tag{D.0.3a}$$

$$\bar{\mu}_1 = \frac{2\hat{k}(\bar{u}_0\bar{u}_1 + \bar{v}_0\bar{v}_1)}{[1 + k^2(\bar{u}_0^2 + \bar{v}_0^2)]}, \tag{D.0.3b}$$

$$\bar{\mu}_2 = \hat{k}\left\{ \frac{2(n-3)(\bar{u}_0\bar{u}_1 + \bar{v}_0\bar{v}_1)^2}{[1 + k^2(\bar{u}_0^2 + \bar{v}_0^2)]^2} + \frac{2(\bar{u}_1^2 + \bar{v}_1^2) + 3(\bar{u}_0\bar{u}_2 + \bar{v}_0\bar{v}_2)}{[1 + k^2(\bar{u}_0^2 + \bar{v}_0^2)]} \right\}, \tag{D.0.3c}$$

where $\hat{k} = k^2(\bar{\mu}_0 - 1)(n-1)$ and

$$\bar{u}_1 = \frac{-1}{2\bar{\mu}_0}\left[1 - \frac{\hat{k}\bar{u}_0^2}{\bar{\sigma}_0}\right], \tag{D.0.4a}$$

$$\bar{v}_1 = \frac{1}{2\bar{\mu}_0}\left[\frac{\hat{k}\bar{u}_0\bar{v}_0}{\bar{\sigma}_0}\right], \tag{D.0.4b}$$

$$\bar{u}_2 = -\frac{\bar{v}_0}{3\bar{\mu}_0} - \frac{\hat{k}\bar{u}_0}{6\bar{\mu}_0^2\bar{\sigma}_0}\left[3 + \frac{k^2\bar{u}_0^2\bar{\sigma}_1}{\bar{\sigma}_0}\right], \tag{D.0.4c}$$

$$\bar{v}_2 = \frac{\bar{u}_0}{3\bar{\mu}_0} - \frac{\hat{k}\bar{v}_0}{6\bar{\mu}_0^2\bar{\sigma}_0}\left[1 + \frac{k^2\bar{u}_0^2\bar{\sigma}_1}{\bar{\sigma}_0}\right], \tag{D.0.4d}$$

with

$$\bar{\sigma}_0 = \bar{\mu}_0[1 + k^2(\bar{u}_0^2 + \bar{v}_0^2)] + \hat{k}(\bar{u}_0^2 + \bar{v}_0^2), \tag{D.0.5a}$$

$$\bar{\sigma}_1 = (n-1)(3 - 2\bar{\mu}_0) - \frac{\bar{\mu}_0}{\bar{\sigma}_0}\left\{ \frac{(n-1)(\bar{\mu}_0 - 1)[(n-1)(\bar{\sigma}_0 - 1) + \bar{\sigma}_0]}{[(n-1)(\bar{\mu}_0 - 1) + \bar{\mu}_0]} + 2[(n-1)(\bar{\mu}_0 - 1) + \bar{\sigma}_0] \right\}. \tag{D.0.5b}$$

List of References

Acrivos, A., Shah, M. J. & Petersen, E. E. 1960 Momentum and heat transfer in laminar boundary-layer flows of non-newtonian fluids past external bodies. *AIChE J.* **6**, 312–317.

Ahmadpour, A. & Sadeghy, K. 2013 Swirling flow of Bingham fluids above a rotating disk : An exact solution. *J. Non-Newtonian Fluid Mech.* **197**, 41–47.

Alibenyahia, B., Lemaitre, C., Nouar, C. & Ait-Messaoudene, N. 2012 Revisiting the stability of circular Couette flow of shear-thinning fluids. *J. Non-Newtonian Fluid Mech.* **183-184**, 37–51.

Andersson, H. I., de Korte, E. & Meland, R. 2001 Flow of a power-law fluid over a rotating disk revisited. *Fluid Dyn. Res.* **28**, 75–88.

Batchelor, G. K. 1951 Note on the class of solutions of the Navier-Stokes equations representing steady non-rotationally symmetric flow. *Q. J. Mech. Appl. Math.* **4**, 29–41.

Bingham, E. C. 1916 An investigation of the laws of plastic flow. *Bull. U. S. Bur. of Standards* **13**, 309–352.

Bird, R. B., Armstrong, R. C. & Hassager, O. 1977 *Dynamics of Polymeric Liquids, Volume 1: Fluid Mechanics*. J. Wiley & Sons.

Bödewadt, U. T. 1940 Die Drehströmung über festem Grund. *Z. Angew. Math. Mech.* **20**, 241–252.

Carreau, P. J. 1972 Rheological Equations from Molecular Network Theories. *Trans. Soc. Rheolo.* **16:1**, 99–127.

Cochran, W. G. 1934 The flow due to a rotating disk. *Proc. Camb. Phil. Soc.* **30**, 365–375.

Colley, A. J., Carpenter, P. W. & Thomas, P. J. 2006 Experimental verification of type-ii-eigenmode destabilization in the boundary layer over a compliant rotating disk. *Phys. Fluids* **18**, 054107.

Cooper, A. J., Harris, J. H., Garrett, S. J., Özkan, M. & Thomas, P. J. 2015 The effect of anisotropic and isotropic roughness on the convective stability of the rotating disk boundary layer. *Phys. Fluids* **27**, 014107.

Corke, T. C. & Knasiak, K. F. 1998 Stationary traveling cross-flow mode interactions on a rotating disk. *J. Fluid Mech.* **355**, 285–315.

Cros, A., Floriani, E., Le Gal, P. & Lima, R. 2005 Transition to turbulence of the Batchelor flow in a rotor/stator device. *Eur. J. Mech. (B/Fluids)* **24**, 409–424.

Dabrowski, P. P. 2004 Boundary-layer Flows in non-Newtonian Fluids. PhD thesis, School of Mathematical Sciences, The University of Adelaide.

Davies, C. & Carpenter, P. W. 2003 Global behaviour corresponding to the absolute instability of the rotating-disk boundary layer. *J. Fluid Mech.* **486**, 287–329.

Decker, M. J., Halbach, C. J., Nam, C. H., Wager, N. J. & Wetzel, E. D. 2007 Stab resistance of shear thickening fluid (STF)-treated fabrics. *Compos. Sci. Technol* **67**, 565–578.

Denier, J. P. & Dabrowski, P. P. 2004 On the boundary-layer equations for power-law fluids. *Proc. R. Soc. Lond. A* **460**, 3143–3158.

Denier, J. P. & Hewitt, R. E. 2004 Asymptotic matching constraints for a boundary-layer flow of a power-law fluid. *J. Fluid Mech.* **518**, 261–279.

Frigaard, I. A., Howison, S. D. & Sobey, I. J. 1994 On the stability of Poiseuille flow of a Bingham fluid. *J. Fluid Mech.* **263**, 133–150.

Gajjar, J. S. B. 2007 Nonlinear critical layers in the boundary layer on a rotating disk. *J. Eng. Math.* **57**, 205–217.

Garrett, S. J. 2010 Linear growth rates of types I and II convective modes within the rotating-cone boundary layer. *Fluid Dyn. Res.* **42**, 025504.

Garrett, S. J., Hussain, Z. & Stephen, S. O. 2009 The cross-flow instability of the boundary layer on a rotating cone. *J. Fluid Mech.* **422**, 209–232.

Garrett, S. J. & Peake, N. 2002 The stability and transition of the boundary layer on a rotating sphere. *J. Fluid Mech.* **456**, 199–218.

Garrett, S. J. & Peake, N. 2004 The stability of the boundary layer on a rotating sphere in a uniform axial flow. *Euro. J. Mech. (B/Fluids)* **23**, 241–253.

Gregory, N., Stuart, J. T. & Walker, W. S. 1955 On the stability of three-dimensional boundary layers with applications to the flow due to a rotating disk. *Phil. Trans. R. Soc. Lond. A* **248**, 155–199.

Griffiths, P. T. 2015 Flow of a generalised Newtonian fluid due to a rotating disk. *J. Non-Newtonian Fluid Mech.* **221**, 9–17.

Griffiths, P. T., Stephen, S. O., Bassom, A. P. & Garrett, S. J. 2014*a* Stability of the boundary layer on a rotating disk for power law fluids. *J. Non-Newtonian Fluid Mech.* **207**, 1–6.

Griffiths, P. T., Garrett, S. J. & Stephen, S. O. 2014*b* The neutral curve for stationary disturbances in rotating disk flow for power-law fluids. *J. Non-Newtonian Fluid Mech.* **213**, 73–81.

Hall, P. 1986 An asymptotic investigation of the stationary modes of instability of the boundary layer on a rotating disc. *Proc. R. Soc. Lond. A* **406**, 93–106.

Hansford, G. & Litt, M 1968 Mass transfer from a rotating disk into power-law liquids. *Chem. Eng. Sci.* **23**, 849–864.

Healey, J. J. 2006 Inviscid long-wave theory for the absolute instability of the rotating-disc boundary layer. *Proc. R. Soc. Lond. A* **462**, 1467–1492.

Healey, J. J. 2010 Model for unstable global modes in the rotating-disk boundary layer. *J. Fluid Mech.* **663**, 148–159.

Huerre, P. & Monkewitz, P. A. 1990 Local and global instabilities in spatially developing flows. *Annu. Rev. Fluid Mech.* **22**, 473–537.

Hussain, Z. 2010 Stability and transition of three-dimensional rotating boundary layers. PhD thesis, School of Mathematics, University of Birmingham.

Hussain, Z., Garrett, S. J. & Stephen, S. O. 2011 The instability of the boundary layer over a disk rotating in an enforced axial flow. *Phys. Fluids* **23**, 114108.

Hussain, Z., Garrett, S. J. & Stephen, S. O. 2014 The centrifugal instability of the boundary-layer flow over slender rotating cones. *J. Fluid Mech.* **755**, 274–293.

Imayama, S., Alfredsson, P. H. & Lingwood, R. J. 2012 A new way to describe the transition characteristics of a rotating-disk boundary-layer flow. *Phys. Fluids* **24**, 031701.

Imayama, S., Alfredsson, P. H. & Lingwood, R. J. 2013 An experimental study of edge effect on rotating-disk transition. *J. Fluid Mech.* **716**, 638–657.

Imayama, S., Alfredsson, P. H. & Lingwood, R. J. 2014 On the laminar-turbulent transition of the rotating-disk flow: the role of absolute instability. *J. Fluid Mech.* **745**, 132–163.

Jasmine, H. A. & Gajjar, J. S. B. 2005 Absolute and convective instabilities in the incompressible boundary layer on a rotating disk with temperature-dependent viscosity. *Int. J. Heat Mass Transfer* **48**, 1022–1037.

Jenekhe, S. A. & Schuldt, S. B. 1984 Coating Flow of Non-Newtonian Fluids on a Flat Rotating Disk. *Ind. Eng. Chem. Fundam.* **23**, 432–436.

von Kármán, T. 1921 Über laminare und turbulente Reibung. *Z. Angew. Math. Mech.* **1**, 233–252.

Lashgari, I., Pralits, J. O., Giannetti, F. & Brandt, L. 2012 First instability of the flow of shear-thinning and shear-thickening fluids past a circular cylinder. *J. Fluid Mech.* **701**, 201–227.

Lee, Y. S., Wetzel, E. D. & Wagner, N. J. 2003 The ballistic impact characteristics of Kevlar® woven fabrics impregnated with a colloidal shear thickening fluid. *J. Mat. Sci.* **38**, 2825–2833.

Levich, V. G. 1962 *Physicochemical Hydrodynamics*. Prentice-Hall.

Lingwood, R. J. 1995*a* Absolute instability of the boundary layer on a rotating disk. *J. Fluid Mech.* **299**, 17–33.

Lingwood, R. J. 1995*b* Stability and Transition of the Boundary Layer on a Rotating Disk. PhD thesis, Sidney Sussex College, University of Cambridge.

Lingwood, R. J. 1996 An experimental study of absolute instability of the rotating-disk boundary-layer flow. *J. Fluid Mech.* **314**, 373–405.

Lingwood, R. J. 1997 Absolute instability of the Ekman layer and related rotating flows. *J. Fluid Mech.* **331**, 405–428.

Lingwood, R. J. & Alfredsson, P. H. 2015 Instabilities of the von Kármán Boundary Layer. *Appl. Mech. Rev.* **67**, 030803.

Lingwood, R. J. & Garrett, S. J. 2011 The effects of surface mass flux on the instability of the BEK system of rotating boundary-layer flows. *Euro. J. Mech. (B/Fluids)* **30**, 299–310.

MacKerrell, S. O. 1987 A nonlinear, asymptotic investigation of the stationary modes of instability of the three-dimensional boundary layer on a rotating disc. *Proc. R. Soc. Lond. A* **413**, 497–513.

MacKerrell, S. O. 2005 Stability of Bödewadt flow. *Phil. Trans. R. Soc. A* **363**, 1181–1187.

Malik, M. R. 1986 The neutral curve for stationary disturbances in rotating-disk flow. *J. Fluid Mech.* **164**, 275–287.

Matsumoto, S., Salto, K. & Takashima, Y. 1973 The thickness of a viscous liquid film on a rotating disk. *J. Chem. Eng. Jpn.* **6**, 503–507.

Matsumoto, S., Takashima, Y., Kamiya, T., Kayano, A. & Ohta, Y. 1982 Film thickness of a Bingham liquid film on a rotating disk. *Ind. Eng. Chem. Fundam.* **21**, 198–202.

Ming, C., Zheng, L. & Zhang, X. 2011 Steady flow and heat transfer of the power-law fluid over a rotating disk. *Int. Commun. Heta Mass Transf.* **38**, 280–284.

Mitschka, P. 1964 Nicht-Newtonsche Flüssigkeiten II. Drehströmungen Ostwald-de Waelescher Nicht-Newtonsche Flüssigkeiten. *Coll. Czech. Chem. Comm.* **29**, 2892–2905.

Mitschka, P. & Ulbrecht, J. 1965 Nicht-Newtonsche Flüssigkeiten IV. Strömung Nicht-newtonsche Flüssigkeiten Ostwald-de Waelescher Typs in der Umgebung Rotierender Drehkegel und Schieben. *Coll. Czech. Chem. Comm.* **30**, 2511–2526.

Nasr-El-Din, H. A., Al-Mohammad, A. M., Al-Aamri, A. M. & Al-Fuwaires, O. 2008 Reaction kinetics of gelled acids with calcite. *SPEPO* **23 (3)**, 353–361.

Nouar, C., Kabouya, N., Dusek, J. & Mamou, M. 2007*a* Modal and non-modal linear stability of the plane Bingham-Poiseuille flow. *J. Fluid Mech.* **577**, 211–239.

Nouar, C., Bottaro, A. & Brancher, J. P. 2007*b* Delaying transition to turbulence in channel flow: revisiting the stability of shear-thinning fluids. *J. Fluid Mech.* **592**, 177–194.

Ostwald, W. 1925 Über die Geschwindigkeitsfunktion der Viskosität disperser Systeme. i. *Colloid Polym. Sci.* **36**, 99–117.

Papanastasiou, T. C. 1987 Flows of materials with yield. *J. Rheol.* **31**, 385–404.

Peng, J. & Zhu, K. Q. 2004 Linear stability of Bingham fluids in spiral Couette flow. *J. Fluid Mech.* **512**, 21–45.

Pier, B. 2003 Finite-amplitude crossflow vortices, secondary instability and transition in the rotating-disk boundary layer. *J. Fluid Mech.* **487**, 315343.

Rashaida, A. A., Bergstrom, D. J. & Sumner, R. J. 2006 Mass transfer from a rotating disk to a Bingham fluid. *Trans. ASME: J. Appl. Mech.* **73**, 108111.

Siddiqui, M. E., Mukund, V., Scott, J. & Pier, B. 2013 Experimental characterization of transition region in a rotating-disk boundary layer. *Phys. Fluids* **25**, 034102.

Smith, F. T. 1979 On the non-parallel flow stability of the Blasius boundary layer. *Proc. R. Soc. Lond. A* **366**, 91–109.

Towers, P. D. 2013 The stability and transition of the compressible boundary-layer flow over broad rotating cones. PhD thesis, Department of Mathematics, University of Leicester.

de Waele, A. 1923 Viscometry and plastometry. *J. Oil Colour Chem. Assoc.* **6**, 32–69.

Zandbergen, P. J. & Dijkstra, D. 1987 Von Kármán swirling flows. *Annu. Rev. Fluid Mech.* **19**, 465–491.

Zhu, H., Kim, Y. D. & De Kee, D. 2005 Non-Newtonian fluids with a yield stress. *J. Non-Newtonian Fluid Mech.* **129**, 177–181.